Université de Lille 1 SCIENCES ET TECHNOLOGIES

N° d'ordre : 41949

Université Lille I – SCIENCES ET TECHNOLOGIES

Ecole Doctorale des Sciences de la Matière, du Rayonnement

et de l'Environnement

Thèse

pour obtenir le grade de

Docteur

Mention : Molécules et Matières Condensée

Par

Jesús GUERRERO

Valorisation du méthane par reformage sec en régimes stationnaire et non-stationnaire sur catalyseurs à base de nickel : mise en œuvre d'un réacteur à alimentation périodique

Valorization of methane through dry reforming in steady and non-steady-state regimes on nickel-based catalysts: application of a periodic feed reactor

11 décembre 2015

Composition du jury :

ARIAS, Pedro Luis	Professeur	Bilbao UPV / EHU	Rapporteur
MIRODATOS, Claude	Directeur de Recherche CNRS	Ircelyon	Rapporteur
ROGER, Anne-Cécile	Professeur	Université de Strasbourg	Examinateur
DUMEIGNIL, Franck	Professeur	Université Lille1	Examinateur
JALOWIECKI-DUHAMEL, Louise	Chargée de Recherches CNRS	Université Lille1	Directeur de thèse
LÖFBERG, Axel	Chargé de Recherches CNRS	Université Lille1	Directeur de thèse

“La vie est un fût vide” *Antonio Caballero, Spanish Philosopher*

“千里之行始于足下” *Lao Tzu, Chinese Philosopher*

ACKNOWLEDGEMENTS

I would like to thank the University of Lille 1 and the French Research ministry to financially support my doctor studies in the Laboratory of Catalysis and Solid state Chemistry (UCCS) in Lille. I thank Pr. L. Montagne and Pr. F. Dumeignil for offering me this opportunity and providing me all the necessary resources for my research.

I owe a lot to Axel Löfberg. His enormous background in alkanes reforming helped me to understand every technical aspect. All his passionate scientific discussions during the last three years let me to enlarge my competences and knowledge on this field. Besides, he was kindly concerned about all the logistical issues at my arrival, which was fundamental for a fast adaptation in the city.

I would like to express my deep gratitude to Louise Duhamel. The fruitful scientific discussions during this thesis help me to understand the complexity from the solid point of view and the different possibilities which can be reached from different synthesis techniques.

I had the extremely great honor to have Pr. Pedro Luis Arias and Pr. Claude Mirodatos as the reporters for my thesis, thank you so much for your valuable reviews. I also would like to sincerely thank Pr. Anne-Cécile Roger and Pr. Franck Dumeignil for their participation in my defense jury.

I would like to extend my sincere gratitude to all the other colleagues who, during more informal discussions, taught me different scientific knowledge. I will keep with me all the wisdom tips. Thanks also to all the people working in the laboratory who did through their humankind and sympathy these last three years much more comfortable. The working atmosphere in this place is priceless.

Finally, let me give the most personal acknowledgement to my lovely family who has always been helping me out and taking care of me despite the distance. Their love and support makes sense to all the rest.

Contents

RÉSUMÉ

La société est préoccupée par l'effet de serre et la nécessité de développer des procédés alternatifs et durables pour fabriquer les produits actuellement dérivés du pétrole. La valorisation du CH_4 avec CO_2 (reformage sec) présente l'avantage de consommer des gaz qui contribuent fortement à l'effet de serre. Simultanément, la réaction produit de l'H_2 et du CO qui, séparément ou ensemble, sont à la base de différents procédés de production d'énergie et de molécules plateformes.

Des catalyseurs du type Ni-Ce-O et Ni-Mg-Al-O, performants pour la production de gaz de synthèse à partir de méthane et de dioxyde de carbone, ont été développés. L'influence de différents paramètres a été étudiée, comme la préparation (imprégnation et coprécipitation), la teneur en Ni et la température de réaction (600°C-800°C). Notamment, une étude a été menée de manière approfondie afin d'optimiser le procédé à une basse température de 600°C.

Les principales difficultés rencontrées sont la formation de coke conduisant à la désactivation rapide des catalyseurs à cause des températures élevées de fonctionnement et la présence simultanée de CO_2 (réactif) et d'hydrogène (produit) qui conduit, par la réaction inverse du gaz à l'eau, à une perte en sélectivité.

Afin d'éviter ce type de problématique un nouveau procédé a été développé. Il implique d'alimenter de manière alternée chacun des réactifs et fait intervenir un solide agissant en tant que vecteur d'oxygène. Dans un premier temps le solide réagit avec le méthane pour former le monoxyde de carbone et le dihydrogène. Le solide étant régénéré à chaque cycle, la déactivation par cokage est évitée. L'hydrogène produit n'est jamais en contact avec le dioxyde de carbone (réactif), évitant ainsi la réaction inverse de gaz à l'eau. L'activité et la sélectivité du solide est assurée par la présence d'un oxyde réductible (CeO_2) faisant office de vecteur d'oxygène, et d'un métal (Ni, Co), non-oxydable dans les conditions de réalisation du procédé, qui assure l'activation du méthane. Différentes caractérisations physico-chimiques ont été effectuées sur les catalyseurs afin d'établir des corrélations entre l'activité catalytique et les propriétés des solides.

ABSTRACT

Nowadays the society is concerned about the greenhouse effect, and the necessity to find alternative procedures and more sustainable and durable processes to obtain the products made from petroleum. The valorization of CH_4 with CO_2 (dry reforming) brings the advantage of consuming gases which contribute strongly to the greenhouse effect. This reaction produces H_2 and CO, which jointly or separately, are the raw materials for different processes producing energy and chemicals.

Ni-Ce-O and Ni-Mg-Al-O based catalysts were successfully prepared by impregnation and coprecipitation. The influence of different parameters was studied, such as the Ni loading and the reaction temperature (600°C-800°C). In particular, a study at 600°C has been deeply developed to optimize the process at such temperature.

The main difficulties are the formation of coke leading to rapid catalyst deactivation due to the high operating temperatures and the simultaneous presence of CO_2 (reactant) and hydrogen (product) which leads, by the reverse water gas shift (RWGS), to a loss in selectivity.

A process which can avoid this kind of problematics consists in exposing alternately each of the reactants. Initially the solid acts as oxygen carrier reacting with methane to form carbon monoxide (1 mole) and hydrogen (2 moles). As the solid is regenerated at each cycle, the deactivation by carbon deposition is avoided. The hydrogen produced is never in contact with the carbon dioxide, preventing the RWGS. The activity and selectivity of the solid is provided by the presence of a reducible oxide (CeO_2) and a metal (Ni, Co), which cannot be reoxidized under the experimental conditions ensuring the activation of methane. Different physicochemical characterizations were performed on catalysts to find correlations between the catalytic activity and properties of the solids.

CHAPTER I:

Introduction and Purpose of the thesis

1. INTRODUCTION and PURPOSE of the thesis

1.1. General introduction

The expected increase in population in the next decades and its proportional energy demand has driven the perspective of the researchers and politicians in the last years. Several studies have been made predicting the increase of energy demand in the horizon of 2050 which point out the need to double the energy production as compared with the one in 2010, considering a growth of population from 7 billion to 9 billion in this lap of time [1.1]. Expecting such enormous rise, several socio-political dilemmas come out, notably the so-called food-water-energy nexus [1.2]. The society needs to face the problematic which will appear in the near future from those three pillars for the sustainability of the human race. The main challenges for the horizon of 2050 are (i) the eradication of hunger preserving sufficient food production and maintaining the biodiversity, (ii) the production of sufficient energy for the imminent vast demand, controlling at the same time the global climate change and the pollution of the air and (iii) the supply of water, mainly due to the population growth in water scarce areas, to avoid the so-called water stress, defined as the ratio of water demand over supply larger than 0.4. A clear example of increasing awareness of some of these obstacles from the political parties is the relevance given to the next United Nations Conference on Climate change (COP21) which will be held in Paris at the end of the year. The organizing committee claims that the main target of the congress is to settle, for the first time in the 20 years of discussions, a binding and universal agreement on climate, from all the nations of the world, with the aim of keeping global warming below 2ºC.

In such context, this thesis is focused on the consensus that sustainable energy production is an urgent need for the future of the humankind. Several technologies are on the way to be optimized for its production in large-scale. This includes an advancement of the know-how to produce energy from different well-known renewable resources such as sunlight, wind, biomass, rain and tides waves [1.3-1.5]. Such improvement is one of the main challenges because nowadays there is the perspective that, in 2050, 80% of the worldwide energy consumption will still depend on fossil fuels [1.1].

Concretely, we focus our effort in the development of technologies for the valorization of CH_4 with the further perspective of making the transition from this fossil fuel to the sustainable production of energy from biogas.

1.2. Valorization of methane

The main and well-known “valorization” of CH_4 is its combustion for energy production. This process is done in large scale with natural gas and petrol. Nevertheless, the challenge is

switching from petrol (liquid) to gas based economy to transform methane in higher hydrocarbons in order to produce liquid fuels. The second challenge is to provide carbon resources for petrochemistry (thus not for energy) using methane as initial carbon source instead of liquid fossil fuels.

The valorization of methane into liquid fuels or higher hydrocarbons has attracted renewed attention in the last years [1.67] due to two main factors, the large volume of methane resources available as compared to petroleum, particularly since the exploitation of shale gas has been developed [1.66], and the remarkable contribution to the greenhouse effect. In fact, even if CH_4 has a much shorter lifetime in the atmosphere than CO_2, the hydrocarbon is more efficient trapping radiation. The impact on the global warming of CH_4 is 25 times greater than the one of CO_2 in a 100-year period [1.64].

The optimization of processes involving the valorization of CH_4 has been studied since several decades [1.6-1.7]. Up to now, the only one which has succeeded in a large industrial scale is the steam reforming of methane (SRM) [1.8].

Eq. 1.1 $\mathrm{CH_4 + H_2O \rightarrow 3H_2 + CO}$ $\Delta H^{\circ}_{298^{\circ}K} = 206 kJ/mol$

This process is mainly used for the production of hydrogen, which is considered one of the main alternatives for an efficient and nonpolluting energy vector in the near future. Even though the industrial application, SRM is still being studied in the attempt of avoiding the carbon deposition from different side reactions [1.9]. One of the main interests of this reaction is the higher production of hydrogen in comparison within other potential methane reforming processes. 3 moles of H_2 are produced instead of 2 for the oxidative reforming of methane (ORM) and the dry reforming of methane (DRM). As a matter of fact, the 48% of the worldwide production of H_2 comes from this process [1.10]. Nevertheless, the two other reforming reactions have been widely studied in order to optimize them as much as being economically competitive for a large-scale process.

Commonly, the catalytic partial oxidation of methane has been postulated as an alternative to SRM [1.11-1.12]. One of the main advantages is the production of synthesis gas (syngas), a mixture of H_2 and CO, with a lower ratio (H_2 / CO = 2) than the one produce in the SRM.

Eq. 1.2 $\mathrm{CH_4 + 0.5O_2 \rightarrow 2H_2 + CO}$

$\Delta H^{\circ}_{298^{\circ}K} = -35.7 kJ/mol$

This ratio is more suitable for further applications, like Fischer-Tropsch or methanol synthesis. Furthermore, the exothermic behavior of the reaction is more attractive from the energetic point of view. One of the main constraints is the explosive limits between CH_4 and O_2, which could cause fire and explosion safety issues [1.13]. Therefore, the process is substantially more dangerous in comparison with the reforming by vapor or CO_2. In addition, selectivity towards syngas in respect to total combustion of methane is also an important issue for this reaction.

Specifically, between the three possible pathways of methane valorization, we choose to study in this thesis the process working with CO_2 (DRM).

1.3. Dry reforming of methane

As mentioned there is a general consensus about the importance of setting a low carbon society for the sustainability of the near future. The link between the emissions of CO_2 with the global warming is well recognized by the scientific community. Concretely, the global surface temperature increased by 0.8°C in the last century.

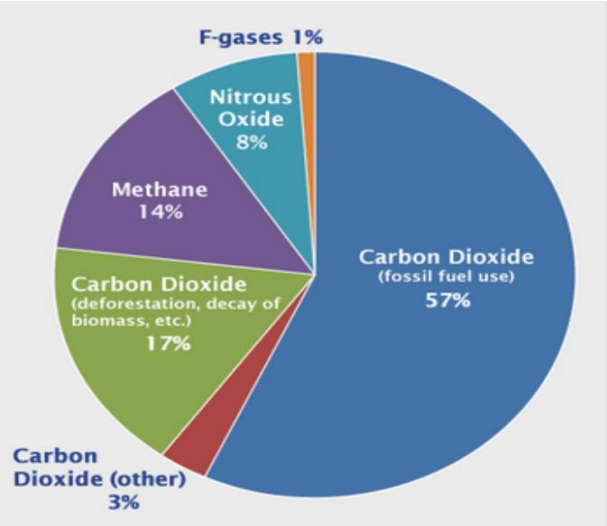

Fig 1.1 Global greenhouse gas emissions by gas (emitted by human activities) [1.65]

The ***Fig 1.1*** shows that CO_2 is the largest gas emitted by human activities (77%). Besides, the lifetime of carbon dioxide in the atmosphere is around 300 years and the 25% of the emissions last forever [1.63]. Some studies show that by 2050, following the present trend, the emission of CO_2 will have increased around 60% in comparison with 2010 [1.1]. The raise will induce an increment of the global temperature of the Earth above the 2ºC target. According to researchers, an increase of only 2ºC or less would be possible if instead of doubling the recent emission of CO_2, we halve them. Thus, several efforts and investments need to be made in the development of technologies in order to reduce net CO_2 emissions. The main solutions would be: (i) the reduction of the energy consumed by enhancing the energy conversion and utilization, (ii) the development of technologies using less carbon intensive fuels, (iii) the increase on the renewable energies implementation, (iv) the improvement of the absorption capacity in forest and (v) the CO_2 consumption as feedstock material for several chemical processes.

Dry reforming of methane is a potential method for such consumption of CO_2 associated to the valorization of methane [1.14, 1.19], gases considered as the least expensive carbon-containing compounds.

Eq. 1.3 $CH_4 + CO_2 \rightarrow 2H_2 + 2CO$ $\Delta H° = 247 kJ/mol$

The reaction between these two gases can generate syngas with a suitable molar ratio of H_2 / CO for the Fischer-Tropsch synthesis to produce light and heavy hydrocarbons [1.15-1.16]**.** Depending on the catalyst and pressure, the required syngas ratio varies from 1 to 2. In addition, another potential product from H_2 and CO is the dimethyl ether (DME) [1.17]. However, DRM has some constraints, (i) a low H_2/CO = 1 ratio in comparison with the two other reforming reactions (2 for the ORM and 3 for the SRM), (ii) the endothermic reaction, on the contrary than in the ORM (iii) the carbon deposition and (iv) the reverse water gas shift (RWGS) [1.18], where CO_2 can react with H_2 to produce H_2O and CO.

Eq. 1.4 $CO_2 + H_2 \rightarrow CO + H_2O$ $\Delta H° = -41 kJ/mol$

H_2/CO ratio is typically lower than 1 due to the consumption of hydrogen and the increase of CO concentration. Besides, another undesired side reaction is the decomposition of methane into carbon and hydrogen [1.20], a process which could occurs potentially in the three cases (SRM, ORM and DRM).

Eq. 1.5 $CH_4 \rightarrow C + 2H_2$ $\Delta H° = 75 kJ/mol$

Finally, the last main side reaction is the disproportionation of carbon monoxide, the so-called Boudouard reaction [1.21].

Eq. 1.6 $2CO \rightarrow C + CO_2$ $\Delta H° = -171 kJ/mol$

The problematic in the last two cases is the formation of carbon which leads to the deactivation of the catalyst due to the deposition on the actives sites.

1.4. Processes in periodic conditions

A periodic feed of the reactants in periodic is a promising solution for energy production from fossil fuels or renewables sources [1.53]. Several industrial techniques have been already applied since decades in order to improve reaction systems [1.22-1.24]. The main difference from the cofeed processes is the ability of decoupling the reaction in two. Therefore the operation conditions can be enhanced independently, obtaining in some cases different selectivity than the one reached in cofeed.

Original reactor systems instead of the classical cofed fixed (or fluidized) bed reactor are necessary. The simplest application, which is most suited for experimental studies at laboratory scale, would consist in a fixed bed reactor fed alternatively with one and the other reactant. Another possibility, which is better adapted for industrial exploitation, would be the use of a circulating bed reactor. The catalysts would be transported from one reactor to the other performing each part of the decoupled reaction in a separate vessel.

One of the most known processes using a circulating bed reactor is the Fluid Catalytic Cracking (FCC) used in petroleum refineries. The aim is to vaporize and crack low value heavy oil into different more valuable products (gasoline, diesel, olefins…) in the first reactor and regenerate the catalyst in the second one. The vaporized petrol gets in contact with a powdered catalyst in order to carry the reaction. The main issue is the deactivation of the catalyst due to carbon deposition on the actives sites from the cracking reactions. Therefore the catalyst is circulated rapidly until a second vessel to be regenerated by air, in other words, burning the carbon by oxygen. In addition, working with fluidized beds helps to avoid hot spots in comparison with fixed beds, which have worse heat transfer. Nowadays the efforts are focused on adapting the technology using different resources as raw material, like resins and biomass-derived oils [1.23].

The chemical looping combustion (CLC) is another process which uses circulating catalysts. The solid is also fluidized between two reactors, but there is an important difference, the catalyst is used as an oxygen carrier. Essentially, a fuel is in contact with a solid oxide which provides the required oxygen to produce total combustion, ideally a mixture of CO_2 and H_2O. Besides, the steam is condensed to recover CO_2 avoiding other energy intensive CO_2 separation procedures and allowing further valorization or trapping. After the combustion, the catalyst is transferred to a second vessel to be reoxidized by air in order to recover the oxygen capacity [1.25]. A general reaction stoichiometry is given as follows:

Eq. 1.7 $C_nH_{2m} + (2n + m)\ M_yO_x \rightarrow (2n + m)\ M_yO_{x-1} + m\ H_2O + n\ CO_2$ $\Delta H° > 0$

Eq. 1.8 $M_yO_{x-1} + ½\ O_2\ (air) \rightarrow M_yO_x$ $\Delta H° < 0$

M_yO_x = oxygen carrier oxidized

M_yO_{x-1} = oxygen carrier reduced

Thus, the CLC offers a flameless combustion without any flammability mixture limitation and a stream free of NO_x during the combustion of the fuel with addition of CO_2 capture.

Finally, the third breakthrough process in periodic is to carry this technique with another attractive property, the selective oxidation. The transformation of butane to maleic anhydride over vanadium phosphorus oxide catalysts was one of the first reactions to work in such conditions [1.26-1.27]. From one side, higher initial concentrations can be applied than working with conventional technologies and from the other side, the butane reacts selectively with the oxygen carrier to produce maleic anhydride. The reduced catalyst is circulated to a second chamber to be reoxidized by air as in the CLC process. In this procedure the main redox process occurs between the V^{5+} and V^{4+} oxidation states of vanadium, as so the stoichiometry for the reactions are as follows:

Eq. 1.9 $C_4H_{10} + xV^{5+} \rightarrow MA + xV^{4+} + 4\ H_2O$

Eq. 1.10 $^1/_2\ O_2 + V^{4+} \rightarrow V^{5+}$

Minimizing as much as possible the oxidation of maleic anhydride into CO_x and H_2O

Eq. 1.11 $MA + yV^{5+} \rightarrow 4\ CO_x + yV^{4+} + H_2O$

Based on all the advantages demonstrated of working in periodic, we tried to develop such technology in the valorization of CH_4.

1.5. Valorization of methane in periodic conditions

Currently researchers try to use such periodic procedures to optimize the processes involving CH_4 with the aim of reducing the cost of CO_2 capture from power generation (e.g. CLC) and H_2 or/and syngas production [1.28]. The main targets are to enhance the stability of the processes minimizing the amount of carbon on the catalyst or reoxidizing it in the regeneration chamber.

1.5.1. Steam reforming

Some studies have already been published using vapor of water as an oxidant reactant. V.Gavita et al. [1.29] proposed the steam reforming of methane in such conditions (P-SRM). Pt-CeO_2-ZrO_2 and Fe_3O_4-CeO_2-ZrO_2 based catalyst were used in order to obtain H_2O and CO_2 (total oxidation of methane). However, some works have focused on the selective oxidation of methane producing 2 mols of H_2 and 1 mol of CO. Zhu et al. [1.30-1.31] obtained a high selectivity towards H_2 and CO (90%) and 10% towards the total oxidation (H_2O and CO_2) at 850ºC using Fe-Ce mixed oxide catalysts. The following system is proposed:

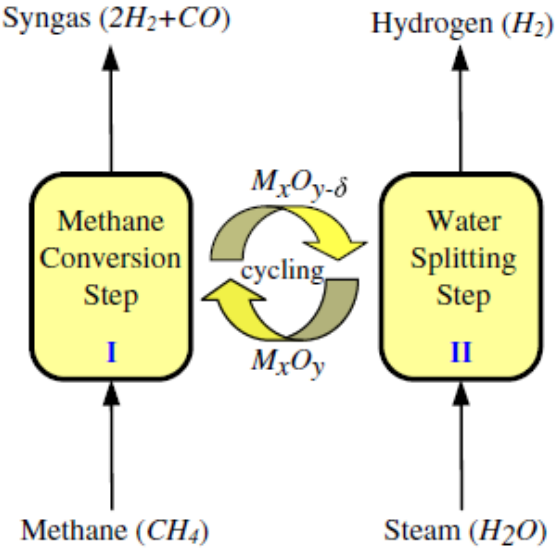

Fig 1.2 Reactor design for SRM in a periodically operated two-layer reactor [1.30]

Dong-Hee et al. also showed the feasibility of such process working with supported Cu-ferrite on Yttria-stabilized zirconia [1.32], obtaining a stable process at 900ºC, but with the inconvenient of producing unselective products at the earliest stage of the reaction. In a

general way, water vapor as oxidant compound is really interesting for some applications, such as the production of pure H_2 stream (if there is not carbon deposition in the reductant step).

1.5.2. Oxidative reforming

The oxidative reforming of methane working with the alternative feed (P-ORM) has also been studied. Some disadvantages encountered in the cofeed system can be solved operating in such way. The two main ones are the absence of limitation on the reactant concentrations due to the limit of flammability, which allows working in a safe reactor process, and the elimination of N_2 from the effluent. S. Bhavsar et al. [1.54] proposed to work with Ni_xFe_{1-x} / CeO_2 oxygen carriers which selectively produce a ratio $H_2/CO = 2$. Nevertheless, the production of H_2O and CO_2 occurs during the first minutes of reaction (as in the case for the P-SRM). Another interesting approach is the one of L. Neal et al. [1.55], who obtained selective and active performances using Fe_2O_3 / $La_xSr_{1-x}FeO_3$. As in the last cases, the main inconvenient is the production of CO_2 at the first stage of the reduction. Probably, H_2O and CO_2 are produced during the first minutes of reaction due to the total reoxidation of iron species. In fact, the unselective oxidation is shown to come mainly from the reduction of Fe_2O_3 to Fe_3O_4. However, the same type of catalyst works more selectively in the study of Zhu et al. [1.30-1.31] thanks to the impossibility of oxidizing by H_2O the Fe_3O_4 state to Fe_2O_3.

1.6. Dry reforming of methane in periodic conditions

Some studies have been done working with CO_2 as a reactant in the catalyst regeneration step. The oxygen depleted by the reaction with CH_4 is regenerated with CO_2. As already mentioned, the main advantages are the valorization of another greenhouse gas on the environmental/societal point of view and the possibility of avoiding the RWGS reaction on the chemistry side.

1.6.1. Cracking of methane and oxidation of the carbon

S. Assabumrungrat et al [1.56] proposed to make the decomposition of methane (***Eq. 1.5***) in a first step (producing carbon and hydrogen) and the reoxidation of the carbon by CO_2 in a second one using $Ni/SiO_2.MgO$ as a catalyst. Obviously, the solid does not act as an oxygen vector in this case. The process claimed is as follows:

$$CH_4 \rightarrow C + 2H_2$$

Eq. 1.12 $$xCO_2 + yO_2 + C \rightarrow zCO$$

As the ***Eq. 1.12*** shows, a flow of oxygen (besides the one of CO_2) is needed for the total reoxidation of the carbon. Concretely, a ratio CO_2 / O_2 = 7:3 gives the best compromise in

terms of activity during the 4h experiment. An optimum step period was found at 10 minutes, after such time the conversion decreases due to a considerable carbon deposition. The study reveals that the periodic operation provides lower performance in terms of methane conversion than steady state operation at the same conditions. Nevertheless, the periodic process is beneficial in terms of product stream separation (H_2 from one side and CO for the other) and regeneration of the catalyst.

1.6.2. Total oxidation of methane and reoxidation by CO_2

A variant of CLC using CO_2 instead of O_2 is another approach using CH_4 and CO_2 in periodic. Although it has been called Chemical Looping Dry Reforming (CLDR), the process aims at total oxidation of methane.

Eq. 1.13 $$CH_4 + 4MO \rightarrow 4M + CO_2 + 2H_2O$$

Eq. 1.14 $$4CO_2 + 4M \rightarrow 4MO + 4CO$$

M = oxygen carrier reduced

MO = oxygen carrier oxidized

One of the main challenges in comparison with the SRM in periodic is to get a suitable oxygen carrier which could be reactive towards CO_2, a molecule less reactive than H_2O. Up to now the most promising carriers are Fe / BHA, Fe /SiO_2 [1.57] and Fe / CeO_2 [1.58] based catalysts. For instance, the main inconvenient for Fe / BHA is the limitation of the carrier utilization (<50%) working below 800°C and incomplete CO_2 conversion. Otherwise, Fe / SiO_2 catalyst shows low activity due to the formation of Fe-silicates which cannot be reoxidized by CO_2. Thus, the addition of air is necessary to maintain the redox capacity of the solid.

CeO_2 as a support has been recently investigated to improve carrier utilization for the conventional CLC, therefore optimizing the activity towards CO_2 [1.59]. According to this study, ceria, which is not involved to the reaction in terms of oxygen contribution, enhances the oxygen vector capacity of Fe_xO_y. Complementary, the XRD analysis showed that CeO_2 was not significantly reduced. However, the kinetics towards CO_2 was found to be much faster than with the other catalysts. From the regeneration point of view is remarkable that Fe_xO_y was reoxidized to Fe_3O_4 instead of the highest oxidation state (Fe_2O_3). This phenomenon has similarities with the study of Zhu et al. [1.31] working with H_2O instead of CO_2 as the oxidant reactant. Such behavior put in evidence another promising property working with CO_2, the selective reoxidation of the solid.

1.6.3. Partial oxidation of methane and reoxidation by CO_2

The third way is the selective oxidation of methane to produce syngas and the regeneration of the solid by CO_2 [1.61]. One of the first researchers to propose such system was Otsuka et al. [1.60] in 1998 on Pt-CeO_2 based catalyst. Evidently, one of the main constraints from the economic point of view is the use of noble metals. Thus, nowadays the efforts are focused on obtaining a similar attractive process with transition metals. The first attempts have been done using Fe-CeO_2 catalysts (as for CLDR process). Bhavsar et al. [1.58] discussed about the relevance of the oxidation state of iron towards the selectivity of the products.

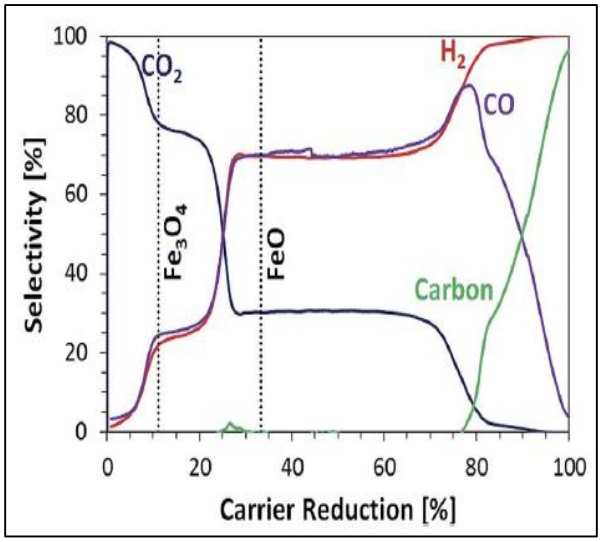

Fig 1.3 Reduction of 100mg Fe-CeO_2 with CH_4 at 900ºC [1.54]

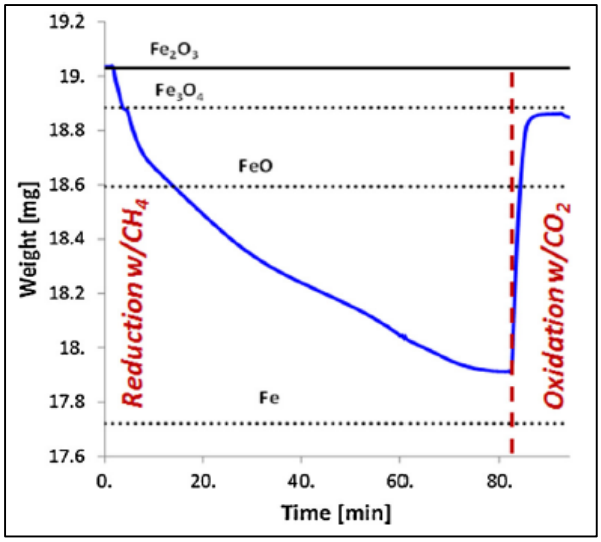

Fig 1.4 CH_4 as a fuel and CO_2 as an oxidant at 900ºC on Fe-CeO_2 catalyst [1.58]

Fig 1.3 shows the products obtained along the different oxidation states. The distribution goes from a total oxidation of CH_4 (Fe_2O_3 to Fe_3O_4), going through a mix of total-partial oxidation (Fe_3O_4 to FeO) and ending with a formation of carbon when the reduction of the solid is almost complete (FeO to Fe).

Even though the ***Fig 1.4*** shows that the reoxidation by CO_2 gives another "initial" state of Fe species (Fe_3O_4) for the next cycle, the system is still not 100% selective towards H_2 and CO. In summary, high oxidation states of iron produce a low selective system towards syngas. On the contrary, low oxidation states lead to less total oxidation but more carbon deposition. Therefore, if the step time of methane was shorter to avoid the carbon formation area, the production of some CO_2 at the first stage of the reaction would be unavoidable.

In conclusion, the main challenge on the first step of the system is to obtain the partial oxidation of methane without neither CO_2 nor H_2O in the syngas stream, keeping a high activity towards methane without producing carbon deposition. Besides, fast kinetics in the reoxidation step still remains an area to explore.

1.7. Discussion the purpose of this thesis

1.7.1. Improvement of DRM by catalyst optimization

Through the last decades different researchers have improved the performance of the DRM thanks to the optimization of the catalyst formulation and synthesis process [1.6,1.33]. The enhancement was achieved mainly by reducing the amount of the noble metal (Rh, Pt, Ru, Ir…) or improving the performance of the transition metals (Ni, Co, Fe…) based catalysts. From one side noble metal catalysts, such as Ru [1.34], Rh, Pt [1.6] and Ir [1.35] show great catalytic activity and a low sensitivity towards carbon deposition, but as usual, their high cost and low availability make them not really interesting compared to transitions metals. From the other side, nickel (the most used transition metal) is an abundant, low-cost and well-known metal to be highly active for DRM [1.36-1.37]. Although there is an increasing concern regarding the toxicity of Ni it remains the most widely studied element for this process.

In this thesis we have mainly worked with Ni based catalysts. Therefore one of the main challenges is to decrease as much as possible the carbon formation and the thermal sintering of actives sites [1.62]. The carbon deposit occurs typically due to the decomposition of CH_4 and the Boudouard reaction (***Eq. 1.5*** and ***Eq. 1.6***). The sintering of Ni can be expected as the typical operating temperatures (700-900ºC) are higher than the Tammann temperature of nickel (590ºC), temperature at which the mobility and reactivity of the molecules become observable [1.47]. Such problematics can be improved modifying the morphology, size and distribution of the nickel particles [1.38]. Obtaining small and well dispersed nanoparticles of nickel is assumed to help diminishing the carbon deposit and the sintering of Ni. Furthermore, the combination of Ni with basic metals, such as K [1.39], Ca, La [1.40] and Mg [1.41] has been proposed in order to enhance the activity and stability of the catalyst. From one side the reaction between CO_2 and carbon is promoted [1.36, 1.46] and from the other side, the chemisorption of CO_2 is improved [1.48] and thus the Boudouard reaction towards CO. However, improved reactivity of CO_2 can enhance RWGS and thus induce a loss in selectivity.

Otherwise the so-called hydrotalcite-like compound which basically is a hydroxycarbonate of magnesium and aluminum ($Mg_6Al_2(OH)_{16}CO_3.4H_2O$) have shown interesting catalytic properties. Concretely, the layered structure can be transformed into mixtures of metal oxides with high surface area, well dispersed, small crystal size and basic properties after high temperature calcination [1.49]. Some studies have focused on the partial substitution of Mg^{2+} by cations of similar size (Ni^{2+}, Co^{2+}…) which reinforces the thermal stability in hydrocarbon reforming reactions [1.50]. Based on that, we found interesting to go deeper in the study and understanding of the Ni-Mg-Al-O based catalyst for DRM [1.44].

Besides, another way to improve the Ni-based catalysts consists of using the redox properties of CeO_2 [1.51], ZrO_2 or Ce-ZrO_2 [1.52]. Researchers relate the ability of reduction

and oxidation between Ce^{4+}/Ce^{3+}, which leads to oxygen release and storage, with the resistance of the catalyst towards carbon deposition. The redox property of CeO_2 is also linked to help the adsorption of CO_2. L. Xu et al. [1.45] shows a mechanism where this improvement could be explained. The driving force of CO_2 is to get adsorbed and refill the vacancies created during the reaction of the solid with CH_4. In addition, the synergetic effect between Ni and CeO_2 can enhance the properties of the Ni-CeO_2 system [1.42]. Based on these interesting properties, Ni-Ce based catalyst is also studied. One of the techniques to synthesize such catalyst consists to obtain the solid by the co-precipitation method [1.43].

Using these two promising types of solids, Ni-Ce and Ni-Mg-Al based catalysts, we aim to understand and optimize the catalytic performances, notably trying to obtain an active, selective and stable performance at 600ºC, which is a temperature considerably lower than the common one (700-800ºC). The results are described in ***Chapter 2*** of this thesis.

1.7.2. Improvement of DRM by innovative process: periodic

As introduced in the ***Paragraph 1.6***, the technology of the reforming of CH_4 in periodic conditions has been developed in the last years. However one of the major challenges which remain to be solved is the total elimination of H_2O and CO_2 in the syngas stream using transition metals-based catalysts. In such context, the second objective of this thesis is to develop and understand the dry reforming in periodic conditions (P-DRM) in order to avoid those issues (***Paragraph 1.6.3***). Therefore, a process where the catalytic solid is exposed in alternative way and repeatedly to each of the reactants of the DRM (methane and carbon dioxide) is proposed. In a first step the solid reacts with methane to produce 1 mole of carbon monoxide and 2 moles of hydrogen. Then, in a second step, the reduced solid reacts with carbon dioxide to be reoxidized, recovering the oxygen lost in the first step. In addition, eventual residues of carbon react with CO_2 avoiding the deactivation of the catalyst. Although the process corresponds globally to the catalytic DRM, in practice the solid acts as an oxygen vector exposed to two independent gas-solid reactions. The principle of this concept consists to employ a solid with some particular properties:

1. It has to have storage and transfer capacity of oxygen
2. It has to activate methane and carbon dioxide
3. It has to, in the suitable working conditions, produce selectively synthesis gas avoiding the RWGS (***Eq. 1.4***) and the total oxidation (***Eq. 1.13***)

Eq. 1.15 $$CH_4 + Sol - O \rightarrow 2H_2 + CO + Sol - R$$

Sol-O = catalyst oxidized

Sol-R = catalyst reduced

Besides, formation of some other side products has to be limited, such as alkenes. In addition the formation of carbon should be desirably avoided. But it is not critical to the extent that the eventual carbon can be reoxidized by CO_2.

Eq. 1.16 $$CO_2 + C \rightarrow 2CO \qquad \Delta H° = 172 kJ/mol$$

4. The storage capacity of oxygen needs to be regenerated by CO_2 in the reoxidation step.

Eq. 1.17 $$CO_2 + Sol - R \rightarrow Sol - O + CO$$

The conditions 1 and 4 have to be assured by a reducible oxide. The condition 2 could be assured by the same oxide or also by another solid phase associated to the first one, for instance a supported metal on the reducible oxide. The condition 3 is mainly defined by the nature of the oxide and the working conditions. From one side, as the solid is regenerated in each cycle, the deactivation by carbon is avoided. From the other side, the hydrogen produced in the first step is never in contact with the carbon dioxide, avoiding the RGWS (***Eq. 1.4***).

We propose in this thesis to carry such reaction exposing the catalytic solid to several reduction-oxidation cycles (CH_4-CO_2). In practice, the experiments are done feeding one fix bed catalytic reactor periodically. This kind of method is one of the easiest ways of doing such process in the laboratory scale. Other possibilities exist, notably in the industrial scale, using a circulated fluidized catalytic bed (***Paragraph 1.4***) which allows optimizing each of the steps. On the contrary, the two steps have to be set at the same temperature in the system used in the laboratory. Another limitation comes from the analytical tool. The mass spectrometer (MS) used to analyze the outlet flow imposes to work with relative low concentrations of the reactants (typically between 5 and 25% in a quantitative way). However, the concept proposed in this thesis would work with pure flow of gases (100% CH_4 in the reductant step and 100%CO_2 in the oxidant one).

The first step of such study consists in determining the potential constituents of solids based on reactivity but also, and mainly, on thermodynamics regarding the feasibility of the oxidation and reduction by CO_2 and CH_4 respectively. Such study is described in ***Chapter 3***. Then, a complete study on the feasibility of the periodic process which comprises an understanding of the activity, selectivity and stability of different solids is presented in the ***Chapter 4***. In principle, the concept of the periodic dry reforming can be extended to other systems which have an economical and societal interest. Biogas is also an important feedstock that could be valorized by reforming processes, especially as the composition consists in a mixture of CH_4 and CO_2. The main drawback would be the need to separate the two components. It is nevertheless conceivable to use a flow of CH_4 with some CO_2 (60-80% and 20-40% respectively) in the first reaction step while still maintaining the contribution of RWGS low and without losing the advantages of reoxidizing the eventual carbon deposit in the second step. In addition this

process is also explored working with ethane instead of methane. Therefore, eventually mixtures of alkanes could also be considered (e.g. shale gas which contains typically 80-100% CH_4 and 0-20% C_2H_6). Thus, preliminary results obtained for biogas and ethane compositions are also presented at the end of the ***Chapter 4 (4.5-4.6)***. Finally, a first approach on the dynamics and apparent kinetics of the periodic process is studied in the ***Chapter 5***.

1.8. References

[1.1] D.P. van Vuuren, M. Kok, P.L. Lucas, A.G. Prins, R. Alkemade, M. van der Berg, L. Bouwman, S. van der Esch, M. Jeuken, T. Kram, E. Stehfest, Pathways to achieve a set of ambitious global sustainability objectives by 2050: Explorations using the IMAGE integrated assessment model, *Technol. Forecast. Soc. Change* 98 **(2015)** 303-323

[1.2] A. Ajanovic, Renewable fuels – A comparative assessment from economic, energetic, and ecological point-of-view up to 2050 in EU-countries, *Renew. Energ.* 60 **(2015)** 733-738

[1.3] R.L. Shrivastava, S.P. Untawale, Solar energy: Review of potential green & clean energy for coastal and offshore applications, *Aquat. Procedia* 4 **(2015)** 473-480

[1.4] F. Bilgili, I. Ozturk, Biomass energy and economic growth nexus in G7 countries: Evidence from dynamic panel data, *Renew. Sust. Energ.* 49 **(2015)** 132-138

[1.5] J. Schallenberg-Rodriguez, A methodological review to estimate techno-economical wind energy production, *Renew. Sust. Energ.* 21 **(2013)** 272-287

[1.6] M. Masai, H. Kado, A. Miyake, S. Nishiyama, S. Tsuruya, Methane reforming by carbon dioxide and steam over supported Pd, Pt and Rh catalysts *Stud. Surf. Sci. Catal.* 36 **(1988)** 67-71.

[1.7] J.H. Edwards, R.J. Tyler, The production of liquid fuels via the catalytic oxidative coupling of methane *Stud. Surf. Sci. Catal.* 36 **(1988)** 395-401.

[1.8] S.D. Angeli, G. Monteleone, A. Giaconia, A.A. Lemonidou, State-of-the-art catalysts for CH_4 steam reforming at low temperature *Int. J. Hydrogen Energ.* 39 **(2014)** 1979-1997.

[1.9] M. Nawfal, C. Gennequin, M. Labaki, B. Nsouli, A. Aboukaïs, E. Abi-Aad, Hydrogen production by methane steam reforming over Ru supported on Ni-Mg-Al mixed oxides prepared via hydrotalcite route *Int. J. Hydrogen Energ.* 40 **(2015)** 1269-1277

[1.10] S.A. Bhat, J. Sadhukhan, Process intensification aspects for steam methane reforming: an overview *AIChE J.* 55 **(2009)** 408-422.

[1.11] B.C. Enger, R. Lodeng, A. Holmen, A review of catalytic partial oxidation of methane to synthesis gas with emphasis on reaction mechanism over transition metal catalyst *Appl. Catal A Gen.* 346 **(2008)** 1-27.

[1.12] A. Scarabello, D.D. Nogare, P. Canu, R. Lanza, Partial oxidation of methane on Rh/ZrO2 and Rh/Ce-ZrO2 on monoliths: Catalyst restructuring at reaction conditions *Appl. Catal. B.* 174-175 **(2015)** 308-322.

[1.13] X. Hu, Q. Yu, N. Sun, Q. Qin, Experimental study of flammability limits of oxy-methane mixture and calculation based on thermal theory *Int. J. Hydrogen* 39 **(2014)** 9527-9533.

[1.14] M.C.J. Bradford, M.A. Vannice CO_2 reforming of CH_4. *Cat Rev – Sci Eng* 41 **(1999)** 1-42

[1.15] J. Yang, W. Ma, D. Chen, A. Holmen, B.H. Davis, Fischer-Tropsch synthesis: A review of the effect of CO conversion on methane selectivity *Appl. Catal A* 470 **(2014)** 250-260

[1.16] M.J. Donnelly, C.N. Satterfield, Product distributions of the Fischer-Tropsch synthesis on precipitated iron catalysts *Appl. Catal.* 52 **(1989)** 93-114

[1.17] S.H. Lima, A.M.S. Forrester, L.A. Palacio, A.C. Faro Jr., Niobia-alumina as methanol dehydration component in mixed catalyst systems for dimethyl ether production from syngas *Appl. Catal A* 488 **(2014)** 19-27

[1.18] D.H. Kim, S.W. Han, H.S. Yoon, Y.D. Kim, Reverse water gas shift reaction catalyzed by Fe nanoparticles with high catalytic activity and stability *J. Ind. Eng. Chem.* 23 **(2015)** 67-71

[1.19] D. Pakhare, J. Spivey, A review of dry (CO_2) reforming of methane over noble metal catalysts *Chem. Soc. Rev.* 3 **(2014)** 7813.

[1.20] A.M. Amin, E. Croiset, W. Epling, Review of methane catalytic cracking for hydrogen production *Int. J. Hydrogen* 36 **(2011)** 2904-2935.

[1.21] P. Lahijani, Z.A. Zainal, M. Mohammadi, A.R. Mohamed, Conversion of the greenhouse gas CO_2 to the fuel gas CO via the Boudouard reaction: A review *Renew. Sust. Energ.* 41 **(2015)** 615-632.

[1.22] L.A. Gould, L.B. Evans, H. Kurihara, Optimal control of fluid catalytic cracking processes *Automatica* 6 **(1970)** 695-703.

[1.23] A. Corma, L. Sauvanaud, FCC testing at bench scale: New units, new processes, new feeds *Catal. Today* 218-219 **(2013)** 107-114.

[1.24] J. Adanez, A. Abad, F. Garcia-Labiano, P. Gayan, L.F. de Diego, Progress in chemical-looping combustion and reforming technologies *Prog. Energ. Combust.* 38 **(2012)** 215-282.

[1.25] M.M. Hossain, H.I. de Lasa, Chemical-looping combustion (CLC) for inherent CO2 separations--a review *Chem. Eng. Sci.* 63 **(2008)** 4433-4451.

[1.26] R.M. Contractor, H.S. Horowitz, G.M. Sisler, E.Bordes, The effects of steam on n-butane oxidation over VPO as studied in a riser reactor *Catal. Today* 37 **(1997)** 51-57.

[1.27] J.R. Fernandez, A.Vega, F.V. Diez, Partial oxidation of n-butane to maleic anhydride over VPO in a simulated circulating fluidized bed reactor *Appl. Catal A* 376 **(2010)** 76-82.

[1.28] Tang M, Xu L, Fan M. Progress in oxygen carrier development of methane-based chemical-looping reforming: A review. *Appl Energ.* 151 **(2015)** 143–156

[1.29] V. Galvita, K. Sundmacher, Hydrogen production from methane by steam reforming in a periodically operated two-layer catalytic reactor *Appl. Catal. A* 289 **(2005)** 121–127

[1.30] X. Zhu, Y. Wei, H. Wang, K. Li, Ce-Fe oxygen carriers for chemical-looping steam methane reforming. *Int. J. Hydrogen Energ.* 38 **(2013)** 4492–4501

[1.31] X. Zhu, K. Li, Y. Wei, H. Wang, L. Sun, Chemical-looping steam methane reforming over a CeO_2-Fe_2O_3 oxygen carrier: Evolution of its structure and reducibility *Energy fuels* 28 **(2014)** 754–760

[1.32] D.H. Lee, K.S. Cha, H.S. Kim, C.S. Park, Y.H. Kim, Syngas and hydrogen production via stepwise methane reforming over Cu-ferrite/YSZ. *Int. J. Energy Res.* 38 **(2014)** 1522–30

[1.33] H. Ay, D. Üner, Dry reforming of methane over CeO_2 supported Ni, Co and Ni-Co catalysts *Appl. Catal. B.* 179 **(2015)** 128–138

[1.34] J. Chen, C. Yao, Y. Zhao, P. Jia, Synthesis gas production from dry reforming of methane over $Ce_{0.75}Zr_{0.25}O_2$-supported Ru catalysts *Int. J. Hydrogen* 35 **(2010)** 1630-1642

[1.35] M. Wisniewski, A. Boréave, P. Gélin, Catalytic CO_2 reforming of methane over $Ir/Ce_{0.9}Gd_{0.1}O_{2-x}$ *Catal. Commun.* 6 **(2010)** 596-600

[1.36] C. Liu, J. Ye, J. Jiang, Y. Pan, Progresses in the preparation of coke resistant Ni-based catalyst for steam and CO_2 reforming of methane *ChemCatChem* 3 **(2011)** 529-541

[1.37] R. Benrabaa, A. Löfberg, J. Guerrero Caballero, E. Bordes-Richard, A. Rubbens, R. N. Vannier, H. Boukhlour, A. Barama, Sol-gel synthesis and characterization of silica supported nickel ferrite catalysts for dry reforming of methane *Catal. Commun.* 58 **(2015)** 127-131

[1.38] J.H. Kim, D.J. Suh, T.J. Park, K.L. Kim, Effect of metal particle size on coking during CO_2 reforming of CH_4 over Ni-alumina aerogel catalysts *Appl. Catal. A* 197 **(2000)** 191-200

[1.39] J. Juan-Juan, M.C. Román-Martínez, M.J. Illán-Gómez, Effect of potassium content in the activity of K-promoted Ni/Al_2O_3 catalysts for the dry reforming of methane *Appl. Catal. A* 301 **(2006)** 9–15

[1.40] M. Muraleedharan-Nair, S. Kaliaguine, F. Kleitz, Nanocast $LaNiO_3$ perovskites as precursors for the preparation of coke-resistant dry reforming catalysts *ACS Catalysis* 4 **(2014)** 3837-3846

[1.41] M. Yu, K. Zhu, Z. Liu, H. Xiao, W. Deng, X. Zhou, Carbon dioxide reforming of methane over promoted $Ni_xMg_{1-x}O$ (111) platelet catalyst derived from solvothermal synthesis *Appl. Catal. B* 148-149 **(2014)** 177-190

[1.42] V.M. Gonzalez-DelaCruz, J.P. Holgado, R. Pereñíguez, A. Caballero, Morphology changes induced by strong metal-support interaction on a Ni-ceria catalytic system *J. Catal.* 257 **(2008)** 307-314

[1.43] W. Fang, C. Pirez, S. Paul, M. Capron, H. Jobic, F. Dumeignil, L. Jalowiecki-Duhamel, Room temperature hydrogen production from ethanol over $CeNi_xH_zO_y$ nano-oxyhydride catalysts *ChemCatChem* 5 **(2013)** 2207

[1.44] W. Fang, S. Paul, M. Capron, A.V. Biradar, S.B. Umbarkar, M.K. Dongare, F. Dumeignil, L. Jalowiecki-Duhamel, Highly loaded well dispersed stable Ni species in $Ni_xMg_2AlO_y$ nanocomposites: Application to hydrogen production from bioethanol *Appl. Catal. B* 166-167 **(2015)** 485-496

[1.45] L. Xu, H. Song, L.Chou, Mesoporous nanocrystalline ceria-zirconia solid solutions supported nickel based catalysts for CO_2 reforming of CH_4 *Int. J. Hydrogen* 37 **(2012)** 18001-18020

[1.46] D.L. Trimm, Catalysts for the control of coking during steam reforming *Catal. Today* 49 **(1999)** 3-10

[1.47] D.L. Trimm, Thermal stability of catalyst supports *Stud. Surf. Sci. Catal.* 68 **(1991)** 29

[1.48] K.H. Kim, The reaction of CO_2 with CH_4 to synthesize H_2 and CO over nickel-loaded Y-zeolites *Catal. Lett.* 28 **(1994)** 41-52

[1.49] F. Cavani, F. Trifiro, A. Vaccari, The reaction of CO_2 with CH_4 to synthesize H_2 and CO over nickel-loaded Y-zeolites *Catal. Lett.* 28 **(1994)** 41-52

[1.50] F. Basile, P. Benito, G. Fornasari, A. Vaccari, Hydrotalcite-type precursors of active catalysts for hydrogen production *Appl. Clay Sci.* 48 **(2010)** 250-259

[1.51] T. Odedairo, J. Chen, Z. Zhonghua, Metal-support interface of a novel $Ni-CeO_2$ catalyst for dry reforming of methane *Catal. Commun.* 31 **(2013)** 25-31

[1.52] H.S. Roh, H.S. Potdar, K.W. Jun, Carbon dioxide reforming of methane over co-precipitated $Ni-CeO_2$, $Ni-ZrO_2$ and $Ni-Ce-ZrO_2$ catalysts *Catal. Today* 93-95 **(2004)** 39-44

[1.53] B. Moghtaderi, Review of the recent chemical looping process developments for novel energy and fuel applications *Energ. Fuel* 26 **(2012)** 15-40

[1.54] S. Bhavsar, G. Veser, Chemical looping beyond combustion: production of synthesis gas via chemical looping partial oxidation of methane *RSC Advances* 4 **(2014)** 47254-47267

[1.55] L. Neal, A. Shafiefarhood, F. Li, Effect of core and shell compositions on MeOx@LaySr1-yFeO3 core-shell redox catalysts for chemical looping reforming of methane *Appl. Energ.* 157 **(2015)** 391-398

[1.56] S. Assabumrungrat, S. Charoenseri, N. Laosiripojana, W. Kiatkittipong, P. Praserthdam, Effect of oxygen addition on catalytic performance of Ni/SiO_2-MgO toward carbon dioxide reforming of methane under periodic operation *Int. J. Hydrogen* 34 **(2009)** 6211–6220

[1.57] S. Bhavsar, M. Najera, G. Veser, Chemical looping dry reforming as novel, intensified process for CO_2 activation *Chem. Eng. Technol.* 35 **(2012)** 1281–1290

[1.58] S. Bhavsar, M. Najera, R. Solunke, G. Veser, Chemical looping: To combustion and beyond *Catal. Today* 228 **(2014)** 96–105

[1.59] S. Bhavsar, G. Veser, Reducible supports for Ni-based oxygen carriers in chemical looping combustion *Energ. Fuel* 27 **(2013)** 2073–2084

[1.60] K. Otsuka, Y. Wang, E. Sunada, I. Yamanaka, Direct partial oxidation of methane to synthesis gas by cerium oxide *J. Catal.* 175 **(1998)** 152-160

[1.61] L.S. Fan, L. Zeng, S. Luo, Chemical-looping technology platform *AIChE.* 61 **(2015)** 1

[1.62] S. Li, J. Gong, Strategies for improving the performance and stability of Ni-based catalysts for reforming reactions *Chem Soc Rev.* 43 **(2014)** 7245

[1.63] D. Archer, Fate of fossil fuel CO_2 in geologic time *J. Geophys. Res.* 110 **(2005)** C09S05 ***doi:****10.1029/2004JC002625*

[1.64] EPA, United States Environmental Protection Agency. Overview of Greenhouse Gases. Methane. *http://epa.gov/climatechange/ghgemissions/gases/ch4.html* Last viewed: **26th July 2015**

[1.65] EPA, United States Environmental Protection Agency. Global greenhouse gas emissions data. *http://www.epa.gov/climatechange/ghgemissions/global.html* Last viewed: **26th July 2015**

[1.66] H. Liu, C. Guan, X. Li, L. Cheng, J. Zhao, N. Xue, W. Ding, The key points of highly stable catalysts for methane reforming with carbon dioxide *ChemCatChem. Geophys. Res.* 110 **(2005)** C09S05 ***doi:****10.1029/2004JC002625*

[1.67] J.W. Thybaut, G.B. Marin, C. Mirodatos, Y. Schuurman, A.C. van Veen, V.A. Sadykov, H. Pennemann, R. Bellinghausen, L. Mleczko, A novel technology for natural gas conversion by means of integrated oxidative coupling and dry reforming of methane, *Chem. Ing. Tech.* 86 **(2014)** 1855-1870.

CHAPTER II:
Dry reforming of methane on Ni-based catalysts

2. DRY REFORMING OF METHANE ON Ni-BASED CATALYSTS

2.1. Introduction

The dry reforming of methane was investigated in the classical way, cofeeding CH_4 and CO_2, as mentioned in the introduction of the thesis (***Paragraph 1.7.1***).

Eq. 2.1 $\mathrm{CH_4 + CO_2 \rightarrow 2H_2 + 2CO}$ $\Delta H° = 247 kJ/mol$

Using CO_2 and CH_4 as reactants, gases largely involved in the global warming, is attractive in the approach of getting green processes [1.19]. To this purpose, Ni based catalysts are very good candidates [1.36, 1.62]. The CH_4 dry reforming activity and the H_2/CO formation is studied over different types of Ni-based composites. Concretely, DRM has been studied on M-Ce-O catalysts (M = Ni, Co and Fe) and Ni-Mg-Al-O based catalysts, the influence of different parameters has been analyzed. The catalysts were successfully prepared by wetness impregnation and coprecipitation method. The influence of different parameters was studied, such as the reaction temperature (600°C-800°C), the nature of the metal, the amount of catalyst, the dilution of the catalyst with SiC, the nature of the precursors, the synthesis method, the influence of the pretreatment under H_2 and the nickel loading. The catalysts were characterized to find correlations between catalytic activity and physico-chemical properties. The outlet gases were analyzed online by a mass spectrometer (MS). The catalytic performance (10-200mg) was conducted under the atmospheric pressure in a fixed-bed quartz reactor fitted in a programmable oven.

2.2. M-Ce-O based catalysts

2.2.1. Catalysts preparation

The catalysts used for the cofeed experiments are named as follows M(*p*)/CeO_2, $CeNi_xO_y$, $Ni_xMg_2AlO_y$ (where M = Ni, Co or Fe; *p* corresponds to the M loading and *x* corresponds to the molar ratio of Ni) were synthesized by impregnation and coprecipitation techniques. In this paragraph the impregnation of the metal on a precipitated ceria is explained in detail as an example.

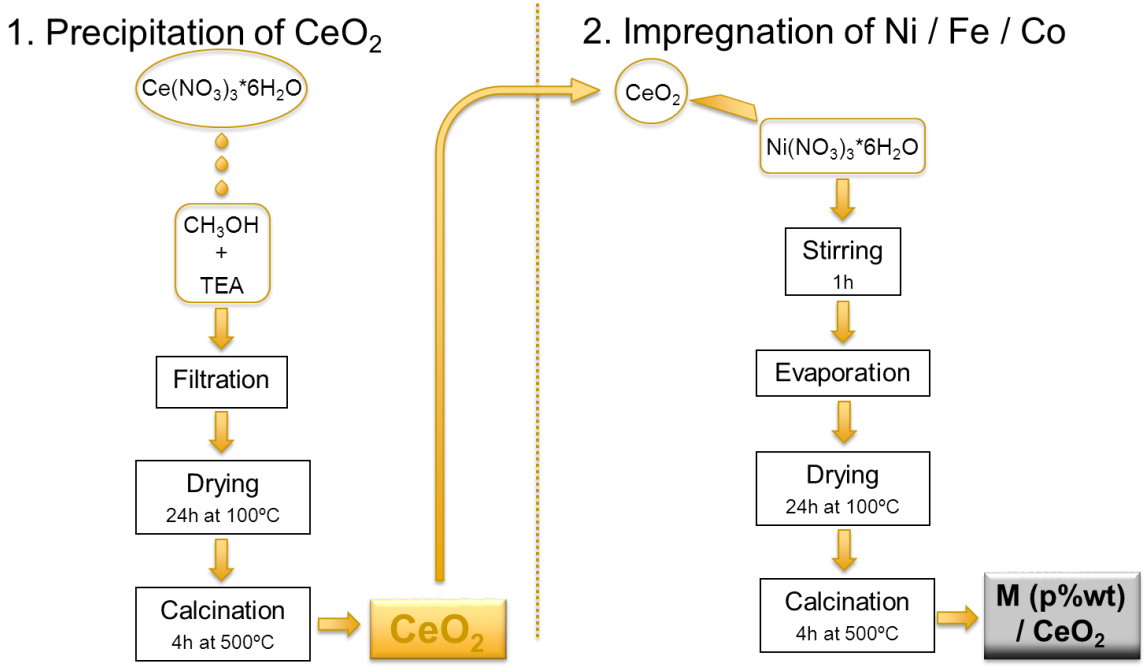

Fig 2.1 Scheme of the catalyst preparation by the wetness impregnation

Firstly, ceria oxide was prepared using triethylamine (TEA) $(C_2H_5)_3N$, (Sigma-Aldrich, ≥99.5% assay) as the precipitant agent. As an example, 21.9g of cerium (III) nitrate hexahydrate $CeN_3O_9.6H_2O$ (Fluka, > 99% assay) were dissolved into 0.1L of distilled H_2O. Separately, 0.1L of methanol CH_3OH (sigma-aldrich, ≥ 99.8% assay) as the media agent, was mixed with 0.0278L of TEA. The solution of cerium nitrate hexahydrate was added slowly (around 1drop/s) into the solution of methanol and TEA, which was mixed under vigorous stirring. The mixing was kept during 2 hours more for aging once the addition was completed. The obtained solid was washed twice with distilled water and methanol. The final product was filtered under vacuum and dried during 24h at 100°C. Finally, the solid was calcined at 500°C during 4 hours in air with a heating ramp of 5°C/min.

Secondly, the metal was loaded onto the home-made ceria by the wet impregnation method. 0.44g of $Ni(NO_3)_2 \cdot 6H_2O$ (sigma-aldrich, ≥98.5%) were dissolved in 20mL of distilled H_2O for a loading of 9.5 wt.% of Ni. Then 1g of ceria was added to the solution. The mixture was stirred during 1h for aging. Afterwards, the water was evaporated at 60-70°C in order to get as much as possible a homogenous solid. Later, the solid was removed from the beaker and dried in an oven during 1h at 100°C. Finally, the catalyst was treated by calcination at 500°C during 4h in air with the heating ramp of 5°C/min. The same procedure was followed to synthesize the catalysts with Co and Fe using as precursors $Co(NO_3)_2 \cdot 6H_2O$ (sigma-aldrich, ≥99%) and $Fe(NO_3)_3 \cdot 9H_2O$ (sigma-aldrich, ≥99%) respectively.

Otherwise the solids were also synthesized by the coprecipitation method. Specifically, well-mixed $CeNi_xO_y$ catalysts were prepared following a procedure developed in our laboratory. All

the specifications about the preparation are well explained in the following reference [1.43]. The solids were calcined in air at 500 °C.

2.2.2. Catalysts characterization

Different physico-chemical characterizations have been performed and are discussed in order to find correlations between catalytic activity and catalysts properties.

The crystalline phases of the catalysts were measured by X-ray diffraction (XRD) using a Bruker D8 Advance X-ray diffractometer equipped with a fast detector type LynxEye with a copper anticathode. The analysis was made in the θ domain (20-90º) with a step of 0.02º and time integration of 0.3s. The mean crystallite size of CeO_2, NiO, CoO, Ni^0 and Co^0 were estimated from the XRD patterns by Scherrer equation.

N_2 physisorption at 77 ºK data were collected on a multipoint and monopoint equipment to obtain the surface area of the different catalysts before and after test.

The metal loadings for all the catalysts were analyzed by X-ray fluorescence (XRF) or inductively coupled plasma (ICP) techniques.

The behavior under H_2 of these catalysts was also studied by TPR on a Micromeritics Autochem II Chemisorption analyzer, the H_2 consumed was analyzed by a TCD detector. 25mg of sample was treated under a flow rate of 50 mL/min (5% H_2/N_2). The temperature was increased at a rate of 10ºC/min up to 900ºC.

Table 2.1 Ni loading, surface area and main crystallite size of the different catalysts

		Atomic ratio			
Catalyst	% M	Ni / M_T	S_{BET} (m^2/g)	d_{M-O} (nm)	d_{CeO2} (nm)
Co (7.2) / CeO_2	7.2	0.19	28	16	10
Fe(10.4) / CeO_2	10.4	0.26	73	n.o.	10
Ni (8.8) / CeO_2	8.8	0.22	29	16	11
Ni(9.5) / CeO_2	9.5	0.24	32	18	10
Ni (10.5) / CeO_2	10.5	0.26	35	n.a.	n.a.
Ni (7.9) / CeO_2[a]	7.9	0.20	9	n.o.	38
$CeNi_{0.3}Oy$	7.9	0.23	79	n.o.	5
$CeNi_{0.5}Oy$	12 (n.a.)	n.a.	96	n.a.	n.a.
$CeNi_{0.6}Oy$	15 (n.a.)	n.a.	96	n.a.	n.a.
$CeNi_{0.8}Oy$	19 (n.a.)	n.a.	77	n.a.	n.a.
$CeNi_1Oy$	24.0	0.50	119	11	4

[a] commercial CeO_2 (Sigma-Aldrich), n.a. = not analyzed, n.o. = not observed

Table above is summarizing the main properties of the M-Ce-O catalysts. The first 5 were prepared by precipitation of CeO_2 and impregnation of the metal. The sixth was made by impregnation of Ni on a commercial CeO_2 provided by Sigma-Aldrich and the last 5 were synthesized by the coprecipitation technique.

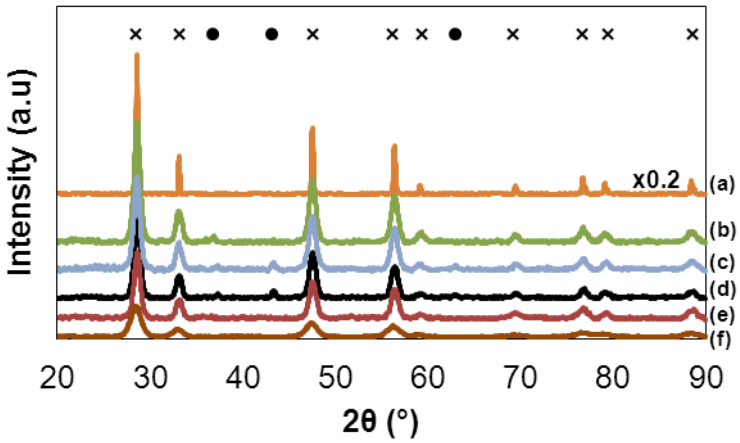

Fig 2.2 XRD patterns for (a) Ni(7.9)/CeO_2(com), (b) Co(7.2)/CeO_2, (c) Ni(8.8)/CeO_2, (d) Ni(9.5)/CeO_2, (e) Fe(10.4)/CeO_2, (f) $CeNi_{0.3}O_y$ x CeO_2, ● NiO and CoO

The X-ray diffraction patterns of the Ni(7.9)/CeO_2(com), Co(7.2)/CeO_2, Ni(8.8)/CeO_2, Ni(9.5)/CeO_2, Fe(10.4)/CeO_2 and $CeNi_{0.3}O_y$ catalysts are shown in ***Fig 2.2*** evidencing characteristic fluorite structure of CeO_2 in all the cases. However, the XRD analysis of Ni(7.9)/CeO_2(com) shows narrower and much higher peaks than the XRD using the home-made ceria. Crystals of the commercial CeO_2 seems to be better defined and crystallized than the one prepared in the laboratory. Otherwise they are 4 times bigger than the ones obtained by the home-made CeO_2 (38nm instead of 10nm). In addition the surface area of the catalyst using CeO_2 from Sigma-Aldrich is 3-4 times lower than the one obtained with the other impregnated ceria (9 m^2/g instead of 29-32 m^2/g). Furthermore, the reproducibility of this method is checked comparing the properties of the Ni(8.8)/CeO_2 and Ni(9.5)/CeO_2, which shows almost an identical XRD pattern, crystal size and surface area.

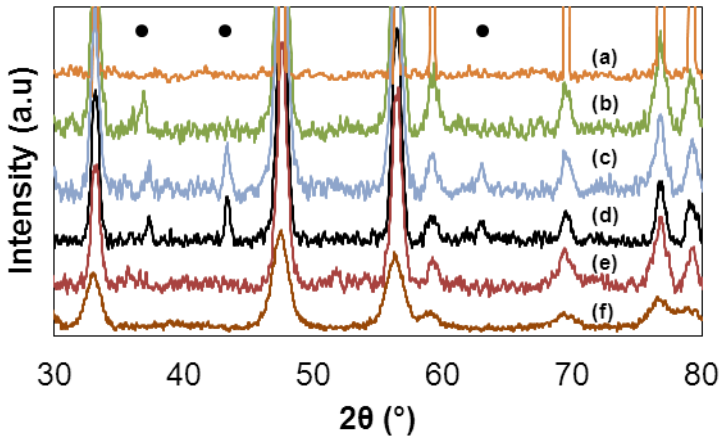

Fig 2.3 Zoom on the XRD patterns

The ***Fig 2.3*** shows a zoom of the XRD patterns in order to distinguish the peaks of the corresponding oxides, CoO (36.8º) and NiO (36.8, 43.2 and 63.1º). Iron oxide for Fe(10.4)/CeO_2 and nickel oxide for Ni(7.9)/CeO_2(com) and $CeNi_{0.3}O_y$ do not appear in the corresponding XRD analysis. Three potential causes could explain the reason, the M related

phase is in an amorphous state, the particles are too small to be detected (the detection limit of the XRD is around 2nm), i.e. the metal oxide is too well-dispersed on CeO_2 to be seen, or a solid solution of cerium and nickel is obtained (as already reported in the literature for the $CeNi_XO_y$ coprecipitated compounds [1.43]). In such case, strong interactions are obtained between Ni and Ce cations inside the solid. Besides, all the studied catalysts correspond to nanomaterials with small average particles size for CeO_2 and/or Ni-Ce-O (5-10nm), NiO (11-18nm) and CoO (16nm), as shown in ***Table 2.1***.

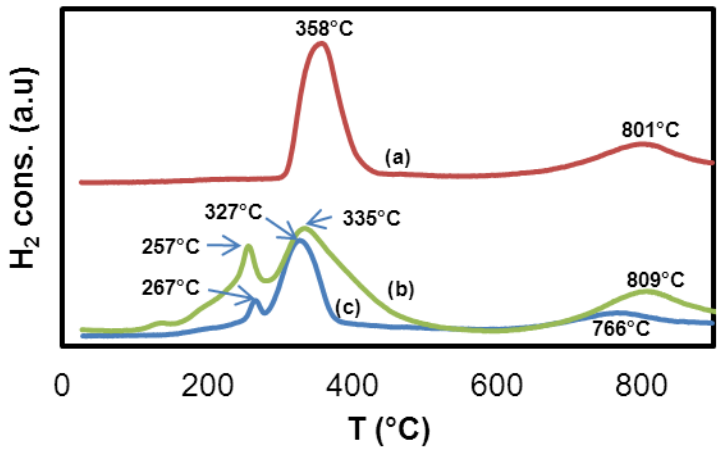

Fig 2.4 TPR profile of (a) Ni(7.9)/CeO_2(com), (b) $CeNi_{0.3}O_y$, (c) Ni(9.5)/CeO_2 under 10% H_2 / N_2 gas

The temperature programmed reduction (TPR) shows for Ni(9.5)/CeO_2 catalyst two peaks at 267ºC and 327ºC, which are related to the reduction of nickel species, and one at 766ºC, related to the reduction of CeO_2. Moreover, the Ni(7.9)/CeO_2(com) catalyst shows only one peak for the reduction of nickel species at 358ºC and a second one at 801ºC for the reduction of CeO_2. Somehow Ni(9.5)/CeO_2 is easier to reduce (hydrogen consumption starts around 150°C) than Ni(7.9)/CeO_2(com). Some researchers relate the first peak at 257-267°C to the Ni species in solid solution or/and to small crystal size of NiO [1.43]. In addition, Ni(9.5)/CeO_2 has 4 times more surface area than Ni(7.9)/CeO_2(com). Therefore Ni would be better dispersed than using the catalyst with the commercial ceria. Some studies also relate the ease on the reduction when the metal is more dispersed onto the support [1.43]. The TPR of $CeNi_{0.3}O_y$ follows relatively the same trend as Ni(9.5)/CeO_2 evidencing a close behavior towards hydrogen from the two synthesis techniques, impregnation and coprecipitation. The fact of using a “home-made” ceria in the two cases seems to be one of the key points to obtain such behavior. Otherwise, the solid obtained by coprecipitation shows a higher consumption of hydrogen, which could mean that such solid is more reduced than the one obtained by impregnation, but a spillover of hydrogen is also possible, in particular, it has been shown that these solids are able to store hydrogen.

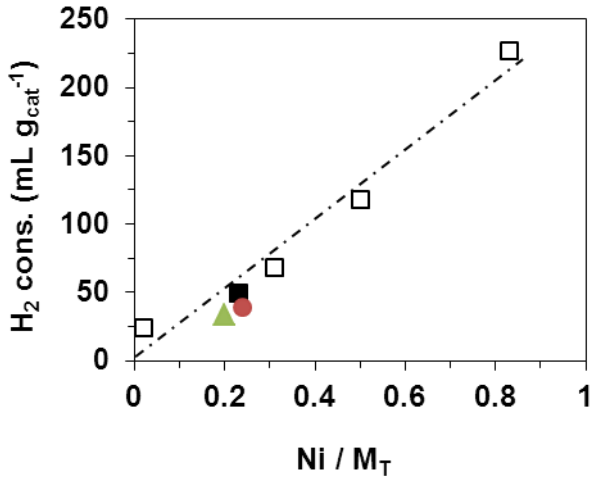

Fig 2.5 H_2 consumption in TPR as a function of the Ni content of (□) $CeNi_XO_Y$ nanocompounds (in black $CeNi_{0.3}O_y$) [1.43], (▲) Ni(7.9)/CeO_2(com) and (●) Ni(9.5)/CeO_2

A linear relationship appeared between the total H_2 consumption and the nickel content for catalysts synthesized by coprecipitation. This previous study made in the laboratory is a good reference to compare those values with the hydrogen consumed on Ni(7.9)/CeO_2(com) and Ni(9.5)/CeO_2. The two of them goes slightly lower than the coprecipitated one in agreement with specific properties of the $CeNi_xO_y$ catalysts and the existing strong Ni-Ce interaction.

2.2.3. Catalytic test

Influence on the nature of the metal (Ni, Co and Fe)

Three different low-cost metals were chosen for the study of the DRM. The noble metals show high activity, selectivity and stability towards carbon deposition but, due to their high cost and low availability, processes based on such compounds are not really competitive in comparison with the transition metals. In particular, period 4 d-block elements such as Ni, Co and Fe based catalysts are very good candidates thanks to their low cost, wide availability (industrial feasibility) and high activity towards the reactants [2.2-2.5], nonetheless the thermal stability is still difficult to solve at the operating conditions. Otherwise, CeO_2 also shows interesting properties for the DRM such as the resistance towards carbon deposition thanks to the redox behavior, as discussed in the ***Paragraph 1.7.1***. Thus, the influence on the nature of the metal was studied for Ni, Co and Fe supported on cerium oxide (CeO_2).

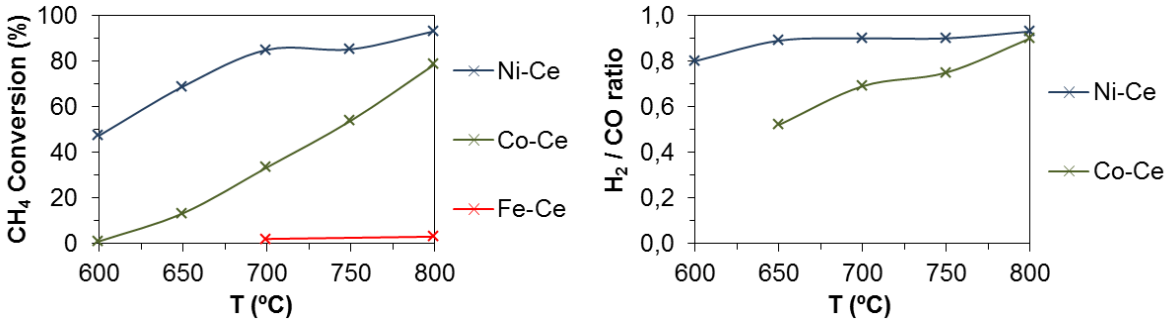

Fig 2.6 ***Left****. Catalytic activity on 200mg of Ni(9.5)/CeO_2, Co(7.2)/CeO_2, Fe(10.4)/CeO_2 at different reaction temperatures, $t_{exp.}$= 2h, CH_4/CO_2/He/Ar (vol%) = 5/5/10/80* ***Right****. Selectivity represented by H_2/CO ratio on Ni/CeO_2 and Co/CeO_2*

The ***Fig 2.6 (left)*** shows the results of the experiments working with the different transition metals. The formulation of Ni/CeO_2 gives the highest activity in the whole range of temperatures in its comparison with Fe and Co. However, there is a common behavior between Ni and Co in terms of activity. The conversion of CH_4 increases with the temperature, which is expected due to the endothermic reaction. Otherwise, there is a low activation on the Fe(10.4)/CeO_2, obtaining only 3% conversion of methane even at the high temperature of 800ºC. In detail, the conversion of CH_4 at 700ºC working with Ni is 85%, 33% for Co and 2% for Fe. Even if the activity of Ni is clearly higher than the one of Co, the selectivity towards the desired products is important to verify as some times the highest active catalyst does not mean the most selective one. Thereby the theoretical ratio of H_2/CO = 1 (***Eq. 2.1***) is taken as a reference. In fact, the high active Ni-catalyst is accompanied by the highest selectivity, obtaining in the whole range of temperatures a ratio between 0.8-0.9, as shown in ***Fig 2.6 (right)***. Otherwise, the selectivity on Co-catalyst decreases with the temperature, the only comparable H_2/CO ratio with Ni is at 800ºC. A discussion about the reasons of the no activation with Fe and the low activity with Co is discussed with the support of the characterization techniques after test (***Paragraph 2.2.4***).

This study was carried without any pretreatment on the solid in order to find out the activation of the catalysts towards the reaction mixture. Based on the results, Ni seems to be the easiest one to get active without any pretreatment within H_2. In addition, this metal shows the best selectivity and activity in the whole range of temperatures. Thus, Ni-Ce catalysts were chosen for further investigation on the DRM.

Optimizing the amount of catalyst

The high conversions obtained in the previous experiment with Ni(9.5)/CeO_2 catalyst without reaching 100% allowed to consider some thermodynamics limitations for DRM. Indeed, the conversions are quite close to such limitations (see ***Paragraph 3.3.1***). One hypothesis is that the amount of solid might be overestimated in the working conditions (needlessly wasting

catalyst). Accordingly, three experiments were carried using 100, 50 and 25mg looking after this optimization. The gas stream of $CH_4/CO_2/He/Ar$ (5/5/10/80%v) was then fed to the reactor (F_T = 100 mL / min).

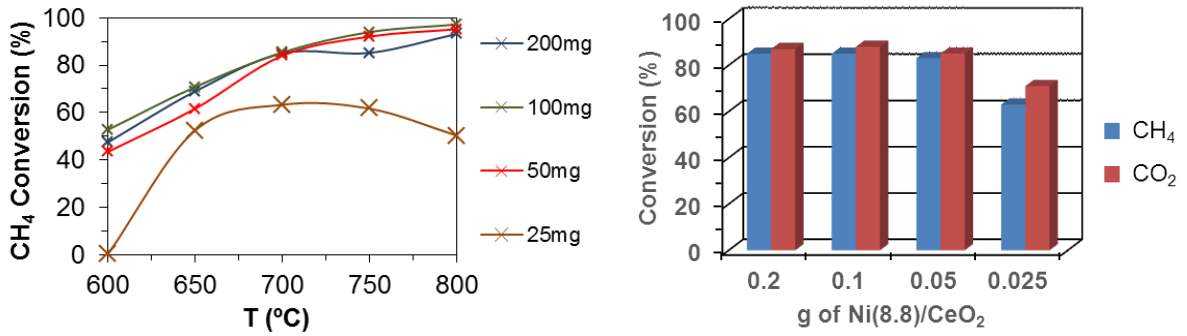

Fig 2.7 ***Left****. Catalytic activity on Ni(8.8)/CeO_2 at different amount of catalyst and reaction temperatures. $t_{exp.}$= 1.5h* ***Right****. Conversion of CH_4 and CO_2 at 700ºC using different amount of catalyst*

Conversions of CH_4 are almost identical using 200, 100 and 50mg in the whole range of temperatures (***Fig 2.7 (left)***). Indeed the amount of 200mg was overestimated. Otherwise, some differences are seen at 25mg, meaning that the catalyst itself gives lower performances as the expected ones. Some different characteristics could explain the low activity, like the relevance of pretreating the catalyst under H_2 when the active sites are not in excess and/or the length of the catalytic bed (around 1 mm) being easier the creation of preferential pathways, death volumes… Moreover, conversions of CH_4 and CO_2 at 700ºC are shown in more detail in the ***Fig 2.7 (right)*** to verify that the conversion of CO_2 follows the same behavior as the one of CH_4, obtaining almost the same one (in average 3% more conversion than CH_4) and decreasing in the same manner working with 25mg.

As a consequence of these results, the possibility of enhancing the performance at 25mg with a wider catalytic bed was raised. For such task, silicon carbide (SiC) is a typical diluent used for this kind of application.

Influence of SiC

Catalysts are commonly diluted with silicon carbide in an industrial application. This material shows inertness, high thermal and chemical stability, avoiding hot spots formation and improving the homogeneity of the catalytic bed (minimizing bypassing and death volumes). The 2700ºC melting point of this compound leads to maintain its physical structure and avoids attrition in extreme conditions [2.6]. The verification of the inertness towards the reaction concerned is important as some reactants could be activated by SiC. Therefore, a considerable amount of SiC in comparison with the one used in the experiments (1.5g instead of 0.075g, 20 times higher) with a particle size of 0.250mm was set into the reactor.

Table 2.2 Catalytic activity on 1.5g of SiC (0.250mm) at different T

T(ºC)	%CH_4	%CO_2
600	0.2	0.2
650	0.4	0.2
700	0.5	0.4
750	0.5	0.2
800	0.2	0.3

Negligible conversions between 0 and 0.5% were obtained in the whole range of temperature, as shown in the ***Table 2.2***. Thereby, SiC can work as a diluent without any significant perturbation from the reactivity point of view. Some advantages appear working with a diluent such as (i) obtaining a better homogenous catalytic bed, (ii) decrease the sintering of the particles, (iii) increase the residence time without changing the amount of catalyst... About this last advantage, there are two factors to take into account, from one side the molecule has more time to react through the catalytic bed, probably enhancing the conversion; but from the other side, consequently, the undesirable side reactions have also more time to occur. Besides, this characteristic allows varying the amount of catalyst without modifying the residence time. Thus, a catalytic bed of 100mg is taken as a reference. Some experiments were carried trying to improve the performance working with 25mg of catalyst and 75mg of SiC.

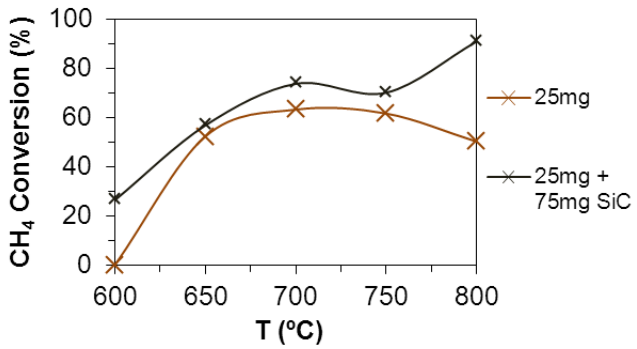

Fig 2.8 Catalytic activity on Ni(8.8)/CeO_2 with 25mg and 25mg+75mg SiC, CH_4/CO_2/He/Ar (vol%) = 5/5/10/80

Indeed, the performance is improved working with a total catalytic bed of 100mg. The results are quite interesting as a relative low mass of catalyst is used without the presence of a noble metal and without any *in-situ* pretreatment of the catalyst, even if low concentrations of reactants are involved.

As a consequence of all the experiments up to this point, the next step was focused on working at 600ºC for several reasons. The performances are quite optimized obtaining results really close to the thermodynamic limitations (see ***Paragraph 3.3.1***) at the high range of temperature (700-800ºC). Otherwise, the energy saving working at 600ºC instead of 800ºC is

another important factor to take into account. In addition, this condition would allow comparing and see differences between the catalysts easier than in the other range of temperatures.

Study at mild conditions (600°C)

Ni(7.9)/CeO_2(com)

The following experiments were carried using only 10mg of catalyst (+90mg SiC) at 600ºC to go further in the optimization "amount of catalyst-working temperature". In this case, a specific pretreatment under H_2 was carried. Concretely, a flow of 25% H_2 / Ar (F_T = 100 mL/min) at a specific temperature was fed through the catalytic bed overnight. Ni(7.9)/CeO_2(com) was synthesized using commercial CeO_2 (Sigma-Aldrich) and loading the Ni by the wet impregnation technique following the same procedure explained above (***Paragraph 2.2.1***). Based on other studies made in the laboratory [1.43] the temperature of the pretreatment under H_2 was set at 250ºC.

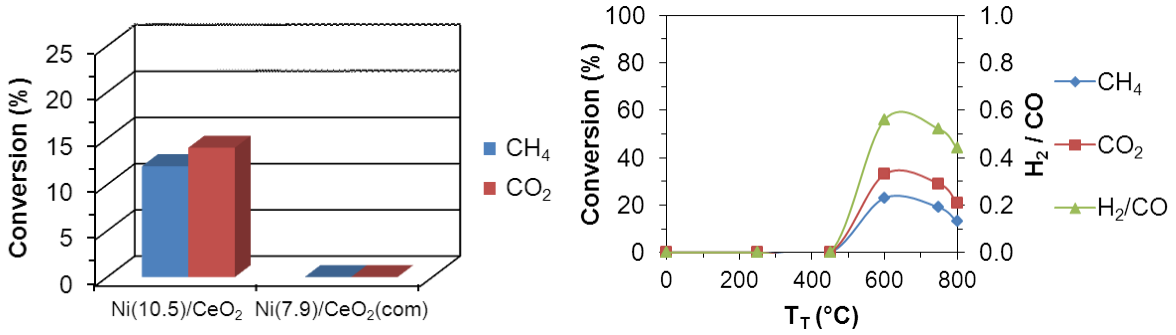

Fig 2.9 ***Left****. Catalytic activity on 10mg of Ni(10.5)/CeO_2 and Ni(7.9)/CeO_2(com) at 600ºC, $t_{exp.}$= 5h, T_T = 250ºC under H_2.* ***Right****. Catalytic activity on 10mg of Ni(7.9)/CeO_2(com) at 600ºC, $t_{exp.}$= 4h, using different T_T under H_2 (the point at zero is without pretreatment)*

The ***Fig 2.9 (left)*** shows the comparison between a catalyst using home-made ceria and the solid using the commercial one. In this first approach, Ni(7.9)/CeO_2(com) is not reactive at the working conditions. However, the pretreatment at 250ºC might be too low for the commercial catalyst. Indeed, Ni(7.9)/CeO_2(com) seems to be more difficult to reduce than impregnating the metal on the home-made ceria from the TPR analysis (***Paragraph 2.2.2)***. Therefore, a complete study was made on the commercial catalyst pretreating the solid in a wide range of temperatures (250, 450, 600, 750 and 800ºC), as shown in ***Fig 2.9 (right)***. The catalyst shows a considerable activity after pretreating the solid at 600ºC, obtaining 23 and 33% conversion of CH_4 and CO_2 respectively. Besides, the decrease on the conversion when the temperature of the pretreatment is higher than 600ºC is another effect to underline from this study. Notwithstanding, some specific remarks need to be made in these results.

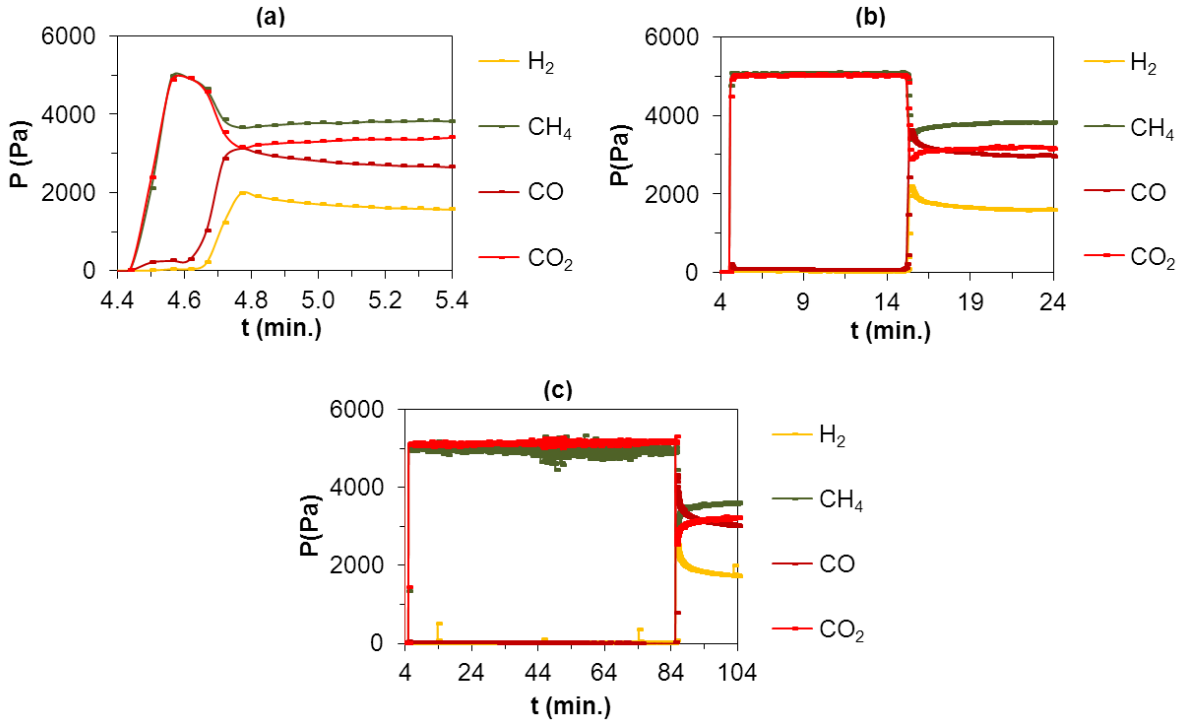

Fig 2.10 Partial pressures of the outlet gases working with 10mg of Ni(7.9)/CeO_2(com) at 600ºC on the initial stage of the experiment, CH_4/CO_2/He/Ar (vol%) = 5/5/10/80. (a) T_T = 800ºC, (b) $T_{T.}$ = 750ºC and (c) $T_{T.}$ = 600ºC under H_2

The activation process of these catalysts seems to be more complex than Ni(10.5)/CeO_2 which goes active after the H_2 treatment. Concretely, besides the corresponding pretreatment under H_2, the activity towards CH_4 and CO_2 appeared after a certain time of feeding the reactant mixture, as shown in the ***Fig 2.10***. The catalyst took around 80min to be active (***Fig 2.10 (c)***) after a pretreatment temperature of 600ºC. Nevertheless, the highest conversions are obtained after such time. Otherwise, the activation process is shorter at the pretreatment temperature of 750 and 800ºC (***Fig 2.10 (a and b)***), obtaining activity after 10 and 0.25 minutes respectively. Nonetheless, the final conversion is slightly lower than in the first case.

The pretreatment under H_2 does not seem to be enough for the proper activation of the catalyst. However some more time under the reactant mixture at 600ºC implies to get somewhat a benefit on the solid leading to the highest performance of this type of catalyst. Even though the conversions at such particular conditions are higher than using Ni(10.5)/CeO_2, a complete study on the temperature of pretreatment of this catalyst would be necessary for a more precise comparison (as the same way done for Ni(7.9)/CeO_2(com)) in order to be sure that the impregnation on the commercial ceria gives a higher performance than the one on the home-made CeO_2.

At this stage, there is a considerable range of improvement for these severe working conditions. Therefore another method was introduced to synthesize the solid, the coprecipitation technique.

$CeNi_xO_y$

The coprecipitation is a well-known method to synthesize catalysts. The main advantages attributed to this technique are the homogenous distribution of different metals in a mixed oxide, the high surface area and the strong interaction between the different metal cations. Typically, the well-dispersed metal and the high surface area allows working with higher loadings of metal than using the impregnation method, basically due to the enhancement for avoiding the sintering effect [2.7]. The same conditions of gas stream (CH_4/CO_2/He/Ar=5/5/10/80 %v) and total flow (F_T = 100 mL/min) was set. Different loadings of metal ($CeNi_{0.3}O_y$, $CeNi_{0.5}O_y$, $CeNi_{0.6}O_y$, $CeNi_{0.8}O_y$ and $CeNi_1O_y$) were prepared. First, $CeNi_{0.3}O_y$, which has the same loading of nickel (7.9 wt.%) as Ni(7.9)/CeO_2(com), was set into the reactor in order to compare the performances between the two catalysts. The first experiment with this solid was pretreated at 600ºC (temperature which gives the best performance for Ni(7.9)/CeO_2(com)).

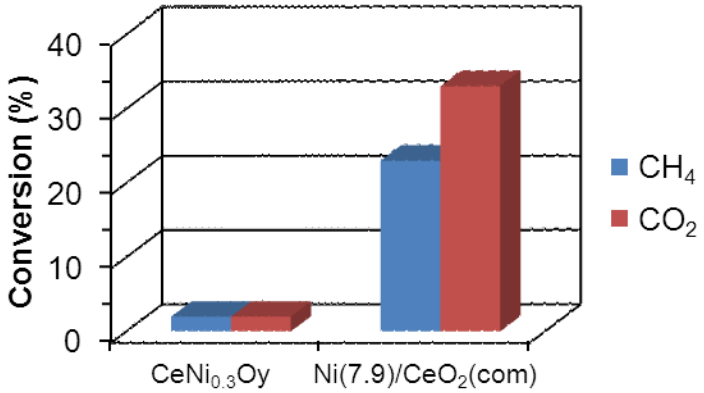

Fig 2.11 Catalytic activity on 10mg of Ni(7.9)/CeO_2(com) and $CeNi_{0.3}Oy$ at 600ºC, $t_{exp.}$= 5h, CH_4/CO_2/He/Ar (vol%) = 5/5/10/80 $T_{T.}$= 600ºC under H_2.

A low activity was reached (***Fig 2.11***) for the coprecipitated catalyst obtaining only 2% conversion of each reactant. Based on that, a complete study on the influence of the pretreatment temperature was made to verify if the catalyst is pretreated under the correct conditions. Experiments were performed after a pretreatment at 250°C, 270°C, 350°C, 450°C, 550°C and 600ºC.

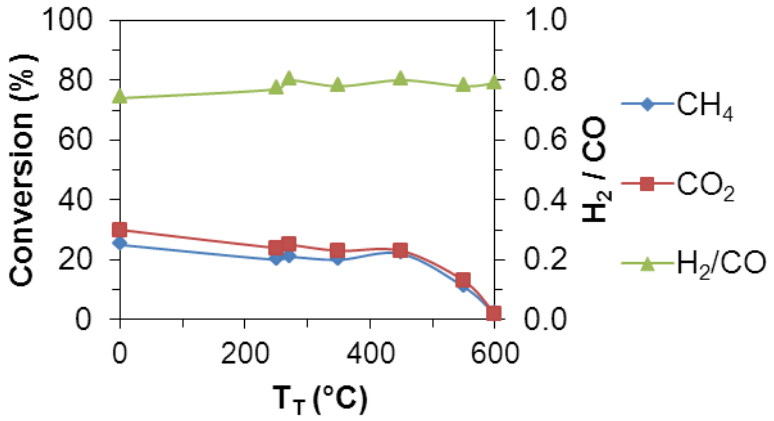

Fig 2.12 Catalytic activity on 10mg of $CeNi_{0.3}Oy$ at 600ºC, $t_{exp.}$= 5h, using different T_T under H_2 (the point at zero is without pretreatment)

The ***Fig 2.12*** shows an interesting effect of the pretreatment under H_2. Lower conversions are achieved pretreating the solid at high temperatures than doing it at low temperatures. This type of behavior leads to consider some hypothesis about the key factor on the activation. A "too" reduced catalyst is not as active as a partial reduced one. Another remarkable characteristic is that, in contrast of the Ni(7.9)/CeO_2(com), the catalyst is already active even without the pretreatment under H_2. The lower temperature which hydrogen starts to be consumed (see TPR) could support the ability of this solid to be active at low pretreatment temperatures. Nonetheless, the no activation of the Ni(7.9)/CeO_2(com) (see ***Fig 2.9***) until at least 600ºC is more difficult to explain from the reduction point of view since the peak for NiO is at 355ºC (see TPR). There is some controversial literature on this subject. V.M. Gonzalez-Delacruz et al. [2.18] also obtained a considerable activity without pretreating the Ni-Ce based catalyst and carrying the reaction at 750ºC. T. Odedairo et al. [1.51] set the temperature of pretreatment at 350ºC, which was enough to active the catalyst at their working conditions. Concretely, I. Luisetto et al. [2.2] reported activity after pretreatment of the catalyst at high temperatures (800°C), and decreasing the experimental temperature from 800ºC to 600ºC with 100mg of $CeNi_xO_y$ (7.5 wt.% Ni) catalyst and 20% initial concentration of the reactants. Maybe, the higher reaction temperature of 800ºC at the beginning of the experiment or even the 20% concentration of the reactants made it easier/faster the activation of their catalyst. In detail, D.K. Kim et al [2.19] proposed one interesting mechanism for this curious behavior. The reduction of their Ni-Ce catalyst at 600ºC under H_2 gives a lower performance than the catalyst pretreated under air (totally oxidized) at the reaction temperature of 600ºC. Based on those results and some experiments working with pulses of CH_4 and CO_2 separately, they related the catalytic activity in the absence of pretreatment to the reactivity of oxygen contained in the compound. Concretely, they proposed the key role of the interfacial oxygen in the Ni-Ce boundary (Ni-O-Ce site). This first interaction leads to the total oxidation of methane and to the creation of selective actives sites for the following reforming reaction towards H_2 and CO

because the unselective consumed oxygen in the Ni-Ce boundary cannot be reoxidized by CO_2.

A too high reduction of the solid seems to decrease the number of active sites for the reforming reaction. Probably there is a direct relationship between the two, without the first unselective and high active reaction, the formation of the actives sites for the selective one cannot be created, as so leading to almost negligible conversions at high pre-reduction temperatures under H_2.

The particular case of Ni(7.9)/CeO_2(com) needs further investigations. From one side the solid needs a much higher temperature (600ºC) to be active than the coprecipitated catalyst. The reason could be due to the nickel particles are more difficult to be reduced in the commercial catalyst (see TPR). Otherwise, the fast activation of Ni(7.9)/CeO_2(com) at 800ºC could be related to the easier migration of nickel at high temperatures. Thus, creating somewhat the high active site in the Ni-Ce boundary, which are partially reduced by H_2 to create the active and selective sites as described above. Finally, a treatment temperature higher than 600ºC leads to lower performances of the experiment. Thereby, the same theory about the decreasing on conversion at a given pretreatment temperature can be applied to the commercial catalyst, as the activity decrease pretreating the catalyst at 750ºC and 800ºC.

Leaving aside the discussion about the particular behavior of the solids towards hydrogen in the pretreatment step, this last study permits comparing strictly the coprecipitated catalyst with the impregnated on commercial CeO_2.

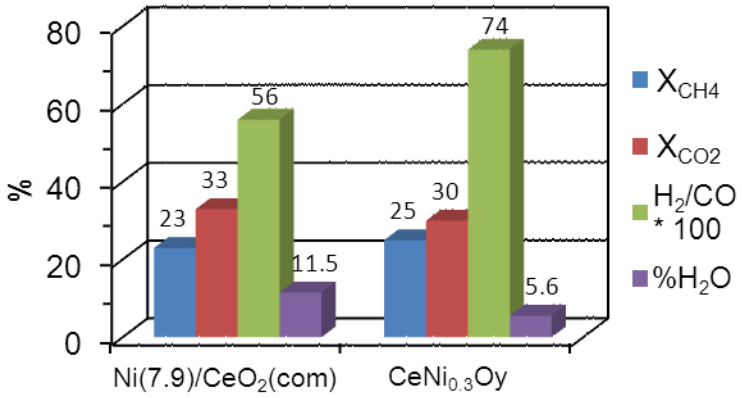

Fig 2.13 Catalytic activity on 10mg of Ni(7.9)/CeO_2(com) T_T = 600ºC under H_2 and $CeNi_{0.3}Oy$ without pretreatment, $t_{exp.}$= 5h, $T_{exp.}$ = 600ºC CH_4/CO_2/He/Ar (vol%) = 5/5/10/80

The ***Fig 2.13*** shows that in terms of conversion the two catalysts gives practically the same, 23% and 25% conversion of methane for the Ni(7.9)/CeO_2(com) and $CeNi_{0.3}Oy$ (which contains also 7.9 wt% Ni). The main differences between the two are (i) the easiest activation procedure for the coprecipitated solid leading to the highest activity even without pretreating the catalyst and (ii) the highest selectivity for $CeNi_{0.3}O_y$ (H_2/CO ratio of 0.74 instead of 0.56). This difference

is supported by the fact of obtaining lower amount of H_2O with $CeNi_{0.3}O_y$ (5.6%) than with Ni(7.9)/CeO_2(com) (11.5%).

Characterizations techniques need to be carried to understand this difference on selectivity. Nevertheless, some predictions can be made based on the crystal size of the mixed oxide (5nm) or commercial CeO_2 (38nm) before experiment (***Table 2.1***). Maybe, the crystal size of $CeNi_{0.3}O_y$ remains smaller than the one of Ni(7.9)/CeO_2(com) working at 600°C. Therefore, the smallest crystal size could be more selective towards syngas producing less RWGS.

Influence on the metal loading

A study on the influence of the metal loading on the coprecipitated catalyst was carried to improve the performance working with 10mg of catalyst at 600ºC. The following graph shows the influence of the nickel content on cerium based compounds using 5% initial concentration of each reactant. The catalyst was pretreated at 250ºC under hydrogen.

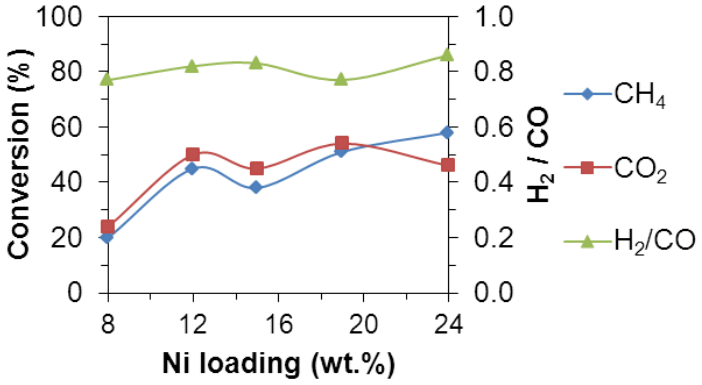

Fig 2.14 Catalytic activity on 10mg of $CeNi_{0.3}Oy$ (7.9% Ni), $CeNi_{0.5}Oy$ (12% Ni), $CeNi_{0.6}Oy$ (15% Ni), $CeNi_{0.8}Oy$ (19% Ni) and $CeNi_1Oy$ (24% Ni) at 600ºC, $t_{exp.}$= 5h, CH_4/CO_2/He/Ar (vol%) = 5/5/10/80, $T_{T.}$= 250ºC under H_2

As expected, CH_4 conversion increases with the Ni loading, while the conversion of CO_2 is slightly higher than the one of methane in all the cases except on $CeNi_1O_y$ which goes lower than CH_4. This shift on the CO_2 conversion normally is related to a considerable carbon deposition, probably at such loading the reaction $CH_4 \rightarrow C + 2\ H_2$ is easily promoted. Therefore, $CeNi_{0.5}O_y$, $CeNi_{0.6}O_y$ and $CeNi_{0.8}O_y$ seem to be the most interesting ones as they show around the same activity and potentially less carbon deposition. Concretely, $CeNi_{0.8}O_y$ gives CH_4 and CO_2 conversions about 54 and 57% respectively with the production of 43% (mol%) of H_2, 52% of CO, 5% of H_2O and the formation of a small amount of carbon. The carbon balance on the $CeNi_{0.5}O_y$, $CeNi_{0.6}O_y$ and $CeNi_{0.8}O_y$ shows a similar % of carbon produced from the methane converted which are 6, 9 and 7% respectively (see ***Paragraph 7.1.3.9*** for calculation method). Otherwise, the visual effect and the more difficulty of removing the catalytic bed from the

reactor as higher is the loading of Ni could mean that the lowest sintering effect occurred at $CeNi_{0.5}O_y$.

Influence on the pretreatment temperature

A study on the influence of the pretreatment temperature was also made for the high nickel loading of 24 wt.% to verify if the same particular behavior (as in the $CeNi_{0.3}O_y$) could happen with bigger particles of NiO. In addition, the influence on the selectivity could also vary.

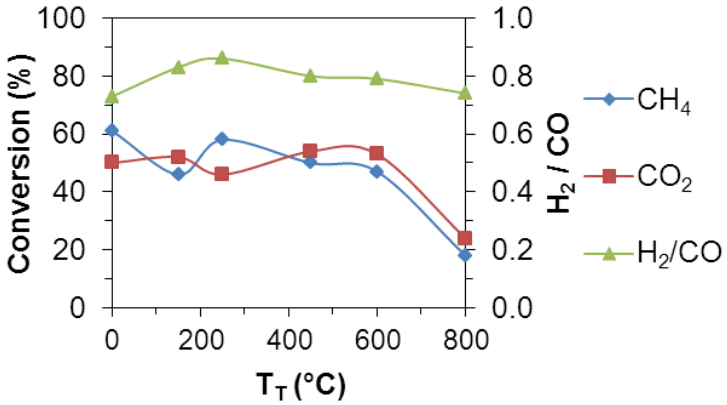

Fig 2.15 Catalytic activity on 10mg of $CeNi_1Oy$ at 600ºC, $t_{exp.}$= 5h, CH_4/CO_2/He/Ar (vol%) = 5/5/10/80, using different T_T under H_2 (the point at zero is without pretreatment)

The ***Fig 2.15*** shows that the conversions follow the same trend as for the $CeNi_{0.3}O_y$. In this case the same activity is obtained at different temperatures up to 600ºC. However, the conversions decrease considerably at 800ºC (18% instead of 50% conversion of methane). Such behavior confirms that for this sort of solids a too high pretreatment temperature is not beneficial for the activation. Nonetheless, the shift on the conversion is at much higher temperature than for $CeNi_{0.3}Oy$ (800ºC instead of 550ºC). One of the hypothesis is that the particles are more difficult to be reduced than at the low loading, as so not being too reduced (not active) until higher pretreatment temperatures.

In summary of the study on the Ni-Ce-O catalysts, the coprecipitated catalyst seems to be the most adequate for DRM. Within the different loadings, the one of $CeNi_{0.5}O_y$ (12.2 wt% of Ni) appears to be the most suitable one as it gives around the same conversion than using higher loading of nickel and exhibits less carbon deposition and qualitatively less sintering effect.

2.2.4. Catalysts characterization after test

XRD, XPS and BET analysis were carried in some of the catalysts ($Fe(10.4)/CeO_2$, $Co(7.2)/CeO_2$ and $Ni(9.5)/CeO_2$) after test trying to understand the properties of the solid after being expose to the DRM. First, it is necessary to have in mind the whole series of experiments

on each catalyst as different working conditions were set, such as the temperature of reaction and the type of process (alternating cofeed and periodic).

Table 2.3 Series of experiments on each catalyst

$Fe(10.4)/CeO_2$			
Exp	T(ºC)	Type	t (min)
1	700	periodic	36
2	**700**	**cofeed**	**20**
3	800	periodic	36
4	**800**	**cofeed**	**20**
5	900	periodic	36
6	**900**	**cofeed**	**20**

$Co(7.2)/CeO_2$			
Exp	T(ºC)	Type	t (min)
1	700	periodic	36
2	**700**	**cofeed**	**20**
3	800	periodic	72
4	750	periodic	72
5	**750**	**cofeed**	**120**
6	**800**	**cofeed**	**120**
7	700	periodic	72
8	**700**	**cofeed**	**120**
9	650	periodic	72
10	**650**	**cofeed**	**120**
11	600	periodic	72

$Co(7.2)/CeO_2$			
Exp	T(ºC)	Type	t (min)
12	**600**	**cofeed**	**120**
13	800	periodic	240

$Ni(9.5)/CeO_2$			
Exp	T(ºC)	Type	t (min)
1	800	periodic	72
2	750	periodic	72
3	700	periodic	72
4	800	periodic	240
5	700	periodic	72
6	750	periodic	72
7	650	periodic	72
8	650	periodic	72
9	700	periodic	72
10	750	periodic	72
11	**700**	**cofeed**	**300**
12	**600**	**cofeed**	**120**
13	**650**	**cofeed**	**120**
14	**750**	**cofeed**	**120**
15	**800**	**cofeed**	**120**

The ***Table 2.3*** shows in detail all the experiments made on each catalyst. Obviously, the characterization techniques were carried after the last experiment in each solid. Besides, the table above emphasizes the versatility and robustness of these types of solids. Concretely, $Co(7.2)/CeO_2$ and $Ni(9.5)/CeO_2$ catalysts were working under the reaction conditions described above during 21h and 28h respectively, showing stable and active performances in all the cases even though the change on the temperature and on the type of process.

XRD and BET surface

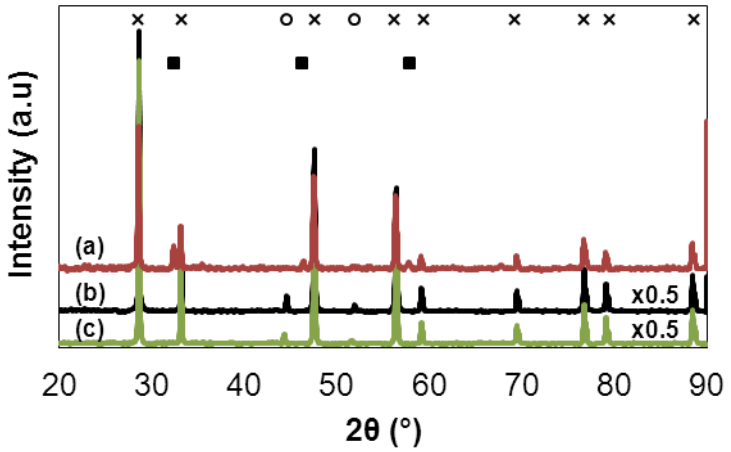

Fig 2.16 XRD patterns for (a) Fe(10.4)/CeO_2, (b) Ni(9.5)/CeO_2, (c) Co(7.2)/CeO_2 after test x CeO_2, o Ni^0 and Co^0, ■ $CeFeO_3$

The ***Fig 2.16*** shows a well-defined pattern of the fluorite structure of CeO_2 in all the cases. The narrower and more intense peaks after experiment could be explained due to the catalysts become more crystallized. Otherwise, the diffraction pattern of Ce_2O_3 does not appear, meaning that in the reaction conditions CeO_2 may be only slightly reduced, without changing the phase of the crystal towards the structure of Ce_2O_3 (***Fig 4.1***).

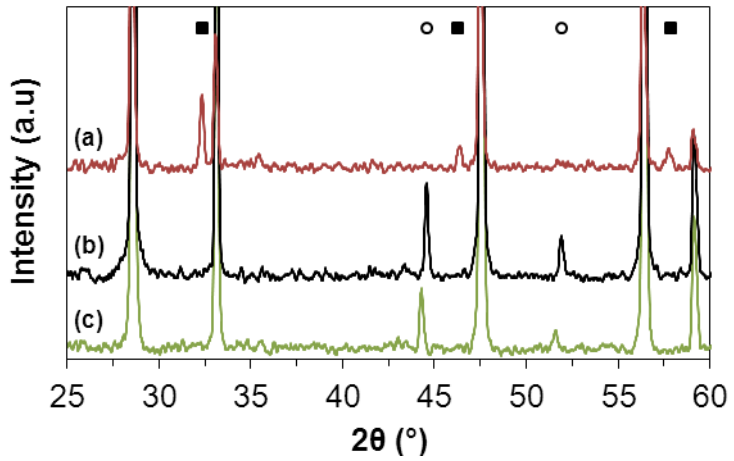

Fig 2.17 Zoom on the XRD patterns after test

From another side, the ***Fig 2.17*** reveals the apparition of the metallic Ni^0 and Co^0 (44.6º and 52.0º) instead of their oxides. Moreover, Fe^0 does not appear after the experiment, being potentially one reason about the low reactivity of this catalyst in the performance of the DRM. However, the phase $CeFeO_3$ appears in the XRD (32.4, 46.3, 57.9º), evidencing the formation of this mixed oxide between Fe and Ce during the reaction. The formation of $CeFeO_3$ is attributed by the solid state reaction 3 CeO_2 + Fe_2O_3 + Fe → $CeFeO_3$ [2.8-2.9] or/and via the reaction CeO_2 + FeO → $CeFeO_3$ [2.10]. Even though the low reactivity shown in the experiments, activation of methane over Fe-Ce based catalysts with the formation of $CeFeO_3$

has been reported in some studies [1.31, 2.11]. The high activity was shown on SRM and ORM feeding the reactants in periodic conditions. Nevertheless, the activation of this type of catalyst under dry reforming conditions has never been reported. Probably, the cofeed atmosphere of CH_4 and CO_2 gives an environment on the catalyst which is somehow not favorable for the activation of the reactants on $CeFeO_3$ species. Further studies would need to be done for a deeper understanding of this behavior, such as pretreating the catalyst under H_2.

Table 2.4 Crystal size and BET surface

Catalyst	d_{M-O} (nm)	d_M (nm)	d_{CeO2} (nm)	S_{BET} (m^2/g)
Ni(9.5) / CeO_2	18	n.o.	10	32
Ni(9.5) / CeO_2 a.e.	n.o.	**33**	**38**	**< 2**
Co(7.2) / CeO_2	16	n.o.	10	28
Co(7.2) / CeO_2 a.e.	n.o.	**30**	**36**	**< 2**
Fe(10.4) / CeO_2	n.o.	n.o.	10	73
Fe(10.4) / CeO_2 a.e.	31	n.o.	**34**	**< 2**

a.e. = after experiment n.o. = not observed

The crystal size of Ni, Co, $CeFeO_3$ and CeO_2 were calculated from the XRD data by the Scherrer equation. In the three cases the crystal size of CeO_2 is around 4 times bigger after test, evidencing some sintering of CeO_2 during the experiment. Otherwise, the crystal size of Ni and Co (33nm and 30nm respectively) is quite close to the one of CeO_2 (36-38nm).

There is also a considerable difference in the surface area before and after experiment. It goes from around 30 m^2/g (in the case of Ni and Co) to lower than 2 m^2/g (detection limit of the equipment) after test. This data is quite relevant because even with a huge loss on the surface area, the catalyst remains active and stable.

X-ray Photoelectron Spectroscopy (XPS)

The Ni $2p_{3/2}$ and the Co $2p_{3/2}$ XPS spectra (before and after test) were analyzed to determine the oxidation state of the particles for the Ni(9.5)/CeO_2 and Co(7.2)/CeO_2 catalysts.

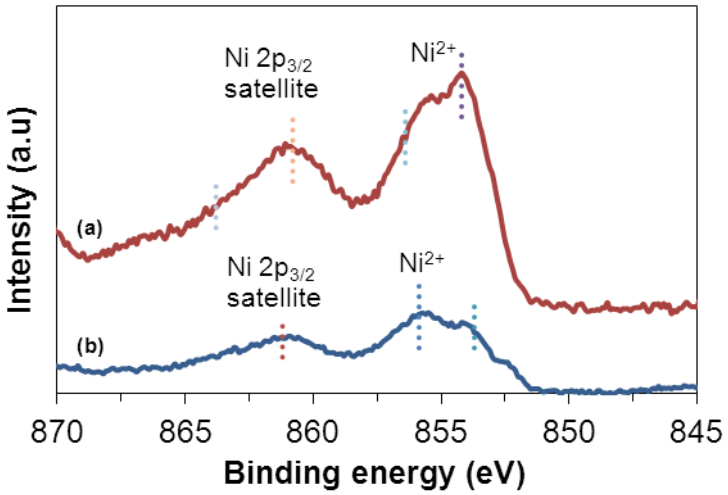

Fig 2.18 XPS pattern of Ni $2p_{3/2}$ core level (a) before and (b) after experiment on Ni(9.5)/CeO_2

First, the XPS before test on the Ni(9.5)/CeO_2 catalyst shows two peaks at 854.2eV and 856.4eV for Ni^{2+} (satellites at 860.8eV and 863.8eV). Otherwise, the analysis after experiment shows a binding energy of Ni^{2+} at 855.9 eV. Therefore, Ni^{2+} cations are present after test. The shift on the binding energy can be explained by the existence of strong interactions between Ni and Ce species after test [2.12-2.13]. In addition the analysis after experiment shows a low intensity. The decrease of Ni species is in good agreement with the increase of the crystallites size observed by XRD corresponding to a sintering effect. Some strong interactions can be obtained between the cations at the interfaces. However, this effect could be also related to a potential migration of nickel species into the ceria phase [2.18]. Raman analysis would be necessary to verify if indeed there is a solid solution after test or not.

Besides, another important characteristic appears after test, which is a small contribution of the metallic nickel that could explain the appearance of a peak at 853.7eV. These results are partially in good agreement with the XRD analysis because from one side the presence of Ni^0 is confirmed but from the other side NiO is not identified by the XRD patterns after test. Therefore, the formation of a solid solution during the reaction thanks to the incorporation of Ni into the structure of CeO_2, with a small amount of metallic Ni on the surface could be one of the potential hypotheses about this behavior.

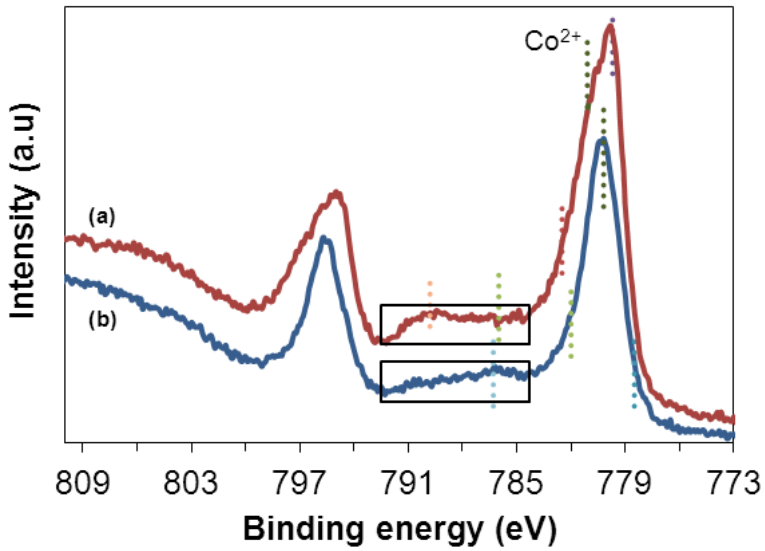

Fig 2.19 XPS pattern of Co $2p_{3/2}$ core level (a) before and (b) after experiment on Co (7.2)/CeO_2

The XPS was also carried for Co(7.2)/CeO_2 catalyst. Before test, the XPS shows the typical binding energies at 779.7eV, 781.1eV, 782.5eV, 786.0eV and 789.8eV, which correspond to the oxidation state of Co related to the Co_3O_4 compound. In addition, a qualitative analysis can be also made as the shape of the Co 2p spectra is identical as the one which gives the Co_3O_4 [2.27]. Otherwise, the same type of behavior, as compared with the one of Ni, occurs on the solid after test. Small contribution of the metallic compound (Co^0) at 778.5eV appears in the XPS spectra, being the major contribution at 780.2eV, 782.0eV and 786.3eV, binding energies related to Co^{2+}. Nonetheless CoO is not shown in the XRD patterns after test, a fact which leads thinking about the possibility of a solid solution between Co and CeO_2 ($CeCo_xO_y$). Otherwise, the decrease on the amount of Co species on the surface after test could be explained as in the case of Ni, the crystallite size is bigger after experiment than before test due to the sintering effect.

Table 2.5 Data from XPS analysis for Ni(9.5)/CeO_2 and Co(7.2)/CeO_2 catalysts

Catalyst	% Atomic concentration				
	Ce	Ni	O	Ni^{2+}	Ni^0
Ni(9.5)/CeO_2	17	30	53	100	-
Ni(9.5)/CeO_2 a.e.	28	13	59	81	19
Catalyst	% Atomic concentration				
	Ce	Co	O	Co^{2+}	Co^0
Co(7.2)/CeO_2	18	20	62	100	-
Co(7.2)/CeO_2 a.e.	22	14	64	96	4

The first value to underline from the ***Table 2.5*** is the overall % of Ni before and after experiment which goes from 30 at% to 13 at%, confirming the visual effect observed in the ***Fig 2.18***. Several hypotheses may come out from these values: (i) there is a decrease of nickel on

the surface of the catalyst, (ii) nickel is covered by another chemical species (potentially carbon) or (iii) the detection is lower due to the sintering of the particles. Moreover, there is a considerable amount of Ni^{2+} (81%) in comparison with the one of Ni^0 (19%) after test. The same type of behavior occurred to Co(7.2)/CeO_2 catalyst, there is a loss of Co species on the surface after experiment and the oxidize compounds remain mostly after test with only 4% of Co^0. The highest amount of metal on the surface of the catalyst in the case of Ni could explain eventually the highest activity obtained in the performance in its comparison with Co (***Fig 2.6***).

In a general way, XPS analysis takes into account around the first 10 atomics layers of the catalyst surface. Thereby, more than the 50% of Ni and Co species, which are not observed on the XPS, could be migrated from the surface and to the bulk CeO_2 to form a solid solution. The fact that the 2+ oxidation state is maintained for Co and Ni species and that there is a shift to higher binding energies after test could be due to the synergistic effect with CeO_2 which allows a redox system. Finally, the oxidation of the metallic nickel during the time between the experiment and the analysis is necessary also to keep in mind. In conclusion, the best way to confirm the guesses extracted from this characterization would be to carry the XPS in-situ, just after the experiment. Besides, more characterizations techniques would need to be carried to verify if in fact there is a solid solution Ni-Ce-O and Co-Ce-O after the experiment.

Leaving aside the discussion of the particular and interesting behavior seen in some of the experiments, the last results obtained at 600°C with 10mg of catalyst show that improvements are still necessary from the conversion point of view. Therefore, another Ni-based catalyst which could give potentially interesting performances was studied.

2.3. Ni-Mg-Al-O based catalyst

The combination of Ni, Mg and Al has shown interesting results towards the DRM. As mentioned in the ***Paragraph 1.7.1***, besides the well-known activity of nickel with CH_4, the basic properties of MgO promotes the activation of CO_2 helping kinetically the Boudouard reaction towards CO (***Eq. 1.6***). In addition, the high melting point of MgO (2850ºC) would assure less sintering. Concretely, the mixed frame-work between Mg and Al, the so-called hydrotalcite-like compound ($Mg_6Al_2(OH)_{16}CO_3.4H_2O$), once is calcined, shows a high thermal stability, surface area and metal dispersion, being quite interesting for high temperature reactions.

In the present study, the influence of different parameters has been studied such as the Ni content (13.2%, 21.9% and 35.7%) and partial pressure of the reactants. The solids were calcined in air at 500°C. Some literature is in agreement about calcining the solids at lower temperature than the experimental one. For instance, Basile et al. [2.25] reported the effect on the calcination temperature, obtaining smaller crystal size of NiO at mild conditions. This effect was indeed verified by A.R. González who obtained larger crystallites of NiO at 650ºC than at

500ºC. In our case, the catalysts were prepared following a method developed in the laboratory using the coprecipitation technique [2.1]. The gas stream of CH_4/CO_2/He/Ar (5-20/5-20/x/y %v) was fed to the reactor (F_T = 100 ml/min). The stoichiometric molar ratio CH_4/CO_2 was maintained at 1 while varying the reactants concentration.

2.3.1. Catalysts characterization

As for Ni-Ce catalysts, different characterizations techniques have been done for a better understanding of the catalytic properties on Ni-Mg-Al-O solids. XRD, BET surface, XPS and TPR are shown in the following paragraph. However, the characterizations are only done before experiment, analysis after test would be necessary for further comprehension after reaction.

Table 2.6 Ni loading, surface area and main crystallite size of the different catalysts

Catalyst	% Ni	Ni / M_T	S_{BET} (m^2/g)	d_{M-O} (nm)	Lattice (nm)
$Ni_{0,5}Mg_2AlO_y$	13.2	0.14	95	3.4	0.42
$Ni_1Mg_2AlO_y$	21.9	0.24	127	3.6	0.41
$Ni_2Mg_2AlO_y$	35.7	0.43	146	3.7	0.39

The small particle size of the solid solution (3-4nm) and the high surface area observed for this type of catalysts (95-146 m^2/g) in the ***Table 2.6*** could enhance the performances in its comparison with the binary Ni-Ce-O based catalysts. The well-dispersion of active sites on the catalyst would give a high activity of the catalyst. In addition, the high surface area of the ex-hydrotalcite-like compound would avoid considerably the sintering phenomenon.

XRD and BET surface

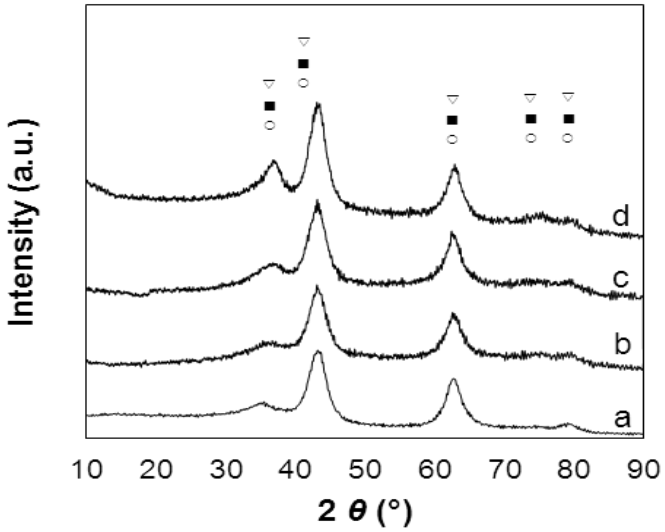

Fig 2.20 XRD patterns for (a) Mg_2Al_1 (b) $Ni_{0.5}Mg_2AlO_y$, (c) $Ni_1Mg_2AlO_y$ and (d) $Ni_2Mg_2AlO_y$ after calcination MgO (O), Ni-Mg-(Al)-O (■), NiO (▽)

The X-ray diffraction patterns of $Ni_{0.5}Mg_2AlO_y$, $Ni_1Mg_2AlO_y$ and $Ni_2Mg_2AlO_y$ are shown in ***Fig 2.20***. The peaks of MgO, Ni-Mg-(Al)-O solid solution and NiO phases are difficult to distinguish separately as they overlap each other. Otherwise, the diffraction pattern of Al_2O_3 does not appear, probably due to three potential causes: (i) high dispersion, (ii) an amorphous state or/and (iii) the insertion of Al species in the Ni-Mg-O phase forming the Ni-Mg-Al-O solid solution. Therefore, as expected the hydrotalcite structures are destroyed after calcination at 500ºC forming the corresponding oxides. This type of XRD pattern for Ni-Mg-Al based catalyst is also obtained by others researchers. A.R. González et al. also correlate the no apparition of NiO to the superpose peak of the mixed oxides, basically MgO and/or Mg(Al,Ni)O [2.22]. Nevertheless, $NiAl_2O_4$, which appears in other preparations methods [2.24], is not formed in this case as its XRD pattern is clearly different as the one shown in the figure above.

TPR

The reducibility of the catalysts was studied by TPR for the three catalysts used on the experiments: $Ni_{0.5}Mg_2AlO_y$, $Ni_1Mg_2AlO_y$ and $Ni_2Mg_2AlO_y$.

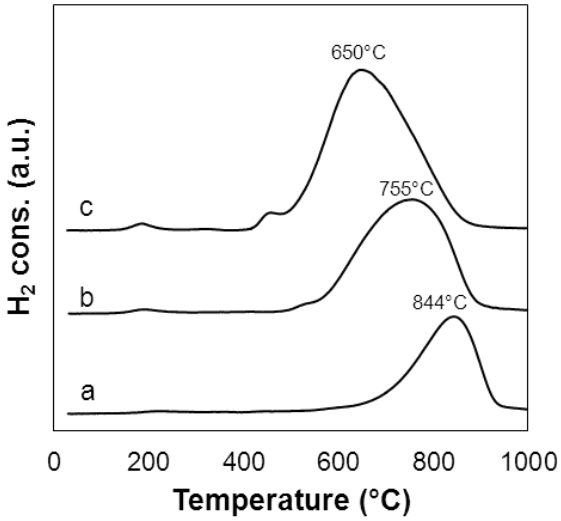

Fig 2.21 TPR profile for (a) $Ni_{0.5}Mg_2AlO_y$, (b) $Ni_1Mg_2AlO_y$ and (c) $Ni_2Mg_2AlO_y$ after calcination

The TPR profile gives only one peak on each sample at much higher temperature than the one for NiO which is around 350-400ºC. Moreover, the shift on the reduction temperature is related to the nickel loading. At high amounts of Ni is easier to reduce the solid than at low ones, giving the highest value at 844ºC working with $Ni_{0.5}Mg_2AlO_y$. The small bound at the beginning of the main peak for $Ni_2Mg_2Al_1O_y$ can be associated to some NiO which has not been mixed in the solid solution. This trend could imply that at high loadings of nickel is more difficult to obtain a well mix solid solution in the whole catalyst. Otherwise the high temperature of reduction with low Ni content could be assigned to the reduction of thermal stable phases involving strong interactions between the cations of the solid solution Ni-Mg-Al-O. This phenomena was also observed by A.R. Gonzalez et al. [2.22] relating that to a strong synergy between nickel species in the mixed oxides resulting from the hydrotalcite-like compound.

X-ray Photoelectron Spectroscopy (XPS)

The oxidation state of Ni was analyzed for the catalyst $Ni_1Mg_2AlO_y$ by XPS in order to corroborate the findings from the XRD patterns about the existence of a solid solution.

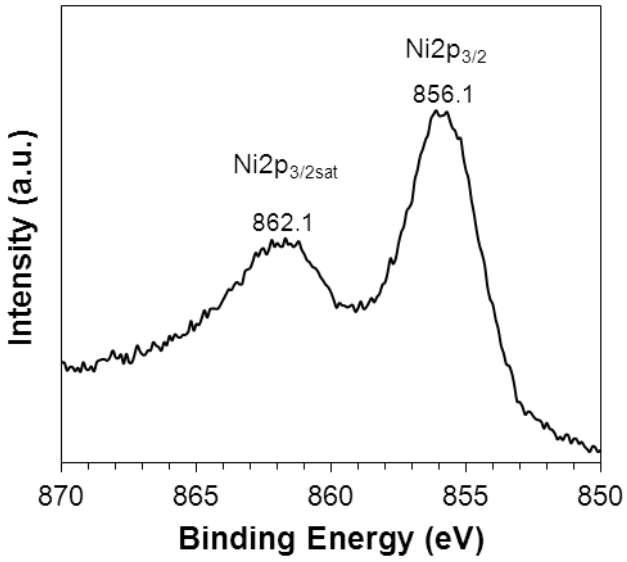

Fig 2.22 XPS pattern of Ni $2p_{3/2}$ core level on $Ni_1Mg_2AlO_y$

The Ni $2p_{3/2}$ XPS spectrum for $Ni_1Mg_2AlO_y$ catalyst before experiment is shown in the ***Fig 2.22***. The binding energy for Ni^{2+} at 856.1eV, which is higher than the one related to pure NiO (853.7-854.6 eV), can be associated to the Ni-Mg-Al-O solid solution phase [2.26]. This shift is due to the strong interactions between the different cations of Ni^{2+}, Al^{3+} and/or Mg^{2+} species (as in the case of Ni and Ce catalyst). The electron transfer between the metals would lead to this deviation on the binding energy. Overall, the XPS analysis revealed the creation of solid solution, as in the XRD was not possible to assume it due to the overlap of the peaks.

In summary, XRD, XPS and TPR confirmed the synergetic effect between the three cations involved in this catalyst (Ni, Mg and Al), which can be beneficial to enhance the activity and stability of the catalyst for DRM.

2.3.2. Catalytic test: Study at 600ºC

Based on the previous study with Ni-Ce catalysts, the working conditions applied to the ternary catalyst were directly 10mg of catalyst and 600ºC of reaction temperature. $Ni_1Mg_2AlO_y$ (22 wt% of Ni) was chosen to carry the experiments as less sintering is expected thanks to the high surface area of the catalyst.

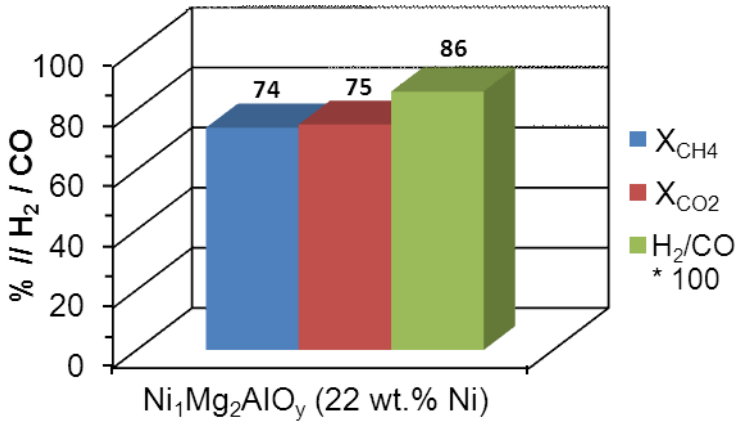

Fig 2.23 Catalytic activity on 10mg of $Ni_1Mg_2AlO_y$ at 600ºC, $t_{exp.}$= 5h, CH_4/CO_2/He/Ar (vol%) = 5/5/10/80, T_T = 450ºC.

The ***Fig 2.23*** shows the conversion of CH_4 and CO_2 and the selectivity obtained after 5h of reaction working with the $Ni_1Mg_2AlO_y$ catalyst. The most interesting fact to underline is that the maximum conversion is reached from the thermodynamic point of view, which is 75% (see ***Paragraph 3.3.1***). Specifically, 74% and 75% conversions of CH_4 and CO_2 are obtained with a high selectivity (for such conditions) towards H_2 and CO of 0.86. This performance can be compared to the one working with $CeNi_1O_y$ as both of them have around the same loading of nickel (24 wt.% for $CeNi_1O_y$ and 22 wt.% for $Ni_1Mg_2AlO_y$). In the best of the experiments CH_4 and CO_2 conversions were 50% and 54% respectively for the binary catalyst which is lower than the 74% and 75% obtained for the ternary solid. Nevertheless, one can expect to enhance the Ni-Ce-O catalysts adding also a third metal, such as Si [2.29] or Al [2.30] to improve different properties like obtaining higher surface area or a better dispersion of the active sites.

20% initial concentrations

Once the optimization at 5% initial concentration of the reactants is close to the ideal behavior, further studies at higher and more realistic concentrations were tested for the following research, concretely at 20%. In addition, as seen in the study on the Ni-Ce-O based catalyst, the treatment temperature can have a negative effect on the catalytic performance. Therefore a study of such parameter is also carried at this new condition.

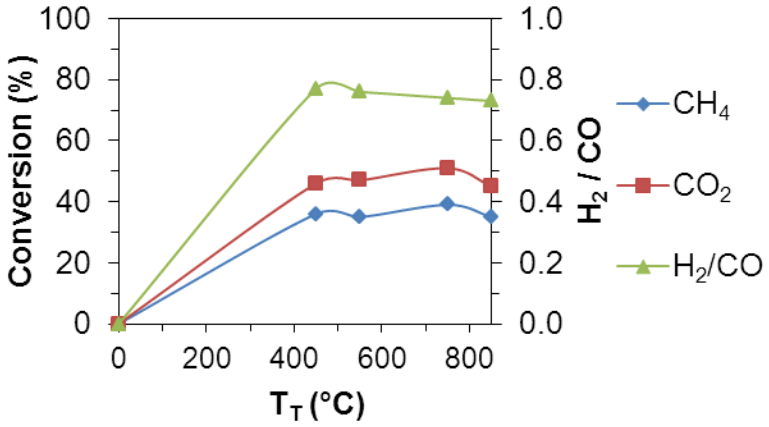

Fig 2.24 Catalytic activity on 10mg of $Ni_1Mg_2AlO_y$ at 600ºC, $t_{exp.}$= 5h, CH_4/CO_2/He/Ar (vol%) = 20/20/20/40, using different T_T under H_2 (the point at zero is without pretreatment)

The ***Fig 2.24*** shows around the same conversions for CH_4 and CO_2 in all the experiments, except for the no pretreating one, which does not show any kind of activation. Thus, Ni-Mg-Al-O catalysts is not capable of being active towards DRM starting directly on the oxide phase, as it was the case for Ni-Ce-O based catalyst. Consequently, prior use of hydrogen is necessary for this type of catalyst. Specifically, 36 and 46% conversion of CH_4 and CO_2 were obtained pretreating the catalyst at 450°C. Researchers use commonly a higher pretreatment temperature between 700-800ºC to reduce these sorts of solids [2.21-2.22, 2.24, 2.28]. Some studies relate the activation of the reactants to the reduction of the NiO species in the framework of NiO-MgO, $NiAl_2O_4$ [2.20] and $Ni(Mg)Al_2O_4$ [2.21].

Leaving aside the behavior towards hydrogen in the pretreatment step, the conversions obtained about 35-40% of CH_4 can be clearly improve as the thermodynamic equilibrium is not reached at such conditions. Therefore, $Ni_2Mg_2Al_1$ catalyst, which corresponds to 36 wt.% of nickel, was carried into the reactor.

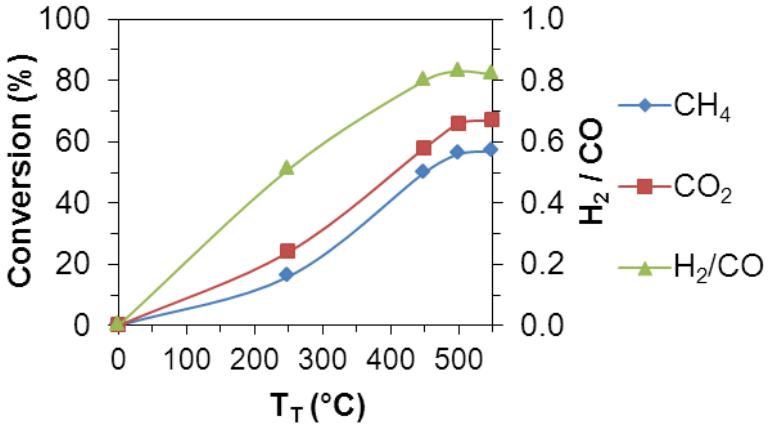

Fig 2.25 Catalytic activity on 10mg of $Ni_2Mg_2AlO_y$ at 600ºC, $t_{exp.}$= 5h, CH_4/CO_2/He/Ar (vol%) = 20/20/20/40, using different T_T under H_2 (the point at zero is without pretreatment)

A whole study was also carried on the influence of the pretreatment under H_2. ***Fig 2.25*** presents the conversions of CH_4 and CO_2 obtained at 600ºC on the $Ni_2Mg_2AlO_y$ compound. From one side, the catalyst shows the same behavior towards hydrogen in the pretreatment step than $Ni_1Mg_2AlO_y$, obtaining high conversions at high temperatures (450-550ºC). Such trend reinforces the importance of reducing this type of solids before experiment. In the optimized pretreatment temperature of 550ºC the conversions of CH_4 and CO_2 are 57% and 67%. Besides, the conversions remain quite stable along all the experiment, and the H_2/CO obtained is close to 0.80. For such results the products distribution and the conversions of CH_4 and CO_2 along the 5h experiment are shown in detail in the following graph.

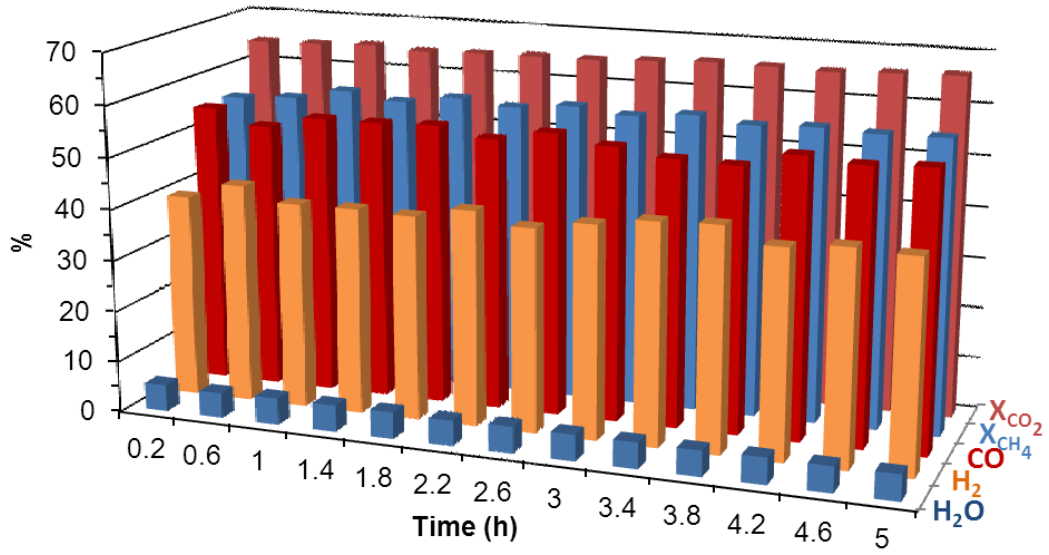

Fig 2.26 CH_4 and CO_2 conversions and products distribution on 10mg of $Ni_2Mg_2AlO_y$ at 600ºC along the 5h experiment, CH_4/CO_2/He/Ar (vol%) = 20/20/20/40 T_T = 550ºC under H_2

Fig 2.26 shows as an example the results obtained after a pretreatment of the catalyst at 550ºC. At 600°C 57% and 67% conversion of CH_4 and CO_2 respectively is observed on $Ni_2Mg_2AlO_y$ (36 wt.% Ni) catalyst with a H_2 and CO formation of about 41 mol% and 54 mol%, while the other product analyzed is H_2O (5 mol%). Besides, the graph above evidences the stability of the test along the 5h experiment without showing any kind of deactivation during this period. As in the case of working with 5% initial concentration of the reactants, the maximum conversions and selectivity towards H_2/CO are achieved for these reaction conditions taking into account the thermodynamic limitations (***Paragraph 3.3.1***), evidencing the high efficiency of the catalyst. At these conditions, the efficiency of the catalyst can be compared to recent results reported on Ni based mixed oxides catalysts [1.51, 2.14 -2.16] or on noble metal based catalyst [2.17].

2.3.3. Stability test (77h)

A stability test was performed at some specific conditions for several reasons. Even though $Ni_2Mg_2AlO_y$ shows a high performance at 600ºC with only 10mg of catalyst, the high loading of nickel used (36 wt.%) could be problematic for a long-run test as the sintering effect is easier to occur than using low loading. Thereby, $Ni_{0.5}Mg_2AlO_y$ which contains almost 3 times less nickel (13.2 wt.%) was chosen for this experiment. Otherwise, 10 times higher amount of catalyst (100mg) was carried in the reactor to balance the low amount of nickel. In addition, the temperature of the experiment was set 50ºC higher, at 650ºC. Commonly, researchers show stability tests working between 700-800°C [2.21, 2.23], so we found interesting to work at 650ºC with the consequent energy savings. The gas stream of CH_4/CO_2/He/Ar (20/20/20/40 vol%) was fed to the reactor (F_T = 100 ml/min).

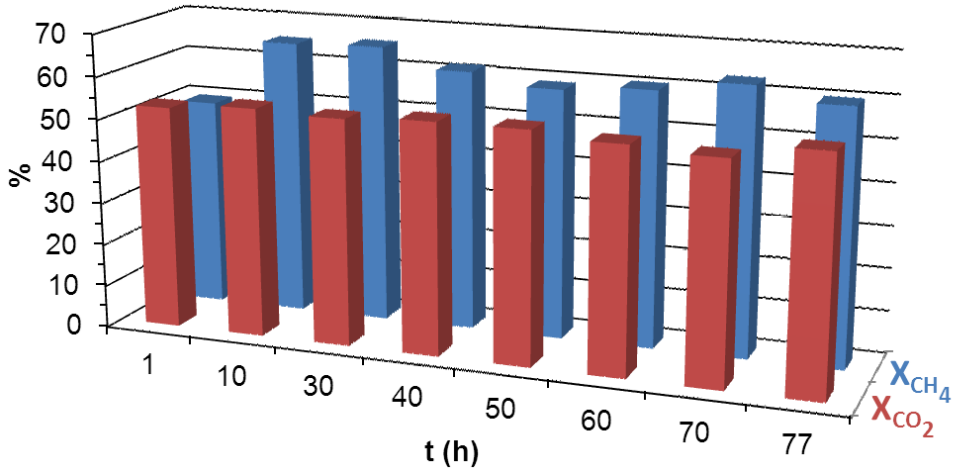

Fig 2.27 Catalytic activity on 100mg of $Ni_{0.5}Mg_2AlO_y$ at 650ºC along the 77h experiment

The ***Fig 2.27*** shows the conversion of CH_4 which is higher than the one of CO_2 along all the experiment. This behavior means commonly the production of some carbon due to the cracking of methane (***Eq. 1.5***). However, it does not seem to be enough for causing the deactivation of the catalyst within the duration of the test (77h). Another reason about this particular trend would be about being too close to the thermodynamic limitations. The possible excess in the amount of catalyst could lead to unusual performances.

Otherwise, in several periods of the experiment the conversions are really close to the theoretical ones, obtaining around 60% for CH_4. To sum, even if some adjustments need to be done for the long-term experiment, a promising performance is obtained in terms of stability which is not negligible considering the few stability tests showed on the literature at this temperature [2.31].

2.4. Conclusions

CH_4 and CO_2 transformation (DRM) has been studied on M-Ce-O (M = Ni, Co and Fe) catalysts and Ni-Mg-Al-O catalysts. The influence of different parameters was studied, such as the synthesis method, the nature of the precursors, the nature and loading of the metal (Ni loading), the amount of catalyst, the dilution of the catalyst with SiC, the influence of the pretreatment in H_2 and the reaction temperature (600°C-800°C). The catalysts were characterized before and after the reaction to find correlations between catalytic activity and physico-chemical properties.

Nanocrystallized compounds and high surface areas (4-20 nm, 30-80 m^2/g) were obtained using the different preparation methods. The Ni-Ce solids prepared by coprecipitation or supported on home-made ceria present smaller crystallites sizes in comparison with the supported catalyst on commercial ceria (~ 40 nm, 9 m^2/g). Moreover, strong interactions between Ni and Ce species can be found in coprecipitated ($CeNi_xO_y$) and Ni supported on home-made ceria compounds. Concerning the Ni-Mg-Al-O catalysts, a solid solution is formed in the Ni-Mg-Al-O formulation with also strong interactions between cations, indicated thanks to the XRD (eliminating some hypothesis about other structures, such as the one of Al_2O_3) and the XPS, which shows binding energies of Ni species higher than the one in NiO. Thus, the hydrotalcite structures are destroyed after calcination at 500ºC forming the corresponding oxides.

Nickel seems to be the most active metal in its comparison with Fe and Co without any pretreatment on the catalyst. The conversion of CH_4 at 700ºC working with Ni is 85%, 33% for Co and 2% for Fe.

In a general way, well tuning heterogeneous catalyst formulation allows obtaining high conversions of methane (84-95%) and carbon dioxide (88-96%) at the range of 700-800°C and a high selectivity (H_2/CO = 0.90-0.94) for the formation of syngas in the DRM without pretreatment under hydrogen of the catalyst at 5% initial concentration of the reactants.

Furthermore, very interesting results are obtained with conversions of 57% CH_4 and 67% CO_2 (close to thermodynamic equilibrium) at the low temperature of 600°C. The results are very promising as an optimization was made to work with a low mass of catalyst (only 10mg). Besides, the presence neither of a noble metal nor of a rare earth metal (Ni-Mg-Al) based catalysts, relative high concentrations of the reactants involved (20%) and the ease of the catalyst preparation method encourage for future studies to work without dilution, using pure 50% CH_4 and 50% CO_2. In addition, the 77h test at 650°C working with 20% concentration of the reactants shows a remarkable stability along the whole experiment.

As regards of the synthesis method between the different Ni-Ce-O based catalysts, the coprecipitation gives the most favorable performance in terms of having the easiest

activation/reducibility of the catalyst and the best selectivity towards the desired products. Specifically, 23% and 25% conversion of methane are achieved for the Ni(7.9)/CeO_2(com) and $CeNi_{0.3}$Oy respectively. However, in terms of selectivity the coprecipitated catalyst provides a H_2/CO ratio of 0.74 instead of 0.56 for the Ni(7.9)/CeO_2(com). The small initial crystallites size on $CeNi_{0.3}O_y$ could be maintained after experiment at the mild conditions of 600°C. Therefore, the small crystal size would be more selective towards syngas producing less RWGS. In addition the coprecipitated catalyst is activated easier (even without pretreatment) than Ni(7.9)/CeO_2(com) (600°C under H_2 + 1.5h under the reaction mixture at 600°C).

Otherwise, some interesting findings are shown about the particular reducibility of the coprecipitated $CeNi_xO_y$ catalysts, obtaining lower performances at higher pretreatment temperatures. A “too” reduced catalyst is not as active as a partially reduced one. The key role of the interfacial oxygen in the Ni-Ce boundary (Ni-O-Ce site) can be one explanation. This first interaction leads to the total oxidation of methane and the creation of selective actives sites for the following reforming reaction towards H_2 and CO because the unselective consumed oxygen in the Ni-Ce boundary cannot be reoxidized by CO_2. A too high reduction of the compounds does not lead subsequently the creation of the active site for the reforming reaction.

2.5. References

2.1 W. Fang, S. Paul, M. Capron, F. Dumeignil, L. Jalowiecki-Duhamel, Hydrogen production from bioethanol catalyzed by $Ni_xMg_2AlO_y$ ex-hydrotalcite catalysts *Appl. Catal. B* 152-153 **(2014)** 370

2.2 I. Luisetto, S. Tuti and E. Di Bartolomeo, Co and Ni supported on CeO_2 as selective bimetallic catalyst for dry reforming of methane *Inter. J. Hydrogen* 37 **(2012)** 15992-15999

2.3 C. Gennequin, M. Safariamin, S. Siffert, A. Aboukais and E. Abi-Aad, CO_2 reforming of CH_4 over Co-Mg-Al mixed oxides prepared via hydrotalcite like precursors *Catal. Today* 176 **(2011)** 139-143

2.4 R. Bouarab, O. Akdim, A. Auroux, O. Cherifi, C. Mirodatos, Effect of MgO additive on catalytic properties of Co/SiO_2 in the dry reforming of methane *Appl. Catal. A* 264 **(2004)** 161-168

2.5 J.R. Mawdsley, T.R. Krause, Rare earth-first-row transition metal perovskites as catalysts for the autothermal reforming of hydrocarbon fuels to generate hydrogen *Appl. Catal. A* 334 **(2008)** 311-320

2.6 R.J. Berger, J. Pérez-Ramírez, F. Kapteijn, J.A. Moulijn, Catalyst performance testing: the influence of catalyst bed dilution on the conversion observed *Chem. Eng. J.* 90 **(2002)** 173-183

2.7 M. Behrens, Coprecipitation: An excellent tool for the synthesis of supported metal catalysts – From the understanding of the well known recipes to new materials *Catal. Today* 246 **(2015)** 46-54

2.8 K. Li, M. Haneda, Z. Gu, H. Wang, M. Ozawa, Modification of CeO_2 on the redox property of Fe_2O_3 *Mater. Lett.* 93 **(2013)** 129-132

2.9 M. Robbins, G.K. Wertheim, A. Menth, R.C. Sherwood, Preparation and properties of polycrystalline cerium orthoferrite ($CeFeO_3$) *J. Phys. Chem. Solid.* 30 **(1969)** 1823-1825

2.10 X. Zhu, H. Wang, Y. Wei, K. Li, X. Cheng, Hydrogen and syngas production from two-step steam reforming of methane over CeO_2-Fe_2O_3 oxygen carrier *J. Rare Earth* 28 **(2010)** 907

2.11 N.L. Galinsky, A. Shafiefarhood, Y. Chen, L. Neal, F. Li, Effect of support on redox stability of iron oxide for chemical looping conversion of methane *Appl. Catal. B* 164 **(2015)** 371-379

2.12 J. Wang, M. Shen, J. Wang, M. Yang, W. Wang, J. Ma, L. Jia, Effects of Ni-doping of ceria-based materials on their micro-structures and dynamic oxygen storage and release behaviors *Catal. Lett.* 140 **(2010)** 38-48

2.13 S. Shan, M. Fleys, F. Lapicque, D. Swierczynski, A. Kiennemann, Y. Simon, P.M. Marquaire, Syngas production from partial oxidation of methane over $Ce_{1-x}Ni_xO_y$ catalysts prepared by complexation-combustion method *Appl. Catal. A* 311 **(2006)** 24-33

2.14 M. Yu, Y.A. Zhu, Y. Lu, G. Tong, K. Zhu, X. Zhou, The promoting role of Ag in Ni-CeO_2 catalyzed CH_4-CO_2 dry reforming reaction *Appl. Catal. B* 165 **(2015)** 43-56

2.15 H. Wu, G. Pantaleo, V. La Parola, A.M. Venezia, X. Collard, C. Aprile, L.F. Liotta, Bi- and trimetallic Ni catalysts over Al_2O_3 and Al_2O_3-MO_x (M = Ce or Mg) oxides for methane dry reforming: Au and Pt additive effects *Appl. Catal. B* 156-157 **(2014)** 350-361

2.16 J.P. Dacquin, D. Sellam, C. Batiot-Dupeyrat, A. Tougerti, D. Duprez, S. Royer, Efficient and robust reforming catalyst in severe reaction conditions by nanoprecursor reduction in confined space *ChemSusChem* 7 **(2014)** 631

2.17 L. Qian, W. Cai, L. Zhang, L. Ye, J. Li, M. Tang, B. Yue, H. He, The promotion effect of hydrogen spillover on CH_4 reforming with CO_2 over Rh/MCF catalysts *Appl. Catal. B* 164 **(2015)** 168-175

[2.18] V.M. Gonzalez-Delacruz, F. Ternero, R. Pereñíguez, A. Caballero, J.P. Holgado, Study of nanostructured Ni/CeO_2 catalysts prepared by combustion synthesis in dry reforming of methane *Appl. Catal. A* 384 **(2010)** 1-9

[2.19] D.K. Kim, K. Stöwe, F. Müller, W.F. Maier, Mechanistic study of the unusual catalytic properties of a new Ni-Ce mixed oxide for the CO_2 reforming of methane *J. Catal.* 247 **(2007)** 101-111

[2.20] X. Du, D. Zhang, L. Shi, R. Gao, J. Zhang, Coke- and sintering-resistant monolithic catalysts derived from *in situ* supported hydrotalcite-like films on Al wires for dry reforming of methane *Nanoscale* 5 **(2013)** 2659-2663

[2.21] Z. Xu, N. Wang, W. Chu, J. Deng, S. Luo, *In situ* controllable assembly of layered-double-hydroxide-based nickel nanocatalysts for carbon dioxide reforming of methane *Catal. Sci. Technol.* 5 **(2015)** 1588-1597

[2.22] A.R. Gonzalez, Y.J. Asencios, E.M. Assaf, J.M. Assaf, Dry reforming of methane on Ni-Mg-Al nano-spheroid oxide catalysts prepared by the sol-gel method from hydrotalcite-like precursors *Appl. Surf. Sci.* 280 **(2013)** 876-887

[2.23] X. Zhang, N. Wang, Y. Xu, Y. Yin, S. Shang, A novel Ni-Mg-Al-LDHs/γ-Al_2O_3 catalyst prepared by in-situ synthesis method for CO_2 reforming of CH_4 *Catal. Commun.* 45 **(2014)** 11-15

[2.24] K. Mette, S. Kühl, A. Tarasov, H. Düdder, K. Kähler, M. Muhler, R. Schlögl, M. Behrens, Redox dynamics of Ni catalysts in CO_2 reforming of methane *Catal. Today* 242 **(2015)** 101-110

[2.25] F. Basile, L. Basini, M. D'Amore, G. Fornasari, A. Guarinoni, D. Matteuzzi, G. Del Piero, F. Trifirò, A. Vaccari, Ni/Mg/Al anionic clay derived catalysts for the catalytic partial oxidation of methane *J. Catal.* 173 **(1998)** 247-256

[2.26] H. Lei, Z. Song, X. Bao, X. Mu, B. Zong, E. Min, XRD and XPS studies on the ultra-uniform Raney-Ni catalyst prepared from the melt-quenching alloy *Surf. Interface Anal.* 32 **(2001)** 210-213

[2.27] H M.Biesinger, "http://www.xpsfitting.com/2012/01/cobalt.html". [Online]. [Accessed: 2013-2015].

[2.28] Z.J. Zuo, C.F. Shen, P.J. Tan, W. Huang, Ni based on dual-support Mg-Al mixed oxides and SBA-15 catalysts for dry reforming of methane *Catal. Commun.* 41 **(2013)** 132-135

[2.29] S. Zhang, S. Muratsugu, N. Ishiguro, M. Tada, Ceria-doped Ni/SBA-16 catalysts for dry reforming of methane *ACS Catal.* 3 **(2013)** 1855-1864

[2.30] N. Wang, K. Shen, L. Huang, X. Yu, W. Qian, W. Chu, Facile route for synthesizing ordered mesoporous Ni-Ce-Al oxide materials and their catalytic performance for methane dry reforming to hydrogen and syngas *ACS Catal.* 3 **(2013)** 1638-1651

[2.31] W. Cai, L. Ye, L. Zhang, Y. Ren, B. Yue, X. Chen, H. He, Highly dispersed nickel-containing mesoporous silica with superior stability in carbon dioxde reforming of methane: the effect of anchoring *Materials* 7 **(2014)** 2340-2355

CHAPTER III:

Thermodynamics

3. THERMODYNAMICS

Dry reforming of methane is an endothermic reaction which needs to be carried out at high temperature, typically above 600°C and it can be limited by the thermodynamic equilibrium. Furthermore, other reactions may take place in these conditions, such as RWGS, methane cracking or the Boudouard reaction. In this chapter, a general overview of the thermodynamics of such reactions is given for traditional cofeed systems. Then, a wide range of metals was studied to know which ones could work in the periodic process taking as a reference the two required properties for the catalyst: the activation of methane and the capacity to provide oxygen to the system. Herein, the reduction of the oxides by CH_4 and the corresponding reoxidation by CO_2 was calculated for several metals (***Paragraph 3.2.6***). Previously, the phase diagram of the different solids was checked [3.1] to know all the intermediates phases between the metallic and the total oxidation state. The main reason of knowing all the intermediate oxides in detail was the significance variation of the thermodynamic properties which can affect the reactivity. In all the cases, the standard Gibbs free energy was followed in order to find out which reactions could be thermodynamically favorable in the different situations. Basically, there are 3 conditions to know about if the reaction could react or not:

$\Delta_f G°$ (reaction) > 0 Non spontaneous reaction

$\Delta_f G°$ (reaction) = 0 Equilibrium

$\Delta_f G°$ (reaction) < 0 Spontaneous reaction

Equation 3.1 $\Delta_f G°\ (reaction) = \sum v\Delta_f G°\ (products) - \sum v\Delta_f G°\ (reactants)$

Besides, the approach of working with shale gas, which has a considerable amount of ethane (typically around 80-100% of CH_4 and 0-20% of C_2H_6), was the main reason to also study the reforming of this gas. The main target was to check if ethane would have the same kind of behavior as methane.

Then, in the third ***Paragraph 3.3*** the theoretical conversions of several reactions are calculated at different temperatures, initial concentrations of reactants and total pressures of the system in order to find out the influence of such parameters on the reactions involved in the process.

The database of the standard Gibbs free energy was obtained from the website "*factsage.com*" [3.2].

3.1. Dry reforming of methane in cofeed

The coexistence of different reactions involved in the DRM has been already discussed in the literature. M. Haghighi et al. [3.3] studied the Gibbs free energy for the reactions involved

in such process. The calculations shown in the graph below are in good agreement with their calculations.

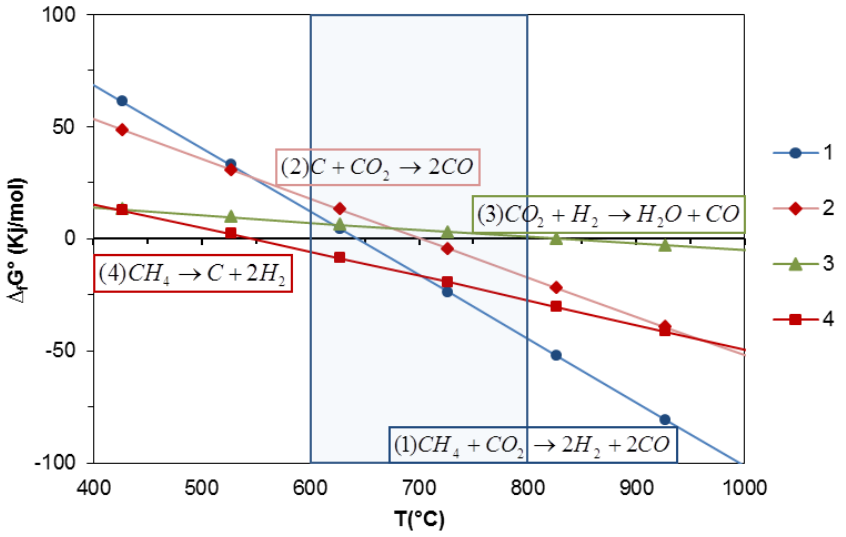

Fig 3.1 Gibbs free energy for DRM and main side reactions

The graph above reinforces the idea about the severe competition between different reactions on the DRM. From one side, DRM ***(1)*** becomes favorable to occur at around 650ºC. Besides, cracking of methane ***(4)*** is more favorable than reaction ***(1)*** up to 725ºC, which may be one of the reasons about obtaining less carbon above 750ºC than at lower temperatures. In addition, the oxidation of the deposited carbon with CO_2 ***(2)*** is favorable above 700ºC but more difficult to occur thermodynamically than the reaction ***(4)*** in the whole working range. Therefore, the eventual carbon would be quite difficult to oxidize at the same time as the DRM occurs due to the competition between CH_4 and C to react with CO_2, as the one of CH_4 is more favorable.

Moreover, the absolute ΔG of RGWS ***(3)*** is very small in all the temperature range. Thus, 100% selectivity towards syngas ***(1)*** is quite difficult to reach from the thermodynamic point of view.

In addition, the experimental data confirms some of the theoretical calculations made from the thermodynamic study. Concretely, the partial pressures of the compounds in the outlet flow of the reactor (at the initial stage of the experiment) working at 800ºC with Ni-Ce is represented in the figure below. The signal of H_2O in the outlet flow working at 800ºC or 600ºC is also shown to understand the difficulty of working at low temperatures, in this case in terms of selectivity.

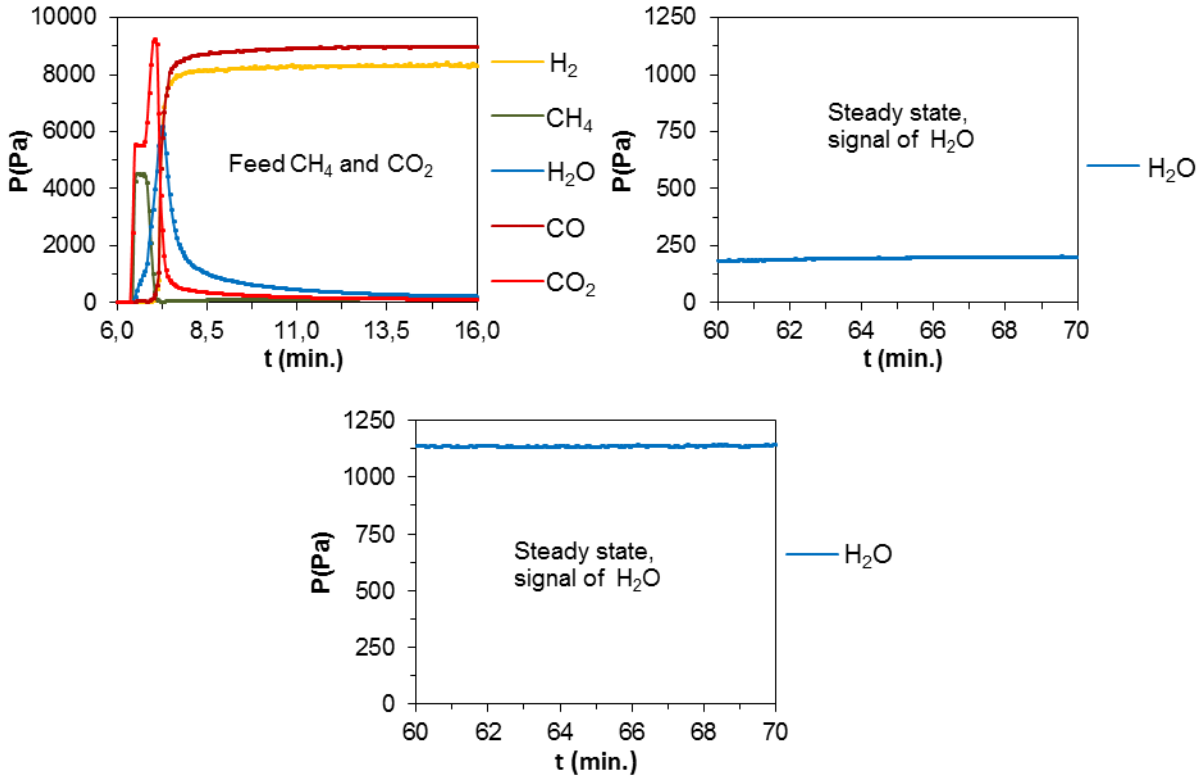

*Fig 3.2 Partial pressures in the outlet flow working with 200mg of Ni(9.5)/CeO_2 at 800ºC on (**Top left**) the initial stage of the experiment, (**Top right**) partial pressure of H_2O at the steady state and (**Bottom center**) at the steady state at 600ºC. CH_4/CO_2/He/Ar (vol%) = 5/5/10/80*

A particular behavior occurs at the beginning of the experiment at 800ºC (***Fig 3.2 (Top left)***). H_2O and CO_2 are majorly produced in the first minutes of the reaction leading afterwards to a much more selective system towards H_2 and CO. This unselective reaction only occurs during the first minutes of the experiment, which is crucial to obtain a selective system after the first stage of the test. Besides, another interesting information can be seen from the graph above: the partial pressure of H_2O is 5-6 times lower working at 800ºC (***Fig 3.2 (Top right)***) than at 600ºC (***Fig 3.2 (Bottom center)***) in the steady state conditions (after 1h). This difference is also in good agreement with the ***Fig 3.1***, which shows a stronger competition (variation of the Gibbs free energy close to each other) between DRM and RWGS at 600ºC than at 800ºC. In this context, M. Haghighi et al. [3.3] and M. Abdollahifar [3.6] calculated the theoretical H_2/CO ratio at different temperatures, being lower as the lower is the temperature as so confirming that somehow hydrogen is consumed, potentially due to the reaction with CO_2 in the RWGS.

In summary, this study on the cofeed system gives us already some clues about why the process in periodic could be selective towards syngas and the reason about the increase on the production of H_2O at low temperatures.

3.2. Dry reforming of methane in periodic feed

As mentioned above, this particular system needs particular properties. The solid plays a role as a reactant of the reaction (besides the catalytic properties of activating CH_4 and CO_2, in this case separately). The following calculations are based on known solid phases for which thermodynamic data is available. Results are illustrated mostly on Ni-Ce system which will prove to be the one with the highest potential towards DRM in the periodic concept.

3.2.1. Reduction by CH_4 of Ni-Ce solids

First, the oxidation of CH_4 was calculated by all the different possibilities of NiO and CeO_2 towards the total or the partial oxidation of the hydrocarbon. About ceria, two redox systems between CeO_2-Ce_6O_{11} and CeO_2-Ce_2O_3 are studied.

Reactivity of NiO

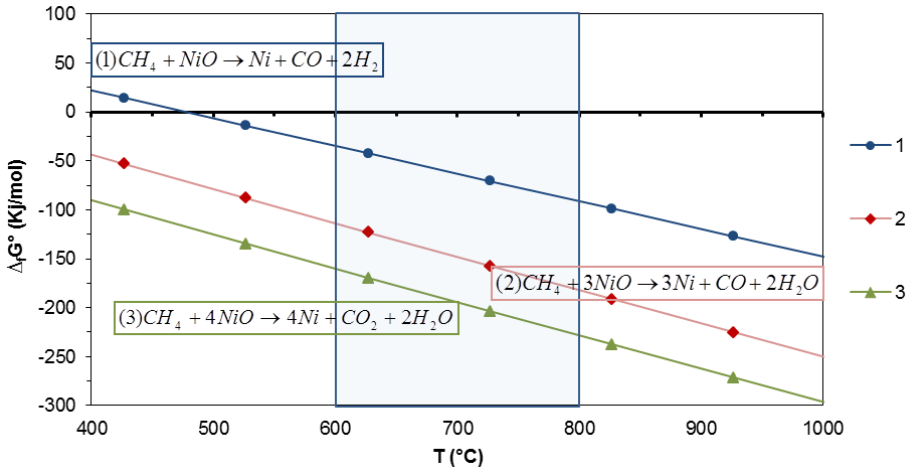

Fig 3.3 Gibbs free energy for the oxidation of CH_4 by NiO

Fig 3.3 shows that the total oxidation of methane towards H_2O and CO_2 ***(3)*** is the most favorable to occur within the different possible pathways to reduce NiO ***(1, 2 and 3)***. This characteristic could be related with the experimental data which shows a production of H_2O and CO_2 in the first minutes of the experiment for cofeed (***Fig 3.2***). The appearance of H_2O and CO_2 at the first stage, when the catalyst is not pre-reduced under hydrogen, it is also in good agreement with the concept of the Chemical Looping Combustion process (CLC) [1.59], where Ni-based catalyst are typically used for the total oxidation of the fuel. In CLC, the selectivity is towards H_2O and CO_2 as the catalyst is periodically oxidized with oxygen, so occurring in each cycle the reaction ***(3)***. Unless the selectivity is somehow controlled by kinetic means, this shows that Ni-NiO system is not adapted to act as oxygen vector for DRM in periodic feed.

Reactivity of CeO_2

The different scenarios for the reduction of CeO_2 are also calculated in the following graph. Particularly, the reduction of CeO_2 to one of its intermediate oxides (Ce_6O_{11}) is also shown.

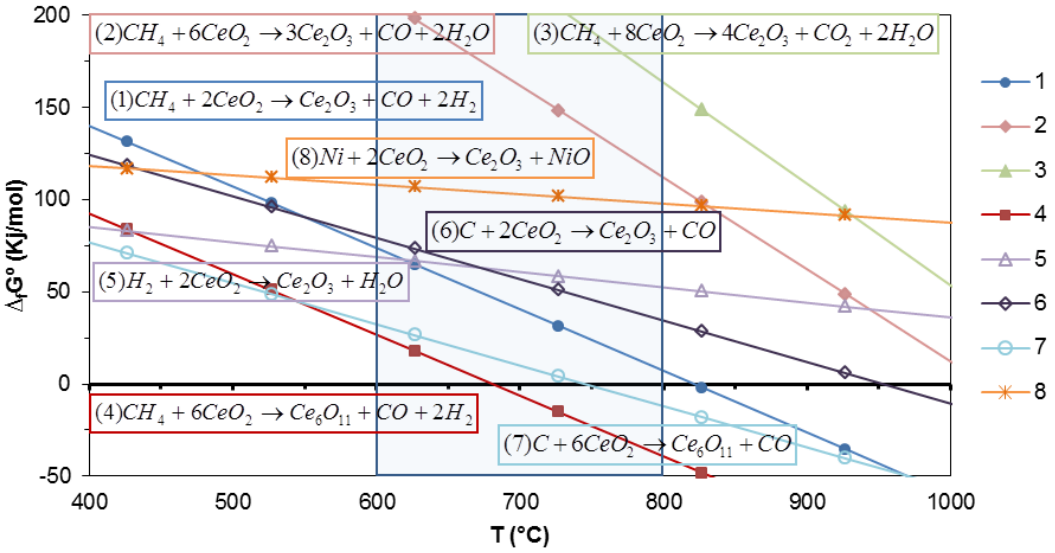

Fig 3.4 Gibbs free energy for the oxidation of CH_4 by CeO_2 and other side reactions

First, the partial oxidation of CH_4 on CeO_2 to Ce_2O_3 ***(1)*** is more favorable than the total oxidation ***(2 and 3)***. Moreover, the selective oxidation of methane between CeO_2 and Ce_6O_{11} ***(4)*** is even more favorable than the direct reduction of CeO_2 to Ce_2O_3 ***(1)***. In this context, Otsuka et al. [1.60] showed that the oxidation of CH_4 over CeO_2 becomes feasible at temperatures above 650ºC, which is quite close to our calculations (680ºC for the reaction ***(4)***). In all cases the selective oxidation of methane towards syngas is more favorable than total oxidation, making CeO_2 a good candidate to act as oxygen vector in P-DRM. Another key point illustrated in ***Fig 3.4*** is that the oxidation of Ni^0 to NiO by the CeO_2 ***(8)*** is not feasible in the temperature range explored. This means that unselective NiO will not be produced during the reoxidation by CeO_2. Besides, the thermodynamic of the reaction ***(8)*** would not change our previous hypothesis about that Ni^{2+} can remain in the system thanks to the synergetic effect with Ce, as the mixed oxide ($CeNi_xO_y$) formed during the experiment should probably have totally different thermodynamic and redox properties. In addition the feasibility of oxidizing carbon by CeO_2 ***(7)*** at high temperatures (above 750ºC) would also help to avoid the deactivation of the catalyst.

Looking back to ***Fig 3.2***, the production of H_2O and CO_2 at the first stage of the experiment can be related to the reduction of the unselective NiO to Ni, which is more favorable, thermodynamically speaking, than the DRM or the reaction ***(4)***. As discussed in the ***Paragraph 2.2.4***, once the nickel oxide is potentially reduced to Ni^0, part of it may migrate to the bulk of CeO_2 to form a mixed oxide Ni-Ce. Thereby the Ni^{2+} observed in the XPS analysis after the

cofeed experiments would be the one in a strong interaction with Ce, which at these new conditions it does not affect the selectivity of the reaction. Furthermore, in terms of deactivation of the system, there is a strong competition between the cracking of methane (see ***Fig 3.1***) and the partial oxidation of CH_4 over CeO_2 ***(4)***. Otherwise, the formation of carbon becomes less important at high temperatures (as in the case of cofeed). Additionally, the Boudouard reaction (see ***Fig 3.1***) is more favorable at 600ºC, which would add more difficulty to avoid carbon deposition at such "low" temperatures.

3.2.2. Reoxidation by CO_2 of Ni-Ce solids

Ni reoxidation

The study of the reoxidation step by CO_2 is also important from the thermodynamic point of view.

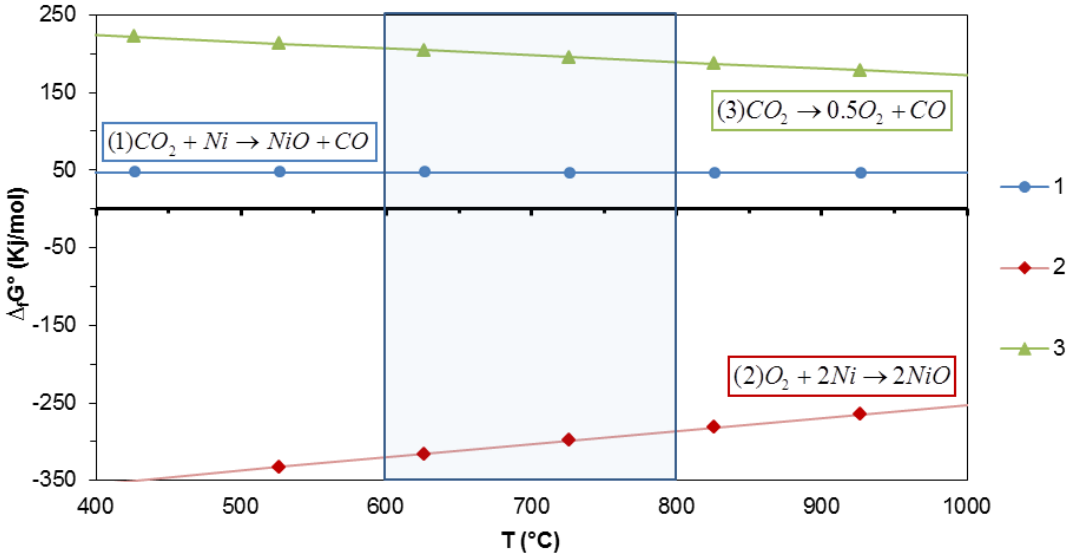

Fig 3.5 Gibbs free energy for the reoxidation of Ni by CO_2 and O_2

The ***Fig 3.5*** shows that the reoxidation of Ni^0 to NiO by CO_2 ***(1)*** is not favorable in the temperature range explored. This is a crucial property from the selectivity point of view. Indeed, the unselective reduction by CH_4 of NiO towards H_2O and CO_2 would react only once, at the beginning of the experiment, which is also confirmed experimentally by Otsuka et al. [1.60]. On this way, Y.H. Taufiq-Yap et al. [3.7] observed Ni^0 without any peak of NiO in the XRD pattern after DRM experiment. This is also in good agreement with the theories mentioned above and the data shown in the ***Paragraph 2.2.4***. In addition, the importance of the oxidation by CO_2 (or H_2O) instead of O_2 is also checked in the reaction ***(2)***, which obviously shows the feasibility of oxidizing Ni by oxygen. This type of behavior can be also correlated with the literature. Bhavsar et al. [1.59] studied the chemical looping combustion over Ni-CeO_2, as so reoxidizing the catalyst by air. They showed clearly the production of CO_2 in the first step of

the reaction, which is in concordance with the reduction of NiO to produce water and carbon dioxide. Finally, the absence of CO_2 dissociation to O_2 and CO is verified in the reaction ***(3)*** in order to check that no oxygen molecules appears in the gas phase, avoiding the reoxidation to unselective NiO.

Ce_xO_y reoxidation

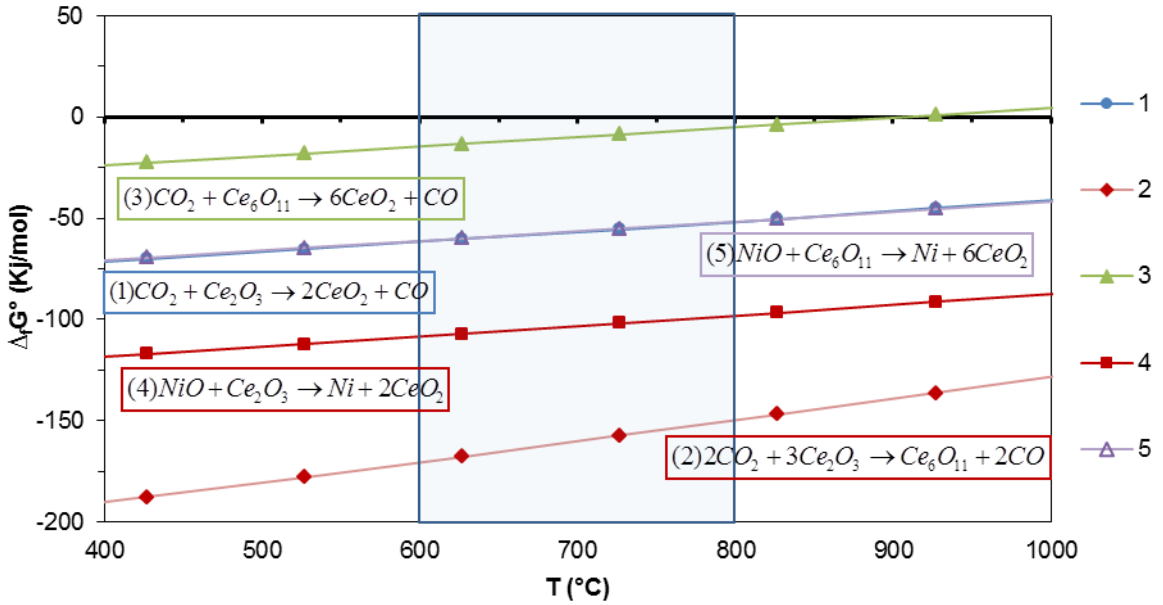

Fig 3.6 Gibbs free energy for the reoxidation of Ce_xO_y by CO_2

Obviously, the other main reaction to have a look is the capacity of CO_2 to reoxidize Ce_xO_y ***(1, 2, 3)***, which in all the cases is thermodynamically favorable at the working temperature range (600-800ºC). Moreover, the Ce_xO_y reoxidation is more feasible as lower is the reaction temperature. Nevertheless, the variation of the Gibbs free energy on the oxidation of Ce_6O_{11} to CeO_2 is really close to zero, so some thermodynamics limitations can be expected in this case. As a reference, Otsuka et al. [1.60] demonstrated that the reduced ceria on a Pt-CeO_2 catalyst can be reoxidized by CO_2. In addition, carbon reoxidation to CO by CO_2 (***Fig 3.1***) or CeO_2 (***Fig 3.4***) is also favorable above 700°C, an important fact in terms of stability. Otherwise, NiO and Ce_xO_y ***(4, 5)*** are always in favor of Ni reduction, which will maintain Ni in metallic state if no O_2 is present.

In summary, Ni-CeO_2 system appears to be a very good candidate for periodic feed DRM although is known to be a good catalytic solid towards CLC. The main difference is that in the case of the reoxidation by CO_2 NiO cannot be formed and CeO_2 acts as unique potential oxygen vector which is selective to syngas production.

3.2.3. Reduction by CH_4 and reoxidation by CO_2 of Co

Besides Ni, some other transition metals can have promising properties to work in a periodic and selective system. Concretely, Co is another transition metal tested in the experimental study as the same kind of thermodynamic behavior as nickel is shown.

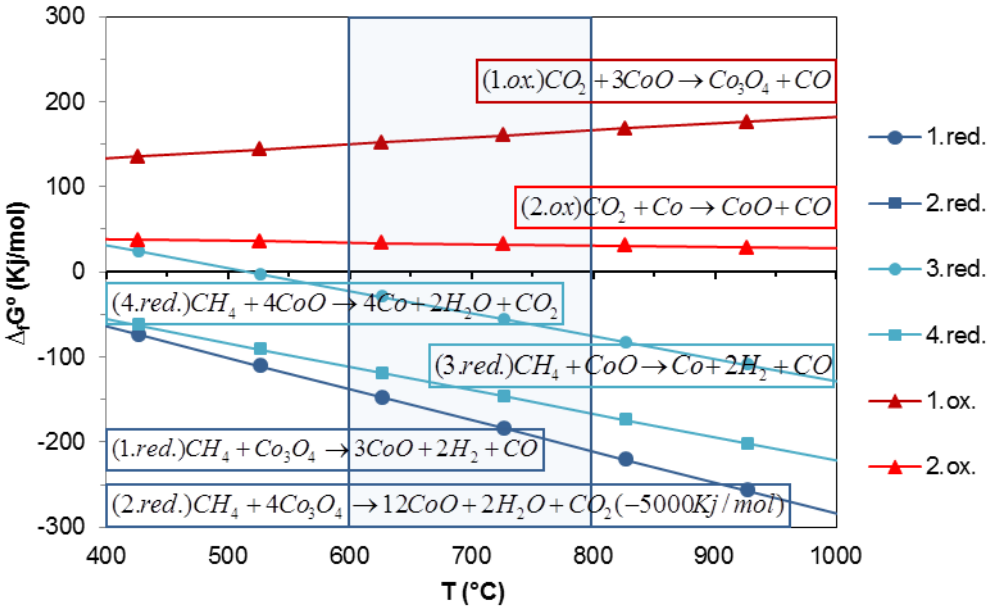

Fig 3.7 Gibbs free energy for the reduction of Co_xO_y by CH_4 and reoxidation by CO_2

The graph above is only focused on Co and their oxides as the behavior of CeO_2 has been already discussed in the previous ***Paragraph 3.2.1***. In this case, the two oxidized phases (Co_3O_4 and CoO) also react with CH_4 more favorably to produce H_2O and CO_2 (***2.red. and 4.red.***) than H_2 and CO (***1.red., 2.red.***). Otherwise, the same crucial property as nickel appears: the metallic state (Co^0) cannot be reoxidized neither towards CoO nor Co_3O_4 by CO_2 ***(1ox. and 2ox.)***. According to this behavior, R. Bouarab et al. [2.4] observed metallic Co in the XRD patterns of Co/SiO_2 catalyst after working under DRM conditions. In addition, C. Gennequin et al. [2.3] also obtained Co^0 after an experiment in DRM working with Co-Mg-Al and Co-Al based catalysts. Thus, this system is also expected to be selective thanks to the role of CeO_2 after the first stage of the reaction.

3.2.4. Reduction by CH_4 and reoxidation by CO_2 of Pt (Otsuka's process)

As mentioned in the introduction of the thesis ***(Paragraph 1.6.3)***, Otsuka et al. [1.60] were the first researchers to show the feasibility of working the DRM in periodic conditions. They used Pt-CeO_2 based catalyst, which makes sense looking at the thermodynamics of platinum having the same behavior as Ni and Co.

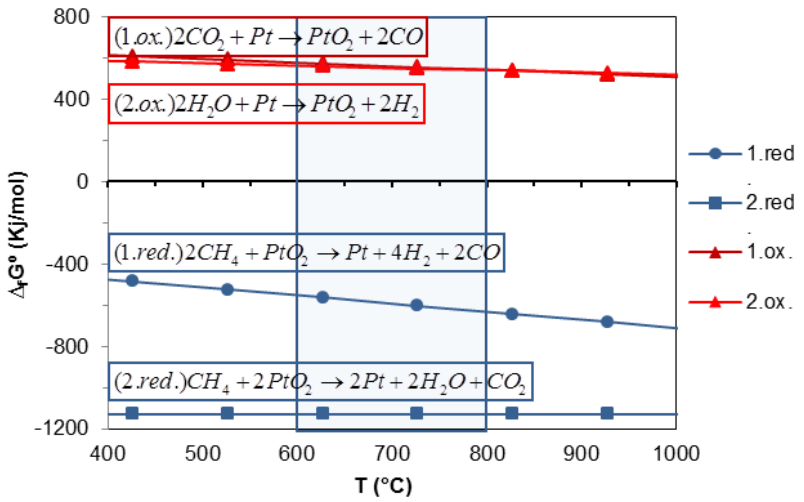

Fig 3.8 Gibbs free energy for the reduction of PtO_2 by CH_4 and oxidation of Pt by CO_2

First the reduction of PtO_2 to Pt by CH_4 is more favorable towards the unselective reaction ***(2.red.)*** than towards H_2 and CO ***(1.red.)***. Nonetheless, Pt cannot be reoxidized by CO_2 ***(1.ox.)*** to the unselective oxide, as so obtaining again a selective system thanks to the role of CeO_2. Obviously, the main difference with our system is the fact of using noble metals. Moreover, the absence of Pt reoxidation by vapor ***(2.ox.)*** is also shown in the ***Fig 3.8***. Some researchers studied the selective oxidation of methane for the SRM in periodic conditions, which works selectively thanks to the same concept. Otsuka et al. [1.60] also demonstrated experimentally the feasibility of the process reoxidizing the reduced Pt-CeO_2 catalyst by H_2O. On this way, V. Galvita et al. [1.29] studied the SRM process on Pt-CeO_2-ZrO_2, obtaining a selective system towards H_2 and CO with small amount of H_2O and CO_2 in the early stage of the reaction at each cycle.

3.2.5. Reduction by CH_4 and reoxidation by CO_2 of Fe

The thermodynamics calculations working with Fe were also made in order to show another possible pathway for this system.

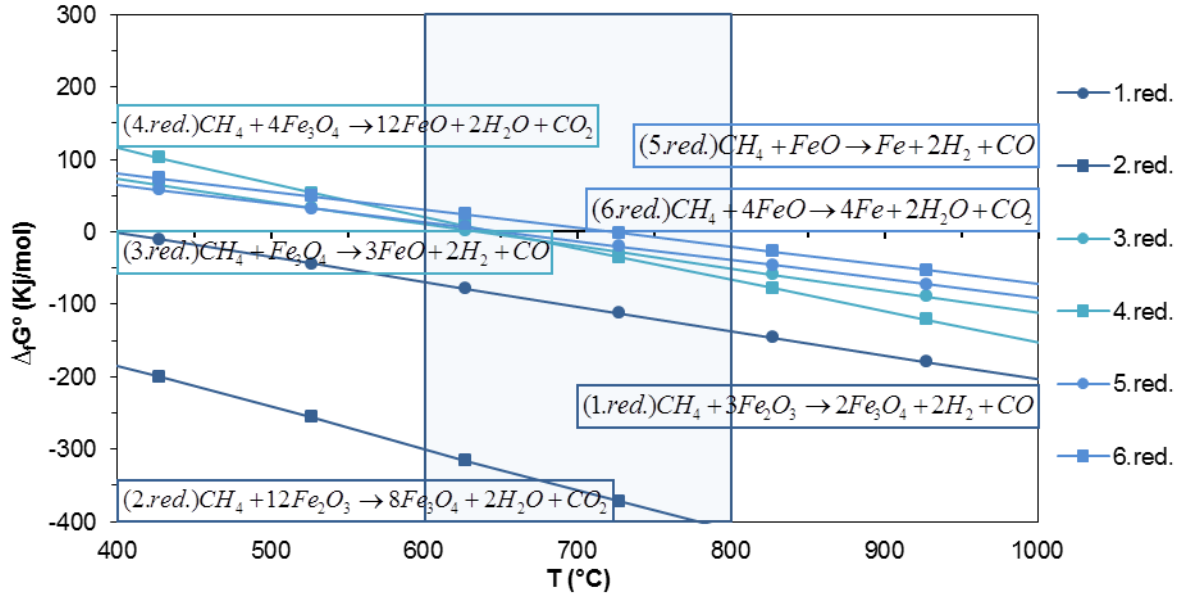

Fig 3.9 Gibbs free energy for the reduction of Fe_xO_y by CH_4

The study on Fe becomes more complex due to the wide range of oxidation states: Fe_2O_3, Fe_3O_4, FeO and Fe were taken for the calculations. First, the reduction of Fe_2O_3 to Fe_3O_4 seems favorable for the total oxidation of CH_4 ***(1.red. and 2.red.)***. Otherwise, the subsequent reduction of Fe_3O_4 to FeO towards the partial ***(3.red.)*** or total ***(4.red.)*** oxidation of methane has almost the same variation of the Gibbs free energy. As the total oxidation needs 4 mols of Fe_3O_4 ***(4.red.)***, probably at the first stage of this reduction the products would be H_2O and CO_2 to afterwards produce H_2 and CO ***(3.red.)***. Finally, the reduction of FeO to Fe has the same kind of behavior, producing potentially H_2O and CO_2 ***(6.red.)*** at first and then H_2 and CO ***(5.red.)***. Bhavsar et al. [1.54] showed nicely the oxidation of CH_4 within all the transition phases of Fe, from Fe_2O_3 to Fe with the corresponding products (***Fig 1.3***), obtaining CO_2 in all the steps.

Besides, the reoxidation of Fe by CO_2 is also important to know which iron oxide would be reached between the several possibilities (Fe_2O_3, Fe_3O_4 or FeO), as the subsequent selectivity of the methane oxidation would depend on that.

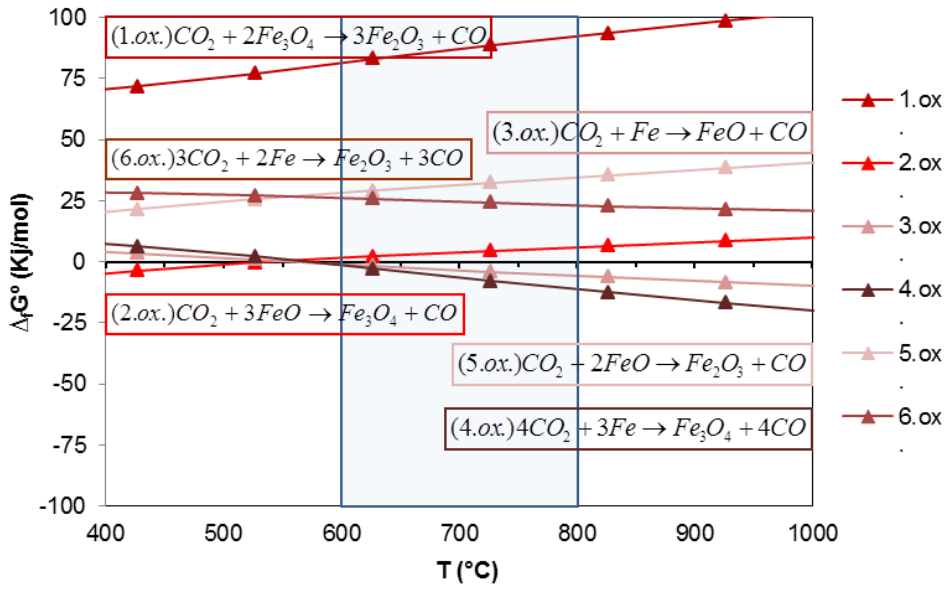

Fig 3.10 Gibbs free energy for the oxidation of Fe by CO_2

The reoxidation of Fe species with CO_2 does not seem to be straightforward because all the possible reactions have a variation of the Gibbs free energy really close to zero, so being difficult to assume which one would actually take place in the experiment. Fortunately, some researchers have already worked with Fe in periodic processes in order to know the potential redox system working with this metal. Bhavsar et al. [1.58] demonstrated that Fe species reduced by CH_4 can be reoxidized by CO_2 until Fe_3O_4 (***Fig 1.3***), as so without obtaining the total oxidation state Fe_2O_3. Besides, Zhu et al [2.10] showed that Fe/FeO species can be also reoxidized by H_2O until Fe_3O_4 working in the periodic SRM, observing a considerable amount of CO_2 at each initial stage for the reduction of CH_4. Therefore, the oxidation by CO_2 or H_2O seems to avoid reaching Fe_2O_3 species. However, the "selective" oxidation of the metal towards an oxide, which is not the initial one, is not enough to obtain a 100% selective system for Fe-based catalyst, producing at each time a mix of H_2O, CO_2, H_2 and CO.

3.2.6. Reduction by CH_4 and reoxidation by CO_2 of several metals (summary table)

The thermodynamic study of several metals and their oxides is shown in the following section. The aim is to show which ones could potentially work in the system proposed, being selective towards the partial oxidation of methane and having the capacity to be reoxidized by CO_2.

Table 3.1 Legend to summarize the function of each metal

Oxyd. CO_2	Red. CH_4	Sel. Red.	Activation	Function
+	+	+	+	Oxygen vector and Activation of CH_4 and CO_2
+	+	+	-	Oxygen vector
+	+	-	-	Non-selective system
-	+	-	+	Activation of CH_4 and CO_2
+	-		+	Activation of CH_4 and CO_2
-	+	-	-	Support/Additive
+	-		-	Support/Additive

The ***Table 3.1*** explains the legend used to classify each metal. Obviously, the sign "+" means YES and the sign "-" means NO (there are some cases which are evaluated as "+ -", meaning that the real behavior is difficult to predict). Then, the classification is based on different properties: if the reduced form can be oxidized by CO_2 (*Oxyd CO_2*), if the oxidized form can be reduced by CH_4 (*Red CH_4*) and if this reduction is selective towards the partial oxidation (*Sel. Red.*). Moreover, the last column shows if the metal specie can activate methane. The best case would be "++++" if the compound can work as oxygen vector and for the activation of the reactants, then "+++-" is the case where the oxide is available to provide oxygen in a selective pathway but without activating the reactants. The case "++--" means that the oxygen carrier provides oxygen in an unselective way, so for the total oxidation of CH_4. Then "-+-+" describes the compounds which activate CH_4 and CO_2 and can be reduced by CH_4 but cannot be reoxidized by CO_2, as so being interesting only for the activation process (typically the case of Ni, as shown previously). Another situation which gives a metal only for the activation is "+- +", meaning that such metal cannot be reduced by CH_4, but its oxide state is active towards the reactants. Finally, there are two other possibilities: (i) to work as a support or (ii) to be an additive compound because neither they activate the reactants nor they are available to work as an oxygen vector. The first one is "-+--" where the metal oxide is reduced by CH_4 but it cannot be reoxidized by CO_2 and the second one is "+- -" where, on the contrary, the oxide cannot be reduced by methane. Therefore, the following table was created based on this classification.

Table 3.2 Function of each metal according with the thermodynamics

Metal	Redox system	Thermodynamics			Activation	Function
		Oxyd. CO_2	Red. CH_4	Sel. Red.		
Ag	Ag_2O-Ag	-	+	-	+	Activation of CH_4 and CO_2
Al	Al_2O_3-Al	+	-		-	Support/Additive
Au	Au_2O_3-Au	-	+	-	+	Activation of CH_4 and CO_2
Bi	Bi_2O_3-Bi	-	+	-	-	Support/Additive
Cd	CdO-Cd	+-	+	-	-	Not interesting Cd (L) 321ºC
Ce	CeO_2-Ce_2O_3	+	+-	+	-	Oxygen vector
	CeO_2-Ce_6O_{11}	+	+	+	-	Oxygen vector
Co	CoO-Co	-	+	-	+	Activation of CH_4 and CO_2
Cr	Cr_2O_3-Cr_3O_4	+	-		+	Activation of CH_4 and CO_2
Cu	Cu_2O-Cu	-	+	-	?	?
Ir	IrO_2-Ir	-	+	-	+	Activation of CH_4 and CO_2
Fe	Fe_2O_3-Fe_3O_4	-	+	-	+	Activation of CH_4 and CO_2
	Fe_3O_4-FeO	+	+	+-	+	Oxygen vector and Activation of CH_4 and CO_2
La	La_2O_3-La	+	-		+	Activation of CH_4 and CO_2
Mg	MgO-Mg	+	-		-	Support/Additive
Mn	Mn_3O_4-MnO	-	+	-	+	Activation of CH_4 and CO_2
	MnO-Mn	+	-		+	Activation of CH_4 and CO_2
Mo	MoO_2-Mo	+	+-	+	+	Oxygen vector and Activation of CH_4 and CO_2
Nb	Nb_2O_5-NbO_2	+	+-	+	-	Oxygen vector
Ni	NiO-Ni	-	+	-	+	Activation of CH_4 and CO_2
Os	OsO_2-Os	-	+	-	+	Activation of CH_4 and CO_2
Pb	PbO_2-Pb	-	+	-	-	Not interesting Pb (L) at 327°C
Pd	PdO-Pd	-	+	-	+	Activation of CH_4 and CO_2
Pt	PtO_2-Pt	-	+	-	+	Activation of CH_4 and CO_2
Re	ReO_2-Re	-	+	-	+	Activation of CH_4 and CO_2
Rh	Rh_2O_3-Rh	-	+	-	+	Activation of CH_4 and CO_2
Ru	RuO_2-Ru	-	+	-	+	Activation of CH_4 and CO_2
Sb	Sb_2O_5-Sb	-	+	-	-	Not interesting Sb (L) at 630°C
Sc	Sc_2O_3-Sc	+	-		+	Activation of CH_4 and CO_2
Si	SiO_2-Si	+	-		-	Support/Additive
Sn	SnO_2-Sn	+-	+	-	-	Not interesting Sn (L) at 232°C
Ta	Ta_2O_5-Ta	+	-		-	Support/Additive
Ti	TiO_2-TiO	+	-		-	Support/Additive
V	V_2O_3-V	+	-		-	Support/Additive
W	WO_2-W	+	+-	+	+	Oxygen vector and Activation of CH_4 and CO_2
Y	Y_2O_3-Y	+	-		-	Support/Additive
Zn	ZnO-Zn	+	+-	+	-	Not interesting Zn (L) at 420°C
Zr	ZrO_2-Zr	+	-		-	Support/Additive

A lot of crucial information is reviewed in the table above. From one side, there are only three possible metals (Mo, Nb and W) which can work as oxygen vector within the 35 metals

studied, besides Ce and Fe (as seen in the ***Paragraph 3.2.1 and 3.2.5***). Molybdenum would work potentially between Mo and MoO_2 as CO_2 can only reoxidize the metal until such oxidation state. C. Shi et al [3.8] also confirmed this limitation. They observed the oxidation of Mo_2C to MoO_2 (instead of MoO_3) after a DRM experiment. Moreover Mo is reported to have low activity during the DRM [3.9], so the most promising combination would be a ternary catalyst formed by Ni (activation) and Mo (oxygen vector) on a high surface area support, such as Al_2O_3. Then Nb may work between Nb_2O_5 and NbO_2 at temperatures around 800ºC, where the variation of the Gibbs free energy becomes negative. In this case, there is no limitation from the oxidation point of view, as it is thermodynamically possible to oxidize Nb from the metallic state (Nb^0) to the total oxide (Nb_2O_5). The limitation appears in the reduction step by CH_4 due to it is only feasible between Nb_2O_5 to NbO_2 producing the syngas products (H_2 and CO). There is not much literature about methane reforming working with niobium. For instance, U.E.S. Amjad et al. [3.10] showed good performances working with a Ru-Mg-Nb based catalyst in the SRM. From there and the similar behavior of the catalyst working in SRM and DRM we can imagine the possibility of using Ni-Nb based catalyst for the DRM in periodic. Finally, tungsten should work between W and WO_2. As in some other cases, the oxidation by CO_2 has some limitations; in this case oxidizing W just until WO_2 instead of WO_3. In summary, the impregnation of Ni-Mo on γ-Al_2O_3 would be really interesting to test in further studies, as molybdenum is the cheapest oxygen vector between the 4 possibilities (Ce, Nb, Mo and W).

On the other hand there are quite a lot of solids to activate methane without interfering the selectivity of the reaction: some noble metals such as Ag, Au, Ir, Os, Pd, Pt, Re, Rh, Ru and some transition metals like Co, Cr, Cu, Mn, Mo, Ni, Sc, Ta and W. Within all of them and besides Ni, Co and Fe (already discussed), Cu on CeO_2 or in MoO_2 (in the last case with Al_2O_3) would be really interesting to consider as Cu is less expensive and more environmentally friendly than Ni. On the contrary, Cu is not well known for being active towards methane, so a binary Ni-Cu catalyst may be eventually necessary.

Finally, there are some solids which would work as a support or an additive such as Al, Bi, Mg, Si, Ta, Ti, V, Y and Zr. For instance some additives can improve the properties of some oxides, like the addition of Zr in CeO_2, creating more oxygen vacancies in the solid, so improving the diffusion of oxygen from the bulk to the surface, maybe being available to work at lower temperatures than 600-800ºC.

3.2.7. Approach to shale gas: Reduction by C_2H_6 and reoxidation by CO_2

The composition of the inlet flow can vary a lot according to the different potential raw material for this kind of reactions. Concretely, we explored the feasibility of the periodic process working with ethane due to the increase in the exploitation of shale gas in the recent years.

Shale gas is mainly composed by CH_4 (80-100%), but there is a remarkable part of ethane (1-20%). Thus, the thermodynamic calculations of the dry reforming of C_2H_6 is relevant to get a theoretical approach.

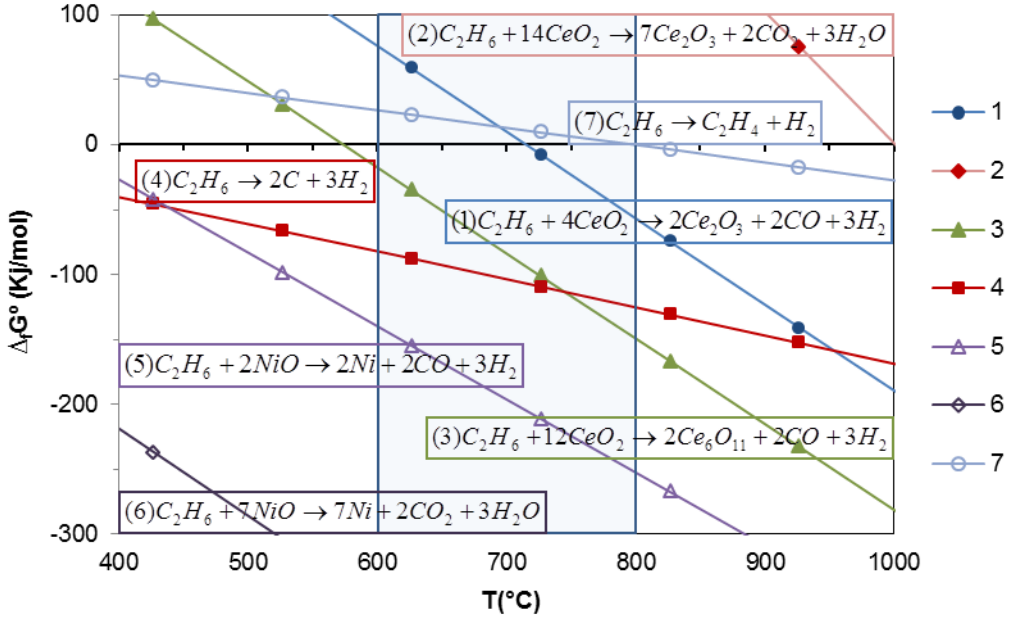

Fig 3.11 Gibbs free energy for the reduction of C_2H_6 on Ni-CeO_2 as a catalyst

The study on the variation of the standard Gibbs free energy shows that the behavior towards NiO would be the same as with CH_4, producing H_2O and CO_2 ***(6)*** instead of H_2 and CO ***(5)*** in the first cycles. Otherwise, the competition between the cracking of C_2H_6 ***(4)*** and the partial oxidation of ethane ***(3)*** would be more delicate than working with CH_4 as the decomposition of C_2H_6 to C and H_2 is thermodynamically more favorable. Furthermore, the oxidation of ethane is more favorable reducing CeO_2 to Ce_6O_{11} ***(3)*** instead to Ce_2O_3 ***(1 and 2)*** as in the case of methane. In addition, the dehydrogenation of ethane to ethylene ***(7)*** appears at 800ºC, adding another factor to take care for the selectivity of syngas.

In summary, the reforming of ethane towards syngas in periodic feed is possible although carbon deposition will probably contribute more extensively to the catalyst deactivation. However, it should be kept in mind that carbon can be periodically reoxidized by CO_2. This approach gives further perspectives for the development of the periodic dry reforming of ethane (P-DRE) or mixtures of methane and ethane (shale gas) without previous separation of the hydrocarbons.

3.3. Conversion at the equilibrium

The theoretical maximum conversion of CH_4 is interesting to compare with experimental values. The cofeed system has some thermodynamic limitations (shown in the ***Paragraph 2***), so a study of the expected conversion was carried taking into account the equilibrium of the

reaction. Even though the aim of periodic is to avoid the equilibrium state, a transient equilibrium could be reached depending on the step time. Thereby, the calculations are also made for the alternative feed. The procedure to calculate these conversions was extracted from the book *"Introduction to Chemical Engineering Thermodynamics"* [3.4]. See ***Paragraph 7.3*** for more details about the calculations.

3.3.1. DRM and P-DRM

The study was made for the main reactions in cofeed and periodic, reacting CH_4 with CO_2 or Ce_xO_y, obtaining the following results.

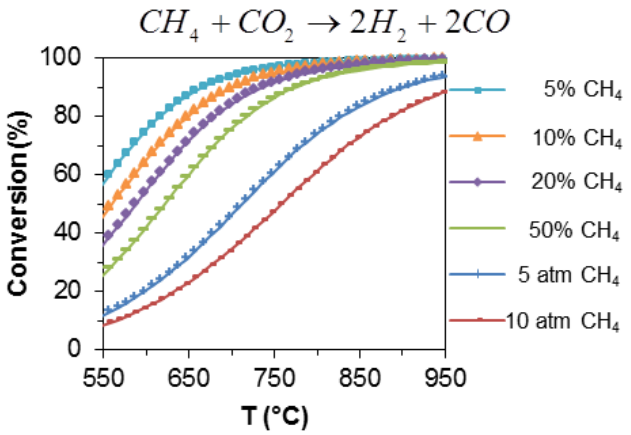

Fig 3.12 Equilibrium conversion at different T, initial concentrations and pressures on DRM

Cofeed DRM (***Fig 3.12***) shows for all the cases thermodynamic limitations to reach 100% conversion. From one side, the dilution of the reactants with an inert gas has a big influence on the equilibrium. The higher is the dilution the higher can be the final conversion. Besides, the influence of working at high pressures is also checked, obtaining lower conversions as higher is the pressure, obviously as four gas molecules are produced whereas two are consumed. Y. Takahashi et al. [3.11] studied the dry reforming at different pressure obtaining the same type of trend. Concretely, they investigated mesoporous Pt/SO-ZrO_2, which showed higher methane conversion at 1 atm (17%) than at 10atm (7%) at 530°C. These values are in good agreement and really close to the maximum conversion shown in the figure above (at 550°C). M. Haghighi et al. [3.3] also calculated the theoretical conversion of CH_4 working at different pressures, showing the negative influence of increasing the total pressure of the system. As in the figure above, the conversions were lower at 5, 10 and 50atm than at 1atm.

In another hand, the periodic DRM is also affected by thermodynamic limitations which can be modified according to the nature of the solid or the redox couple.

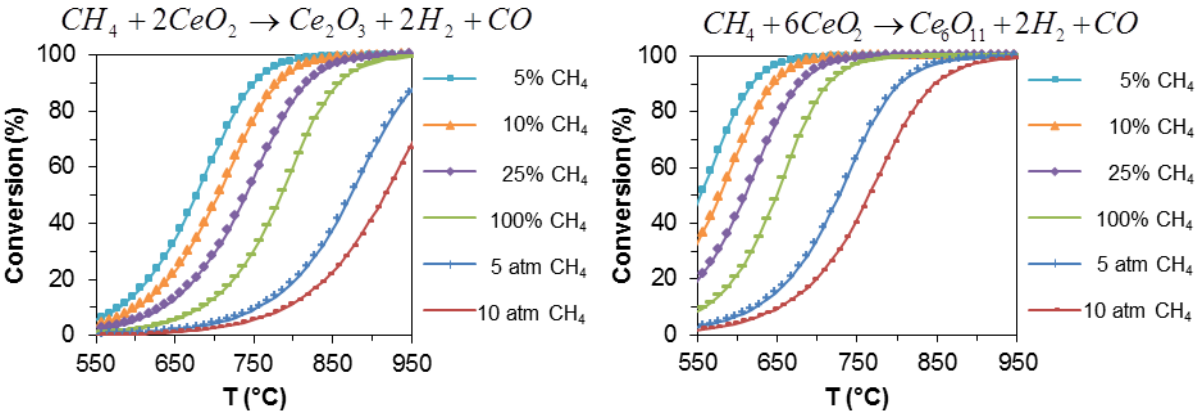

*Fig 3.13 Equilibrium conversion at different T, initial concentrations and pressures on periodic DRM over (**left**) CeO_2 to Ce_2O_3 and (**right**) CeO_2 to Ce_6O_{11}*

In this case, CeO_2 shows more thermodynamic restrictions towards Ce_2O_3 (***Fig 3.13 (left)***) rather than Ce_6O_{11} (***Fig 3.13 (right)***).

Otherwise, Nb, Mo and W oxides have been evidenced as other potential candidates, besides Ce for the P-DRM (***Paragraph 3.2.6***). Therefore the equilibrium conversions are also calculated for the following reactions:

$$2CH_4 + MoO_2 \rightarrow Mo + 4H_2 + 2CO$$

$$CH_4 + Nb_2O_5 \rightarrow 2NbO_2 + 2H_2 + CO$$

$$2CH_4 + WO_2 \rightarrow W + 4H_2 + 2CO$$

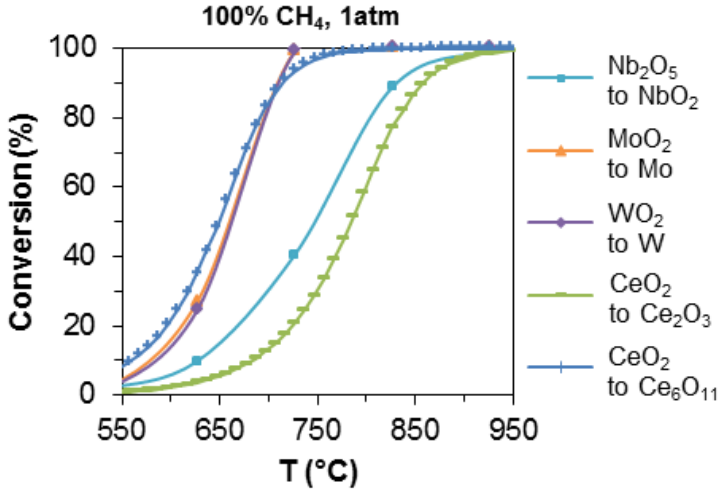

Fig 3.14 Equilibrium conversion at different T, initial concentrations and pressures on periodic DRM over Nb, Mo, W and Ce

Fig 3.14 shows that the most favorable oxides to provide oxygen to the system are Ce (from CeO_2 to Ce_6O_{11}), Mo and W, obtaining an almost identical behavior for the last two cases. These calculations show the importance of the nature of the solid respect to the thermodynamic limitations working in periodic feed. This is obviously not the case in cofeed

where only reactant and product of DRM intervene in the calculations. Such behavior opens new perspectives for the optimization of the periodic process at high pressures as it may be possible to modify the solids in order to improve the thermodynamics of the system.

3.3.2. Side reactions: RWGS, Cracking of CH_4, oxidation of C

The maximum theoretical conversions of the different side reactions were also calculated to have a better understanding about the potential behavior of the whole system.

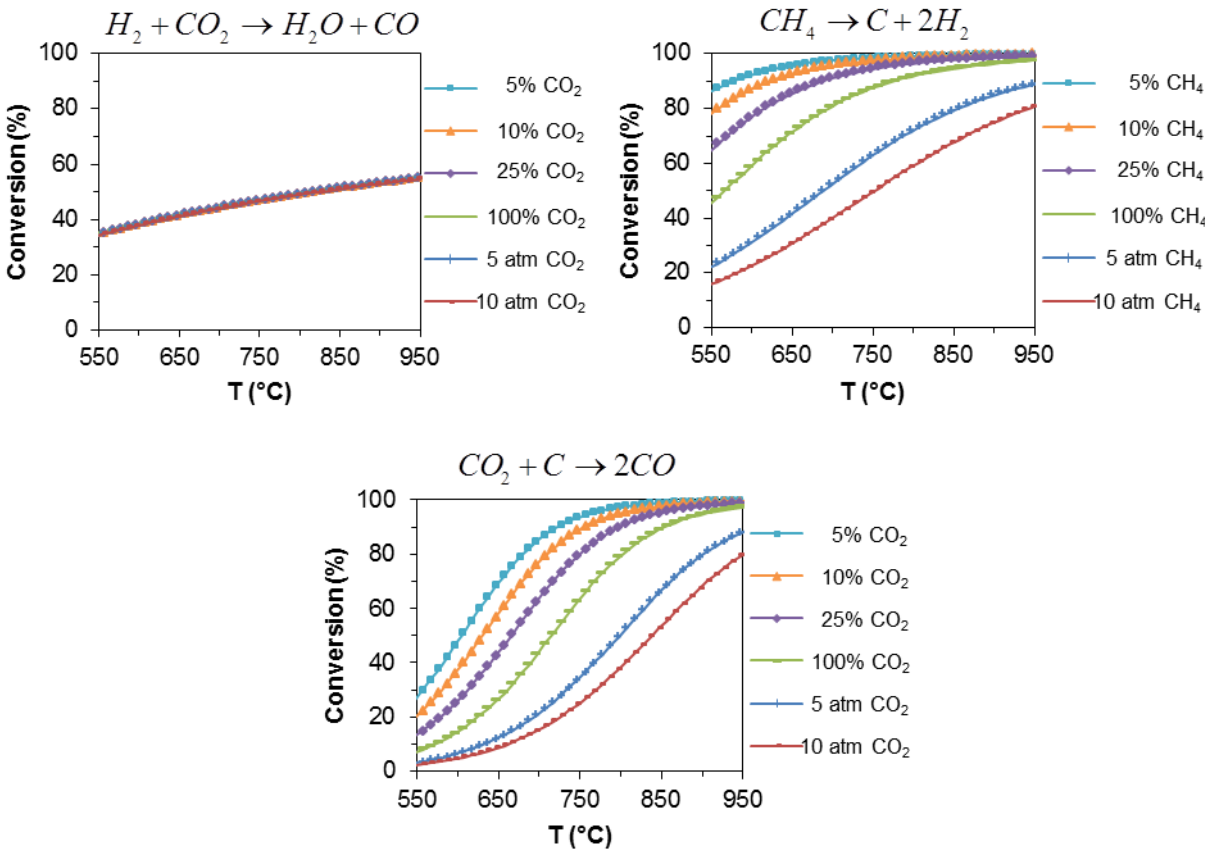

*Fig 3.15 Equilibrium conversion at different T, initial concentrations and pressures on the RWGS (**Top left**), the cracking of CH_4 (**Top right**) and the Boudouard reaction (**Bottom center**)*

From one side, the conversion of the reactants in the RWGS (***Fig 3.15 (Top left)***) is obviously not affected whatever the concentration or the pressure is on the system, as v = 0 (equal amount of moles in the inlet and in the outlet). The same values were obtained by D.H. Kim et al [1.18] who showed a theoretical 38% conversion of CO_2 at 600°C based on the thermodynamic consideration. The data calculated by K. Oshima et al can also corroborate our values, they showed a conversion around 35% at 527°C which is really close to the 37% at 550°C illustrated in the figure above. In addition, the results show why the RWGS becomes more important as higher is the initial concentration of CH_4 and CO_2. From one side the equilibrium conversion of DRM decrease (***Fig 3.14 (Bottom center)***) but from the other side the conversion of RWGS remains at the same level (***Fig 3.15 (Top left)***). Therefore, it appears a

stronger competition between the two. Otherwise, the decomposition of methane (***Fig 3.15 (Top right)***) follows the same trend as the DRM, obtaining some limitations at high initial concentration of CH_4. In this case, A.M. Amin [1.20] also studied the thermodynamic of this reaction showing the same sort of values, such as 60% conversion of CH_4 at 600°C (working with 100% CH_4 in the inlet flow at 1atm). The trend of this reaction is really important to know as the DRM in periodic at the same conditions gives theoretically a maximum conversion of 20% (***Fig 3.14 (Bottom center)***). Thereby, the production of carbon would be potentially more favorable in such case. Finally, the oxidation of C by CO_2 (***Fig 3.15 (Bottom center)***) has also some thermodynamic limitations at the equilibrium, another important reason to avoid the steady state process.

3.3.3. Reoxidation of Ce_xO_y by CO_2

Finally, the thermodynamic limitations of CO_2 in the reoxidation step are studied for the two potential cases (Ce_2O_3 or Ce_6O_{11}).

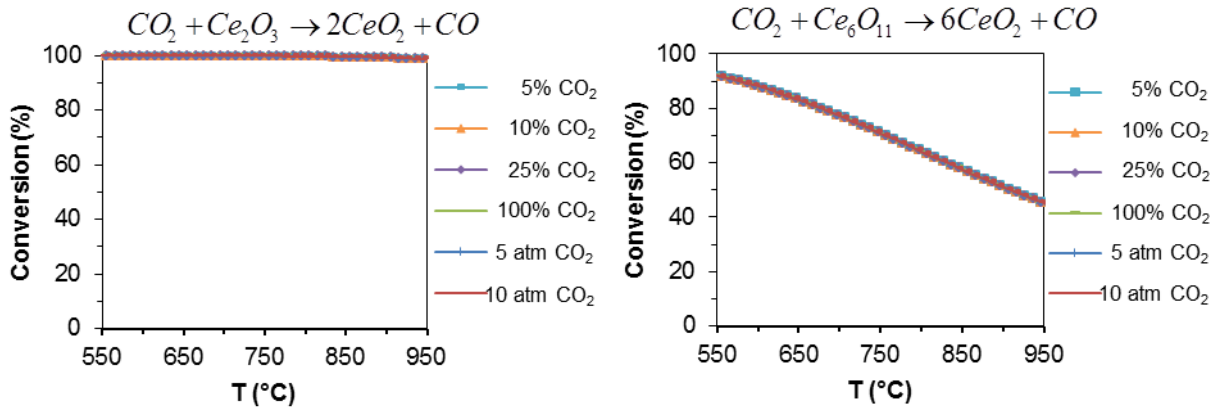

Fig 3.16 Equilibrium conversion at different T, initial concentrations and pressures on the oxidation of Ce_2O_3 ***(left)*** *and Ce_6O_{11}* ***(right)*** *by CO_2*

First, the oxidation of Ce_2O_3 by CO_2 (***Fig 3.16 (left)***) does not have any equilibrium limitations towards CeO_2, behavior which is corroborate for other researchers [4.11, 3.13]. On the contrary, the oxidation of Ce_6O_{11} to CeO_2 by CO_2 would have some limitations in the steady state, as shown in the ***Fig 3.16 (right)***. Obviously neither of the two reactions is affected by CO_2 partial pressure.

The study on this ***Paragraph 3.3*** is interesting to know the behavior of each reaction separately, but for the experimental point of view where all the reactions occur at the same time, another method is considered by several researchers to involve all the products and sub products in the calculations (typically H_2, CO, H_2O and/or C). R. Bouarab et al. [2.4] calculated the theoretical conversion of CH_4 and CO_2 for 50% initial concentration at 600ºC obtaining 43% and 56% respectively, considering H_2O as another product (besides H_2 and CO) and using the

Gibbs free energy minimization method. Really close to those values, C.N. Ávila-Neto et al. [3.5] found a theoretical conversion of 38% for methane. Otherwise, J.P. Dacquin et al [2.16] calculated a thermodynamic equilibrium of 58% and 66% conversion of CH_4 and CO_2 with a ratio $H_2/CO=0.73$. On this way, M. Abdollahifar et al. [3.6] are in good agreement with data shown by J.P. Dacquin. They also obtained around 58% and 66% conversion for CH_4 and CO_2 and H_2/CO ratio of 0.73 (based on the minimization of the Gibbs free energy). Probably, the high conversion obtained in the last two cases is due to the consideration of the carbon formation (the compounds considered are not specified in the scientific papers). Some other researchers have shown the same kind of calculations but working with an inert gas as a diluent. M. Haghighi et al. [3.3] calculated the maximum conversion by the same procedure (using the Chemkin software) and considering C, C_2H_2, C_2H_4, C_2H_6 (besides CH_4, CO_2 and H_2O) with an initial concentration of 10%, reaching 63% conversion of CH_4 and $H_2/CO = 0.86$ at 600°C. Identical to this study, A. Pietraszek et al. [3.12] calculated the theoretical CH_4 conversion (software ProSim Plus) using a stream made by CH_4/CO_2/Inert (v.%) = 10/10/80 and reaching the same value as Haghighi, 63%.

3.4. Conclusions

Several important clues can be extracted from this third chapter. The first one is that unfortunately for our target of making pure syngas, a lot of side reactions can occur thermodynamically at the working temperature range, being the concurrence between them much stronger at low temperatures (notably at 600°C) than at high temperatures. For instance, this competition is verified showing a higher amount of H_2O produced at 600°C than 800°C in cofeed conditions.

Otherwise, the production of H_2O and CO_2 on the initial stage of the cofeed experiment is in good agreement with the reduction of NiO to Ni^0 by CH_4, which is thermodynamically more favorable to produce the total oxidation of the hydrocarbon than the partial oxidation. In such context, the unfeasible reoxidation of Ni by CO_2 is a key property to keep the system selective after the first minutes of the experiment. This type of correlation is also translatable to the periodic system, as shown in the thermodynamic calculations. Moreover, the comparison between the two processes (cofeed and periodic) show the same kind of trend on the Gibbs free energy and the same maximum conversion in the “steady state”. Nevertheless, such limitation would not be reached if the transient equilibrium is avoided in the periodic process.

The thermodynamic difference of various intermediate ceria oxides is shown between CeO_2, Ce_6O_{11} and Ce_2O_3. The most feasible pathway to oxidize methane is from CeO_2 to Ce_6O_{11}. This variation shows the marge of improvement from the thermodynamic point of view working with a solid as oxygen vector instead of CO_2.

The reason about the 100% selectivity working with Ni, Co or Pt seems to be the absence of reoxidation of those metals by CO_2. On the contrary, the thermodynamic on the reduction of the Fe_3O_4 by CH_4 explains why some H_2O and CO_2 are produced at each step working with this metal.

The wide study of the reduction by CH_4 and oxidation by CO_2 of 35 metals shows from one side that there are really few ones (4) which can work as an oxygen vector for the DRM in periodic (Ce, Nb, Mo and W) and from the other side that there are quite a lot (17) which would activate methane keeping a good selectivity towards syngas at the same time. As usual, the transition metals would be the most interesting due to their lower cost and higher availability than the noble ones. Within all the combinations, Ni-Mo-Al, Ni-Cu-Ce and Ni-Cu-Mo-Al seem to be the most promising to verify experimentally in further studies.

Then, the study on the conversion at the equilibrium allows to know if the experimental results are close or not to this limitation. Otherwise, the absence of variation of CO_2 conversion for the RWGS working at different conditions and the decrease of activity for the DRM at high initial concentrations and high pressures could explain why the influence of the undesired reaction is higher as the initial concentration of CH_4 and CO_2 increased. Moreover, this study also shows the importance of working in periodic to avoid some constraints at the steady state, such as the thermodynamic limitations on the reduction of CeO_2 and the oxidation of carbon and Ce_6O_{11}. In addition, the possibility of changing the thermodynamics limitations modifying the solid opens the path for further optimization of the process.

Finally, the thermodynamics working with C_2H_6 demonstrate the potential feasibility of applying the same concept to this gas, even though a process without any carbon formation would be more difficult to obtain than in the case of CH_4.

3.5. References

3.1 Alloy phase diagrams. Volume 3. Committees, ASM International Alloy Phase Diagram and the Handbook (**1992)**

3.2 C. Bale, E. Bélisle, P. Chartrand, S. Decterov, G. Eriksson, K. Hack, I. Jung, Y. Kang, J. Melançon, A. Pelton, C. Robelin, S. Petersen, "www.factsage.com" FactSage Thermochemical Software and Databases - Recent Developments, Calphad, 33 **(2009)** 295-311 [Online] [Accessed 2013-2015]

3.3 M. Haghighi, Z.Q. Sun, J.H. Wu, J. Bromly, H.L. Wee, E. Ng, Y. Wang, D.K. Zhang, On the reaction mechanism over a bed of coal char *P. Combust. Inst.* 31 **(2007)** 1983-1990

3.4 Introduction to Chemical Engineering, 5th edition. J.M. Smith, H.C. Van Ness, M.M. Abbott **(1997)**

3.5 C.N. Ávila-Neto, S.C. Dantas, F.A. Silva, T.V. Franco, L.L. Romanielo, C.E. Hori, A.J. Assis, Hydrogen production from methane reforming: Thermodynamic assessment and autothermal reactor design *J. Nat. Gas Sci. Eng.* 1 **(2009)** 205-215

3.6 M. Abdollahifar, M. Haghighi, A.A. Babaluo, Syngas production via dry reforming of methane over Ni/Al_2O_3-MgO nanocatalyst synthesized using ultrasound energy *J. Ind. Eng. Chem.* 20 **(2014)** 1845-1851

3.7 Y.H. Taufiq-Yap, Sudarno, U. Rashid, Z. Zainal, CeO_2-SiO_2 supported nickel catalysts for dry reforming of methane toward syngas production *Appl. Catal. A* 468 **(2013)** 359-369

3.8 C. Shi, A. Zhang, X. Li, S. Zhang, A. Zhu, Y. Ma, C. Au, Ni-modified Mo_2C catalysts for methane dry reforming *Appl. Catal. A* 431-432 **(2012)** 164-170

3.9 T. Hirose, Y. Ozawa, M. Nagai, Preparation of a nickel molybdenum carbide catalyst and its activity in the dry reforming of methane *Chinese J. Catal.* 32 **(2011)** 771-776

3.10 U.E.S. Amjad, G.G. Lenzi, N.R.C. Fernandes-Machado, S. Specchia, MgO and Nb_2O_5 oxides used as supports for Ru-based catalysts for the methane steam reforming reaction *Catal. Today* 257 **(2015)** 122-130

3.11 Y. Takahashi, T. Yamazaki, Behavior of high-pressure CH_4/CO_2 reforming reaction over mesoporous Pt/ZrO_2 catalyst *Fuel* 102 **(2012)** 239-246

3.12 A. Pietraszek, B. Koubaissy, A.C. Roger, A. Kiennemann, The influence of the support modification over Ni-based catalysts for dry reforming of methane reaction *Catal. Today* 176 **(2011)** 267-271

3.13 J.H. Earley, R.A. Bourne, M.J. Watson, M. Poliakoff, Continuous catalytic upgrading of ethanol to n-butanol and >C_4 products over Cu/CeO_2 catalysts in supercritical CO_2 *Green Chem.* 17 **(2015)** 3018

CHAPTER IV:

Dry reforming of CH_4 in non-steady state regime

4. DRY REFORMING OF CH_4 IN NON-STEADY STATE REGIME

4.1. Introduction

The second part of this thesis is focused on working DRM in periodic conditions. Indeed, it has been shown in the previous chapter that the insurmountable thermodynamic barrier of cofeed DRM could be overcome by working in a complete different concept, as the thermodynamics properties would depend on the CH_4-solid and CO_2-solid reactions and not exclusively on the gas phase reactants/products equilibrium. Besides this feature, working in periodic feed also can have important effects on the selectivity, e.g. avoiding RWGS, as explained in the introduction (***Paragraph 1.7.2***).

4.1.1. Catalyst considered for DRM in periodic: M-CeO_2

One of the key factors working in periodic conditions is to provide oxygen from the solid to react with CH_4, as seen in ***Paragraph 1.5*** and ***1.6***. Therefore, the redox property is required to bring oxygen during the feed of methane and recover it during the reoxidation by carbon dioxide. Besides, the system needs to be selective towards syngas. This will certainly depend on the nature of the oxygen vector but can also depend on the diffusion rate of oxygen which needs to be optimal for the partial oxidation. If the rate is too high the total oxidation of methane can take place producing H_2O and CO_2, on the contrary, if it is too slow some carbon deposition can be produced from the decomposition of methane. From all the potential candidates viewed in the literature for SRM in periodic such as Cu-Fe / YSZ [1.32], Fe / CeO_2 [1.31]… and notably for DRM in periodic like Fe / CeO_2 [1.58], Fe / BHA and Fe /SiO_2 [1.57] and Pt-CeO_2 [1.60], metal-CeO_2 based catalysts were chosen to carry the process in the present work. Concretely, S. Bhavsar et al. [1.58] already worked with Fe-CeO_2, but the main difference from their approach is that the main oxygen reservoir consists on the iron oxide species while we consider CeO_2 as the main oxygen provider. Thus, the redox system using CeO_2 as the oxygen carrier would be as follows:

Eq. 4.1 $$CH_4 + 2CeO_2 \xrightarrow{\Delta H<0} 2H_2 + CO + Ce_2O_3$$

Eq. 4.2 $$CO_2 + Ce_2O_3 \xrightarrow{\Delta H>0} CO + 2CeO_2$$

The rare earth oxide ceria (CeO_2) has the property required for this system, the solid release oxygen under reduction conditions forming Ce_2O_3 (Ce^{3+}), which turns easily to CeO_2 (Ce^{4+}) taking up oxygen under oxidizing conditions. From the catalytic point of view, the oxygen from the bulk migrates up to the supported metal particle and oxidizes the adsorbed species on the metal [4.6].

At this point the oxygen amount released in the conversion from CeO_2 to Ce_2O_3 is important to know. The structure of Ce_2O_3 can be constructed out of eight unit cells of CeO_2 with 25% oxygen vacancies ordered in a particular way [4.7].

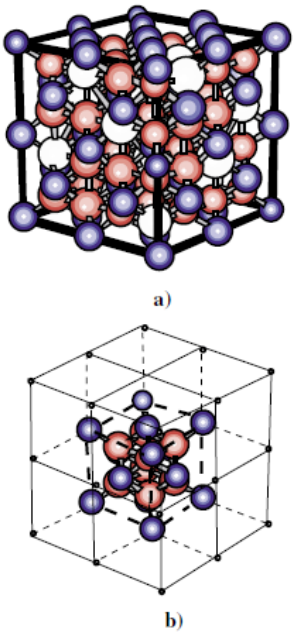

FIG. 1 (color). Lattice unit cells for Ce_2O_3 (*C*-type) (a) and CeO_2 (b). A cubic unit cell of *C*-type Ce_2O_3 can be constructed out of eight CeO_2 unit cells by increasing their volume by 3% and removing 25% of the oxygen atoms along four noninter-secting ⟨111⟩ diagonals. Blue, red, and white spheres indicate the cerium, oxygen atoms, and vacancies, respectively.

Fig 4.1 Structure of CeO_2 and Ce_2O_3 [4.7]

Another key factor of the system is the ability to reoxidize the reduced ceria by CO_2. Several hypotheses have been made about the feasibility of the re-oxidation of Ce_2O_3 to CeO_2 by carbon dioxide. From the thermodynamic point of view the reaction is favorable at 25°C up to more than 1000°C [4.8]. Otherwise, the main constrains comes from the slow kinetics at low temperatures, even using noble metals to accelerate the process. Li et al. [4.9] attributed the activation of CO_2 on CeO_2 to the rapid formation of carbonates and carboxylates species on partially reduced CeO_{2-x}, which could remain on the surface of the solid up to 500ºC. However, some other studies concluded that CO_2 can be directly dissociated to CO and active oxygen species by the metal-ceria catalyst, donating oxygen to a lattice vacancy and producing CO, which is totally desorbed at around 450ºC [4.5,4.20]. In addition, Jin et al. [4.10] observed in a Temperature Programmed Desorption for CO_2 on Pt (2 wt.%) / CeO_2, the production of CO around 280°C (the catalyst was pre-reduced under H_2). Moreover, Sharma et al. [4.11] noted that the oxidation of ceria by CO_2 was negligible in measurements using Pd / ceria at 200°C, implying that indeed there are kinetic limitations to its oxidation by carbon dioxide. Nevertheless they demonstrated that at 350ºC the catalyst is somehow reoxidized. CO was produced when a pulse of CO_2 was fed on the reduced CeO_2 (the CeO_2 was pre-reduced by

CO). In addition O. Demoulin et al. [4.5] showed that pure CO_2 is capable to oxidize reduced (under H_2) $Pd/Ce_{0.21}Zr_{0.79}O_2$ catalyst at 300°C. Nevertheless, the key factor is again the kinetics of the oxidation, as 34min. is necessary to oxidize completely the solid (instead of 12min. under O_2 and 46min. under He). Otherwise, Staudt et al. [4.12] claimed that CO_2 is activated in the defect sites of ceria, even without noble metals, if the concentration of Ce^{3+} is high enough. Finally, one of the most interesting studies for our research was the one of Otsuka et al. [1.60], which showed almost total reoxidation of CeO_2 by CO_2 at 450°C with the formation of CO (after been reduced by CH_4 at 700°C), getting a recovery degree of about 82%.

In summary, from all the approaches mentioned above it seems that the reoxidation of CeO_{2-x} by CO_2 can be possible at the working conditions of our experiments. Therefore, Fe-CeO_2, Co-CeO_2, Ni-CeO_2 (different loadings and preparation methods) and Ni-Ce-Zr-O based catalysts were chosen to work in the periodic concept. In addition, Ni-Mg-Al-O catalyst was also studied in order to see the feasibility of using MgO as oxygen carrier.

4.2. Catalysts characterization

Different physico-chemical characterizations have been performed for the catalysts mentioned above. All the experimental setup and solids described in the chapter dedicated to cofeed (see ***Paragraph 2.2.2***) were also used for the periodic process. Besides, three other catalysts were studied for the periodic reaction. The characterization of all of them is presented as follows.

Table 4.1 Ni loading, surface area and main crystallite size of the different catalysts

		Atomic ratio			
Catalyst	wt.% M	Ni / M_T	S_{BET} (m^2/g)	d_{M-O} (nm)	d_{CeO2} (nm)
CeO_2	-	-	53	-	6
Ni(2.1)/CeO_2	2.1	0.06	27	n.o.	12
Ni (8.8) / CeO_2	8.8	0.22	29	16	11
Ni(9.5) / CeO_2	9.5	0.24	32	18	10
Ni (10.5) / CeO_2	10.5	0.26	35	-	-
Ni(38.5)/CeO_2	38.5	0.65	33	21	12
Co (7.2) / CeO_2	7.2	0.19	28	16	10
Fe(10.4) / CeO_2	10.4	0.26	73	n.o.	10
Ni (7.9) / CeO_2(com)	7.9	0.20	9	n.o.	38
$CeNi_{0.3}Oy$	7.9	0.23	79	n.o.	5
$CeNi_{0.5}Zr_{0.5}O_y$	Ni: 9.9 // Zr: 14.1	0.25	129	n.o.	$d_{CeNi0.5Zr0.5}$: 4
$Ni_1Mg_2AlO_y$	21.9	0.24	127	4	-

n.o. = not observed

The ***Table 4.1*** shows the main characteristics of the catalysts including those already presented in ***Chapter 2***. Two catalysts synthesized by impregnation with 2.1 wt.% and 38.5 wt.% Ni (following the method explained in ***Paragraph 2.2.1***) are also used in the periodic

experiments. Moreover, a ternary Ni-Ce-Zr-O based catalyst, which is synthesized by coprecipitation following a method developed in the laboratory [4.19], is also tested in the following experiments.

XRD

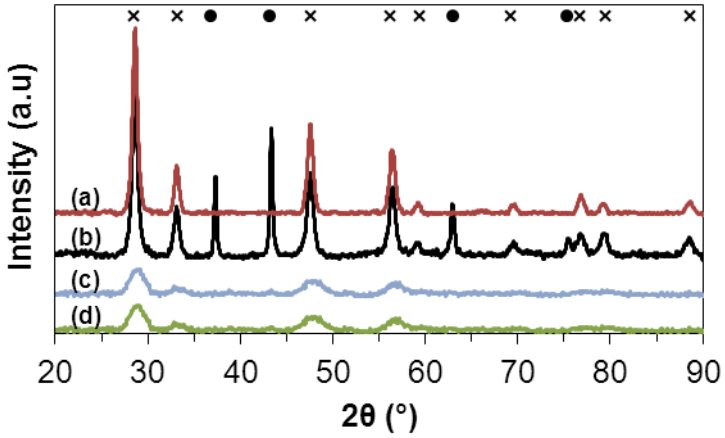

Fig 4.2 XRD patterns for (a) Ni(2.1)/CeO_2, (b) Ni(38.5)/CeO_2, (c) CeO_2, (d) $CeNi_{0.5}Zr_{0.5}O_y$ x CeO_2 and/or $CeNi_{0.5}Zr_{0.5}O_y$ mixed oxide ● NiO

The X-ray diffraction patterns of Ni(2.1)/CeO_2, Ni(38.5)/CeO_2, CeO_2 and $CeNi_{0.5}Zr_{0.5}O_y$ are shown in ***Fig 4.2*** evidencing characteristic fluorite structure of CeO_2 in the four cases. Otherwise, no phase related to the presence of Zr has been observed for the fourth catalyst. From another side NiO is not observed at the low nickel content. As for Ni(7.9)/CeO_2(com) (***Paragraph 2.2.2***), it can be concluded that the particles are well dispersed and the crystal size is too small to be detected or/and the particles are amorphous. On the contrary, narrow peaks are observed for NiO using 38.5 wt.% Ni, even at 75.4° (besides the ones at 36.8°, 43.2° and 63.1°), peak which was not observed for the other catalysts (Ni(9.5)/CeO_2, Ni(10.5)/CeO_2…). This forth peak indicates that at high loading of nickel is easier to obtain the whole XRD pattern of NiO, probably due to a big crystal size. Indeed 21nm is obtained for NiO crystals in Ni(38.5)/CeO_2 instead of 16nm for Ni(8.8)/CeO_2 and 18nm for Ni(9.5)/CeO_2. Nevertheless, the same crystal size of CeO_2 (12nm) is obtained at high (38.5%) and low (2.1%) loadings of nickel. In addition the surface area of the catalysts are really similar, 27 m^2/g for Ni(2.1)/CeO_2 and 33 m^2/g for Ni(38.5)/CeO_2 to the ones observed for Ni(8.8)/CeO_2 (29 m^2/g) and Ni(9.5)/CeO_2 (32 m^2/g). Thereby, the loading of nickel, at least even up to 38.5%, does not seem to affect the total surface area of the catalyst using the impregnation method.

TPR

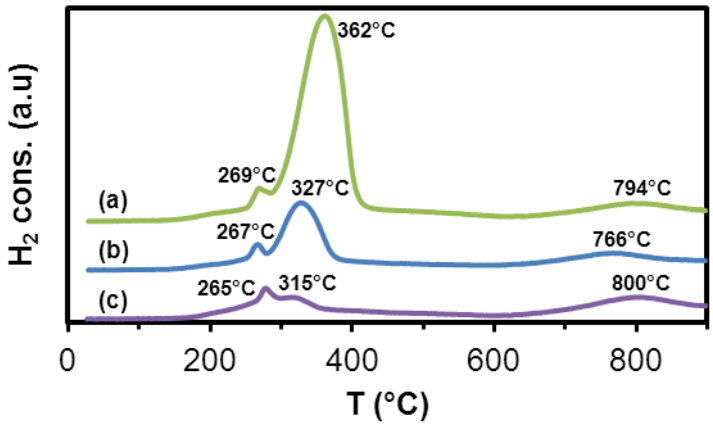

Fig 4.3 TPR profile of (a) Ni(38.5)/CeO_2, (b) Ni(9.5)/CeO_2, (c) Ni(2.1)/CeO_2 under 10% H_2 / N_2 gas

The temperature programmed reduction (TPR) of Ni(38.5)/CeO_2, Ni(9.5)/CeO_2 and Ni(2.1)/CeO_2 shows interesting trends for the reduction of nickel. Large NiO crystallites seems to be more difficult to reduce as the main peak related to the reduction of nickel shifts from 315°C for Ni(2.1)/CeO_2, going to 327°C for Ni(9.5)/CeO_2 (18nm NiO) and 362°C for Ni(38.5)/CeO_2 (21nm NiO). Otherwise, the peak found around 268°C could be attributed to the presence of the Ni species in very small NiO crystallites and/or in a solid solution between Ni and Ce [4.4]. Besides, the peaks of the ceria reduction are at 760-800°C.

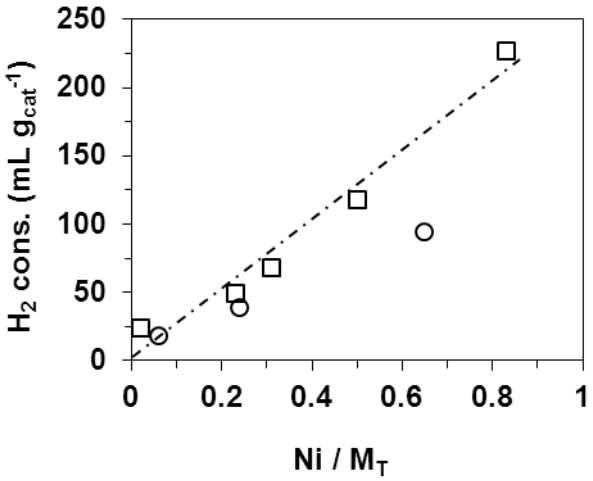

Fig 4.4 H_2 consumption in TPR as a function of the Ni content of (□) $CeNi_XO_Y$ nanocompounds [1.43] and (o) Ni(x)/CeO_2 catalysts

A linear relationship appears between the total H_2 consumption and the nickel content for catalysts synthesized by impregnation, as in the previous study made in the laboratory on the same type of ceria. The values fit well with the other study except at the highest loading of 38.5 wt.% Ni (Ni/M_T=0.65).

4.3. Catalytic test

4.3.1. Catalytic performance

The catalytic performance (25 – 400 mg) test was conducted under atmospheric pressure in a fixed-bed quartz reactor fitted in a programmable oven. The gas stream of CH_4/He/Ar (5-25/x/y %v) named reductant step and CO_2/He/Ar (5-25/x/y %v) named oxidant step was fed to the reactor (F_T = 100 mL/min). The stoichiometric molar ratio CH_4/CO_2 was maintained at 1 while varying the reactant concentration. The outlet gases were analyzed online by a mass spectrometer (MS). The influence of different parameters has been studied such as the Ni loading, reaction temperature, the initial concentration of the reactants, the nature of the active metal and the influence of the support. The following paragraphs show some of the most representative results. It is mainly reported the conversion of each reactant integrated on a full cycle, which should be the same in the best of the cases, and the H_2/CO ratio during the reductant step. Ideally, such ratio would be equal 2. The different values take into consideration to evaluate the selectivity of the reaction are explained in detail in the annex (***Paragraph 7.1.3.9 - 7.1.3.11***). Each experiment is made by 12 complete cycles. Typically, a cycle 1/2/1/2 includes 1min. CH_4, 2min. Ar, 1min. CO_2 and 2min. Ar., obtaining a 72 minutes experiment. The values shown on the tables come from the average of the last 4 cycles. There are also some experiments made by 60 cycles in order to show the stability of the process. An exhaustive description of the set up and the treatment of the raw data from the mass spectrometer are given in the annex (***Paragraph 7.1***).

4.3.2. Activity of CeO_2 towards periodic DRM

The role of the CeO_2 without an active metal was investigated. The experiments were carried at 700°C, 750°C and 800°C. The performance obtained at 800°C is shown in the following figures. The other two experiments are not shown as the activities were negligible.

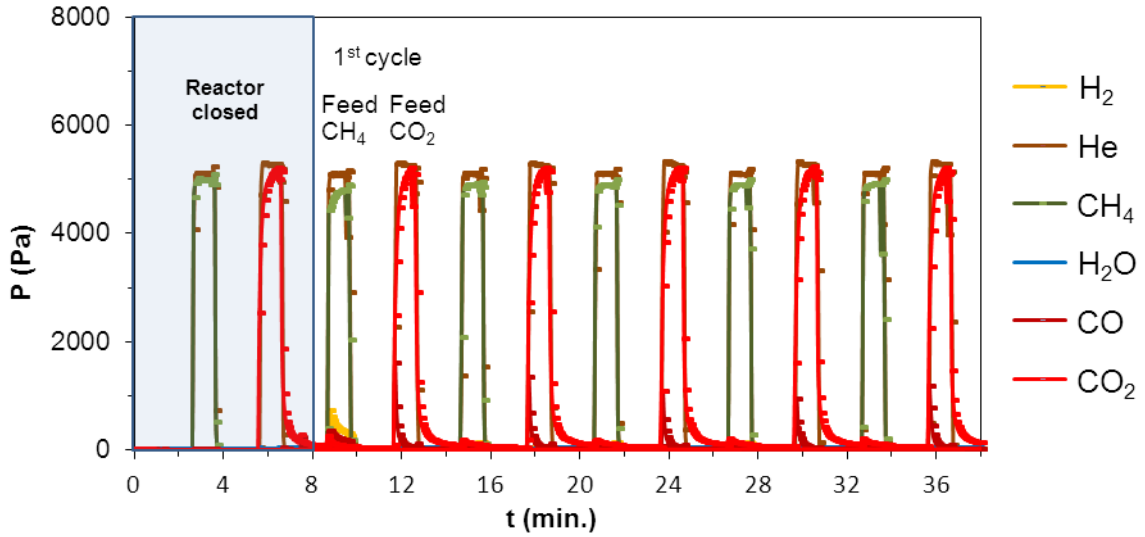

Fig 4.5 Partial pressures in the outlet flow working with 150mg of CeO_2 at 800°C $F_{T,0}$ = 100 mL/min. Cycle: 1/2/1/2. 5% CH_4, 5 % CO_2

The ***Fig 4.5*** shows the partial pressures in the outlet of the reactor. From there, it can be seen that the partial pressure of CH_4 goes to almost the nominal value in each reductant step. Concretely, the conversions of CH_4 and CO_2 are around 0.5-1%. A zoom on the partial pressures is necessary to verify the residual compounds produced.

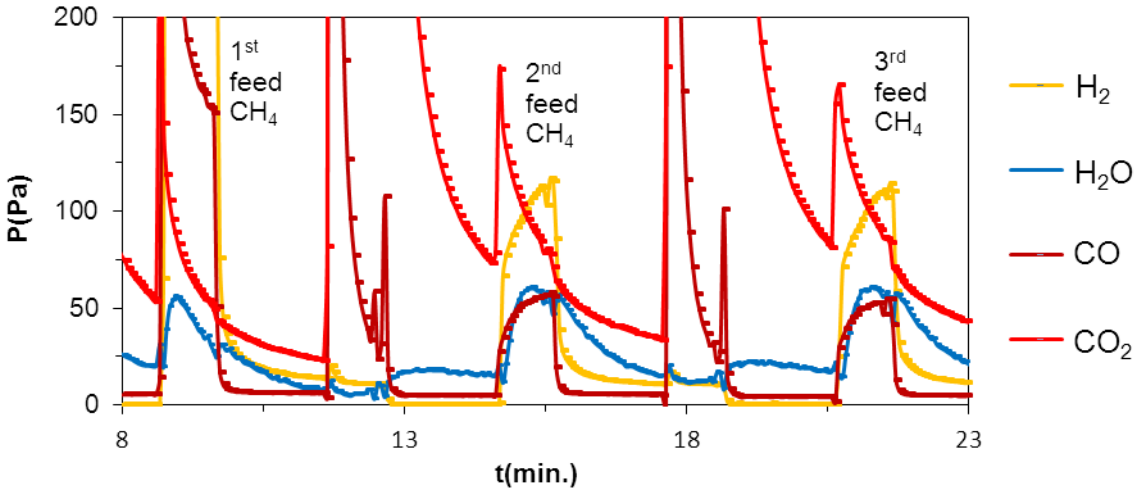

Fig 4.6 Partial pressures of H_2, H_2O, CO and CO_2 in the outlet flow, zoom from ***Fig 4.5***

The ***Fig 4.6*** shows the partial pressures of H_2, CO, CO_2 and H_2O. Even though the really low conversion of CH_4, it is interesting to see the products proportion. A mix between H_2 and CO (from the partial oxidation) and H_2O and CO_2 (from the total oxidation) is produced. Interestingly, this kind of behavior is in good agreement with the thermodynamics shown in the complete study of Ce (***Paragraph 7.2.1***). The partial and total oxidation of CH_4 (within the redox couple CeO_2-Ce_6O_{11}) is thermodynamically favorable and with ΔG quite near to each other at 800°C. Such thermodynamics can explain the mix of products seen during the experiment.

Besides, these results show the importance of the active metal (Ni, Co…) in the catalyst. Obviously, the excellent redox property of CeO_2 is useless for our reaction if there is not a good activation of the reactants.

4.3.3. Ni/CeO_2

For the sake of clarity one representative experiment for the well-working periodic process is shown and explained in detail. First, the partial pressures of the different compounds along the whole experiment are represented in the following figure.

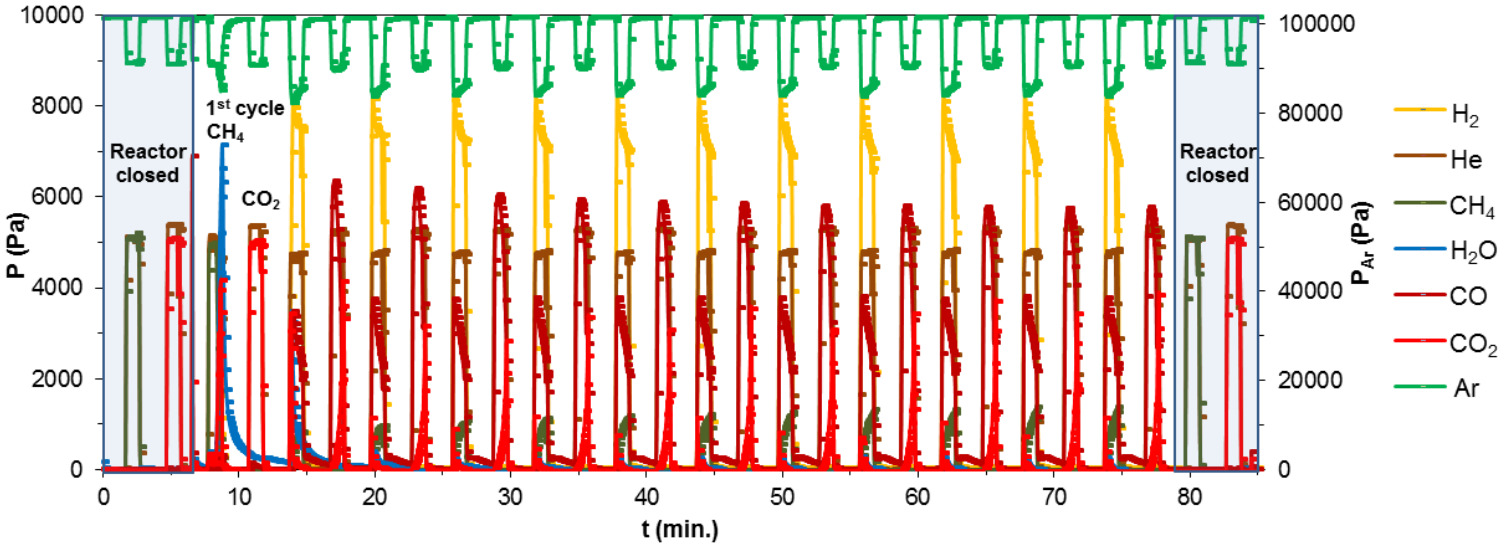

Fig 4.7 Partial pressures in the outlet flow working with 200mg of Ni(8.8)/CeO_2 (0.1-0.2mm) + 100mg SiC at 700°C $F_{T,0}$ = 100 mL/min. Cycle: 1/2/1/2. 5% CH_4, 5 % CO_2

Following the ***Fig 4.7*** from the left to the right, firstly one step of CH_4 and one of CO_2 are fed to the system with the reactor closed in order to calculate different valuable data for the calculations (see annex ***Paragraph 7.1.3.2***). Then, the experiment starts showing a different behavior for the first redox cycle in respect to the following. From one side, a considerable amount of H_2O and CO_2 is produced during the reductant step (CH_4). From the other side, the oxidant step (CO_2) shows an almost negligible variation on the partial pressure of CO_2, so without production of CO. This interesting behavior will be explained in detail in the ***Paragraph 4.3.8***. Then the following cycles become almost 100% selective towards H_2 and CO during the reductant steps with an almost negligible production of H_2O and CO_2. Finally, the same procedure of feeding CH_4 and CO_2 when the reactor is closed it is made at the end of the experiment.

Then, ***Fig 4.8*** shows a zoom in the last two cycles of the experiment in order to verify the excellent reproducibility from one cycle to the other.

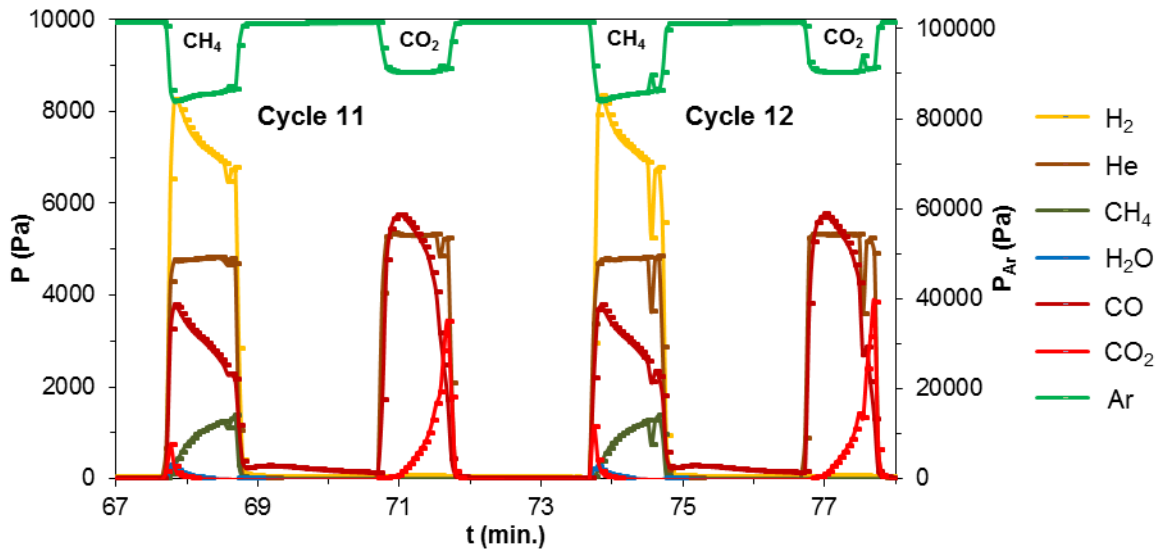

Fig 4.8 Partial pressures in the outlet flow, zoom of the ***Fig 4.7***

First, H_2 and CO are produced majorly during the reductant step with a really small contribution of H_2O and CO_2. Then, the same production of H_2 and CO is obtained for the two cycles showing a remarkable reproducibility between the two, even after 10 cycles. In addition, the production of CO decreases progressively during the reductant step which can be due to a lack of oxygen in the carrier. However, the amount of oxygen in CeO_2 (2064 µmoles) is largely enough to react with the CH_4 feed (205 µmoles). Even considering the redox couple between CeO_2 and Ce_2O_3 where only 25% of the oxygen in CeO_2 is released, the oxygen available is still high (516 µmoles). This would discard the hypothesis that the decrease in CO is due to the depletion of oxygen in ceria. Otherwise, the CO_2 partial pressure does not reach the nominal value of 5000 Pa during the oxidant step. Probably, CO_2 needs more time to reoxidize completely the Ce_xO_y species at the given working conditions. As expected, there is also an important production of CO during this step due to the reoxidation of Ce_xO_y species and eventually some carbon deposited during the reductant step.

Otherwise, a graph with the main values of conversion and selectivity is shown as follows. Concretely, the properties from the reductant step in the cycle 1 are shown above the number 1 along the x-axis, but differently, the properties for the oxidant step in the cycle 1 are shown above the number 1.5 along the x-axis to make the difference between the two and do not get confused with classic results of DRM in cofeed. In addition, the ***Fig 4.9*** shows the values taking into account the whole step (Ex. Total moles of CH_4 inject to the system in the 1 minute step – total moles of CH_4 out along the 1 minute).

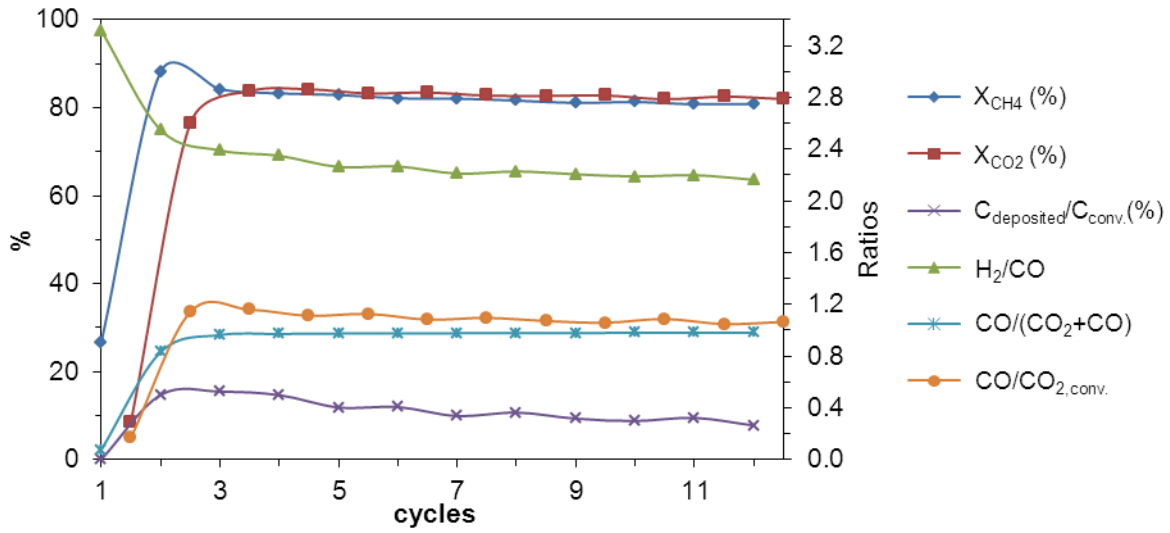

Fig 4.9 ***Reductant step:*** *Conversion of CH_4 (%), $C_{deposited}/C_{conv.}$(%), H_2/CO and CO/(CO_2+CO) ratios.* ***Oxidant step:*** *Conversion of CO_2 (%) and CO/$CO_{2,conv}$. ratio. 200mg of Ni(8.8)/CeO_2 (0.1-0.2mm) + 100mg SiC at 700°C $F_{T,0}$ = 100 mL/min. Cycle: 1/2/1/2. 12 cycles, 5% CH_4, 5 % CO_2*

As expected from the ***Fig 4.7***, there is an evolution of the conversion between the first cycle and the following ones. During the first cycle 28% conversion of CH_4 and only 9% of CO_2 are obtained. Then, the two of them become stable around 80% until the end of the experiment. Besides, H_2/CO ratio goes from 3.2 in the first cycle to 2.2 in the last one. Even though H_2/CO is equal 3.2, the ratio CO/(CO_2+CO) is almost zero, meaning that there is no or negligible production of CO. Therefore the H_2/CO value at that first cycle is not relevant as it would come from some residual production of CO. Otherwise, some real trends about the selectivity between H_2, CO, H_2O and carbon deposit become more coherent from the cycle 2. The CO/(CO_2+CO) ratio goes close to 1 (0.98), which corroborates the small production of CO_2 during the selective cycles. Then, the $C_{deposited}/C_{conv.}$ (%) goes down from 15% in the cycle 2 to 8% in the cycle 12, at the same time the H_2/CO ratio goes also down from 2.5 to 2.2. Logically this trend makes sense, less cracking of methane occurs in the system, less production of hydrogen would come from this reaction. In addition, the low deposition of carbon during the reductant step is also corroborated thanks to the $CO/CO_{2,conv.}$ ratio obtained in the oxidant step, which goes around 1.1. Such value means that almost all the CO_2 reoxidized the ceria species and only a small amount was used to oxidize the carbon deposit (see ***Paragraph 7.1.3.10*** for an explanation in detail about $CO/CO_{2,conv.}$ ratio).

Moreover, the following figure shows the instantaneous conversion in order to follow the behavior of the reactants within the step.

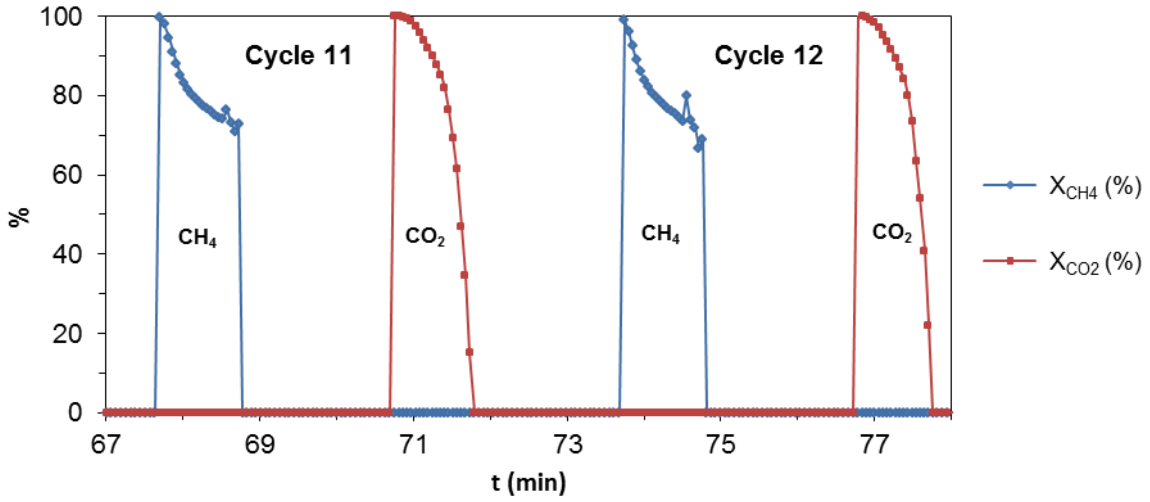

Fig 4.10 ***Reductant step:*** *Instantaneous conversion of CH_4 (%)* ***Oxidant step:*** *Instantaneous conversion of CO_2 (%) in the last two cycles*

The ***Fig 4.10*** shows that the conversion of CH_4 goes from 100% to around 70% evidencing the dynamic behavior of the periodic process. Probably, the kinetics is faster when ceria is totally reoxidized and then it is slower as the oxygen reservoir starts to decrease. In addition, the fact of obtaining 100% conversion at the beginning of the reductant step in each cycle reinforces the advantage of working in a dynamic process from the thermodynamic point of view, as the limitations are more difficult to reach than working in cofeed (stationary state). From the other side, the CO_2 conversion goes almost to zero at the end of the oxidant step. This trend is favorable for our interest. CO_2 conversion going to zero would mean that all the species are already reoxidized, as so the optimization about using the minimum amount of CO_2 is quite close. Therefore, this experiment is a good opportunity to compare the mass balance on the catalyst towards oxygen and carbon in the whole cycle.

Table 4.2 Catalyst mass balance of oxygen and carbon for the last four cycles of the experiment

	Oxygen (µmols)			Carbon (µmols)		
Cycle	MB.R	MB.O	MB.T cycle	MB.R	MB.O	MB.T cycle
9	-152	165	**13**	15	-13	**2**
10	-153	152	**-1**	14	-17	**-3**
11	-151	166	**15**	15	-11	**5**
12	-154	158	**3**	13	-13	**-1**

MB.R : Mass Balance in Reductant step

MB.O : Mass Balance in Oxidant step

MB.T : Mass Balance in the whole cycle

The ***Table 4.2*** shows the mass balance of oxygen out – oxygen in (the same for carbon) in the catalyst during the two steps of the last four cycles. The µmoles of oxygen released in the reductant step are around the same as the ones insert during the oxidant step. In addition, the µmoles of carbon deposit during the reductant step are oxidized during the feed of CO_2. Mass

balances on the catalyst confirm the hypothesis about CO_2 being capable to oxidize at the working conditions the two species desired, the reduced ceria and the eventual carbon deposit.

In an overall view, this paragraph has shown the principles and the procedures that we follow to process and understand the data of the different experiments in periodic. Besides, the experiment shown demonstrates the feasibility of working in such conditions even at 700ºC, obtaining promising conversions and selectivity.

4.3.4. Stability test

The stability of the process was checked on $Ni(8.8)/CeO_2$ and $CeNi_{0.3}O_y$ catalysts. 60 cycles (4h using a cycle 1/1/1/1) were carried at 800°C in order to obtain a longer stability test than the typical 12 cycles experiment.

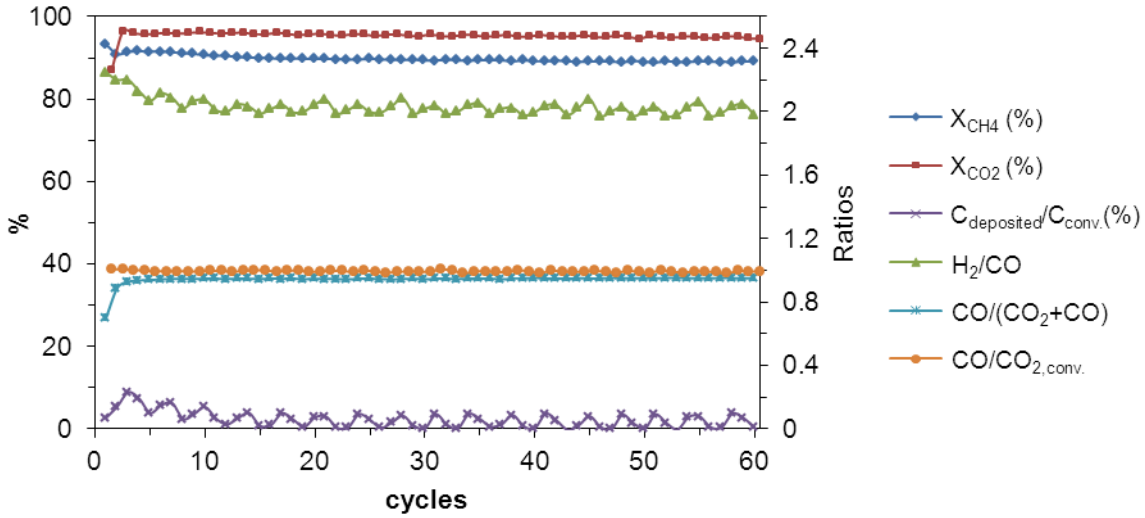

Fig 4.11 ***Reductant step:*** *Conversion of CH_4 (%), $C_{deposited}/C_{conv.}$(%), H_2/CO and $CO/(CO_2+CO)$ ratios.* ***Oxidant step:*** *Conversion of CO_2 (%) and $CO/CO_{2,conv.}$ ratio. 200mg of $CeNi_{0.3}O_y$ at 800°C $F_{T,0}$ = 100 mL/min. Cycle: 1/1/1/1, 5% CH_4, 5 % CO_2*

The ***Fig 4.11*** shows the performance working with the coprecipitated catalyst. The conversion of CH_4 goes up to 89% while the one of CO_2 reaches 95%. In addition, around 100% selectivity is found obtaining H_2/CO = 2.0, $CO/(CO_2+CO)$ = 0.96 and $C_{deposited}/C_{conv.}$ = 0-2%. The performance underlines clearly the feasibility of DRM in periodic conditions with the advantages associated on it, such as avoiding the RWGS.

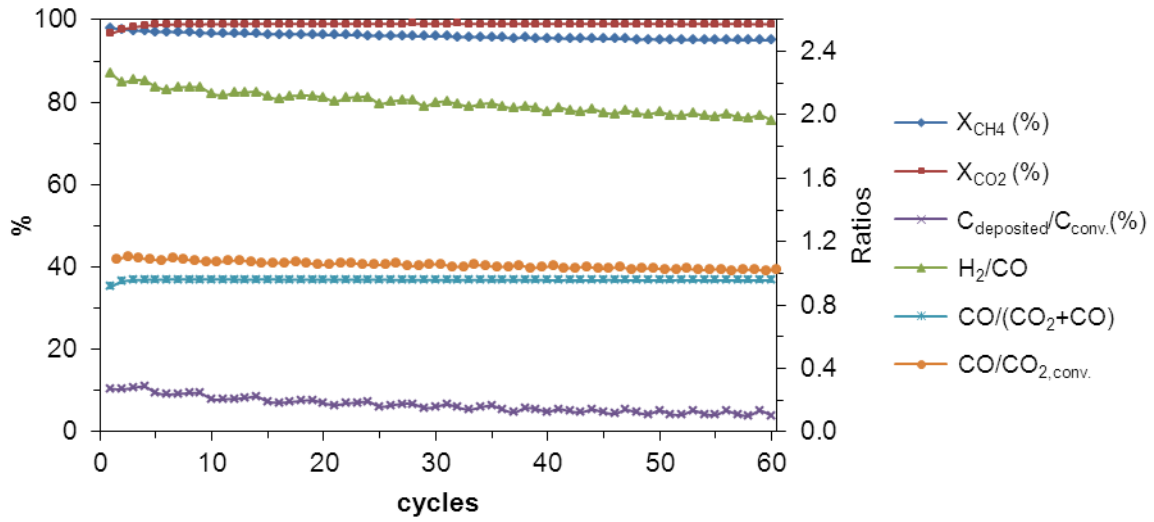

Fig 4.12 ***Reductant step:*** *Conversion of CH_4 (%), $C_{deposited}/C_{conv.}$(%), H_2/CO and $CO/(CO_2+CO)$ ratios.* ***Oxidant step:*** *Conversion of CO_2 (%) and $CO/CO_{2,conv.}$ ratio. 200mg of Ni(8.8)/CeO_2 (0.1-0.2mm) + 100mg SiC at 800°C $F_{T,0}$ =100 mL/min.Cycle:1/1/1/1,5% CH_4,5 % CO_2*

In addition, the ***Fig 4.12*** shows the performance working in this case with the impregnated catalyst. The same promising results are obtained for Ni(8.8)/CeO_2. Concretely, the conversion of CH_4 is 95% and the one of CO_2 99%. About selectivity, H_2/CO = 2.0, $CO/(CO_2+CO)$ = 0.96 and $C_{deposited}/C_{conv.}$ = 4%. The performance is thus very near to the coprecipitated catalysts. The fact of using 100mg of SiC, so increasing the catalytic bed can be an explanation of the improvement in conversion from the experiment shown in the ***Fig 4.11***.

25% initial concentration

The stability tests shown up to now are made working with $[CH_4]_0$ = 5%. Even if it is already a great success to prove the periodic concept at such stage, an experiment with higher concentrations ($[CH_4]_0$ = 25%) was carried to know if we can prove such behavior at higher scale.

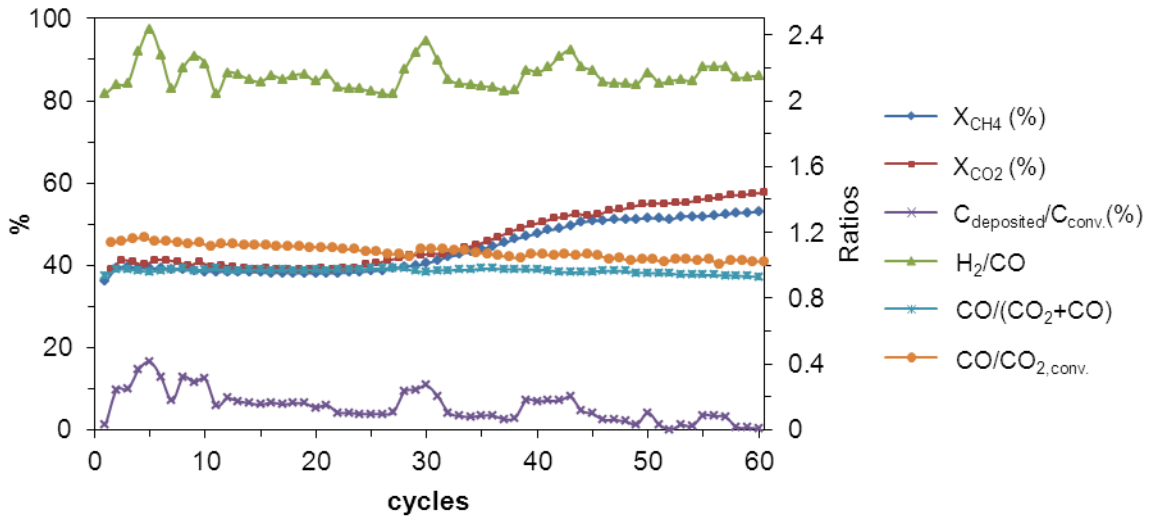

Fig 4.13 ***Reductant step:*** *Conversion of CH_4 (%), $C_{deposited}/C_{conv.}$(%), H_2/CO and $CO/(CO_2+CO)$ ratios.* ***Oxidant step:*** *Conversion of CO_2 (%) and $CO/CO_{2,conv}$. ratio. 400mg of $Ni(9.5)/CeO_2$ at 800°C $F_{T,0}$ =100 mL/min.Cycle:1/1/1/1, 25% CH_4, 25 % CO_2*

The ***Fig 4.13*** shows some interesting behaviors. The evolution of the conversion along the experiment (from 40% at the beginning of the experiment to 53% at the end) indicates that the performance of the system can be improved with an adequate activation of the catalyst. The working conditions are somehow beneficial for the activation of the solid. Besides, in terms of selectivity the results are quite close to ideal ones and are not affected by the evolution in conversion. In this case the H_2/CO = 2.2, $CO/(CO_2+CO)$ = 0.94 and $C_{deposited}/C_{conv.}$ = 1-2%. These results are encouraging for the perspective of looking forward in an industrial process. Even if the results are not as good as working with 5% concentration, they are quite close in terms of almost pure H_2 and CO production. Therefore, the matter of obtaining higher conversion than 50% would be an issue of reducing the step time (if the conversion decreases through the time as in the case of working with 5% initial concentration) or/and increasing the amount of catalyst.

4.3.5. Influence on the working temperature

The working temperature is another key factor for the feasibility of the process, as the temperature plays a crucial role towards the oxygen diffusion from the bulk to the surface of the catalyst. The values below are again the average of the last four cycles of each experiment.

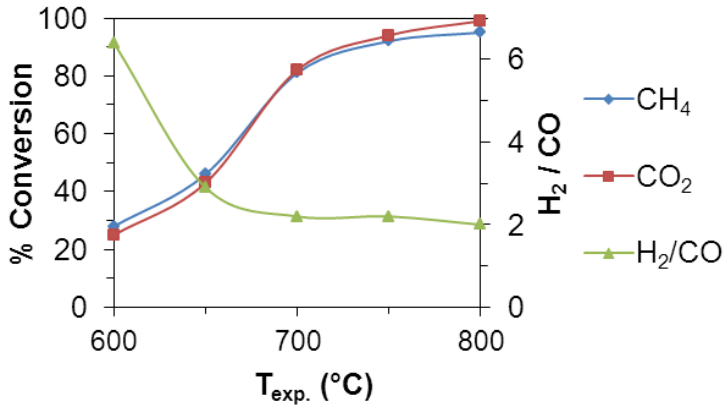

Fig 4.14 Catalytic activity on 200mg of Ni(8.8)/CeO_2 (0.1-0.2mm) + 100mg SiC at different T, $F_{T,0}$ = 100 mL/min. Cycle: 1/2/1/2. 5% CH_4, 5 % CO_2

The figure above is a clear example about the activity-selectivity effect on the reaction temperature. From one side the conversion increases with the temperature going from 30% at 600ºC to 95% at 800ºC. The highest improvement within the 50°C difference is between 650°C and 700°C. This behavior can have an explanation from the thermodynamic point of view, as the reaction $CH_4+6CeO_2 \rightarrow Ce_6O_{11}+CO+2H_2$ becomes theoretically favorable to react ($\Delta G<0$) at 680°C (***Paragraph 3.2.1***). Moreover, the H_2/CO ratio also varies with temperature. The highest value of 6.5 is obtained at 600ºC. Such high H_2/CO ratio is due to the important role of the cracking of methane reaction at such temperature. Concretely, the $C_{deposited}/C_{conv.}$ (%) is 64%, meaning that only 36% of the CH_4 is converted by the partial and/or the total oxidation reaction. Nevertheless, the selectivity is considerably improved at 650ºC (H_2/CO = 2.9) and almost ideal towards syngas products above 700°C (H_2/CO = 2.0, CO/(CO_2+CO) = 0.96 and $C_{deposited}/C_{conv.}$(%) = 4%, at 800°C). This kind of behavior reveals also the effect of the temperature on the oxygen diffusion rate obtaining low selectivity towards CO at 600°C. Some studies are made focusing in such property. J. El Fallah et al. [4.16] claimed that in the 300–500°C temperature range, the surface reduction process is faster than the O diffusion from the bulk to the surface. Some other researchers found correlations between the oxygen diffusion and (i) the working temperature [4.13], (ii) the reduction state of CeO_2 (the more the ceria is reduced the slower is the rate of oxygen diffusion) [4.14], (iii) the surface area (improvement of diffusion at higher surface area) [4.15] and (iv) the incorporation of nickel [4.17] which also accelerates the oxygen mobility.

4.3.6. Influence on the metal loading

Three different loadings of nickel were prepared onto the home-made ceria in order to see the influence on the conversion and selectivity. Concretely, Ni(38.5)/CeO_2, Ni(9.5)/CeO_2 and Ni(2.1)/CeO_2 were tested for the periodic DRM reaction. The results come from the average of the last 4 cycles. The carbon balance is not shown in these results as it was not totally reliable

due to the use of the nitrogen liquid in the mass spectrometer area (see ***Paragraph 7.1.2.4*** for explanation).

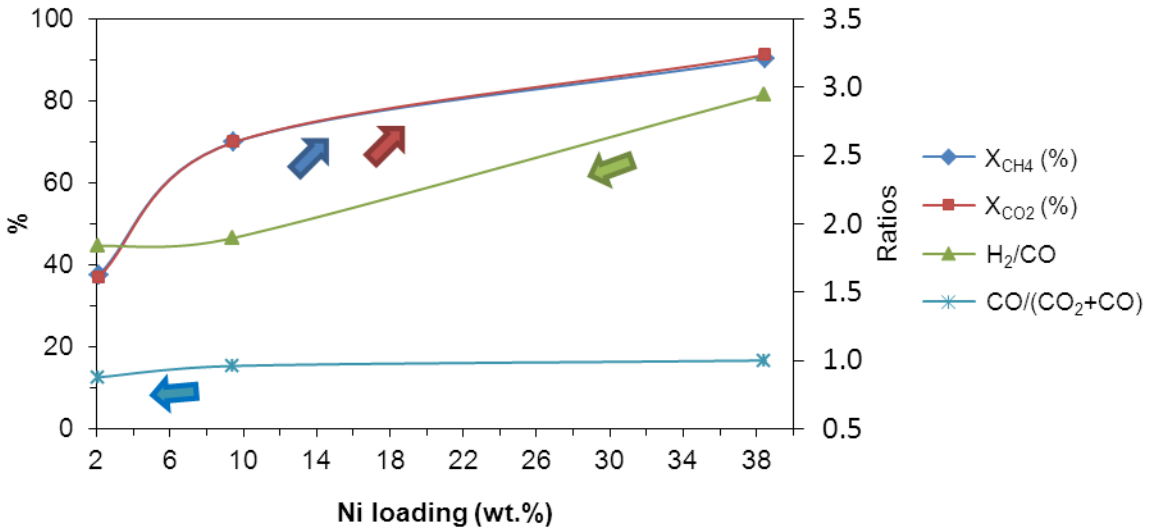

Fig 4.15 ***Reductant step:*** *Conversion of CH_4 (%), H_2/CO and CO/(CO2+CO) ratios.* ***Oxidant step:*** *Conversion of CO_2 (%). 200mg of catalyst Ni(x)/CeO_2 at 700°C $F_{T,0}$ = 100 mL/min. Cycle: 1/2/1/2. 5% CH_4, 5 % CO_2, 12 cycles*

The ***Fig 4.15*** shows the importance of nickel in terms of conversion and selectivity. The Ni(2.1)/CeO_2 gives low activity but interesting selectivity towards H_2/CO. Otherwise, it produces a little bit more of CO_2 as the CO/(CO_2+CO) ratio is lower than in the other two cases (0.88 instead of 0.96 for 9.5% Ni and 1.00 for 38.5% Ni). In the other extreme, Ni(38.5)/CeO_2 shows the highest conversion but accompanied with an undesired selectivity, the H_2/CO ratio is far from the ideal one and the qualitative trend of the carbon deposited was much higher than the one obtained in the two other experiments. Therefore, a good compromise between activation and selectivity seems to be the one working with 9.5% Ni. There, the conversion is considerably enhanced from the Ni(2.1)/CeO_2 catalyst and at the same time the selectivity towards syngas products remains around 100%. Besides, as expected the overall conversion of CH_4 increases with the loading of nickel.

4.3.7. Influence on the nature of the catalyst (Ni-Ce, Ni-Ce-Zr, Co-Ce, Fe-Ce, Ni-Mg-Al)

A comparison is made within different kind of catalyst with different preparation methods:

- Impregnation on home-made CeO_2 → Ni(9.5)/CeO_2
- Impregnation on commercial CeO_2 → Ni(7.9)/CeO_2(com)
- Coprecipitation → $CeNi_{0.3}O_y$

different active metals:

- Impregnation of Fe on home-made CeO_2 → $Fe(10.4)/CeO_2$
- Impregnation of Co on home-made CeO_2 → $Co(7.2)/CeO_2$

doped ceria:

- Coprecipitation Ni-Ce-Zr → $CeNi_{0.5}Zr_{0.5}O_y$

other type of support:

- Coprecipitation Ni-Mg-Al → $Ni_1Mg_2Al_1O_y$

In the following graphs CH_4 conversion, carbon deposition, H_2/CO ratio and CO_2 conversion are shown at different temperatures. The H_2/CO ratio is multiplied by a factor of 10 as a matter of visibility on the graph. In addition the ideal H_2/CO ratio is shown as a reference.

Activation towards reactants mixture at 700ºC

Normally the serial of experiment started working at 700°C. Therefore, the results obtained at such temperature are presented first.

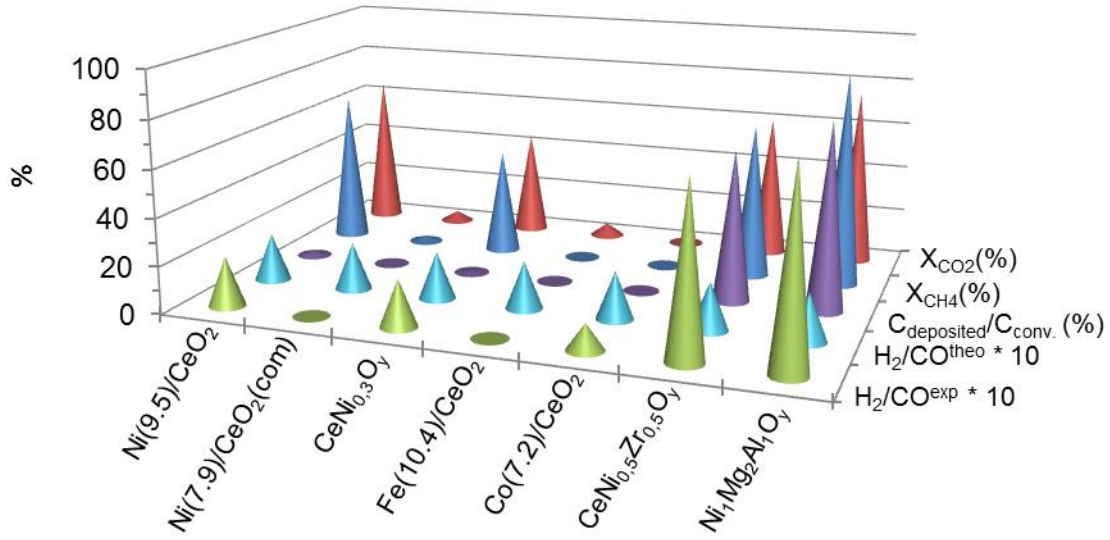

Fig 4.16 ***Reductant step:*** *Conversion of CH_4, $C_{deposited}/C_{conv.}$(%), H_2/CO ratio.* ***Oxidant step:*** *Conversion of CO_2. 200mg of catalyst at 700°C $F_{T,0}$ = 100 mL/min. Cycle: 1/2/1/2. 5% CH_4, 5 % CO_2*

Some interesting information can be extracted from the figure above. The catalyst impregnated on the commercial CeO_2 ($Ni(7.9)/CeO_2(com)$) shows only 2% conversion of CH_4 in comparison with the 65% conversion obtained with the impregnated on the home-made CeO_2 ($Ni(9.5)/CeO_2$). On the other side, the coprecipitated catalyst ($CeNi_{0.3}O_y$) reaches 45% conversion which is 20% less than in the impregnated one. Besides, $Fe(10.4)/CeO_2$ and $Co(7.2)/CeO_2$ show almost negligible conversion. $CeNi_{0.5}Zr_{0.5}O_y$ shows a similar conversion (66%) as $Ni(9.5)/CeO_2$, but on the contrary the selectivity is much worse, obtaining a H_2/CO = 7.2 (instead of 2.1) and $C_{deposited}/C_{conv.}$ = 64% (instead of 2%). The high amount of carbon is surprising as the doping of Zr on the CeO_2 structure commonly helps the oxygen diffusion.

Finally, the $Ni_1Mg_2Al_1O_y$ catalyst shows the relevance of working with an adequate oxygen reservoir which releases easily oxygen as almost all the conversion comes from the cracking of methane ($C_{deposited}/C_{conv.}$ = 79%), obtaining H_2/CO ratio equal 8.2. Nevertheless, $Ni_{0.5}Mg_2Al_1O_y$ should be also tested in future studies to be in the same range of nickel content (13 wt.% instead of 24 wt.% for $Ni_1Mg_2Al_1O_y$).

Otherwise, some of the catalysts had shown interestingly an evolution during the serial of experiments, as so we redid the 700°C experiments on those solids.

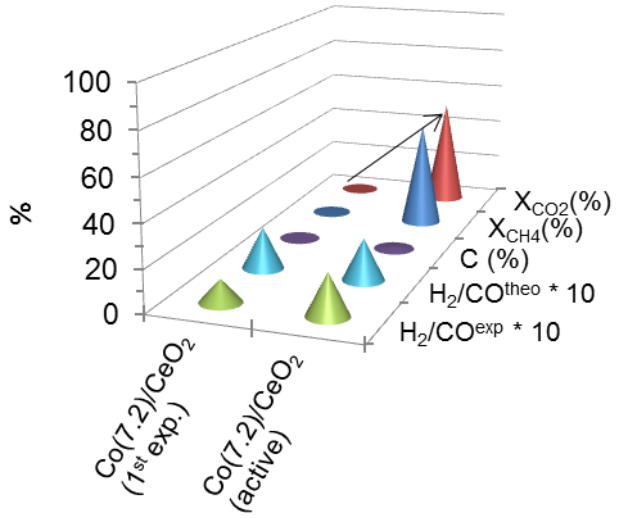

Fig 4.17 Evolution of some catalysts

The ***Fig 4.17*** shows a huge difference between the first experiment on the Co(7.2)/CeO_2 catalyst at 700ºC and the results obtained with the same catalyst after a serial of experiments. Concretely, the catalyst got activated working at 800ºC. Probably at such temperature, the activation of the solid under the reaction mixture is feasible/faster than at 700ºC. Specifically, the conversion obtained was 51% for CH_4 and 52% for CO_2 accompanied with an excellent selectivity of H_2/CO=2.0 and $C_{deposited}/C_{conv.}$ = 0-1%. Probably, an optimized stoichiometry of Ni-Co-Ce catalyst could be one of the most promising combinations to obtain the best ratio activation-selectivity, based on these results.

800°C

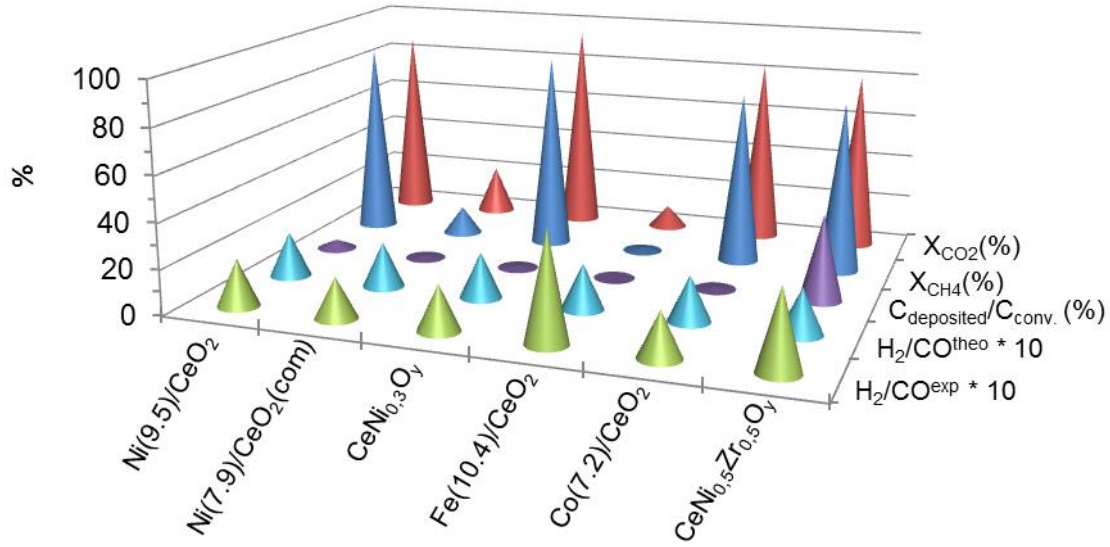

Fig 4.18 ***Reductant step:*** *Conversion of CH_4, $C_{deposited}/C_{conv.}$(%), H_2/CO ratio.* ***Oxidant step:*** *Conversion of CO_2. 200mg of catalyst at 800°C $F_{T,0}$ = 100 mL/min. Cycle: 1/2/1/2. 5% CH_4, 5 % CO_2*

Firstly, Fe(10.4)/CeO_2 only activates negligibly methane even at the high temperature of 800ºC. Co(7.2)/CeO_2 and Ni(9.5)/CeO_2 are active and selective. The coprecipitated catalyst $CeNi_{0.3}O_y$ also works well evidencing that the two different approaches about the synthesis method can work, with the appropriate elements. Secondly, $CeNi_{0.5}Zr_{0.5}O_y$ catalyst shows the same trend as working with 700ºC. From one side there is still more carbon deposition than working with the other solids ($C_{deposited}/C_{conv.}$(%) = 38 instead of nearly zero). From the other side, there is also more H_2O and CO_2 than in the other cases ($CO/(CO_2+CO)$ = 0.87 instead of 0.98-1.00). As mentioned before, the introduction of Zr should create more defects in the structure of ceria improving the oxygen diffusion, which could explain the high amount of H_2O and CO_2. However, this behavior is contradictory with the fact of obtaining more carbon deposition. Typically, less carbon is expected at such conditions, when the oxygen diffusion is enhanced. Nevertheless, some researchers already found this type of behavior. Kambolis et al [4.22] relate the whisker type of carbon, which is favored in the presence of low zirconium content, to the increase in the carbon deposition in comparison with the binary Ni-Ce catalyst. Otherwise, they reached less carbon at high loadings of Zr, but without being lower than the one obtained with Ni-Ce.

Finally, Ni(7.9)/CeO_2(com) shows some considerable conversion (13%) in comparison with the one at 700ºC (2%) but still much lower than the one obtained with Ni(9.5)/CeO_2 catalyst (88%). Some hypothesis came out from these results:

- The diffusion of oxygen is worse due to the bigger crystal size of CeO_2 (38nm instead of 10nm) and/or the lower surface area (9 m^2/s instead of 32 m^2/s)

- The interaction between Ni and the home-made CeO_2 brings somehow more activity in CH_4 than using the commercial one, maybe the synergetic effect is stronger in the first case.
- Ni(7.9)/CeO_2(com) has more difficulties to be activated in the reaction mixture. The solid may need specific pretreatment under hydrogen, which can be the case as it was for the experiment in cofeed.

600°C

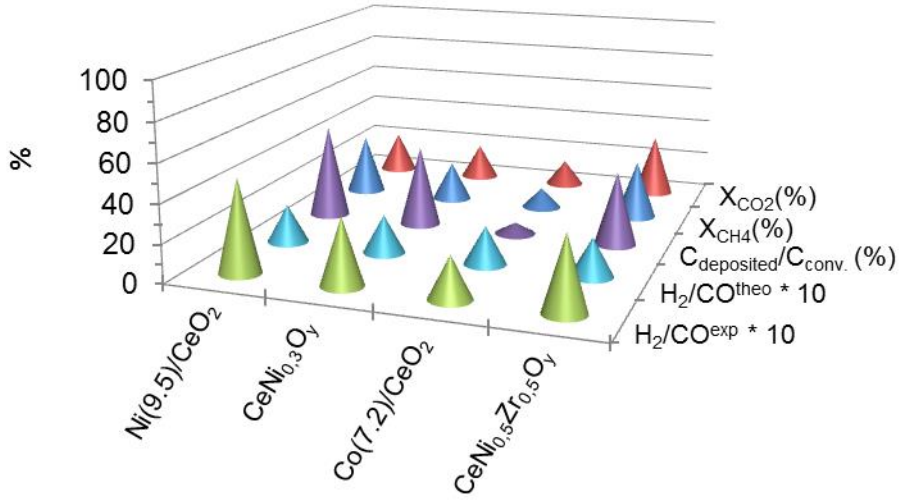

Fig 4.19 ***Reductant step:*** *Conversion of CH_4, $C_{deposited}/C_{conv.}$(%), H_2/CO ratio.* ***Oxidant step:*** *Conversion of CO_2. 200mg of catalyst at 600°C $F_{T,0}$ = 100 mL/min. Cycle: 1/2/1/2. 5% CH_4, 5 % CO_2*

Some differences between the catalysts are easier to see at 600ºC, for instance the difference between the selectivity of Co(7.2)/CeO_2 and Ni(9.5)/CeO_2. In the first case $C_{deposited}/C_{conv.}$(%) is "only" 6% whereas it goes up to 50% for the Ni catalyst which corroborates the hypothesis made for the experiments at 700ºC. Cobalt is more efficient to avoid the cracking reaction than nickel, event at the mild conditions of 600ºC. Notwithstanding, the drawback of the low activation is even clearer seen in this case obtaining 3 times less CH_4 converted (11% instead of 32% CH_4 conversion).

From all this set of experiments, some interesting clues can be extracted about the periodic process. The system works well at the range of temperatures between 700 and 800ºC obtaining around 90-100% selectivity with a small carbon deposition. Of course, as explained before, the conversion shown in the last figures is the average of the 1 minute step. Therefore, if the step time was shorter, higher conversion would be obtained. In this section, the absence of activity on Fe(10.4)/CeO_2 is observed as it was the case working in cofeed, emphasizing again the ease of Ni and Co to be already active without prior activation other than the reaction mixture. Besides, the experiment working with $Ni_1Mg_2AlO_y$ has also emphasized the importance of using a proper oxygen carrier. Finally, the low performances obtained at 600ºC

shows the challenge and the huge improvement which can be done at such mild conditions. Otherwise some interesting hints are already found to look forward in the optimization of the process at such temperature, such as a potential combination of Co with Ni on CeO_2.

4.3.8. H_2O and CO_2 production on the initial stage

Ni-Ce catalyst

The thermodynamics calculations have given some hints about some production of water and carbon dioxide due to the reduction of NiO to Ni^0 by CH_4 ($CH_4 + 4NiO \rightarrow 4Ni + CO_2 + H_2O$). This hypothesis is already in good agreement with the experimental data from the cofeed tests. Therefore, this particular and key role behavior is also checked in detail for the periodic process.

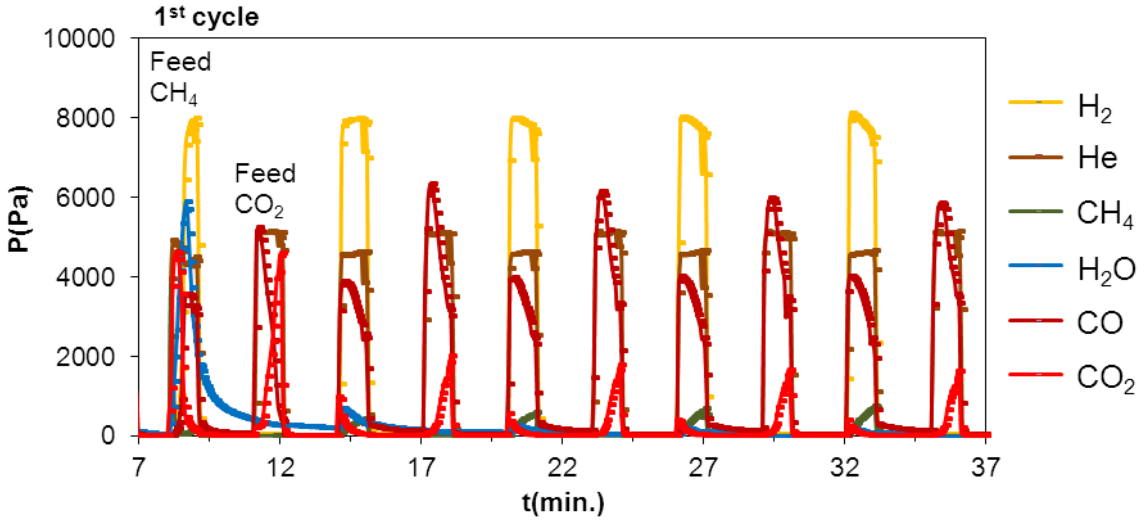

Fig 4.20 Partial pressures in the outlet flow working with 200mg of Ni(9.5)/CeO_2 at 800°C $F_{T,0}$ = 100 mL/min. Cycle: 1/2/1/2. 5% CH_4, 5 % CO_2

The figure above shows the partial pressures in the outlet flow after the reaction. The production of H_2O and CO_2 decreases until almost zero after the first 2 cycles, leading to a highly selective system towards syngas products.

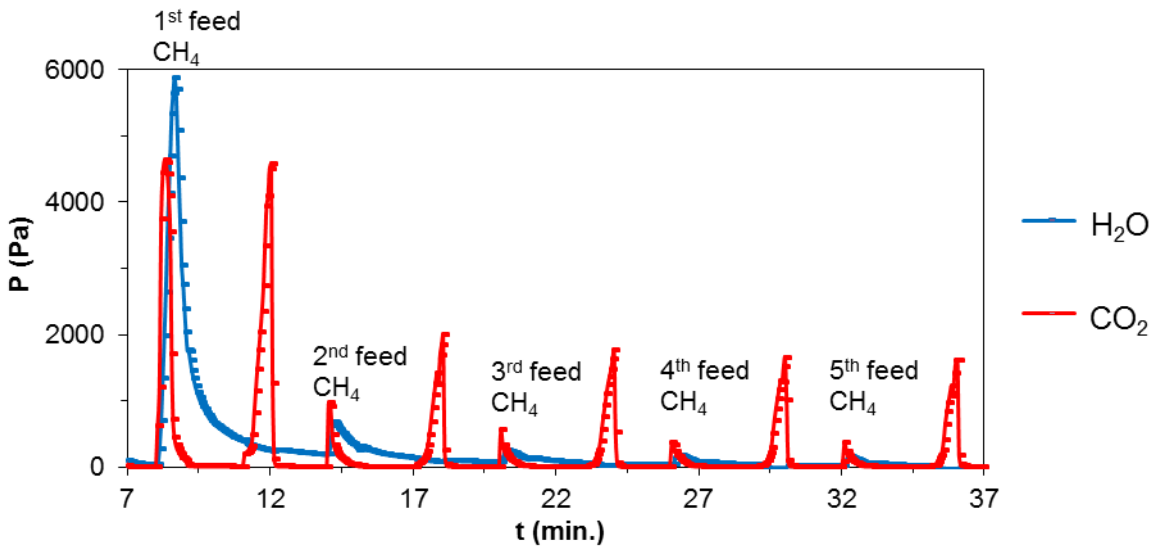

Fig 4.21 Partial pressures of H_2O and CO_2 in the outlet flow, zoom from ***Fig 4.20***

The ***Fig 4.21*** shows clearly the trend of H_2O and CO_2, where indeed there is a considerable amount of the products from the total oxidation of CH_4 which disappear after the first cycle. It should be reminded that the catalysts used were not prereduced before test. Therefore, the production of H_2O and CO_2 in this first cycle can be ascribed to the reduction of NiO species that are subsequently not reoxidized by CO_2. V. Galvita et al. [1.29] also observed H_2O and CO_2 in the early stage of the reaction working with Pt-Ce-Zr based catalyst on the periodic SRM. The results above reinforce again the idea about the absence of reoxidation of Ni^0 to pure NiO in the oxidant step. Thanks of that, one of the main undesired side reaction is avoided, leaving "only" two competitive reactions ($CH_4 + 2CeO_2 \rightarrow Ce_6O_{11} + 2H_2 + CO$ and $CH_4 \rightarrow C + 2H_2$). Consequently, this is one of the key points about the good selectivity towards syngas. If not, the same kind of production as in the first cycle would appear during the whole experiment, a mixture between H_2, CO, H_2O and CO_2.

ORM for NiO theory verification

The importance of oxidizing the catalyst with CO_2 for the good selectivity towards syngas is also verified carrying the oxidative reforming of methane in periodic. Basically using oxygen instead of carbon dioxide in the oxidant step. Thereby, a series of experiments in periodic was made as follows: P-DRM (20 cycles) / P-ORM (12 cycles) / P-DRM (12 cycles). Only the first four cycles of each experiment are shown in the following graphs for a proper visibility.

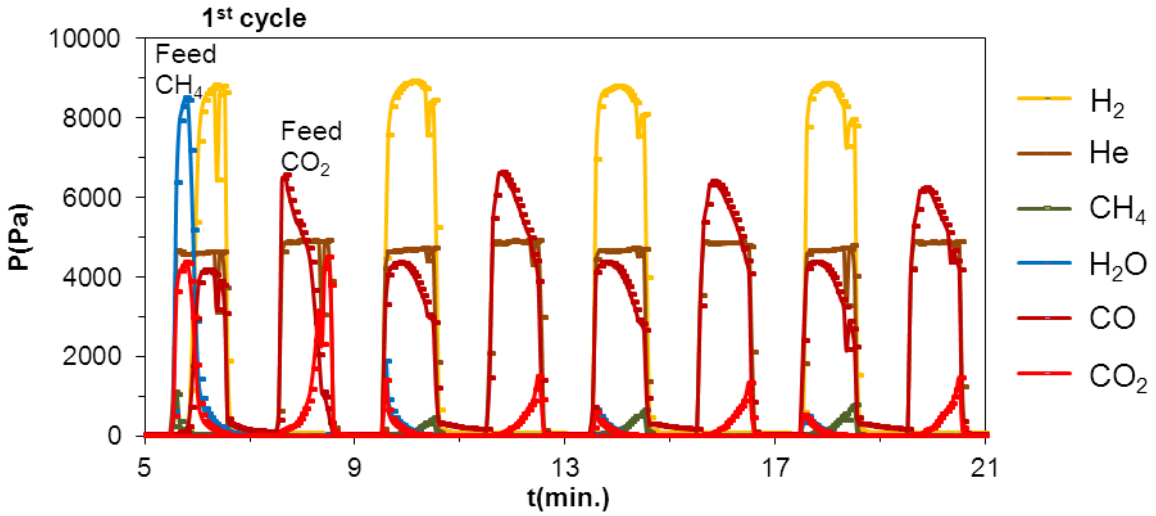

Fig 4.22 Partial pressures in the outlet flow working with 200mg of Ni(10.5)/CeO_2 at 800°C $F_{T,0}$ = 100 mL/min. Cycle: 1/1/1/1. 5% CH_4, 5 % CO_2

First, the ***Fig 4.22*** shows the behavior seen in some of the previous experiments, meaning production of H_2O and CO_2 in the first cycle and afterwards leading to syngas products. After 20 cycles, once the catalyst was "stable" at those conditions, the oxidant feed was changed to oxygen.

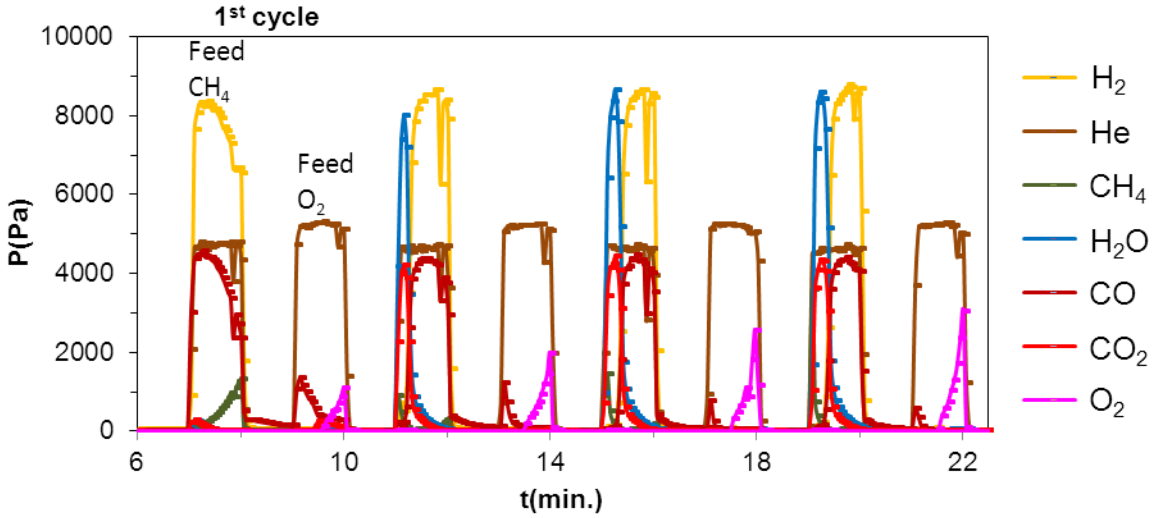

Fig 4.23 Partial pressures in the outlet flow working with 200mg of Ni(10.5)/CeO_2 at 800°C $F_{T,0}$ = 100 mL/min. Cycle: 1/1/1/1. 5% CH_4, 5 % O_2

Obviously, the first step with CH_4 gives still H_2 and CO, but the most important point comes after the first reoxidation with oxygen. From there, H_2O and CO_2 appear at each initial stage of the CH_4 steps, leading after 20-25s to syngas products. This kind of behavior is exactly the same as during the first step of CH_4 in the ***Fig 4.22***. From the literature, Bozo et al. [4.6] also observed, working by separate pulses of CH_4 and O_2 on the ORM, a formation of CO_2 which was decreasing rapidly as the oxygen from the carrier was consumed for Pt-Ce-Zr-O based

catalyst. The thermodynamic data of PtO reduction by CH_4 (***Paragraph 3.2.4***) makes sense with their results, as the potential reaction to occur is the total oxidation of the hydrocarbon. Therefore, it is proved that CO_2 cannot oxidize the unselective species of the catalyst which produces H_2O and CO_2.

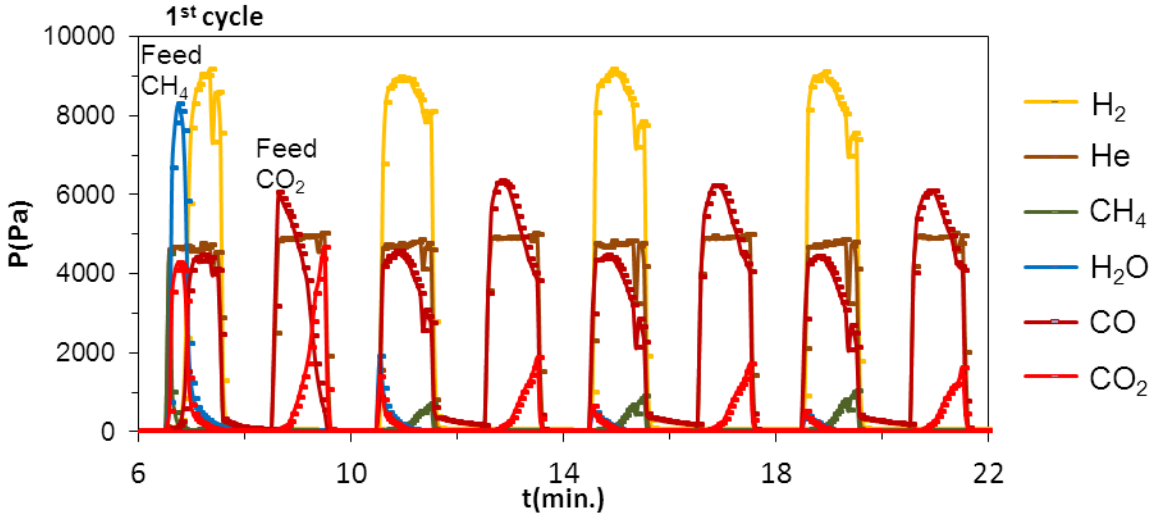

Fig 4.24 Partial pressures in the outlet flow working with 200mg of Ni(10.5)/CeO_2 at 800°C $F_{T,0}$ = 100 mL/min. Cycle: 1/1/1/1. 5% CH_4, 5 % CO_2

In addition, the last experiment of the series allows observing the robustness and versatility of the catalyst, being capable to be again selective towards H_2 and CO even after being fully oxidized by oxygen (from the previous experiment) and by simply switching to CO_2 again.

Co-Ce catalyst

Cobalt seems to have the same type of behavior as nickel, at least from the thermodynamic point of view. Therefore, this similarity is experimentally checked in this paragraph.

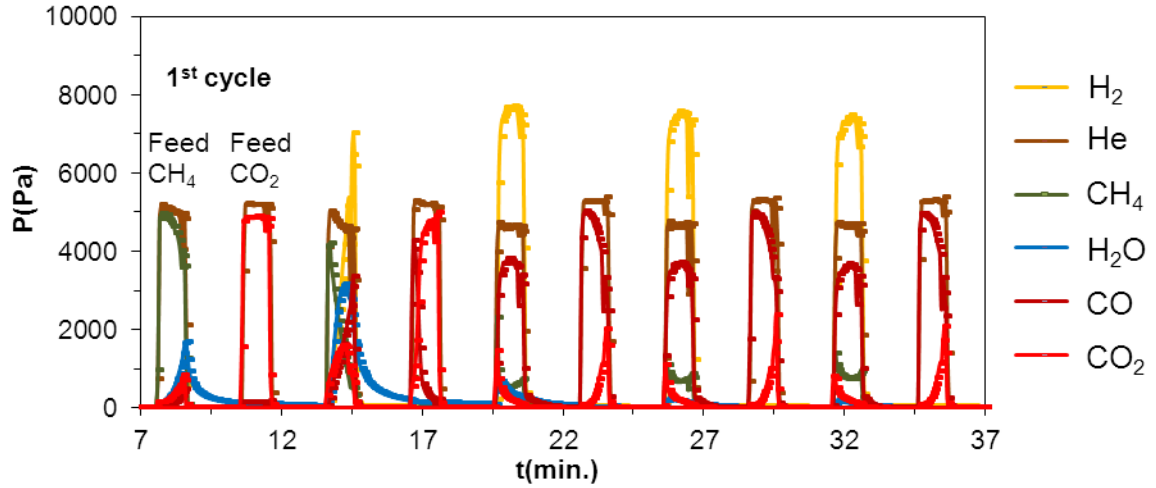

Fig 4.25 Partial pressures in the outlet flow working 200mg of Co(7.2)/CeO_2 at 800°C $F_{T,0}$ = 100 mL/min. Cycle: 1/2/1/2. 5% CH_4, 5 % CO_2

Although the activity in the first cycle is lower, the same kind of behavior appears working with Co. The ***Fig 4.25*** shows a production of water and carbon dioxide in the first two cycles leading to a selective system in the following ones.

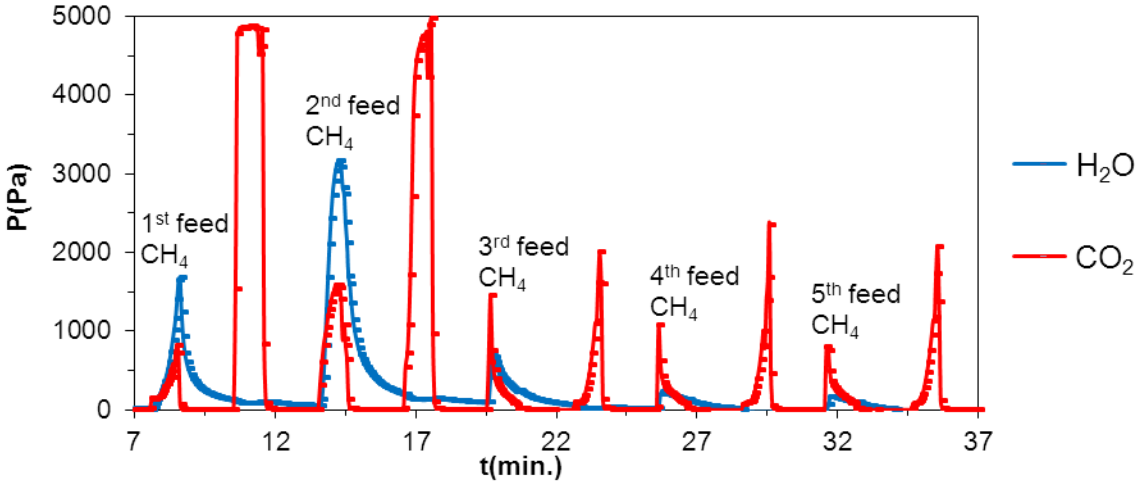

Fig 4.26 Partial pressures of H_2O and CO_2 in the outlet flow, zoom from ***Fig 4.25***

As shown in the ***Paragraph 3.2.3***, this behavior can be linked to the reduction of Co_3O_4 ($CH_4 + 4Co_3O_4 \rightarrow 12CoO + CO_2 + 2H_2O$) and the one of CoO ($CH_4 + 4CoO \rightarrow 4Co + CO_2 + 2H_2O$). The results on the oxidant step are also in good agreement with the thermodynamic study which showed the unfeasible oxidation of Co^0 by CO_2. Thereby, two undesired side reaction are eluded of the system, remaining only the competition between the partial oxidation and the cracking of CH_4 (as in the case of nickel). The hypothesis about the absence of cobalt reoxidation is also consistent looking at the X-ray diffraction after the experiment, which is shown in the Chapter of cofeed (***Paragraph 2.2.4***).

Fe-Ce catalyst

The correlation between total or partial oxidation of CH_4 is also made for the Fe-Ce catalyst.

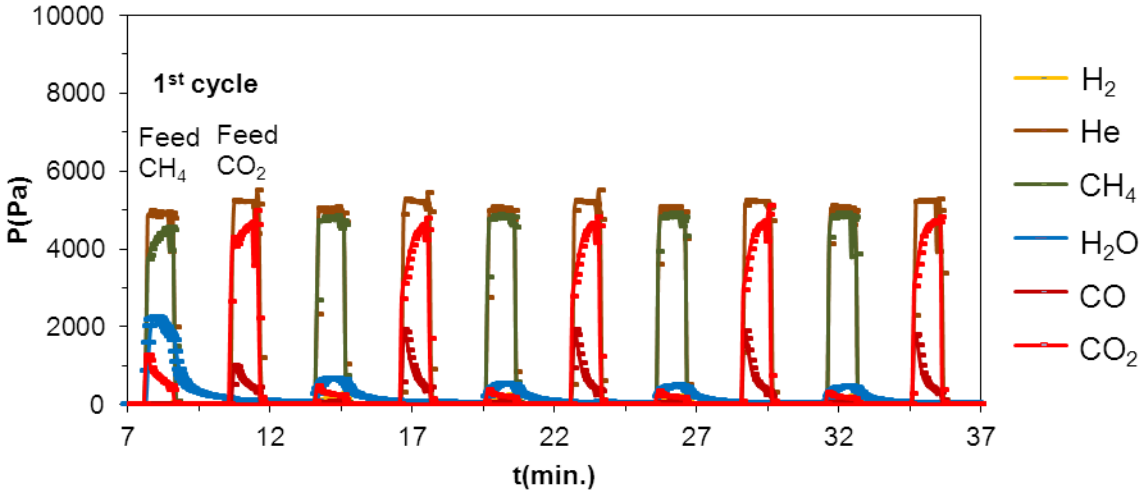

Fig 4.27 Partial pressures in the outlet flow working 200mg of Fe(10.4)/CeO_2 at 900°C $F_{T,0}$ = 100 mL/min. Cycle: 1/2/1/2. 5% CH_4, 5 % CO_2

The ***Fig 4.27*** shows the performance working at 900ºC instead of 800°C as only 1-2% conversion of CH_4 was obtained at the low temperature. At 900ºC, 5% of CH_4 and 17% of CO_2 were converted. As usual, the first cycle gives the highest amount of H_2O and CO_2, probably due to the reduction of Fe_2O_3 to Fe_3O_4 [1.58]. However, on the contrary of Ni and Co systems, significant selectivity towards H_2O and CO_2 remains during all the experiment in comparison with the production of H_2 and CO.

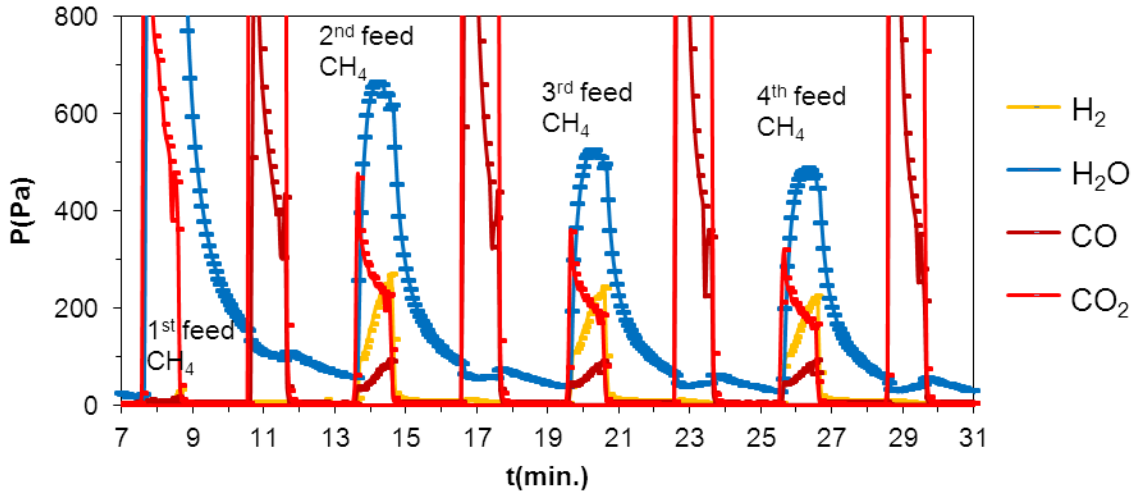

Fig 4.28 Partial pressures of H_2, H_2O, CO and CO_2 in the outlet flow, zoom from ***Fig 4.27***

The figure above presents the mix of products between the partial and total oxidation of methane (H_2O, CO_2, H_2 and CO). This type of behavior fits also well with the thermodynamic study (***Paragraph 3.2.5***) which shows that the reduction of Fe_3O_4 to FeO is thermodynamically favored for the two reactions, even a little bit more for the production of H_2O and CO_2. S. Bhavsar and G. Veser [1.54] also observed that the reduction of Fe_3O_4 to FeO is partially unselective. Furthermore, the reoxidation of Fe or/and FeO to Fe_3O_4 by CO_2 is also confirmed in such study. Otherwise, based on the XRD analysis after test, shown in the cofeed chapter

(***Paragraph 2.2.4***), $CeFeO_3$ oxide phase seems to be the unselective species which leads to the products observed. Even though the last test of the serial experiments was in cofeed (***Table 2.3***), the hypothesis about obtaining the same species on the catalyst after cofeed and periodic is assumed.

4.3.9. Tuning the working conditions (RT, PSD)

Influence of the volume flow rate (≠ RT)

Tuning the working conditions is always relevant and important, even more in an industrial application. The influence of a high or low total flow could be significant depending on the reaction and process. Thereby this parameter is checked increasing the residence time (RT) by two (50 mL/min) and decreasing it by 1.4 times (140 mL/min) as compared to the previous experiments (100 mL/min).

Table 4.3 Results (average 4 last cycles) working 200mg of Ni(9.5)/CeO_2 at 700°C $F_{T,0}$ = 50, 100 and 140 mL/min. Cycle: 1/2/1/2, 12 cycles, 5% CH_4, 5 % CO_2

F_T (mL / min)	X_{CH4} (%) ± 1	H_2/CO ± 0.1	$C_{deposited}$ / $C_{conv.}$ (%) ± 2	$CO/(CO_2+CO)$ ± 0.02	X_{CO2} (%) ± 1
50	73	2.1	3	0.96	77
100	65	2.1	2	0.98	65
140	44	2.0	1	0.98	46

The ***Table 4.3*** shows the results obtained from this study. As expected, the conversion decreases with the increase of flow, from 73% to 44% CH_4 conversion. Otherwise, the selectivity remains quite stable in the whole range of flows with a tiny difference about the carbon formation and the production of CO_2. Nevertheless, a high space velocity is also important for the industrial process approach, so probably the 100 mL/min is the best compromise from this point of view as the loss in conversion (8%) is not so high in comparison with the experiment using 50 mL/min and 20% conversion is gained in the comparison with the one working at 140 mL/min..

Influence of the mixing with SiC

Different catalytic bed lengths were studied looking forward in the improvement of the performance. SiC was used as a diluent thanks to its inert properties towards the reactions (explained in detail ***Paragraph 2.2.3***). As for the cofeed system, the inertness of SiC towards the two reactions was verified, in this case flowing separately CH_4 and CO_2 and no measurable conversion could be observed up to 800°C. Then, 3 experiments were carried working with 200mg of catalyst: (i) without SiC, (ii) with 100mg of SiC and (iii) with 300mg of SiC. Thus, the influence of mixing the catalyst with SiC was studied.

Table 4.4 Results (average 4 last cycles) working 200mg of Ni(8.8)/CeO_2 at 700°C $F_{T,0}$ = 100 mL/min. Cycle: 1/2/1/2, 12 cycles, 5% CH_4, 5 % CO_2

Weigth catalytic bed (g)	X_{CH4} (%) ± 1	H_2/CO ± 0.1	$C_{deposited}$ / $C_{conv.}$ (%) ± 2	CO/(CO_2+CO) ± 0.02	X_{CO2} (%) ± 1
0.2 cat.	65	2.1	2	0.98	65
0.2 cat. + 0.1SiC	74	2.1	5	0.99	73
0.2 cat. + 0.3SiC	77	2.3	12	0.93	77

The ***Table 4.4*** shows a summary of the results for the three experiments. Some differences are seen between them. As it could be expected, the conversion is enhanced working with SiC. Concretely, the conversion of CH_4 is 77% for 0.5g catalytic bed instead of 65% for the 0.2g. Otherwise, the selectivity decreases slightly. From one side there is more carbon deposit (12% instead of 5%), a fact which is also reflected in the increase of the H_2/CO ratio (2.3 instead of 2.1). From the other side, the high activity leads to produce a little bit more of CO_2, CO/(CO_2+CO) ratio is slightly lower (0.93 instead of 0.98). Otherwise, trying to find a balance between conversion and selectivity, the experiment working with 200mg of catalyst and 100mg of SiC seems to be the optimum within the three as the conversion is improved by 8-9% and at the same time the selectivity is the same as working without silicon carbide.

Influence of the particle size distribution (PSD)

The mean size of the grain could also play an important role on the activity, selectivity or/and stability of the system. Therefore, some experiments were carried using powder and some others with the catalyst sieved between 0.1-0.2mm.

Table 4.5 Results (average 4 last cycles) working 200mg of Ni(8.8)/CeO_2 + 100mg SiC (0.250mm) at different T. $F_{T,0}$ = 100 mL/min. Cycle: 1/2/1/2, 12 cycles, 5% CH_4, 5 % CO_2

T(°C)	PSD (mm)	X_{CH4} (%) ± 1	H_2/CO ± 0.1	$C_{deposited}$ / $C_{conv.}$ (%) ± 2	CO/(CO_2+CO) ± 0.02	X_{CO2} (%) ± 1
700	pw	74	2.1	5	0.99	73
	0.1 - 0.2	81	2.2	9	0.98	82
750	pw	81	2.1	6	0.99	79
	0.1 - 0.2	92	2.2	7	0.96	94
800	pw	89	1.9	< 2	0.98	86
	0.1 - 0.2	97	2.1	8	0.96	99

The ***Table 4.5*** shows the results working with or without sieving the catalyst for the reaction temperatures of 700, 750°C and 800ºC. For all the cases the set of experiments using the sieved catalyst is considerably more active, increasing the conversion 7%, 11% and 8% respectively. About the selectivity, the carbon and CO_2 production seems to be slightly higher for the sieved catalyst than the powder one. In an overall view it remains quite interesting to look forward in an optimization of such parameter. Thus, the PSD seems to be another property

to keep into account as the grain size can have some relevance influence on the activity-selectivity of the process.

4.4. Characterization after test

4.4.1. XRD

The XRD patterns of some of the solids used in the experiments discussed above are shown in the following paragraph in order to understand some of the changes in the solid after test.

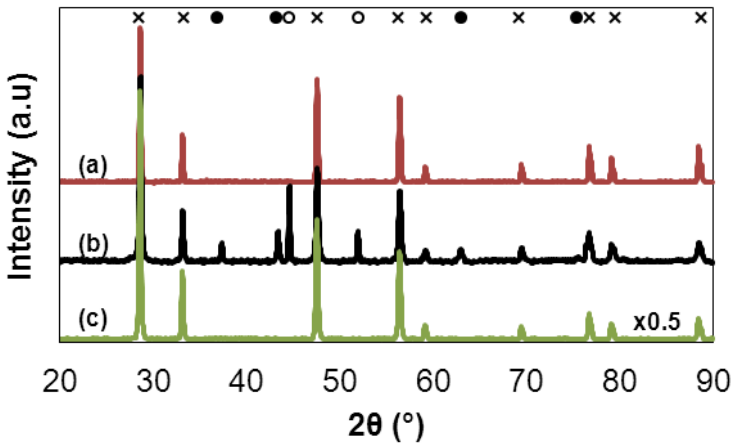

Fig 4.29 XRD patterns for (a) CeO_2 (b) Ni(38.5)/CeO_2 (after O_2), (c) Ni(2.1)/CeO_2 x CeO_2, o Ni^0, ● NiO

First, the figure above reveals some interesting characteristics on the CeO_2 experiment (***Paragraph 4.3.2***). The peaks are narrower and more intensive than the ones before test (***Paragraph 4.2***). Probably during the process the solid was more crystallized and the average crystal size was increased. Indeed, the particle size calculated by the Scherrer equation (***Table 4.6***) indicates a length of 35nm after experiment instead of the 6nm before experiment. This data is quite important as during the experiments almost negligible activity was shown. Otherwise, all the catalysts which activate the reactants and work correctly during several experiments reach around the same crystal size of CeO_2. Therefore, the sintering effect, at least from the CeO_2 side, is mostly related to the temperature independently of the DRM reaction. In addition, the surface area is much lower after experiment (1 m^2/g) than before test (53 m^2/g).

Then, the black line shows the XRD pattern on the Ni(38.5)/CeO_2 catalyst with an important particularity. After the P-DRM experiment, 12-cycles P-ORM experiment at 600°C was carried out on this sample in order to see the differences on the structure working with oxygen in the oxidant step. Indeed, there is an expected difference, the NiO diffraction pattern appears on this solid. These data can support the results found on the ***Fig 4.23*** and link again the fact of having NiO on the solid for the production of H_2O and CO_2.

Finally, the XRD on Ni(2.1)/CeO_2 after test (last exp. done in that catalyst was P-DRM at 700°C) does not show Ni^0. As already mentioned in other paragraphs the Ni particles are probably too small or amorphous to be detected by XRD.

Different Ni-Ce synthesis methods and Ni-Ce-Zr

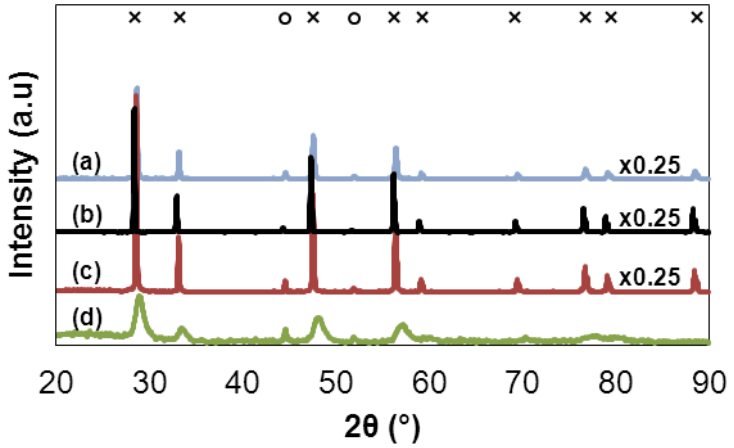

Fig 4.30 XRD patterns for (a) $CeNi_{0.3}O_y$ (b) Ni(7.9)/CeO_2(com) (c) Ni(9.5)/CeO_2 (d) $CeNi_{0.5}Zr_{0.5}O_y$ x CeO_2 and/or $CeNi_{0.5}Zr_{0.5}O_y$ o Ni^0

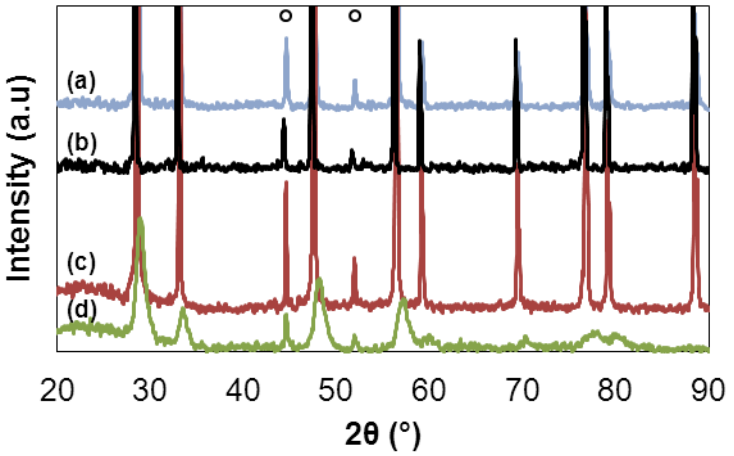

Fig 4.31 Zoom XRD patterns

The figures above show the XRD patterns of the solid made by different preparation methods and the one using zirconium. The same type of pattern is shown in all the cases evidencing CeO_2 and Ni^0 phases. Therefore, the hypothesis about the absence of reoxidation of nickel gains consistence looking at the X-ray diffraction after the experiment, showing in all the cases the peaks of Ni^0 without the ones of NiO. Even though, a main difference is seen on the $CeNi_{0.5}Zr_{0.5}$ catalyst, the peaks have much lower intensity than the other ones. In addition, the calculation by the Scherrer equation reveals CeO_2 crystal size of 8nm, only 4 more than before test. On the contrary, crystal of CeO_2 after test for the rest of the catalysts is in the range of 38-40nm (38nm for $CeNi_{0.3}O_y$, 40nm for Ni(7.9)/CeO_2(com) and 39nm for Ni(9.5)/CeO_2),

evidencing an important effect of the sintering. Thus, the improvement towards sintering with the addition of Zr is proved, as some researchers mentioned in the literature [1.45]. These values encourage us to look forward working with this type of catalyst from this point of view. Notwithstanding, the problematic on the selectivity towards H_2O, CO_2 and carbon deposition needs to be also considered. The catalyst used contains 10 wt.% Ni and 14 wt.% Zr, thereby a catalyst with the same amount of nickel but for instance the double of zirconium would be really interesting to test in further experiments, due to the low carbon formation at high loadings of Zr [4.22].

The comparison before and after experiment of the CeO_2 crystal size on Ni(7.9)/CeO_2(com) can be made from the data obtained by the Scherrer equation.

Table 4.6 Crystal size and BET surface before and after test

Catalyst	d_{M-O} (nm)	d_M (nm)	d_{CeO2} (nm)	S_{BET} (m^2/g)
CeO_2	-	-	6	53
CeO_2 a.e.	-	-	35	1
Ni(2.1)/CeO_2	n.o	n.o	12	27
Ni(2.1)/CeO_2 a.e.	n.o	n.o	33	3
Ni(9.5)/CeO_2	18	n.o	10	32
Ni(9.5)/CeO_2 a.e.	n.o	34	39	2
Ni(38.5)/CeO_2	21	n.o	12	33
Ni(38.5)/CeO_2 a.e. (O_2)	28	33	28	5
Ni(7.9)/CeO_2(com)	n.o	n.o	38	5
Ni(7.9)/CeO_2(com) a.e.	n.o	31	40	3
$CeNi_{0.3}O_y$	n.o	n.o	5	79
$CeNi_{0.3}O_y$ a.e.	n.o	30	38	1
$CeNi_{0.5}Zr_{0.5}$	n.o	n.o	$d_{CeNi0.5Zr0.5}$: 4	129
$CeNi_{0.5}Zr_{0.5}$ a.e.	n.o	n.o.	$d_{CeNi0.5Zr0.5}$: 8	10

n.o. = not observed

Before test is 38nm and after test is 40nm, which means that there is a kind of limitation on the segregation phenomena. For all the type of Ni-CeO_2 catalyst no matters the experiments done on different temperature and processes (periodic and cofeed) that always end at such size. Meaning that from the sintering point of view, the crystal of CeO_2 would reach that range at any time, even starting with a really small size before test (4 nm for $CeNi_{0.3}O_y$). Although these are average values and do not consider size distribution, this means that eventual differences in catalytic properties of the solid cannot be ascribed by different sintering properties of the support.

4.4.2. XPS

XPS analyses were made for the $CeNi_{0.3}O_y$ and $CeNi_{0.5}Zr_{0.5}O_y$ catalysts (besides the XPS described in the cofeed chapter). In the following figures the Ni $2p_{3/2}$ spectra is shown for both solids in order to understand the oxidation state of Ni on the surface before and after test.

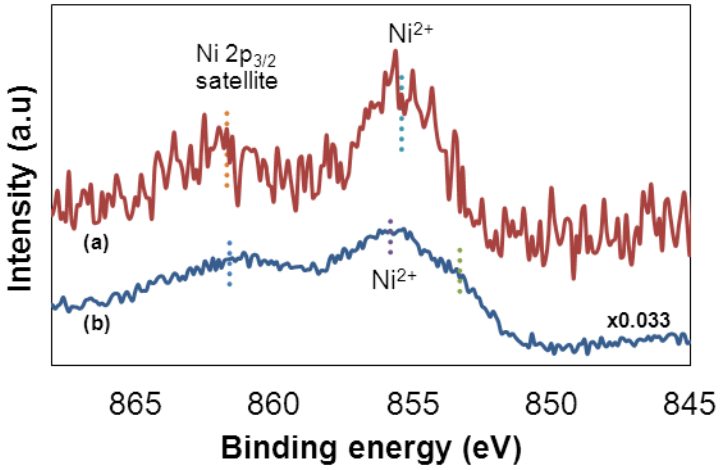

Fig 4.32 XPS pattern of Ni $2p_{3/2}$ core level (a) before and (b) after experiment on $CeNi_{0.3}O_y$

The *Fig 4.32* shows the XPS spectra on the $CeNi_{0.3}O_y$. First, the sample before experiment (in red) shows a binding energy of 855.4eV for Ni^{2+} with satellite at 861.7eV. Otherwise, the XPS after experiment reveals some particular differences. The peak of Ni^{2+} shifts to higher binding energies (855.8eV). In addition, a small contribution of metallic nickel appears at 853.3eV. The cause on the shift of the peaks is related by some researchers by a stronger synergetic effect between Ce and Ni [2.12-2.13]. Moreover, the total amount of nickel on the surface increased after experiment from 5% to 12 at.%. Besides, the distribution of nickel is 80% for Ni^{2+} and 20% for Ni^0. Reinforcing again the idea about that even NiO species are not found in the XRD spectra, Ni^{2+} species are still majorly on the surface, as discussed in the cofeed chapter probably in a strong interaction with CeO_2.

Otherwise, Ni species on the surface after experiment are almost the same as the one obtained for $Ni(9.5)/CeO_2$ catalyst (12% for 13% in the impregnated catalyst). In addition the distribution Ni^{2+}-Ni^0 is also almost the same (80%-81% Ni^{2+} and 20-19% Ni^0). Meaning that from the oxidation point of view, the two type of catalyst reach the same properties after working in such processes.

Table 4.7 Data from XPS analysis for $CeNi_{0.3}O_y$ and $CeNi_{0.5}Zr_{0.5}O_y$ catalysts

Catalyst	% Atomic concentration					
	Ce	Ni	-	O	Ni^{2+}	Ni^0
$CeNi_{0.3}O_y$	16	5	-	79	100	-
$CeNi_{0.3}O_y$ a.e.	28	12	-	61	80	20
Catalyst	% Atomic concentration					
	Ce	Ni	Zr	O	Ni^{2+}	Ni^0
$CeNi_{0.5}Zr_{0.5}O_y$	21	8	7	64	100	-
$CeNi_{0.5}Zr_{0.5}O_y$ a.e.	23	5	8	64	80	20

a.e. = after experiment

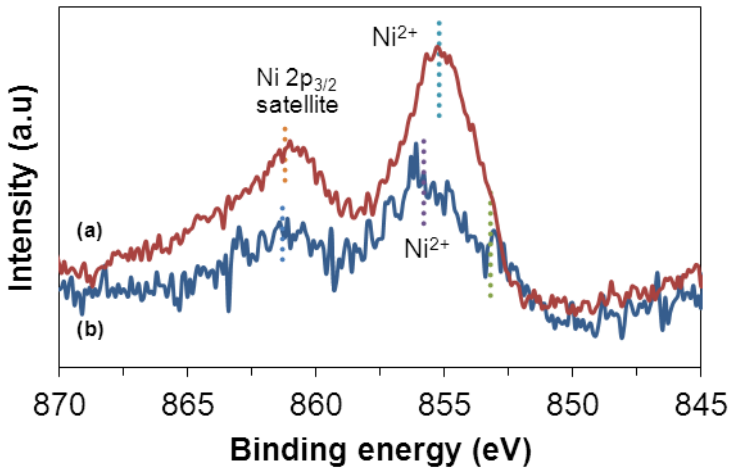

Fig 4.33 XPS pattern of Ni $2p_{3/2}$ core level (a) before and (b) after experiment on $CeNi_{0.5}Zr_{0.5}O_y$

Some important information is obtained from the XPS of the $CeNi_{0.5}Zr_{0.5}O_y$ catalyst before and after test. The binding energy of Ni^{2+} is 855.2eV with satellite at 861.2eV. This binding energy is at the same as the one obtained in $CeNi_{0.3}O_y$, underlying a strong interaction between Ni-Zr-Ce. Then, the XPS spectra after experiment gives a peak of Ni^{2+} at 855.8eV (satellite at 861.3eV) and a contribution of Ni^0 at 853.2eV. Moreover, the distribution of Ce, Ni and O species on the surface remains more stable than working with the coprecipitated catalyst. This trend is in good agreement with the data found from the XRD analysis which shows a similar crystal size of CeO_2 before (4nm) and after (8nm) test. Curiously, the contribution of Ni^0-Ni^{2+} remains the same as in the other cases: 20% for Ni^0 and 80% for Ni^{2+}. Therefore the contribution of zirconium does not seem to affect the nickel behavior. On the contrary, Zr could have a direct or an indirect role (for instance creating more defects in ceria) on the catalytic performance.

4.4.3. XPS: Difference after reduction and oxidation pulse

A specific study using the XPS technique was made to show in detail the differences on the surface of the solid after each step (reduction by CH_4 and oxidation by CO_2) at two different temperatures (600°C and 800°C). 200mg of Ni(10.5)/CeO_2 catalyst was used for each of the

experiments, which were stopped at the convenient moment after 30 cycles in order to be sure that the solid is “stable” in terms of the internal evolution.

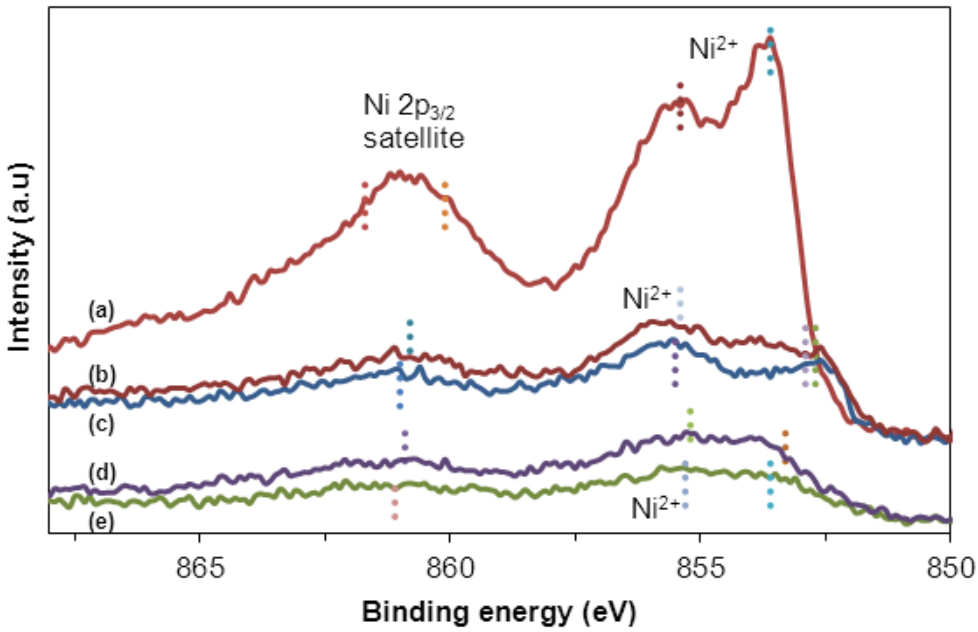

Fig 4.34 XPS pattern of Ni $2p_{3/2}$ core level (a) before test (b) after oxidant step at 800°C (c) after reductant step at 800°C (d) after oxidant step at 600°C (e) after reductant step at 600°C on Ni(10.5)/CeO_2

The ***Fig 4.34*** shows the XPS of the catalyst before and after each of the experiments. The binding energies of the two main peaks of Ni^{2+} before test are 853.6eV and 855.4eV (satellites at 860.1eV and 861.7eV respectively). Then, the Ni^{2+} binding energy after experiment at 800°C shift to 855.4eV (oxidant step) and 855.5eV (reductant step). There is also a contribution of metallic nickel in the two steps (852.9eV for the oxidant step and 852.7eV for the reductant step). Otherwise, the decrease of Ni species is seen again going from 31 at.% to 13-14 at.% after test (in terms of quantitative data). In addition the same kind of distribution is found about the oxidation state of nickel, obtaining 75-80% for Ni^{2+} and 20-25% for Ni^0. The quantitative differences between the two steps are almost negligible (see ***Table 4.8***). Moreover, some interesting clues can be also underlined from the experiments working at 600°C. First, the same trend as the experiments at 800°C is seen. In this case the binding energies for Ni^{2+} are located at 855.3eV and 855.2eV and the contribution of Ni^0 is at 853.6eV and 853.3eV (oxidant and reductant step respectively). In addition the oxidation state of nickel has the same distribution as in the experiment working at 800°C, in this case 70-80% for Ni^{2+} and 20-30% for Ni^0.

Table 4.8 Data from XPS analysis for Ni(10.5)/CeO_2 before and after experiments

Catalyst	% Atomic concentration				
	Ce	Ni	O	Ni^{2+}	Ni^0
Ni(10.5)/CeO_2	15	31	55	100	-
Ni(10.5)/CeO_2 a.e. 800°C, R	24	13	63	79	21
Ni(10.5)/CeO_2 a.e. 800°C, O	22	14	64	76	24
Ni(10.5)/CeO_2 a.e. 600°C, R	27	7	66	71	29
Ni(10.5)/CeO_2 a.e. 600°C, O	27	11	62	79	21

a.e. = after experiment

Furthermore, the spectra of the Ce $3d_{3/2.5/2}$ are also shown to verify the oxidation state of cerium after working at the different conditions mentioned above.

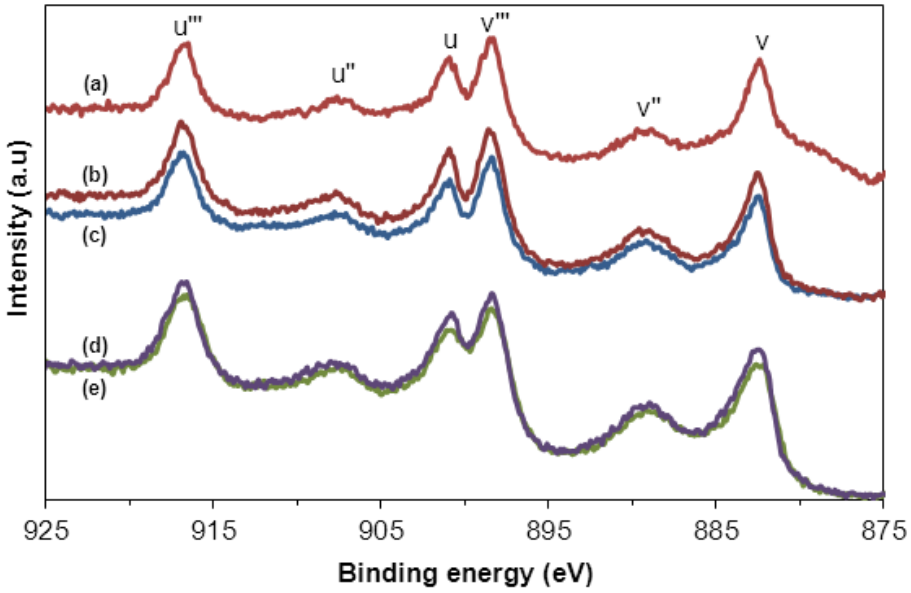

Fig 4.35 Ce $3d_{3/2.5/2}$ XPS spectrum (a) before test (b) after oxidant step at 800°C (c) after reductant step at 800°C (d) after oxidant step at 600°C (e) after reductant step at 600°C on Ni(10.5)/CeO_2

Cerium compounds have XPS spectra with rather complex features due to numerous initial and 4f electronic configurations. The 3d spectrum, registered on pure ceria, can be resolved into three spin-orbit doublets, $3d_{3/2}$-$3d_{5/2}$, denoted (u, v), (u'', v'') and (u''', v'''). The ***Fig 4.35*** shows the Ce $3d_{3/2.5/2}$ spectrum, observing the typical pattern of Ce^{4+} species before experiment. The characteristic peak of Ce^{4+} is the one observed at 916.7eV. Typically, this peak does not appear for the Ce^{3+} spectrum, as shown as a reference in the Annex (***Fig 7.15***). Otherwise, such peak appears in all the cases after experiment. Therefore, the surface CeO_2 is not completely reduced to Ce^{3+}. This could be explained by a rapid diffusion of oxygen species towards the surface, which is more expected at 800°C than at 600°C. Otherwise, some other phenomena can explain the Ce^{4+} at the low temperature, such as the time cooling down the reactor under argon. Indeed, surface Ce_xO_y can be slowly reoxidized even feeding only noble gases, just because of the oxygen diffusion from the bulk [4.5]. Nevertheless, a long

reduction by methane seems to be necessary to reach Ce^{3+} species on the first layers of the catalyst or/and an in-situ XPS experiment.

4.5. Biogas composition

4.5.1. Carbon neutral cycle

The relevance of using biogas from the environmental point of view is shown in the following figure.

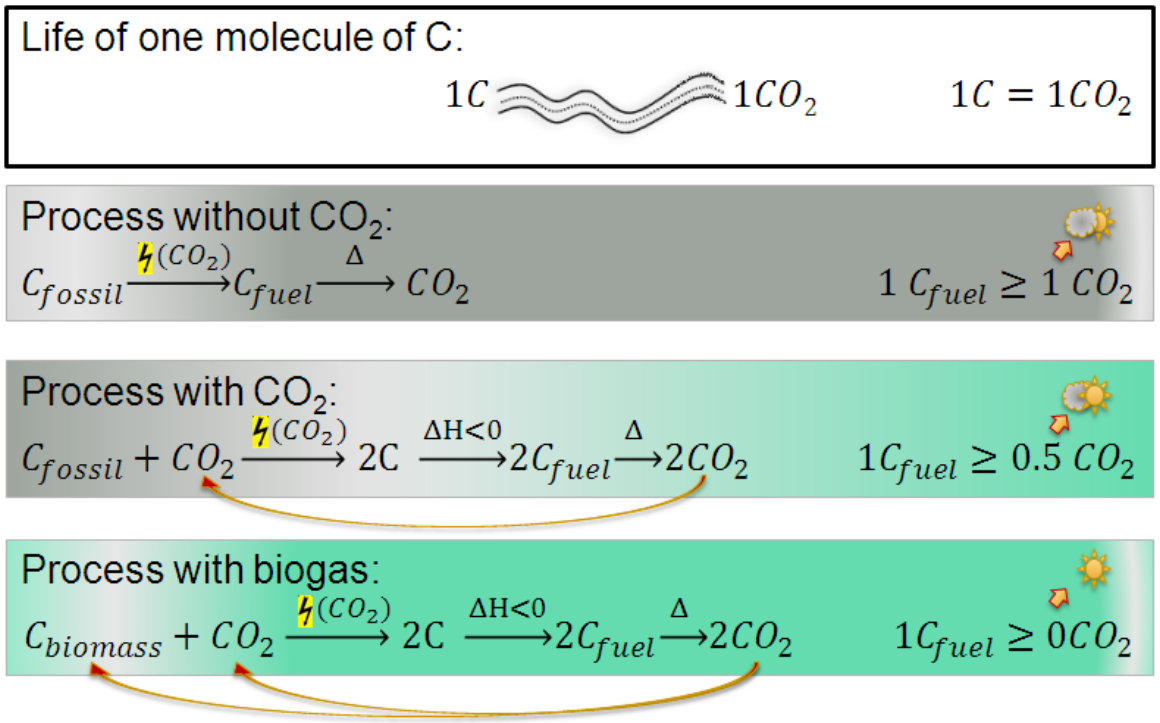

Fig 4.36 Carbon cycle in different scenarios

The life of one molecule of C ends up sooner or later as one molecule of CO_2. The ***Fig 4.36*** shows the comparison between working in a process without CO_2 (Ex. transformation from petrol to gasoline), with CO_2 (DRM) and with CO_2 using biogas as raw material. For instance, the process in this Chapter is already more favorable from the CO_2 emissions point of view than the one working without carbon dioxide, releasing the half of CO_2 to the atmosphere. Nevertheless, biogas is the greenest pathway, as the carbon balance would be nearly zero. Absolute zero carbon balance is difficult to state as the production of the required energy during the process would produce some. Based on that, an approach of the periodic concept working with biogas compositions (without H_2S) is studied in the following paragraphs.

4.5.2. Biogas composition: Influence of CO_2 in reductant step

The main compounds of biogas are CH_4 and CO_2, so another potential raw material for the process. There is a wide range of biogas sources, consequently they do not have the same proportion of the reactants. The most common range is 60-80% for CH_4 and 20-40% for CO_2. Thereby, a set of experiments was carried covering the whole range (83.3%, 71.4%, 62.5%, and 55.5% of CH_4 with the corresponding concentration of CO_2). The following graphs shows the comparison from 100% CH_4 in one side and 100% CO_2 in the other (typical periodic system) until 55.5%CH_4 - 44.5% CO_2 in one side and the equivalent of CO_2 to get the stoichiometry CH_4/CO_2 = 1 (whole cycle) in the other side. The conversion of CO_2 is expressed in terms of the whole cycle (taking into account the $CO_{2,in}$, and the $CO_{2,converted}$ during the reductant and the oxidant step). The main idea of such experiments is to prove the feasibility of the periodic system for the biogas compositions without needing prior separation of CH_4 and CO_2 and simply “completing” the CO_2 feed in periodic way.

Table 4.9 H_2/CO ideal ratio

$[CO_2]_0$ in R step (%)	H_2/CO ideal
0	2.00
1	1.67
2	1.43
3	1.25
4	1.11
5	1.00

The ***Table 4.9*** shows one of the main differences working with some CO_2 in the reductant step. The ideal H_2/CO ratio is lower as higher is the concentration of CO_2 going from 1.67 at $[CO_2]_0$=1% to 1.11 at $[CO_2]_0$=4% (CH_4 is maintained at 5%).

800°C

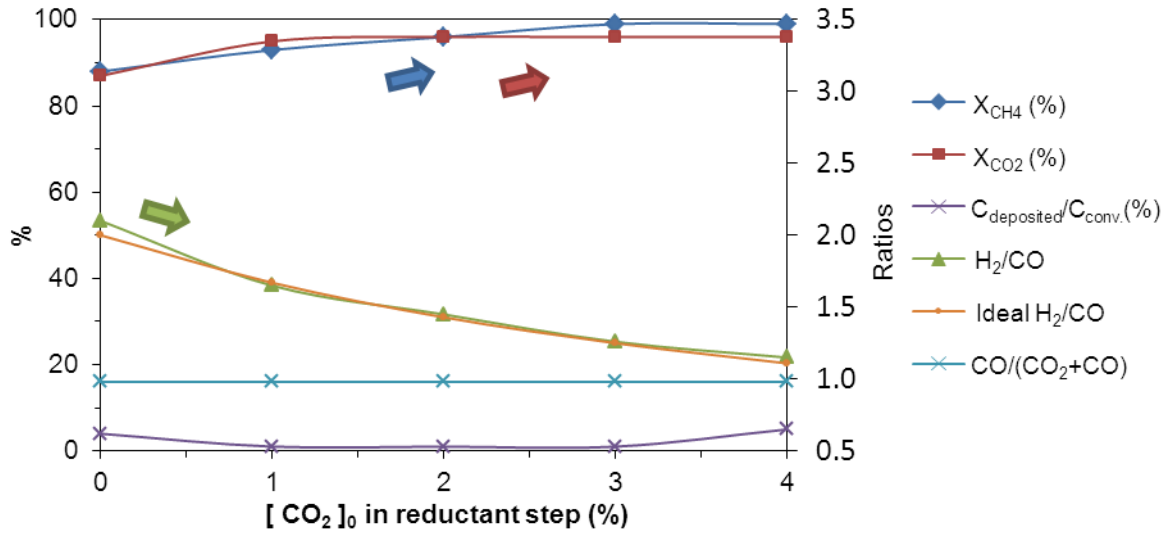

Fig 4.37 ***Reductant step:*** *Conversion of CH_4 (%), $C_{deposited}/C_{conv.}$(%), H_2/CO and CO/(CO_2+CO) ratios.* ***Whole cycle:*** *Conversion of CO_2 (%).200mg of Ni(9.5)/CeO_2 for 5% CH_4 0% CO_2, 200mg of Ni(8.8)/CeO_2 for 5% CH_4 1% CO_2 and 200mg of Ni(10.5)/CeO_2 for the rest of the experiments. 800°C $F_{T,0}$ =100 mL/min. Cycle:1/2/1/2, 5% CH_4, x% CO_2*

In this case, 90-100% selectivity and quite high conversions (90-100%) are obtained in the whole range of compositions. Otherwise, H_2/CO ratio goes down as the concentration of carbon dioxide increase, as mentioned previously, but follows the ideal selectivity curve. Otherwise, few real differences can be seen in the figure due to the high performances in all the cases.

600°C

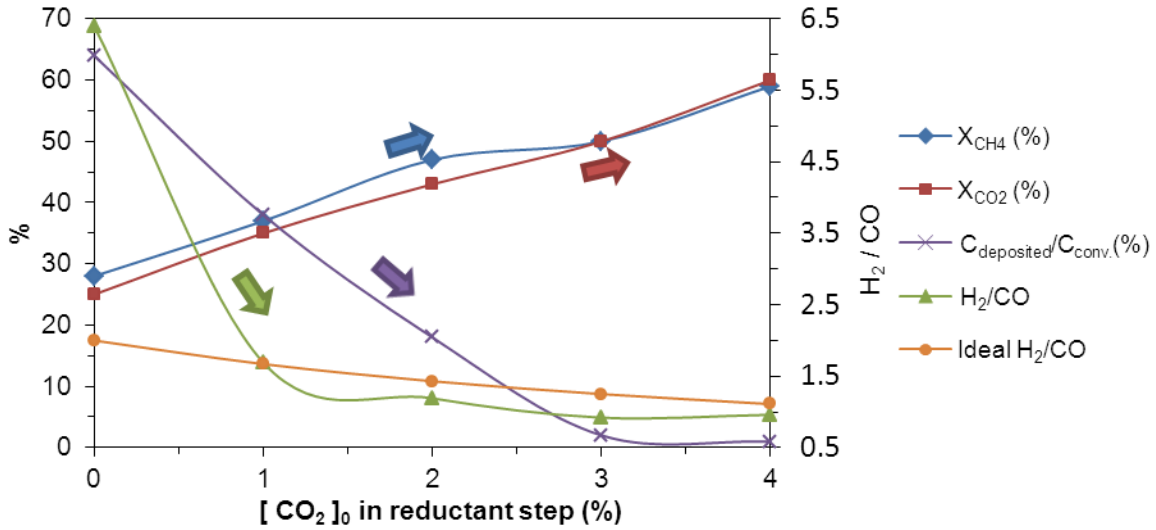

Fig 4.38 ***Reductant step:*** *Conversion of CH_4 (%), $C_{deposited}/C_{conv.}$(%), H_2/CO ratio.* ***Whole cycle:*** *Conversion of CO_2 (%).200mg of Ni(8.8)/CeO_2 for 5% CH_4 1% CO_2 and 5% CH_4 0% CO_2 in reductant step and 200mg of Ni(10.5)/CeO_2 for the rest of the experiments. 600°C $F_{T,0}$ =100 mL/min. Cycle:1/2/1/2, 5% CH_4, x% CO_2*

The ***Fig 4.38*** evidences more differences of working with some CO_2 in the reductant step at low temperature. At 600ºC the carbon deposition decreases clearly as the percentage of CO_2 increases. Logically, CeO_2 loses step by step the role of being the only oxygen vector to oxidize methane. Another point to underline is that at 2%, 3% and 4% concentration of CO_2 in the reductant step, H_2/CO ratio is lower than the ideal one showing a strong influence of the reverse water gas shift.

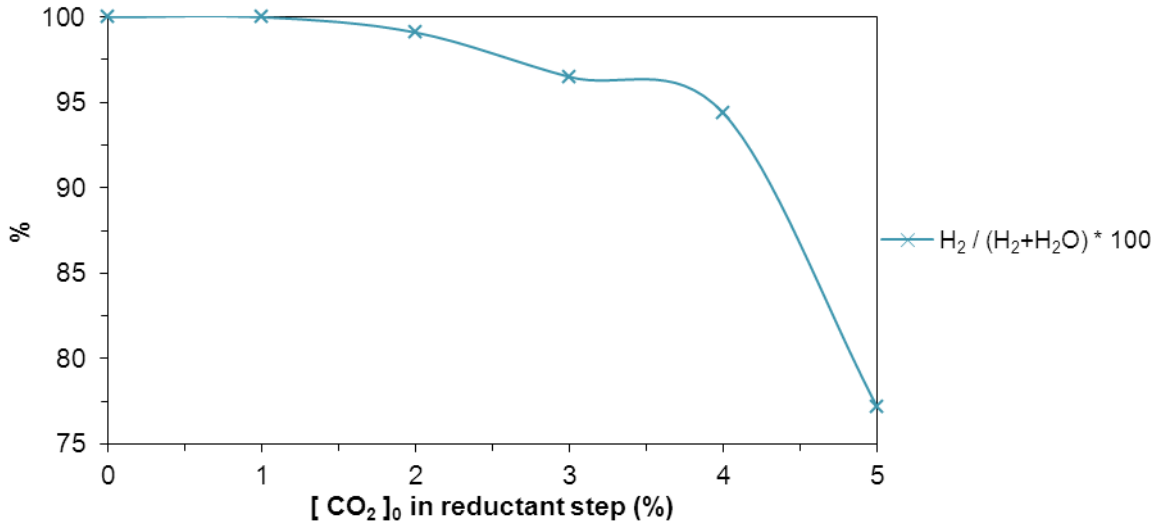

Fig 4.39 ***Reductant step:*** *Production of H_2O working at 600°C*

The prediction of more RWGS is verified in the ***Fig 4.39***. The variation in the H_2 selectivity between H_2 and H_2O goes from 100% working only with CH_4 to 77% in the classical DRM

(5%CH_4 5%CO_2). This evidences one of the main advantages working with pure CH_4 at the first step. The results obtained above verify that biogas composition can also work well in the periodic concept, keeping in mind the main differences mentioned before.

These experiments were made using rather low reactant concentrations (5%). Thus, differences between pure periodic and mixed cofeed-periodic processes could be more relevant at higher concentrations but give good opportunities for process optimization.

Another relevant issue about working with biogas is the presence of H_2S in the feed which can poison the catalysts and lead to deactivation. Some experiments have been performed in the presence of such gas. For this purpose a new set-up has been built and equipped with all the safety issues related with this chemical (ventilation, alarms, emergency protocols…). Results of such preliminary tests are not shown. Indeed, as it could be expected, Ni-CeO_2 catalysts are fully deactivated after few cycles in presence of H_2S (H_2S/CH_4/He/Ar (vol.%) = 0.2/5/3.7/91.1, F_T = 99.9mL/min). The design of H_2S resistant catalysts for periodic DRM is therefore a subject of further development.

4.6. Shale gas approach

Some tests on the Periodic Dry Reforming of Ethane (P-DRE) were carried out considering the encouraging results for the periodic dry reforming of methane (P-DRM). This extension of the process to other raw materials is based on the enormous market development in the last years concerning shale gas, which typically contains between 0-20% of C_2H_6. Obviously, some properties change working with C_2H_6 instead of CH_4. For instance, the ideal ratio H_2/CO is 1.5 instead of 2:

Eq. 4.3 $$\mathbf{C_2H_6 + 4CeO_2 \rightarrow 3H_2 + 2CO + 2Ce_2O_3} \qquad \mathbf{H_2/CO = 1.5}$$

Eq. 4.4 $$\mathbf{2CO_2 + 2Ce_2O_3 \rightarrow 4CeO_2 + 2CO}$$

Eq. 4.5 $$\mathbf{C_2H_6 + 2CO_2 \rightarrow 3H_2 + 4CO} \qquad \mathbf{H_2/CO = 0.75}$$

4.6.1. Catalytic test

Pure C_2H_6 was fed to the reactor in place of CH_4 in order to see the behavior of this hydrocarbon towards the periodic process. Another particularity is the 2 minutes feed (instead of 1) of CO_2 in the oxidant step to be in the stoichiometry amount of each reactant in the whole cycle, as seen in the equations above.

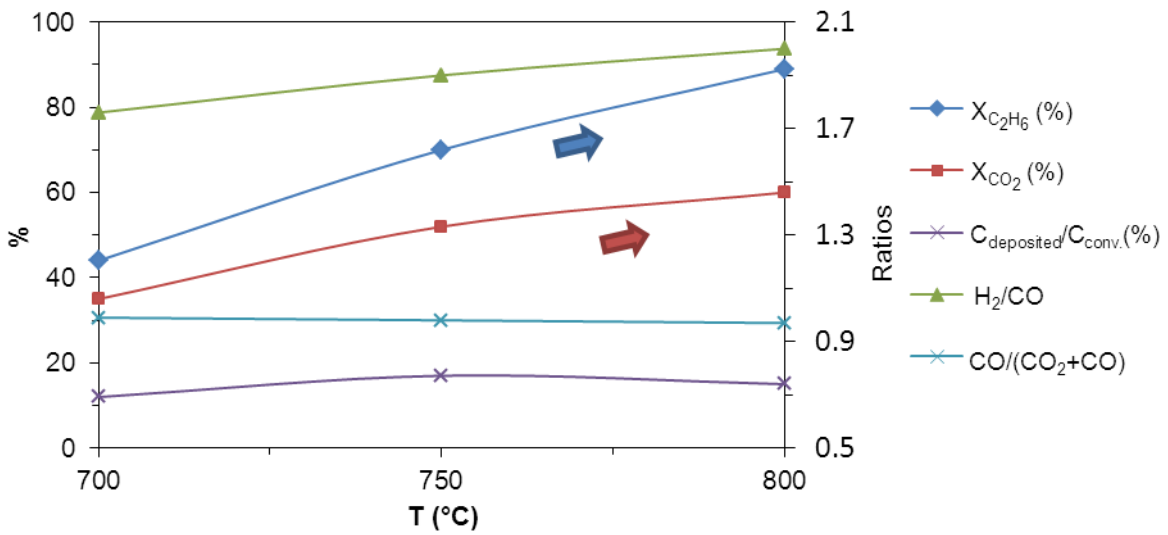

Fig 4.40 ***Reductant step:*** *Conversion of C_2H_6 (%), $C_{deposited}/C_{conv.}$(%), H_2/CO and $CO/(CO_2+CO)$ ratios.* ***Oxidant step (2min.):*** *Conversion of CO_2 (%). 200mg of $Ni(8.8)/CeO_2$ at different T $F_{T,0}$ =100 mL/min. Cycle:1/2/**2**/2, 5% C_2H_6, 5% CO_2*

The ***Fig 4.40*** shows the results obtained at 700ºC, 750ºC and 800ºC. The conversion of C_2H_6 increases with temperature from 44% at 700°C to 89% at 800ºC. Focusing at the lowest temperature of 700ºC, the conversion is 20% lower than working with methane, which is unexpected as ethane is easier to activate than methane. This lower activity could be explained by the history of the sample studied. Indeed, experiments made in the catalyst at 700°C, 750°C and 800°C working with only 1 minute of CO_2 instead of the 2 stoichiometry minute was performed on this sample which may partially deactivated the catalyst. In fact, taking the first reductant step operating with ethane at 700°C the conversion goes up to 97% instead of the 64% for methane at the same conditions. However, the selectivity is worse than working with methane, potentially due to a rise in the carbon deposition. It gets around the double (11% instead of 5% at 700°C). Otherwise, CO_2 conversion is considerably lower than the one of C_2H_6. The outlet partial pressures in the last two cycles working at 700ºC is shown in the following figure in order to understand such behavior.

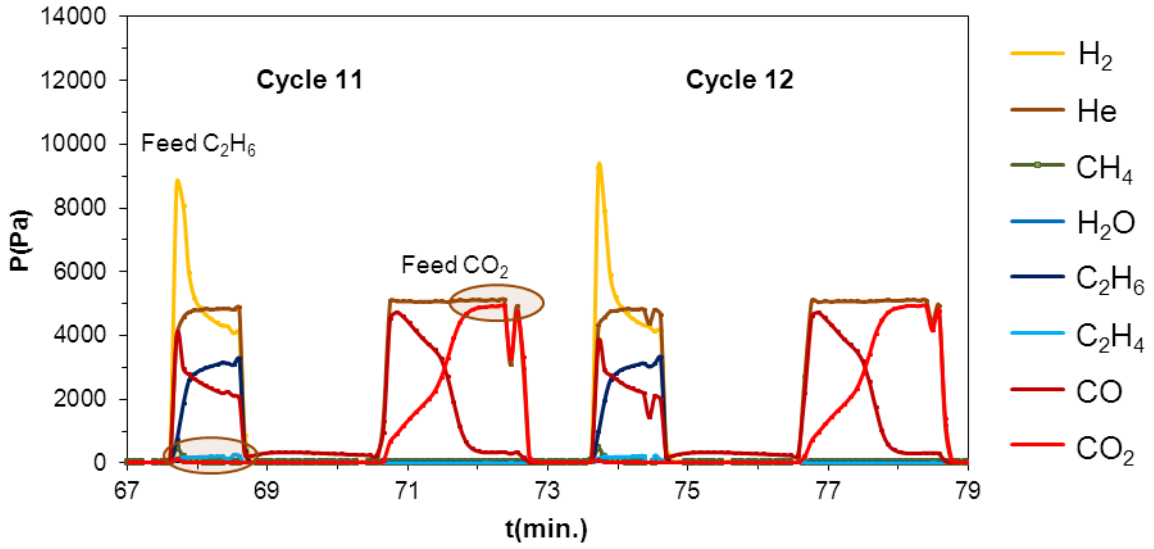

Fig 4.41 Partial pressures in the outlet flow working with 200mg of Ni(8.8)/CeO_2 at 700°C $F_{T,0}$ = 100 mL/min. Cycle: 1/2/2/2. 5% C_2H_6, 5 % CO_2

Fig 4.41 shows interesting indications about some differences from the P-DRM. First, some ethylene is seen in the reductant step (light blue line) evidencing some other side products working with C_2H_6. In addition the low conversion of CO_2 can be understood from the graph above, there is a point where the partial pressure of CO_2 remains stable but slightly lower than its nominal value. CO_2 is still converting something but much slower than the rest of the species. Eventually, some of the carbon deposit is another type than the one working with CH_4, which at the same time has more difficulties to be oxidized by CO_2.

In addition, another correlation between the theoretical thermodynamics and the experimental data is found in the next figure, working the P-DRE at 800ºC.

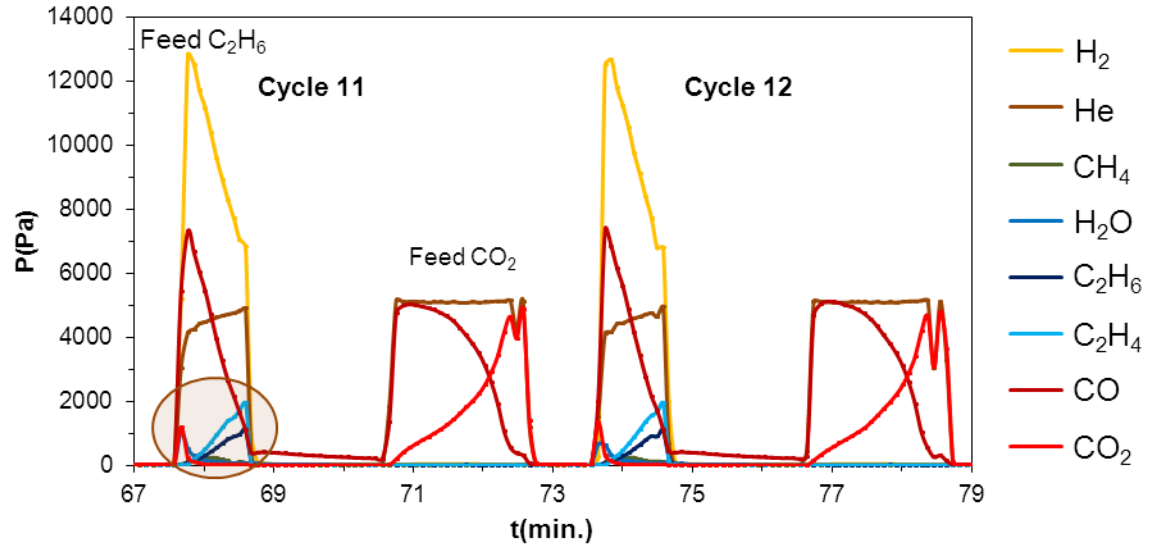

Fig 4.42 Partial pressures in the outlet flow working with 200mg of Ni(8.8)/CeO_2 at 800°C $F_{T,0}$ = 100 mL/min. Cycle: 1/2/2/2. 5% C_2H_6, 5 % CO_2

A considerable amount of ethylene is produced at such temperature. On the contrary, a really small amount was produced at 700°C, as seen in the ***Fig 4.41***. The $C_2H_6 \rightarrow C_2H_4+H_2$ reaction becomes more favorable at 800°C (***Paragraph 3.2.7***). Notwithstanding, the main point of this first approach is to show that the periodic concept can work with this hydrocarbon obtaining reproducible cycles through the experiment.

In general terms, P-DRE shows promising results especially as the system has not been optimized for ethane conversion. For example, a way to reduce the carbon deposition working with ethane would be to expose more oxygen available to react in the system by increasing the amount of catalyst. In summary, these results encourage to try mixtures CH_4 - C_2H_6 in the inlet as shale gas contains typically 20% maximum concentration of ethane. Such mixtures would probably be more favorable to produce less carbon than the results shown above.

4.7. Conclusions

The principle of periodic dry reforming of methane has been successfully demonstrated using a solid based on particles of nickel (Ni) supported or coprecipitated with cerium dioxide (CeO_2). The support reacts as an oxygen vector by reduction and oxidation under CH_4 and CO_2 respectively. The metal is necessary to provide the good activation of methane, leading to high conversions. Nickel cannot be reoxidized back to the original oxide state in presence of CO_2 under the working conditions, which is also corroborated with the thermodynamic calculations. In such conditions, the selectivity coming from the oxidation of methane is practically ideal towards syngas, on the contrary to when the catalysts is reoxidized by oxygen. In addition, the main differences from other studies made in the literature are the high selectivity towards H_2/CO without a high production of H_2O thanks to work with Ni-CeO_2 instead of Fe-CeO_2 formulations and the ease of the synthesis technique. Impregnation and coprecipitation methods, the most practical ones for the industry, have shown promising performances for this process.

These results evidence that in a wide range of conditions: different concentrations of the reactants, reaction temperature, amount and nature of the solid…the performances obtained are quite close to the ideal selectivity. The main difference may be about the reactivity and the percentage of carbon deposition. Thus, the robustness of this process is shown when the conditions mentioned above are respected. Besides, a large margin of optimization is also discussed, in particular by:

- The control of the amount and the nature of the metallic phase, see mixed metals phase to optimize the activation of CH_4 and CO_2.
- The control of the oxygen available to react in the oxygen carrier modifying the nature of the support (oxides, mixed oxides…)

4.8. References

4.1 P. Danielson, Creating a vacuum. A journal of practical and useful vacuum technology. http://www.surface.mat.ethz.ch/education/courses/surfaces_interfaces_and_their_applications/ Last viewed: **29th October 2012**

4.2 NIST Chemistry Webbook. http://webbook.nist.gov/webbook.nist.gov/ Last viewed: **2012-2015**

4.3 The vacuum technology book. Pfeiffer vacuum Volume 1 **(2008)** 110-136

4.4 L. Jalowiecki-Duhamel, H. Zarrou, A. D'Huysser, Hydrogen production at low temperature from methane on cerium and nickel based mixed oxides *Int. J. Hydrogen* 33 **(2008)** 5527-5534

4.5 O. Demoulin, M. Navez, J.L. Mugabo, P. Ruiz, The oxidizing role of CO_2 at mild temperature on ceria-based catalysts *Appl. Catal. B* 70 **(2007)** 284-293

4.6 C. Bozo, N. Guilhaume, J.M. Herrmann, Role of the ceria-zirconia support in the reactivity of platinum and palladium catalysts for methane total oxidation under lean conditions *J. Catal.* 203 **(2001)** 393-406

4.7 N.V. Skorodumova, S.I. Simak, B.I. Lundqvist, I.A. Abrikosov, B. Johansson, Quantum origin of the oxygen storage capability of ceria *Phys. Rev. Lett.* 89 **(2002)** 16

4.8 P. Kumar, Y. Sun, R.O. Idem, Comparative study of Ni-based mixed oxide catalyst for carbon dioxide reforming of methane *Energ. Fuel.* 22 **(2008)** 3575-3582

4.9 C. Li, Y. Sakata, T. Arai, K. Domen, K.I. Maruya, T. Onishi, Carbon monoxide and carbon dioxide adsorption on cerium oxide studied by fourier-transform infrared spectroscopy *J. Chem. Soc., Faraday Trans. 1* 85 **(1989)** 929-943

4.10 T. Jin, T. Okuhara, G.J. Mains, J.M. White, Temperature-Programmed desorption of CO and CO_2 from Pt/CeO_2. An important role for lattice oxygen in CO oxidation *J. Phys. Chem.* 91 **(1987)** 3310-3315

4.11 S. Sharma, S. Hilaire, J.M. Vohs, R.J. Gorte, H.W. Jen, Evidence for Oxidation of Ceria by CO_2 *J. Catal.* 190 **(2000)** 199-20

4.12 T. Staudt, Y. Lykhach, N. Tsud, T. Skala, K.C. Prince, V. Matolin, J. Libuda, Ceria reoxidation by CO_2: A model study *J. Catal.* 275 **(2010)** 181–185

4.13 M. Kamiya, E. Shimada, Y. Ikuma, M. Komatsu, H. Haneda, Intrinsic and extrinsic oxygen diffusion and surface exchange reaction in cerium oxide *J. Electrochem. Soc.* 147 **(2000)** 1222–1227

4.14 S. Ackermann, J.R. Scheffe, A. Steinfeld, Diffusion of oxygen in ceria at elevated temperatures and its application to H_2O/CO_2 splitting thermochemical redox cycles *J. Phys. Chem. C* 118 **(2014)** 5216–5225

4.15 C.E. Whiting, C.D. Barklay, D.P. Kramer, E.A. Kaufman, J.M. Douglas, Mechanisms and kinetics of the oxygen exchange reaction with CeO_2 at high temperatures *Solid State Ionics* 272 **(2015)** 18–23

4.16 J.E. Fallah, S. Boujana, H. Dexpert, A. Kiennemann, J. Majerus, O.Touret, F. Villain, F.L. Normand *J. Phys. Chem.* 98 **(1994)** 773.

4.17 D. Garcia, A. Juan, B. Irigoyen, Oxygen vacancy formation on the $Ni/Ce_{0.75}Zr_{0.25}O_2$ (111) surface. A DFT + U study *Int. J. Hydrogen Energy 37* **(2012)** 4937-*4944*

4.18 T.Marrero,E.Mason. http://www2.bren.ucsb.edu/~dturney/WebResources_13/GasInWaterProperties_files/BinaryDiffusionOfGases.pdf **1972**. [Online]. [Accessed 2013-2015].

4.19 L. Jalowiecki-Duhamel, H. Zarrou, A. D'Huysser, Low temperature hydrogen production from methane on cerium nickel- and zirconium-based oxyhydrides, *Catal. Today* 138 **(2008)** 124–129.

4.20 F. Dury, E.M. Gaigneaux, P. Ruiz, The active role of CO_2 at low temperature in oxidation processes: the case of the oxidative dehydrogenation of propane on $NiMoO_4$ catalysts *Appl. Catal. A* 242 **(2003)** 187–203.

4.21 E. Bêche, P. Charvin, D. Perarnau, S. Abanades, G. Flamant, Ce 3d XPS investigation of cerium oxides and mixed cerium oxide ($Ce_xTi_yO_z$) *Surf. Interface Anal.* 40 **(2008)** 264–267.

4.22 A. Kambolis, H. Matralis, A. Trovarelli, Ch. Papadopoulou, Ni/CeO_2-ZrO_2 catalysts for the dry reforming of methane, *Appl. Catal. A* 377 **(2010)** 16-26.

CHAPTER V:

Kinetic approach for periodic DRM

5. KINETIC APPROACH FOR PERIODIC DRM

5.1. Bibliography discussion

In a parallel way of the optimization of the process, the understanding of the surface chemistry through different kinetic approaches has been studied in detail, mainly based on the Langmuir-Hinshelwood approach [5.2-5.6] or detailed multi-step surface reaction mechanisms describing the elementary-like processes occurring on the catalysts surface [5.1,1.57]. In our case, we are focused in the second approach, obviously due to the concept of working in periodic conditions. Some researchers already studied the chemistry of CH_4 and CO_2 on the surface independently.

From the literature, different catalysts formulations lead to different mechanism proposals. Bychkov et al. [5.3,5.4] showed that for traditional catalysts such as alumina-supported Pt, Ni and Co the CO_2 is activated via direct interaction with the carbon atoms on the metal surface, which is the slowest step of DRM. Otherwise for Ni/SiO_2 catalyst, Y. Schuurman and C. Mirodatos [5.5] said that CO_2 is activated by direct dissociation on Ni atoms and the rate-limiting step is interaction between C and O adsorbed on Ni. For Ni/lanthana catalyst, Slagtern et al. [5.6] proposed that methane is activated on the Ni particles, and carbon dioxide interacts with La_2O_3 to form carbonates which scavenge carbon from nickel at the $Ni–La_2O_3$ interface. Specifically, the attractiveness of the fluorite-like oxide (CeO_2 in our case) for such reactions is commonly explained by the bifunctional scheme of reaction mechanism including CH_4 activation and CO_2 on the oxide sites followed by fast transfer of oxygen species to the metal-support interface, where they interact with activated CH_x species producing syngas [5.1].

From all these approaches CH_4 and CO_2 can be activated by several different interactions with the catalyst, depending on the nature of the solid. Thus, the discussion of the evidence for such mechanism is still open. One of the main points is to know the rate-determining step and if the activation of both reagents is independent or not. The pulse technique is typically used for these kinds of studies (cofeeding together or independently the two reactants) towards the steady state catalyst to figure out the reaction mechanism [5.1-5.5]. However, few studies have been made to study such reaction in metal-supported catalysts with high mobility and reactivity of oxygen in oxide supports.

Sadykov et al. [5.1] studied the mechanism in such conditions. Concretely, a pulse of CH_4 or CO_2 is fed once the catalysts reach steady state in cofeed conditions at 700°C. The catalyst was based on metal nanoparticles on perovskite / fluorite supports with high oxygen mobility. They concluded that CH_4 molecules dissociate on metal sites yielding H_2 and surface C atoms or CH_x fragments, which are rapidly transformed into CO or/and H_2. Thus, the reaction is made with oxygen species at the metal/oxide support interface. Ni clusters supported on

nanocrystalline complex fluorite-like provides the partial oxidation of CH_4 by the feed of oxygen species from the support, assigning such step as the rate-limiting stage. Besides, the reoxidation of the reduced oxide sites was also carried by CO_2 to produce CO. There, it is shown that indeed the carbon can be reoxidized with CO_2, which is in agreement with the thermodynamic study mentioned above (***Fig 3.1***) and the experimental data obtained (***Table 4.2***). In addition it was assumed that CO_2 is consumed by dissociation into CO and oxygen species filling oxide support vacancies. To sum, they showed that reactive oxygen forms responsible for CH_4 transformation into syngas are efficiently regenerated by CO_2 dissociation on the surface vacancies of fluorite or perovskite supports. In addition, the variation of the heat (ΔH) showed a low positive value at the first pulse of CO_2, and afterwards a higher one in the following pulses. Knowing that the reoxidation of the fluorite-like support is commonly exothermic ($\Delta H<0$) and the one of carbon is endothermic ($\Delta H>0$), such behavior can be related as having faster kinetics for the reoxidation of the support and some of the carbon and lower one for the rest of the carbon (maybe another type of C). This approach of Sadykov is explained in more detail as it is one of the fundamental concepts for the availability of the process proposed in the ***Chapter 4***. In the same direction, Bhavsar et al. [1.57] underline the importance of the activation of CO_2 on the reactivity of the carrier through the use of nano-sized particles (in their case Fe) because the small particles may be expected to be more reactive due to the minimization of solid-state diffusion limitations during formation of dense oxide over-layers during carrier oxidation. They also show that kinetics of the reoxidation by CO_2 of a silica support is much slower than when a barium hexaaluminate support (BHA) is used. This study confirms the importance on the nature of the support for the activation and fast kinetics of CO_2. In addition, an important dependence of the temperature with the kinetics of the carrier oxidation was also observed, being slower at 600°C than at 800°C.

As a conclusion, all the approaches from the literature confirm the bifunctional mechanism of CH_4 dry reforming in periodic conditions (independent steps), one for the reductant and the other for the oxidant.

5.2. Partial oxidation of CH_4

Going further in the study of Sadykov et al. [5.1], we can make some interesting comparison with our experimental data. They showed that up to 2-3% of the overall oxygen content in the samples, the heat effects of the reaction are controlled by CH_4 interaction with oxygen species rapidly migrating to the metal/support interface from the surface sites of the fluorite-like oxides (at 700°C). They also concluded that the presence of some CO_2 could be explained by the interaction of CO with the surface hydroxyls. Otherwise, a deep reduction degree, when the oxygen storage capacity of the subsurface layers is depleted, the reaction heat declines

approaching values corresponding to the enthalpy of CH_4 dissociation into C (graphite) and H_2.

In the previous chapter the catalytic behavior of the solids where analyzed by integrating the reactant consumed and products on a whole reductant or oxidant step. In the following discussion, periodic DRM results will be analyzed in more details looking at the dynamics occurring within a single step. Usually, at least 10 cycles are performed in order to reach a "steady" periodic behavior. The following figure shows the accumulation of the CH_4 consumed and the oxygen removed from the solid along the one minute feed of CH_4 for different amounts of solid in the reactor at 700°C. Ideally, one mole of CH_4 consumed should remove one mole of oxygen from the solid in order to get 2 H_2 and 1 CO. Thus, 100% selectivity should be reached if the lines of CH_4 and oxygen consumed overlap each other and follow a parallel trend (considering that a time shift can occur) to the black line which represents the cumulated CH_4 fed into the reactor. Otherwise, if the consumption of CH_4 is higher than the one of oxygen, some carbon is deposited on the catalyst. On the contrary, if the consumption of oxygen is higher than the one of CH_4, the total oxidation of CH_4 is involved in the system producing some H_2O and CO_2 (besides or not some carbon deposition).

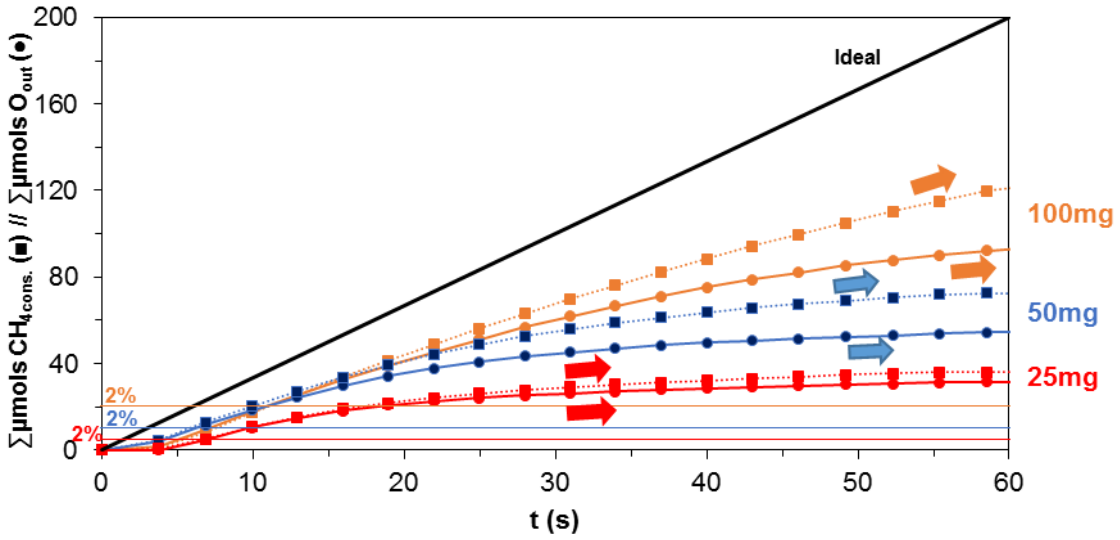

Fig 5.1 O removed (●) and CH_4 consumed (■) at 700ºC, Ni(8.8)/CeO_2, $[CH_4]_0$ = 5% after 11 cycles

Fig 5.1 shows that the two lines (O removed and CH_4 consumed) tend to separate after about 2% of oxygen is consumed. From there, the distance between the two curves is progressively bigger, meaning that the decomposition of CH_4 is becoming more and more important than the partial oxidation towards syngas. Probably, at such temperature, the migration of the oxygen from the bulk to the surface has no kinetics limitations until the 2-4% of oxygen is consumed. Then, the cracking of methane becomes more important due to a lack of enough oxygen on the surface. Therefore, these results are in good agreement with the Sadykov's study [5.1]. Otherwise, the 2-4% value cannot be extrapolated to other temperatures

because the diffusion of oxygen is extremely dependent on such parameter. As evidence, the following figure shows the consumption of CH_4 and oxygen along the 1 minute feed at different temperatures.

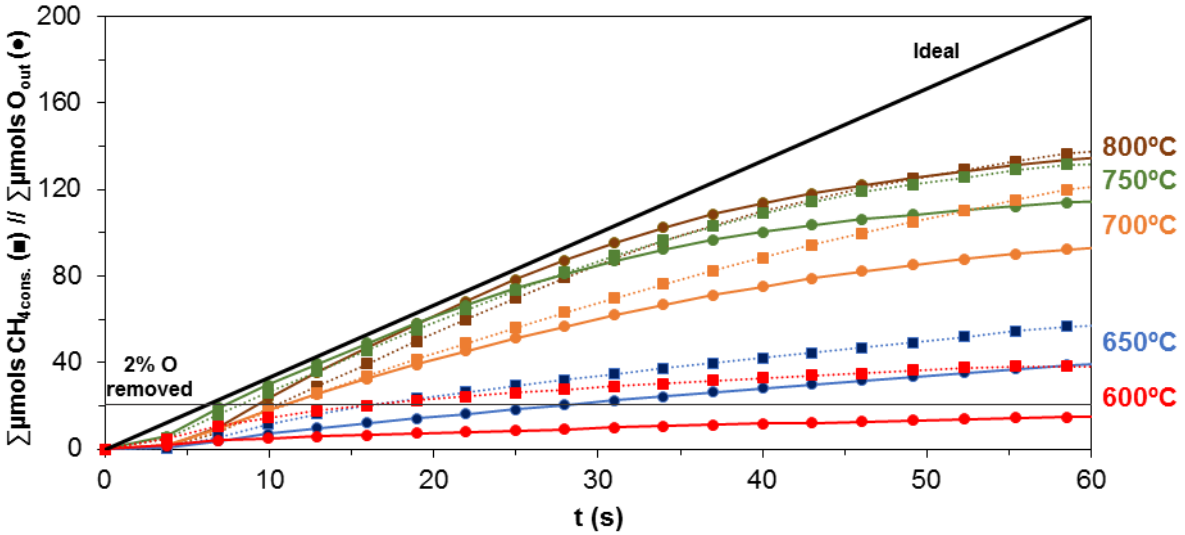

Fig 5.2 O removed (●) and CH_4 consumed (■) at different T, 100mg Ni(8.8)/CeO_2, $[CH_4]_0$ = 5% after 11 cycles working in periodic

The ***Fig 5.2*** shows that at 650ºC, when the solid reaches approximately 2% of oxygen removed, the selectivity is already quite far from the ideal one. In fact, at such temperature almost from the beginning of the step the consumption of CH_4 is more important than the one of oxygen, underlying the big influence on the diffusion of oxygen at such range of temperature. Otherwise, at the initial stage of the 1 minute step appears the fastest kinetics of oxygen diffusion in all the cases, probably thanks to the oxygen from the first layers of the surface. Knowing such behavior, it would be a matter of adjusting the amount of catalyst to keep 100% selectivity along the whole step. For instance, in the example showed in the ***Fig 5.2***, such ideal situation is reached at 800ºC for the whole 1 minute or at 750°C during the first 30 seconds. However, the oxygen available to react is a little bit in excess during the first 40 second working at 800ºC, as the curve of oxygen consumed goes above of the one of the CH_4 consumption, so potentially producing some CO_2 and H_2O.

Moreover, Bhavsar et al. [1.57] also correlates the increase of the total carrier utilization (C.U.) with the increase in temperature. Therefore, another set of experiments were carried working at different temperatures, in this case using 200mg of catalyst.

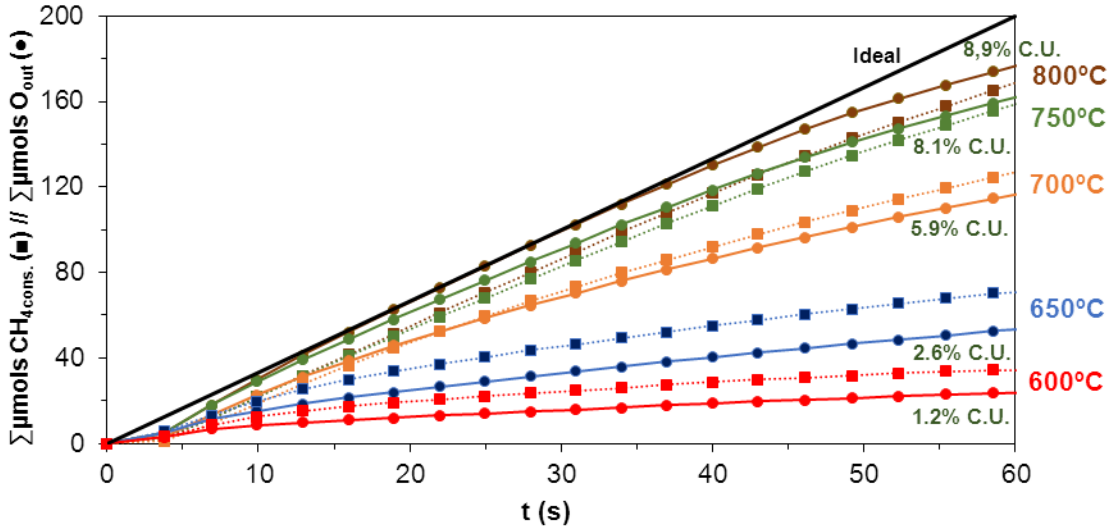

Fig 5.3 O removed (●) and CH_4 consumed (■) at different T, 200mg Ni(8.8)/CeO_2, $[CH_4]_0$ = 5% after 11 cycles working in periodic

The ***Fig 5.3*** shows carrier utilization of 1.2% at 600ºC and 8.9% at 800ºC. This trend agrees from one side to the thermodynamics of the potential main reaction which is more favorable at higher temperatures and from the other sides with fast kinetics of oxygen diffusion from the bulk to the surface of the fluorite structure at high temperatures.

Based on the studies above, the best conditions activity-selectivity would be a matter of adjusting the timing step, temperature and/or the amount of catalyst.

Oxygen diffusion length

Oxygen diffusion can be related to the morphology of CeO_2 crystals and is strongly influenced by temperature. The characteristic oxygen diffusion length can be calculated from diffusion coefficient data from the literature.

Diffusion length (cm):

Eq. 5.1 $$L = 2 \cdot \sqrt{D \cdot t}$$

t = residence time (s) = 1.2s

D = diffusion coefficient (m^2/s)

Table 5.1 Oxygen diffusion coefficient and diffusion length in CeO_2

T(°C)	D_{int} (m^2/s)	L_{bulk} (nm)
300	7.37E-25	0.002
600	9.04E-18	7
650	4.90E-17	15
700	2.23E-16	33
750	8.75E-16	65
800	3.02E-15	120
850	9.35E-15	212

Table 5.1 shows the diffusion coefficient and characteristic diffusion length calculated using the data provided by M. Kamiya et al. [4.13]. Even if they consider such correlation at the range temperature above 900°C it reflects the intrinsic diffusion properties in such solid. It is however difficult to obtain concordant diffusion data for CeO_2 because it is strongly affected by the presence of impurities which generate vacancies and thus improve diffusion, especially at low temperatures. The characteristic time considered is the residence time of gases inside the reactor (typically 1.2s).

One would expect that with a diffusion length shorter than the crystal size of the oxygen carrier, the diffusion of oxygen from the bulk would be limited, and become rate determining for the process. On the contrary, if the diffusion length is larger than the crystal size, oxygen would have enough time to migrate from the bulk to the surface within the time considered. The average crystallite size of CeO_2 of "equilibrated" P-DRM solid is in the range of 35 to 40 nm (***Table 4.6***). At 600°C the diffusion length is indeed shorter that the crystal size whereas it is 3 to 4 times larger at 800°C. Although such considerations should be used cautiously, this shows that the transition between a process where diffusion limits oxygen transfer from bulk to a process wherein all the bulk oxygen is directly involved occurs in the temperature range explored within this study.

CeO_2-Ce_6O_{11} redox couple

An interesting correlation can be found between working at 700-750°C with 200mg, 100mg and 50mg of catalyst.

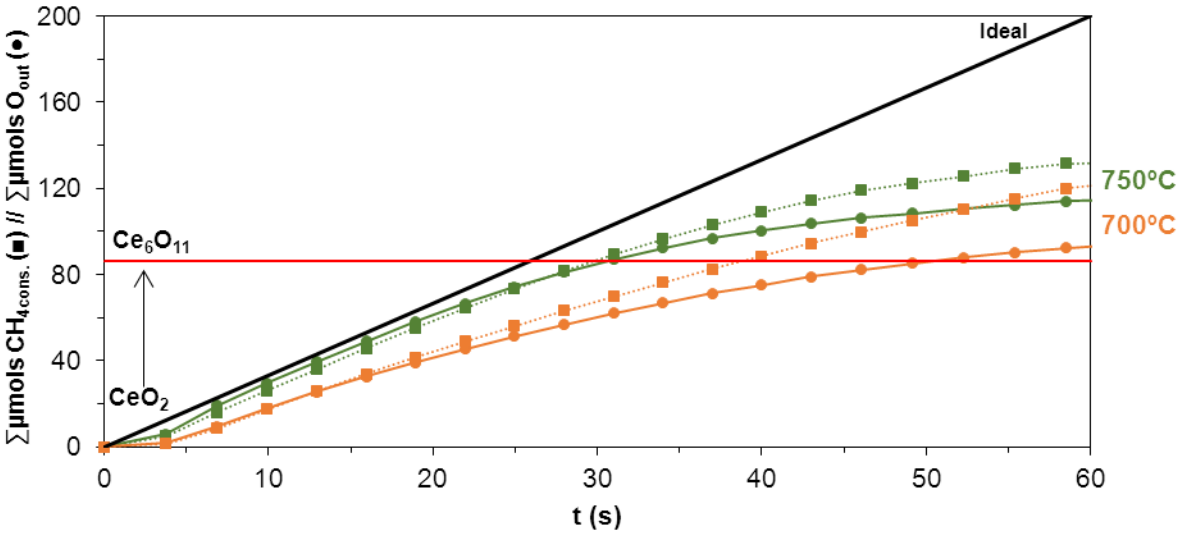

*Fig 5.4 O removed (●) and CH_4 consumed (■) at 700°C and 750°C, **100mg** Ni(8.8)/CeO_2, $[CH_4]_0$ = 5% after 11 cycles working in periodic*

First, ***Fig 5.4*** shows that at 750°C the system is selective until the oxygen consumed reached a C.U. of approx. 8% which corresponds to Ce_6O_{11} oxide phase, producing afterwards some

carbon. This effect could mean that at a given temperature there is an important difference between the kinetics from CeO_2 to Ce_6O_{11} than the kinetics at a lower reduction phase. Interestingly, the split of the oxygen and CH_4 consumed is at 30 seconds, therefore we should expect to keep the good selectivity with the double amount of solid. The importance of the temperature on the oxygen diffusion is also checked looking at the curves at 700°C. Being in the range between CeO_2-Ce_6O_{11}, it does not mean to obtain directly good selectivity. At such temperature the two consumption curves split much earlier than at 750°C.

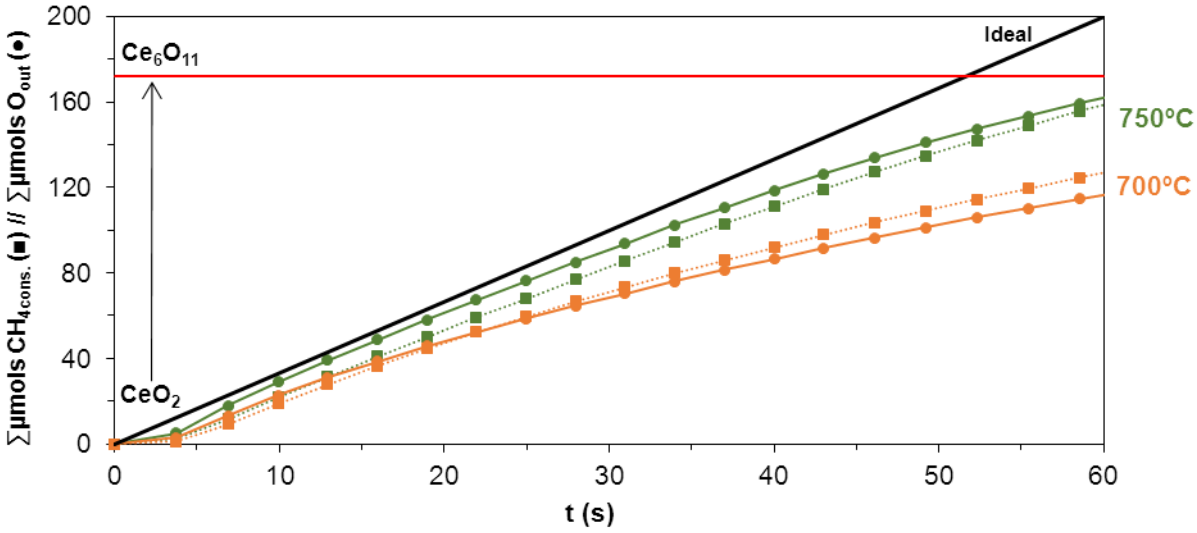

*Fig 5.5 O removed (●) and CH_4 consumed (■) at 700°C and 750°C, **200mg** Ni(8.8)/CeO_2, $[CH_4]_0$ = 5% after 11 cycles*

The predictions made from the ***Fig 5.4*** are verified and shown in ***Fig 5.5***. Indeed, the consumption of methane and oxygen have the same rate during the one minute step. From these two figures we can say that our solid can diffuse oxygen at a proper rate at 750°C to keep an excellent selectivity during the whole step, concretely between the CeO_2 and Ce_6O_{11} oxide phases.

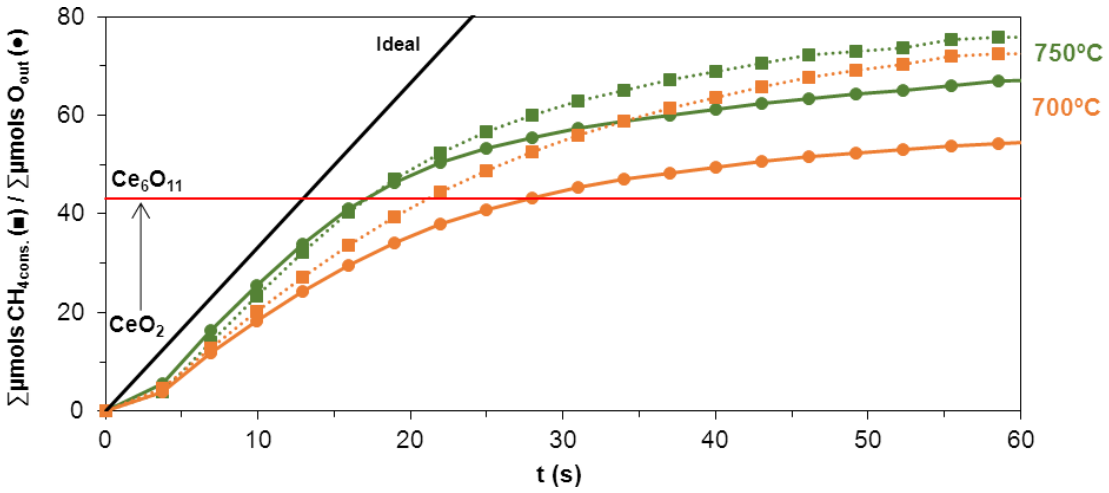

*Fig 5.6 O removed (●) and CH_4 consumed (■) at 700°C and 750°C, **50mg** Ni(8.8)/CeO_2, $[CH_4]_0$ = 5% after 11 cycles*

This trend is also checked in the figure above working with 50mg. The consumption of CH_4 and oxygen splits once the redox couple CeO_2-Ce_6O_{11} is completed (at 750°C).

5.3. Total reoxidation of the catalyst by CO_2

Sadykov et al. [5.1] showed that for all steady-state catalysts based on supports with high lattice oxygen mobility, CO_2 pulses provide reoxidation of only the surface sites. Hence, bridging surface oxygen species regenerated by CO_2 pulses do not migrate into the subsurface layers/bulk of oxide support particles. However, in our case the reoxidation seems to be complete, providing all the oxygen consumed in the reductant step even when the solid is reduced up to 18% of the oxygen. Such degree of reduction cannot be related only to the surface oxygen of CeO_2. As a reminder, 25% of oxygen can be removed from CeO_2 to Ce_2O_3. This can be shown looking at the oxidant step of the experiment with low amount of solid (25mg) in order to ensure such deep reduction.

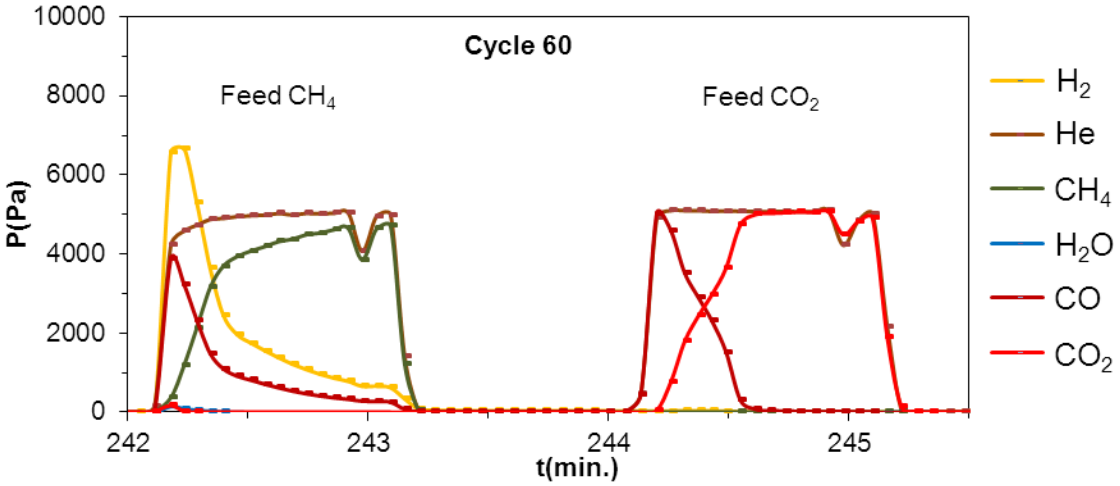

Fig 5.7 Partial pressures in the outlet flow working with 25mg of Ni(8.8)/CeO_2 at 800°C $F_{T,0}$ = 100 mL/min. Cycle: 1/1/1/1. 5% CH_4, 5 % CO_2

The ***Fig 5.7*** shows that the partial pressure of CO_2 reaches the nominal value of 5000Pa. Thereby the species available to be oxidized by CO_2 have enough time to react. The cycle shown above is the last one of a 60 cycles experiment. Therefore taking into account that 25mg of CeO_2 contains 256 µmoles of O and that at each reductant step 45-50 µmols of O are consumed, we can assume that the reinjection of such amount of oxygen by CO_2 is possible. If not, the selectivity of the reaction should shift to the decomposition of methane due to the depletion of oxygen after the first few cycles, so without any CO production.

Table 5.2 Conversion of CH_4 and CO_2 along the experiment

cycle	X_{CH_4} (%)	H_2/CO	CO/(CO_2+CO)	$C_{deposited}/C_{conv.}$(%)	X_{CO_2} (%)
2	**25**	2.2	0.98	7	**24**
5	**24**	2.1	0.97	5	**24**
10	**24**	2.0	0.97	2	**24**
15	**24**	2.0	0.98	0	**24**
20	**24**	2.1	0.99	5	**24**
25	**24**	2.0	0.98	1	**24**
30	**24**	2.4	0.98	4	**24**
35	**23**	2.1	0.98	0	**23**
40	**23**	2.1	0.98	2	**24**
45	**24**	2.1	0.99	5	**23**
50	**24**	2.2	0.99	3	**24**
55	**24**	2.3	0.99	4	**24**
60	**24**	2.1	0.99	6	**24**

Somewhat the total reoxidation of Ce_xO_y species to CeO_2 seems to be feasible at the working conditions showing stable results, as seen in ***Table 5.2***.

5.4. Activation energy

The activation energy of CH_4 and the one of "mobile" oxygen of CeO_2 were calculated from two different experimental approaches, modifying the amount of catalyst and the partial

pressure of the reactants. The method is the one of the initial rates (taken into account the first 15 seconds of the step). The same calculations were carried for the activation energy of CO_2. Unfortunately, the rate of CO_2 consumption on the reoxidation step was too high at the working conditions to obtain reliable values.

The Arrhenius equation gives the quantitative basis of the relationship between the activation energy and the rate at which a reaction proceeds. Thus, the equations used were the following ones:

Eq. 5.1 $r = k * P_{CH4}^{a} * P_{CeO2}^{b}$

Eq. 5.2 $k = A \exp (-Ea / R * T)$

Eq. 5.3 $r = (A * \exp(- Ea / R * T)) * P_{CH4}^{a} * P_{CeO2}^{b}$

Eq. 5.4 $\ln r = \ln A - \mathbf{Ea} / R * T + a * \ln P_{CH4} + b * \ln P_{CeO2}$

To get **Ea**: P_{CH4} = ct. P_{CeO2} = ct. $T \neq$ ct

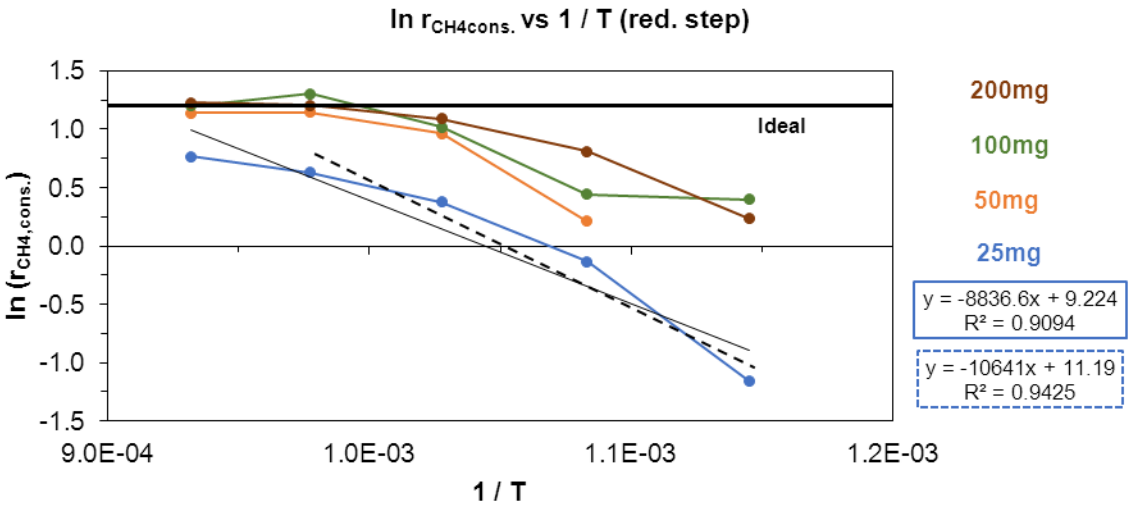

Fig 5.8 Arrhenius plots of the CH_4 consumption rate (expressed as µmol/s). Exp: Different amounts of Ni(8.8)/CeO_2 working between 600-800°C Reductant step: $F_{T,0}$ = 100 mL/min. 1 minute 5% CH_4

First, the figure above shows the difficulty of obtaining reliable curves for the calculation of the activation energy as in almost all the cases the initial rate of CH_4 consumption reaches the rate of reactant feed into the reactor (instantaneous 100% conversion) meaning that the rate is not kinetically governed by the catalysts properties. This limit is indicated as the “ideal” rate in the figure. This maximum conversion is rapidly approached by increasing the amount of solid and temperature. Therefore, the most reliable data to obtain a first approach is the one using 25mg of catalyst. From there, the activation energy of CH_4 appears to be between 73-88 Kj/mol.

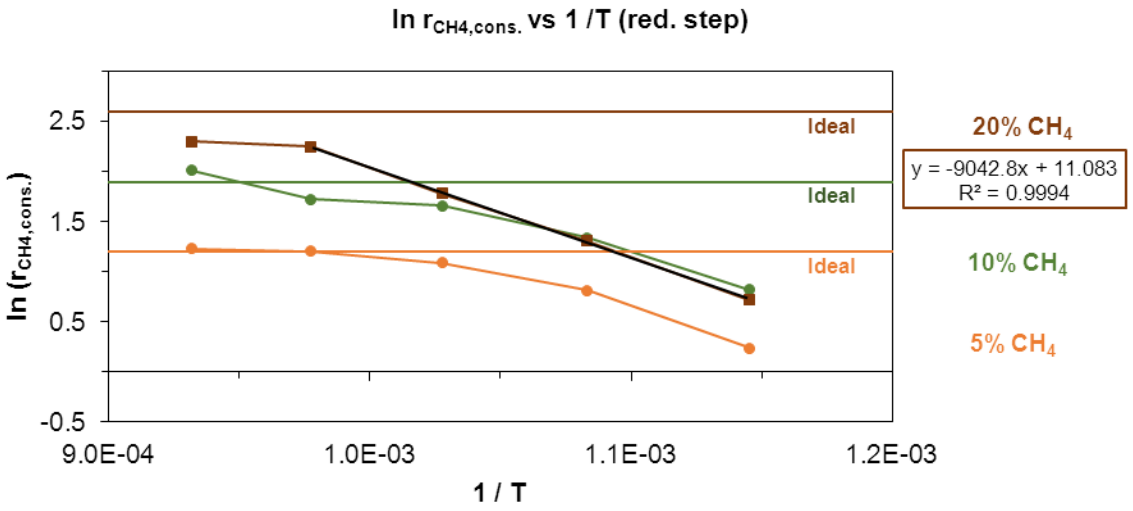

Fig 5.9 Arrhenius plots of the CH_4 consumption rate (expressed as µmol/s). Exp: Different partial pressures of CH_4, 200mg Ni(8.8)/CeO_2 working between 600-800°C Reductant step: $F_{T,0}$ = 100 mL/min. 1 minute 5% CH_4

The same kind of issue was found working at different partial pressures of CH_4, the initial rates were too high to obtain a trustable correlation at 5% and 10% of CH_4. Thus, only the one obtained on the first four points (from 600°C to 750°C) working at 20% concentration of CH_4 was taken into account even though the low temperature points for all concentrations tend to be parallel. There, the Ea obtained is 75 Kj/mol which is in good agreement with the one got by the other procedure. In addition, these two values are quite close to some from the literature. A. Kambolis et al [4.22], working with a similar catalyst composition (Ni(5)/CeO_2), shows a value a little bit lower than the ones obtained in the present study, 67 Kj/mol. The same type of calculation was made for the initial rate of oxygen consumed from the solid.

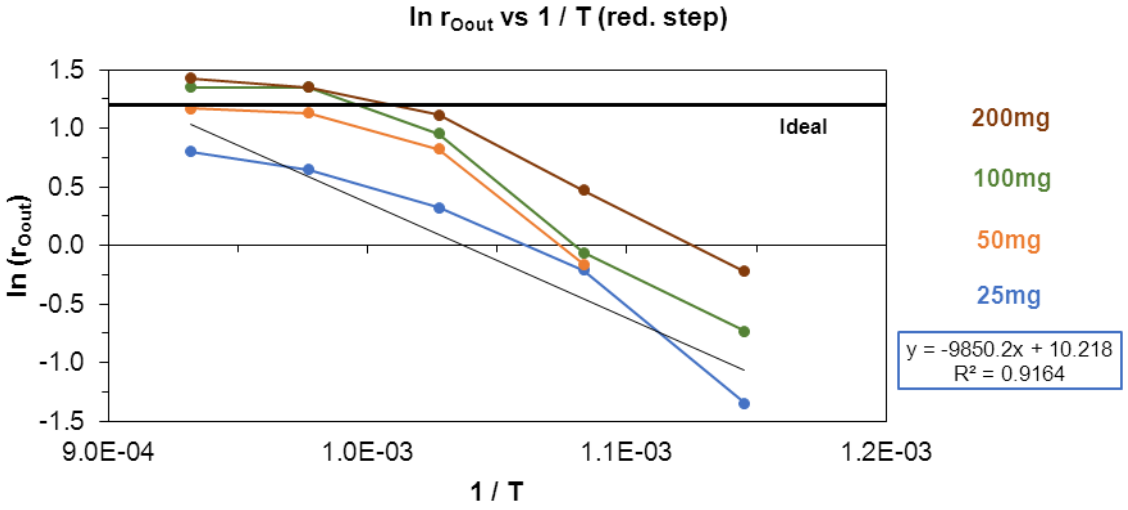

Fig 5.10 Arrhenius plots of the oxygen consumption rate (µmol/s). Exp: Different amounts of Ni(8.8)/CeO_2 working between 600-800°C Reductant step: $F_{T,0}$ = 100 mL/min. 1 minute 5% CH_4

As for the case of CH_4 the most interesting curve in terms of kinetics was the one obtained working with 25mg. In this case the activation energy of the oxygen diffusion is 82 Kj/mol. Again, the curves tend to become parallel at low temperatures, as it can be seen also with different CH_4 concentrations.

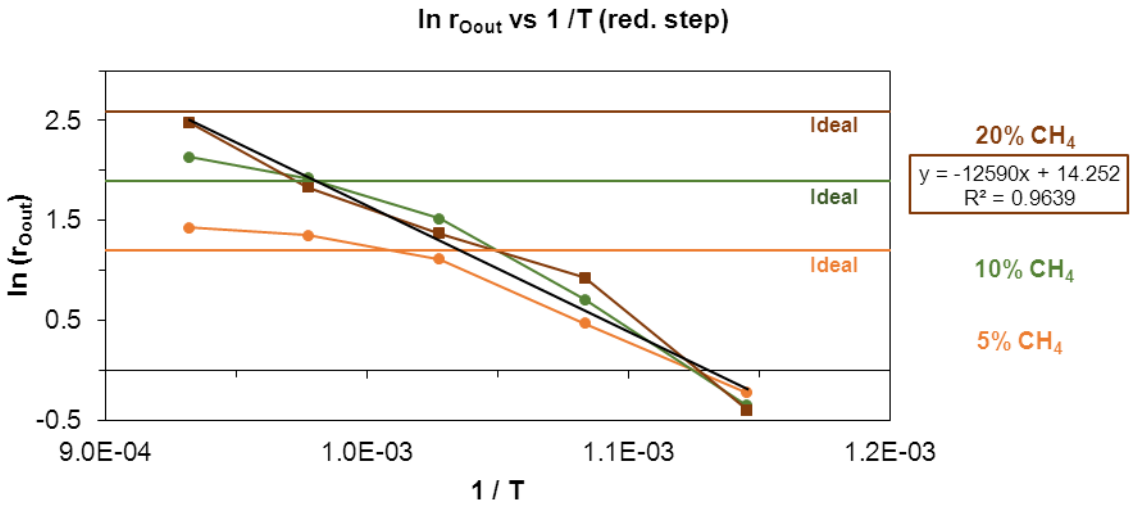

Fig 5.11 Arrhenius plots of the oxygen consumption rate (µmol/s). Exp: Different partial P of CH_4, 200mg Ni(8.8)/CeO_2 working between 600-800°C Reductant step: $F_{T,0}$ = 100 mL/min.1 minute 5% CH_4

Otherwise some variation is observed from the Ea calculated in the figure above. The activation energy is equal to 105 Kj/mol. Even if it is different than the one calculated by the other experiments, this one seems to be more reliable as in the other case the point at 800°C does not have a significant variation from the one at 750°C, maybe due to a too high rate at such temperatures for the kinetic calculation.

The difference between the E_a of CH_4 and "mobile" oxygen can be associated to the experimental data which shows a higher conversion/activation of CH_4 than oxygen at low temperatures, notably at 600°C.

5.5. Partial orders of reaction

The partial orders of reaction are calculated based on ***Eq. 5.4*** as follows:

$$\ln r = \ln A - Ea / R * T + a * \ln P_{CH4} + b * \ln P_{CeO2}$$

To get *a*: $P_{CH4} \neq$ ct. P_{CeO2} = ct.

To get *b*: P_{CH4} = ct. $P_{CeO2} \neq$ ct.

Reductant step

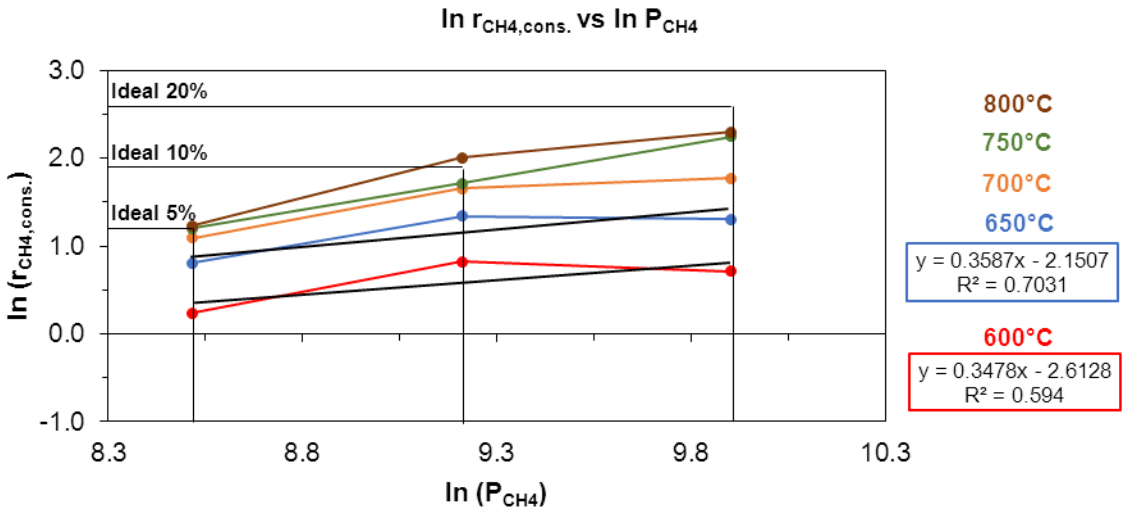

Fig 5.12 ln (r_{CH4}) vs ln(P_{CH4}). Exp: 200mg of Ni(8.8)/CeO_2 working between 600-800°C Reductant step: $F_{T,0}$ = 100 mL/min. 1 minute 5% CH_4, 10%CH_4, 20% CH_4

As in the case for the activation energy some of the experiments cannot be taken into account due to the proximity to the ideal rate. Therefore, only the curves at 650°C and 600°C are taken in consideration. From one side the partial order of CH_4 is the same in the two cases (0.35), evidencing low influence of the partial pressure on the rate of methane consumption. If the points at 10% and 20% CH_4 are taken without the one at 5%, the partial order goes to zero or even negative values at 600°C, 650°C and 700°C. This behavior is sometimes related to the saturation of the active sites by the reactant. Otherwise at the high temperatures of 750°C and 800°C the trend is different which can mean that the active sites are not saturated maybe due to a fast desorption of the species from the catalyst.

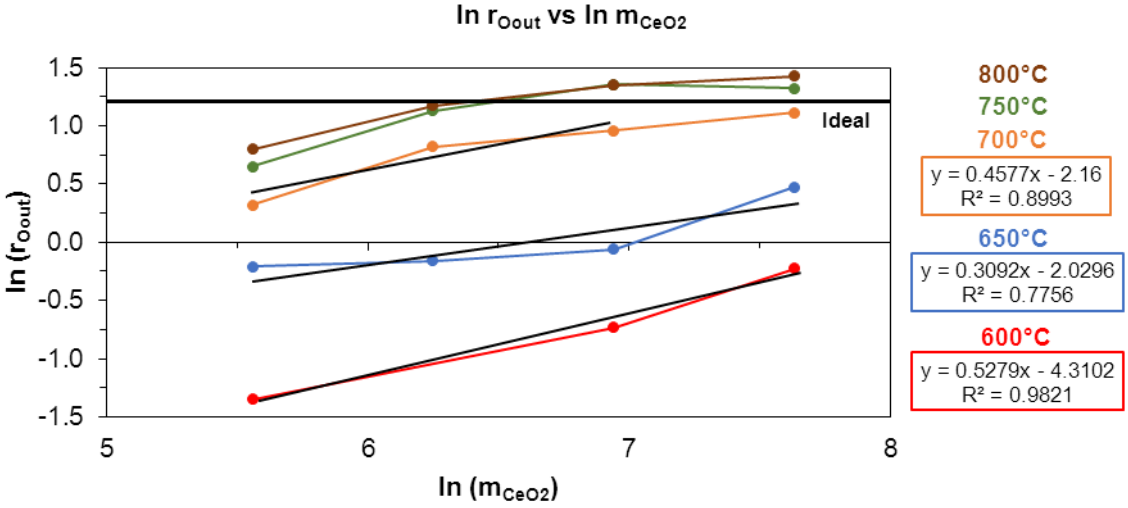

Fig 5.13 ln (r_{Oout}) vs ln(m_{CeO2}). Exp: different amounts of Ni(8.8)/CeO_2 working between 600-800°C Reductant step: $F_{T,0}$ = 100 mL/min. 1 minute 5% CH_4

Fig 5.13 shows some interesting trends about the influence of the amount of CeO_2 on the oxygen diffusion rate. As it was predicted in the ***Paragraph 5.2***, it seems that the amount of CeO_2 has an influence, even if it is not too high, on the oxygen availability, showing partial orders between 0.5 and 0.3 in the range of 600°C-700°C where mostly surface oxygen species seem to be involved in the reaction. This influence seems to be less important at high temperature when bulk oxygen becomes available.

Oxidant step

As mentioned in the introduction of this ***Paragraph 5.4***, the same calculations were carried for the activation energy of CO_2. Unfortunately, the initial rate of CO_2 consumption on the reoxidation step was too high at the working conditions to obtain reliable values. However, a first approach can be done for the partial orders. Thus, the same procedure is followed:

$\ln r = \ln A - Ea / R * T + a * \ln P_{CO2} + b * \ln P_{CexOy}$

To get *a*: $P_{CO2} \neq ct.$ $P_{CexOy} = ct.$

To get *b*: $P_{CO2} = ct.$ $P_{CexOy} \neq ct.$

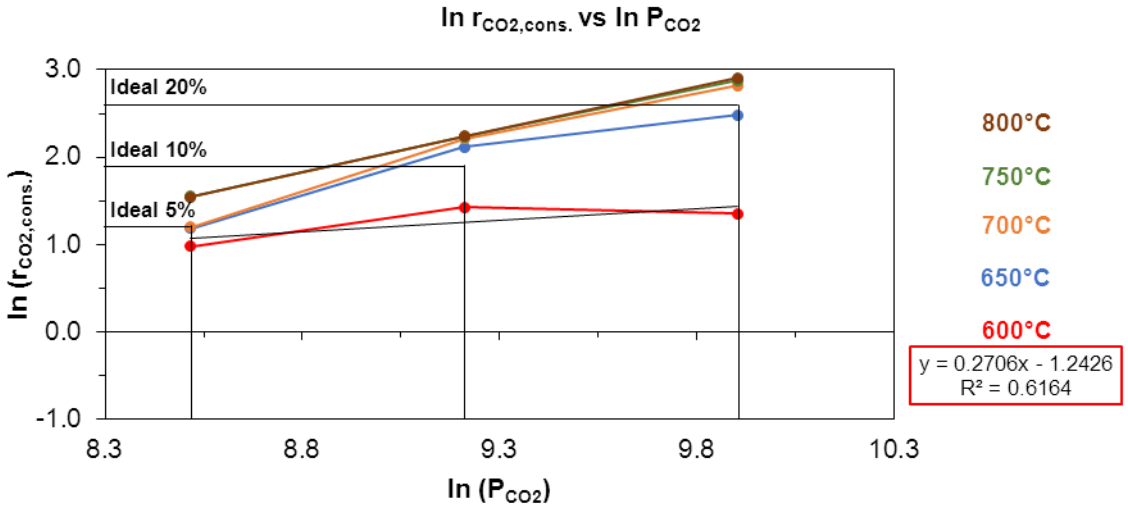

Fig 5.14 ln (r_{CO2}) vs ln(P_{CO2}). Exp: 200mg of Ni(8.8)/CeO_2 working between 600-800°C Oxidant step: $F_{T,0}$ = 100 mL/min. 1 minute 5% CO_2, 10%CO_2, 20% CO_2

The partial order of CO_2 at 600°C goes to 0.3, which is close to the value obtained for CH_4. Thereby, the partial pressure of CO_2 has a low effect on the consumption rate at least at such temperature. A drastic decrease on conversion would be necessary to study kinetics at 650-800°C.

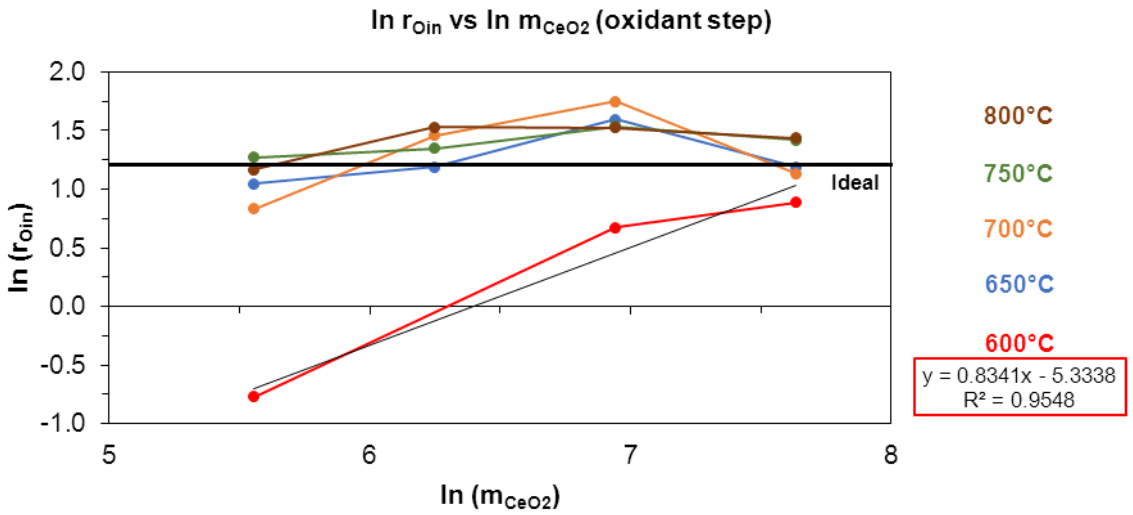

Fig 5.15 ln (r_{Oin}) vs ln(m_{CeO2}). Exp: different amounts of Ni(8.8)/CeO_2 working between 600-800°C Oxidant step: $F_{T,0}$ = 100 mL/min. 1 minute 5% CO_2

Finally, the figure above shows that the partial order of Ce_xO_y goes to 0.8 which is a bit higher than the one obtained for the reduction of CeO_2 (0.5) at 600°C. High amount of CeO_2 seems to have more influence in the reoxidation rate of Ce_xO_y than in the reduction of CeO_2. Maybe, the higher amount of oxygen vacancies helps the activation of CO_2, as it is mentioned in some of the literature exposed above [4.12].

5.6. Influence of the Ni loading

The next figure shows the influence of the nickel loading on the consumption of CH_4 and oxygen.

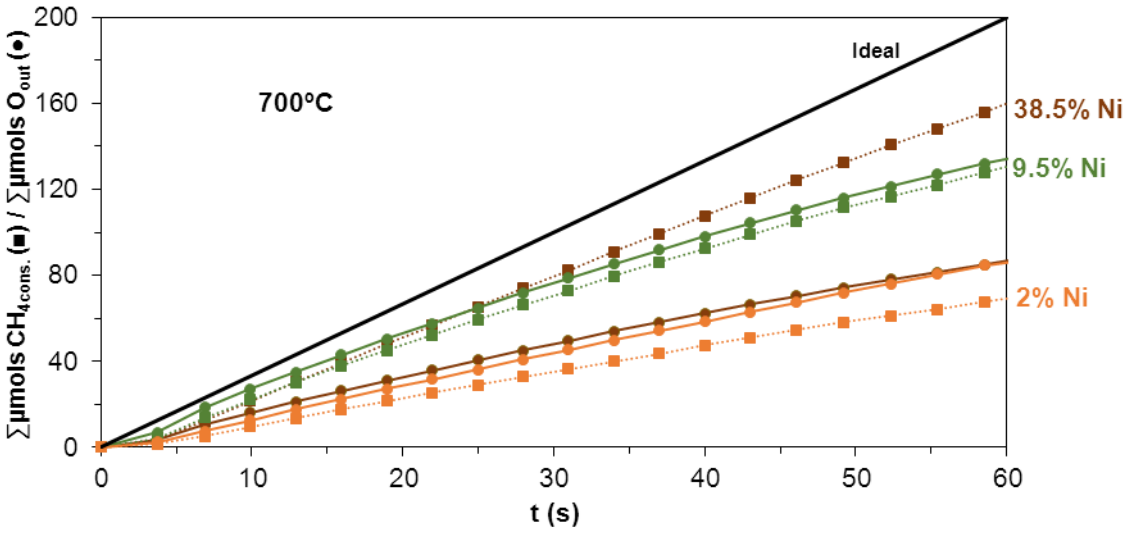

Fig 5.16 O removed (●) and CH_4 consumed (■) at 700ºC, 200mg of Ni(x)/CeO_2, $[CH_4]_0$ = 5% after 11 cycles working in periodic

First the 2 wt.%Ni curve of oxygen consumption is above the one of CH_4, meaning that in such case the relation oxygen diffusion – activity of CH_4 is more favorable to the first one, producing potentially more H_2O and CO_2 than in the other cases. On the contrary, the trend is the reverse at the highest loading of 38.5 wt.%Ni, the curve of CH_4 consumption is much higher than the one of oxygen, so forming a lot of carbon. Finally, the loading of 9.5 wt.%Ni shows a good compromise between the two consumptions, CH_4 and oxygen have the same rate, so producing potentially the partial oxidation of the alkane. This confirms that Ni is mainly responsible for the activation of methane in such process as it could be expected.

Interestingly, the rates of oxygen removal are very similar with 2 and 38.5 wt.%Ni whereas it is much higher for the 9.5 wt.%Ni catalyst, an evidence of a synergetic effect between Ni and CeO_2. Specific intermediate loading of nickel can lead to an optimum solid solution which may be necessary to enhance the oxygen diffusion. High loadings would be prejudicial as independent phases can be created, forming majorly a mixed oxide of Ni and Ce species. On the contrary, a too low % of Ni creates partially a solid solution with Ce but not in the optimum range, creating few vacancies. However, the 9-10% loading of Ni can create a solid solution near to the optimum without forming separate phases. Thus, the oxygen diffusion is improved at such loading.

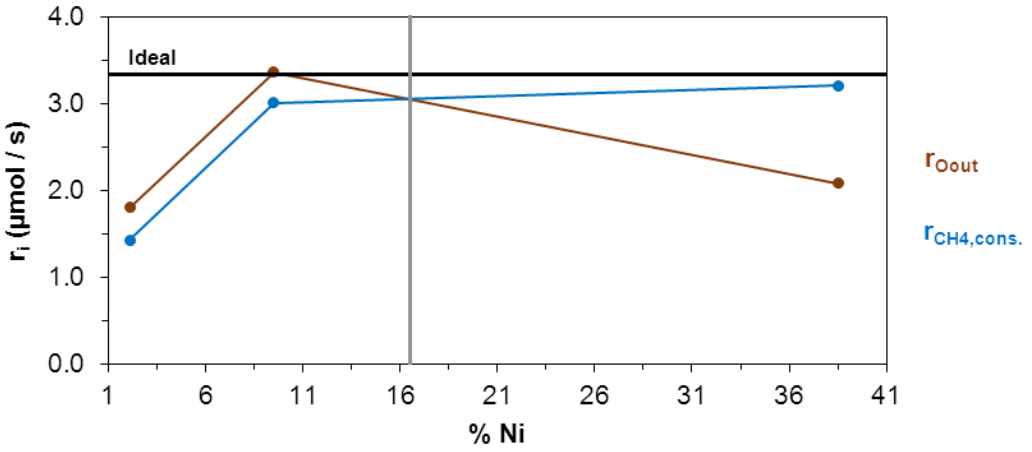

Fig 5.17 r_i (µmol/s) vs %Ni. Exp: 200mg of Ni(x)/CeO_2 working at 700°C Reductant step: $F_{T,0}$ = 100 mL/min. 1 minute 5% CH_4

The correlation between the rates of each reactant in the reductant step towards the amount of nickel shows an optimum at approx. 16.5 wt.%Ni working at 700°C during 1 minute. More intermediate Ni loading would however be necessary to get a more precise value. It is also probable that such optimum will depend on other experimental conditions such as methane partial pressure in particular.

Otherwise, the calculation are not made in the oxidant step as the experiments with 2% and 38.5% Ni were carried using nitrogen liquid, so the mass balance of oxygen is less accurate

due to a considerable adsorption/desorption phenomenon on CO_2 within the mass spectrometer (explained in ***Annex 7.1.2.4***).

5.7. Comparison between Ni and Co

The curves of CH_4 and oxygen consumption on the experiments working with $Co(7.2)/CeO_2$ are shown as follows.

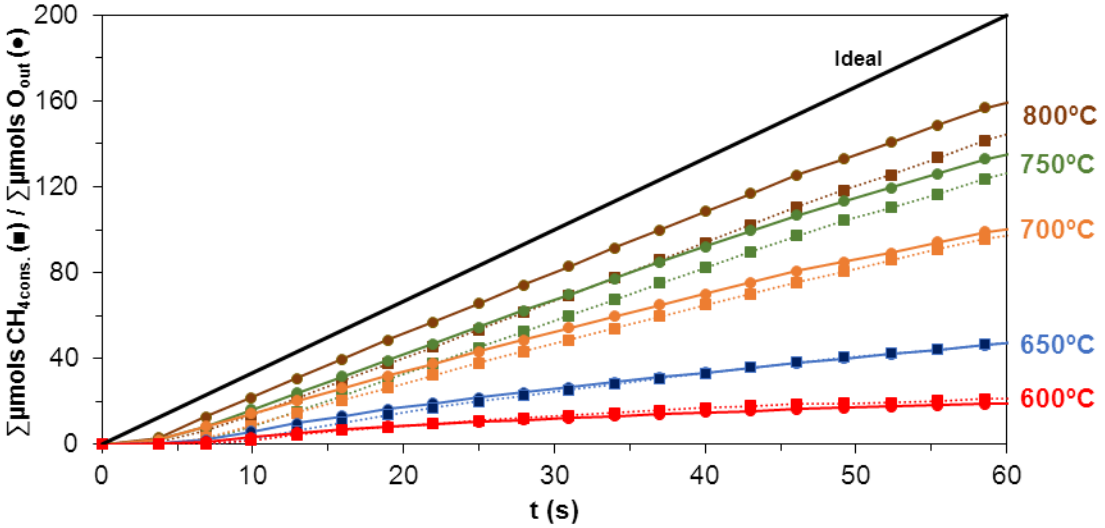

Fig 5.18 O removed (●) and CH_4 consumed (■) at different T, 200mg $Co(7.2)/CeO_2$, $[CH_4]_0$ = 5% after 11 cycles

The ***Fig 5.18*** shows a clear influence of temperature on the oxygen diffusion, going above the methane consumption at 800°C to slightly below at 600°C.

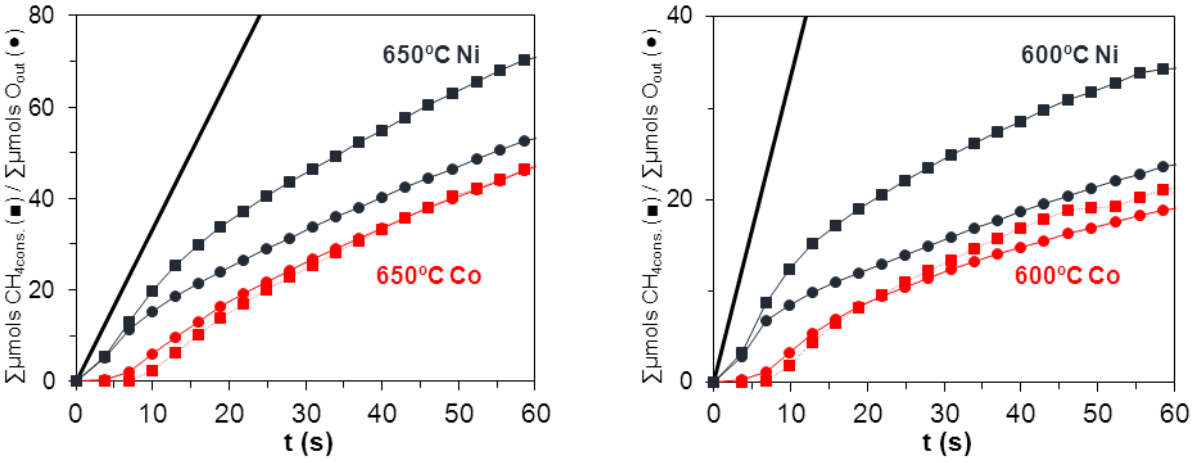

*Fig 5.19 O removed (●) and CH_4 consumed (■) comparison between nickel and cobalt at **(left)** 650°C and **(right)** 600°C, 200mg $Ni(8.8)/CeO_2$ and $Co(7.2)/CeO_2$, $[CH_4]_0$ = 5% after 11 cycles*

The figure above put in evidence the assumptions made in the ***Paragraph 4.3.7*** about better selectivity of cobalt compared to nickel at low temperatures. The consumption of CH_4 and oxygen are almost the same for 650°C and 600°C with $Co(7.2)/CeO_2$. On the contrary, the

difference is much higher working with nickel. Probably, low activation of CH_4 with cobalt is in better adequacy to slow oxygen diffusion at such temperatures.

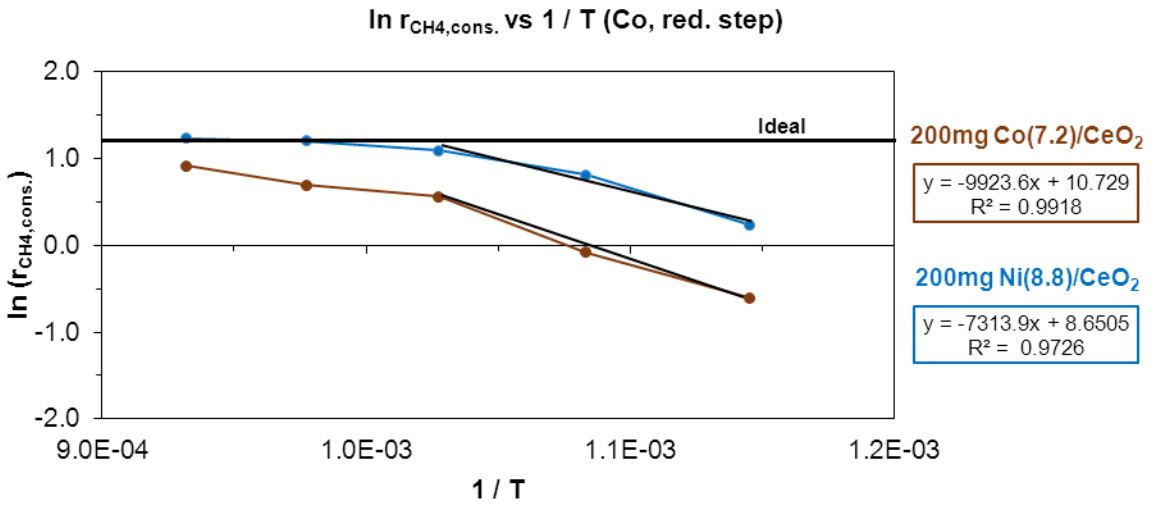

Fig 5.20 Arrhenius plots of the CH_4 consumption rate (µmol/s). Comparison between 200mg of $Co(7.2)/CeO_2$ and 200mg of $Ni(8.8)/CeO_2$ at 600-700°C R step: $F_{T,0}$ = 100 mL/min. 1 minute 5% CH_4

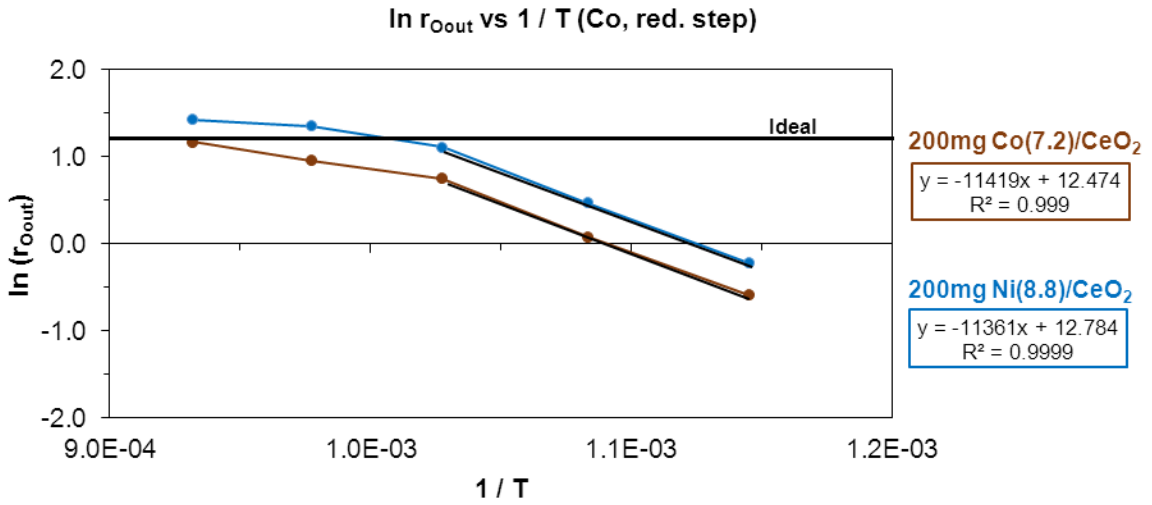

Fig 5.21 Arrhenius plots of the oxygen consumption rate (µmol/s). Comparison between 200mg of $Co(7.2)/CeO_2$ and 200mg of $Ni(8.8)/CeO_2$ at 600-700°C R step: $F_{T,0}$ = 100 mL/min. 1 minute 5% CH_4

Table 5.3 Activation energies

Catalyst	Ea_O (kJ / mol)	Ea_{CH4} (kJ / mol)	**Δ (kJ / mol)**
$Co(7.2)/CeO_2$	95	82	**12**
$Ni(8.8)/CeO_2$	94	61	**34**

Indeed as seen in the figures and the table above, the reason about obtaining a good selectivity at low temperatures with Co is due to a close proximity between the activation of CH_4 and the one of “mobile” oxygen. Unfortunately the data available is not sufficient to discuss the potential of Co based solid as most of the work was focused on Ni. Nevertheless this indicates that Co and eventually ternary Ni-Co-Ce catalysts would be interesting to study at

low temperatures. Obviously, the modification of the oxygen carrier to obtain low activation energies is also a main target for future works.

5.8. Conclusions

At the temperature of 700°C, the results seem to be in good agreement with the literature about the shift on selectivity once about 2% of oxygen is removed from the carrier, which is related to the oxygen depletion on the surface of the solid. Otherwise, it is shown that this assumption cannot be extrapolated to other temperatures due to the big influence of this parameter on the oxygen diffusion. Indeed only 1% of the oxygen available can be removed selectively to produce syngas at 600°C whereas 9% can be removed at 800°C

The most feasible reaction from the thermodynamic point of view (CeO_2-Ce_6O_{11}) is also confirmed from the kinetic one. Concretely, it is shown that this redox couple is highly selective around 750°C.

The 60 cycles stability test using 25mg of catalyst show stable periodic behavior although around 20% of the oxygen from the sample is removed at each cycle. This proves that CO_2 is capable to reoxidize ceria once it is highly reduced at high temperatures. Therefore, the oxygen species on the surface are potentially capable to migrate into the bulk and vice-versa in such conditions.

The results indicate that in the temperature range of 600 to 800°C the process is governed by the bulk properties, that is oxygen diffusion within CeO_2. At low temperature the surface reactivity of methane is high and the oxygen supply from the solid is too slow and thus leads to carbon deposit. On the other hand at high temperatures, diffusion is not limited anymore and all the methane can be oxidized to syngas and eventually some carbon dioxide.

Even though the working conditions were not very favorable to do nice kinetics, some experiments allowed calculating the activation energy of methane and the one of “mobile” oxygen from the solid. Results, in particular for methane activation are in good agreement with the literature. Otherwise, further experiments in better conditions need to be made for the oxidant step as in all the cases the initial rates were too high for this kind of calculations.

The reactants partial pressure seems to have a low influence on the rate of the reaction as the partial order of the reaction is around 0.3 in the two cases (CH_4 for the reductant step and CO_2 for the oxidant step), at least in the low temperatures of 600°C and 650°C. The partial order of oxygen diffusion on the reduction of CeO_2 goes to 0.5 and 0.8 on the oxidation of Ce_xO_y evidencing the influence on the amount of CeO_2 which is in good agreement with the study made on the oxygen available in the redox couple CeO_2-Ce_6O_{11}.

The effect of nickel loading shows that methane is activated on the metal particles. However, Ni also has an important role on the rate of oxygen supply from the solid, especially

in the intermediate loading showing an important synergetic effect that does not appear at very low and very high loadings. This could be linked to the insertion of part of the nickel in the cerium oxide forming mixed Ce-Ni oxides of particular interest.

In addition, the difference in selectivity between nickel and cobalt at 600°C and 650°C is clearly shown in the comparison of the CH_4 and oxygen consumption along the 60 seconds step. Low CH_4 reactivity on Co is in better accordance with the oxygen supply at such low temperatures thus producing more selective oxidation and producing less carbon.

Although these results are fragmentary and need a more in depth study, they give interesting indications for further optimization of the system and show the importance of such kinetic approach.

5.9. References

5.1 V. Sadykov, V. Rogov, E. Ermakova, D. Arendarsky, N. Mezentseva, G. Alikina, N. Sazonova, A. Bobin, S. Pavlova, Y. Schuurman, C. Mirodatos. Mechanism of CH_4 dry reforming by pulse microcalorimetry: Metal nanoparticles on perovskite/fluorite supports with high oxygen mobility *Thermochim Acta* 567 **(2013)** 27-34.

5.2 J.H. Bitter, K. Seshan, J.A. Lercher, Mono and bifunctional pathways of CO_2/CH_4 reforming over Pt and Rh based catalysts *J. Catal.* 176 **(1998)** 93-101.

5.3 V. Bychkov, Y. Tyulenin, O. Krylov, V. Korchak, Methane reforming with carbon dioxide on the Co/ α-Al2O3 catalyst: the formation, state, and transformations of surface carbon, *Kinet. Catal.* 43 **(2002)** 724–730.

5.4 V. Bychkov, Yu. Tyulenin, V. Korchak, The mechanism of methane reforming with carbon dioxide: comparison of supported Pt and Ni (Co) catalysts, *Kinet. Catal.* 44 **(2003)** 353–359

5.5 Y. Schuurman, C. Mirodatos, Uses of transient kinetics for methane activation studies, *Appl. Catal. A: Gen.* 151 **(1997)** 305–331

5.6 A. Slagtern, Y. Schuurman, C. Leclercq, X. Verykios, C. Mirodatos, Specific features concerning the mechanism of methane reforming by carbon dioxide over Ni/La_2O_3 catalyst, *J. Catal.* 172 **(1997)** 118–126.

5.7 Advances in Chemical Engineering. Volume 3. Edited by G.B. Marin **(2008)** Link: http://books.google.fr/books?id=4ndCfvToqcMC&pg=PA18&lpg=PA18&dq=diffusion+coefficient+oxygen+in+CeO2&source=bl&ots=m1RWUso6Fj&sig=noOZael5rCiFzDIU

General discussion and conclusion

6. GENERAL DISCUSSION AND CONCLUSION

6.1. General discussion

The experiments on the classical dry reforming of methane have shown some interesting results. In the comparison between some of the cheapest transition metals (Ni, Co and Fe), nickel shows the highest activity towards DRM. Concretely, almost full conversions of the reactants have been obtained at the high temperatures of 750-800ºC. Otherwise the system at 600ºC has been optimized working with 20% concentration of the reactants with only 10mg of catalyst and with some of the most abundant and cheapest metals (Ni-Mg-Al). In such case, the conversions were close to thermodynamic equilibrium. Besides, the 77h test at 650°C shows a remarkable stability along the whole experiment. Therefore, further studies are needed to allow working with higher concentrations (see pure mixtures).

Some interesting concepts have been verified by the thermodynamic study like the reason about a higher amount of H_2O at 600°C than at 800°C due to at the low temperature the competition between the main and side reactions is much stronger than at the high one.

In addition, the specific comparison study between the solids synthesized by Ni impregnated on commercial CeO_2 and by coprecipitation has shown the similarities between the two in terms of activity but considerable differences in terms of selectivity (obtaining a better one for the coprecipitated solid) and in the pretreatment conditions. Indeed, the commercial catalyst needs a pretreatment under H_2 at high temperatures to be active whereas the coprecipitated solid reaches the same catalytic performance even without pretreatment. Besides, the conversion decreases after treating the catalyst at a given temperature under H_2. This particular behavior can be explained by the key role of the interfacial oxygen in the Ni-Ce boundary (Ni-O-Ce site). This first interaction leads to the total oxidation of methane and the creation of selective active sites for the following reforming reaction towards H_2 and CO because the unselective consumed oxygen in the Ni-Ce boundary cannot be reoxidized by CO_2. Maybe, a too high reduction of the solid does not lead subsequently to the existence of the active site for the reforming reaction.

Although interesting results were obtained performing DRM in cofeed conditions, the thermodynamic limitations between CH_4 and CO_2 will always limit the conversions if we want to keep working without any addition of oxygen in the flow. Otherwise, the DRM and the P-DRM working with CeO_2 as oxygen carrier have shown similar thermodynamics limitations. However, this problematic is avoided in periodic conditions as the transient equilibrium is not reached. This study also helps to understand that different thermodynamic behaviors could happen between different oxide phases. In the case of ceria different properties are found between CeO_2-Ce_6O_{11} and CeO_2-Ce_2O_3. Concretely, the most feasible one is CeO_2-Ce_6O_{11}.

Such differences encourage looking forward in the optimization of the oxygen carrier to obtain even better thermodynamic properties. In addition the thermodynamic calculations hold some of the main theories claimed in this thesis, such as the logical production of H_2O and CO_2 in this first step due to the total oxidation of CH_4 by NiO, which is the most favorable reaction, and the absence of reoxidation of Ni by CO_2 to NiO. This last behavior is one of the key points to maintain the system selective after the first cycle. This property can be extrapolated to other metals such as Co (tested in this work) or Pt (Otsuka's process). In this context, the study also helps to explain the reason about the high production of H_2O and CO_2 working with iron, results in good agreement with recent literature. The 35 metals-study only shows 4 potential metals, Ce, Nb, Mo and W, which can work as oxygen carrier providing the required properties. This evidences the uncommon specific properties needed for the type of process. Besides, Ni and/or Co seem to be the most low-cost and abundant metal to activate the reactants without interfering in the selectivity of the reaction.

The Periodic Dry Reforming of Methane (P-DRM) process was proposed to avoid some of the issues involved in DRM. The principle of the process has been proved using Ni-Ce and Co-Ce based catalyst. CeO_2 reacts with CH_4 providing selective oxygen at the optimize conditions, notably at 750°C along the whole 1 minute feed. The system becomes selective after the first cycles thanks to the "preferential" reoxidation by CO_2, which provides oxygen to the carrier but does not oxidize Ni to NiO. In addition, the experimental data is in good agreement with the thermodynamic study. Indeed, the same oxide state is shown after the reductant and the oxidant step for Ni by the XPS analysis, which is different than the one before experiment. In addition the influence of working with oxygen instead of carbon dioxide in terms of selectivity has also been shown. Overall, the P-DRM experiment showed high performances in a wide range of conditions (different concentrations of the reactants, reaction temperature, amount and nature of the solid…).

Dynamics of the system have shown good agreement with the literature at 700°C, showing a shift on the selectivity after a given %age of the oxygen is consumed by CH_4. Moreover, such study has been spread to other temperatures, covering from 600°C to 800°C due to the big influence of such parameter in the oxygen diffusion. Such study also shows that the redox couple CeO_2-Ce_6O_{11} is the most favorable from the kinetic point of view and highly selective at optimized working conditions. From the oxidation point of view, it is important to underline that our solid seems to be capable to be fully regenerated by CO_2. A long test where the initial oxygen available in the solid would not be enough for the good selectivity along the whole experiment without the reoxidation of the oxygen carrier corroborates such assumption. In some studies only the surface of the carrier was reoxidized due to oxygen diffusion limitations from the surface to the core.

The partial pressures of CH_4 and CO_2, at least up to 20%, do not have a strong influence on the reaction rate obtaining in all the cases partial orders lower than 1.

The study at 700°C between the rates of CH_4 and oxygen with different loadings of nickel allows obtaining an optimum wt% Ni, where an equal rate between the two consumptions would be reached in such operating conditions. This kind of approach shows a tool which can be really useful for the optimization at each different situation. The loading of nickel has shown to be quite important for the balance between the activation of CH_4 and the oxygen diffusion from CeO_2. Indeed, an optimal intermediate loading is necessary to enhance the oxygen diffusion. High loadings would be prejudicial as independent phases can be created, forming majorly oxides of Ni and Ce. On the contrary, a too low % of Ni creates a solid solution of cerium and nickel but not in the optimum range, creating few anionic vacancies. However, the 9-10% loading of Ni leads to the creation of a solid solution near to the optimum one without forming separate phases. Thus, the oxygen diffusion is improved at such loading.

The comparison between Ni and Co catalysts shows a better selectivity in the case of Co. This may be due to the activation energies of CH_4 and “mobile” oxygen which are closer to each other than the ones using nickel. Although these results need to be verified by a deeper study, they give interesting indications for further optimization of the system and show the importance of such kinetic approach.

The proven feasibility on P-DRM has to encourage further studies on such process due to the promising advantages in comparison with the traditional DRM: the elimination of the RWGS side reaction, the reoxidation of the eventual carbon and the promising H_2/CO ratio equal 2 for further applications, such as Fischer-Tropsch. In addition, the catalysts are synthesized by impregnation and coprecipation, techniques which are already applied in an industrial scale. Besides, the periodic concept has shown interesting performances for other raw hydrocarbon feed compositions, such as biogas and shale gas.

6.2. General conclusion

CH_4 and CO_2 transformation (DRM) has been studied on M-Ce-O (M = Ni, Co and Fe) catalysts and Ni-Mg-Al-O catalysts. Nickel based catalyst shows the highest activity towards DRM (85% conversion of CH_4 instead of 33% for Co and 2% for Fe). High conversions of the reactants have been obtained at 750-800ºC. Besides, 57% for CH_4 and 67% for CO_2 conversions were obtained at 600ºC (20% initial concentration) working with 10mg of $Ni_2Mg_2Al_1O_y$. In addition, the long test on $Ni_{0.5}Mg_2Al_1O_y$ at 650°C shows a remarkable stability along the whole experiment. The comparison between two different synthesis ($CeNi_{0.3}O_y$ with 7.9 wt% Ni obtained by coprecipitation and Ni(7.9)/CeO_2(com)) shows the same conversion but different selectivity (higher for the coprecipitated catalyst). Some interesting findings are

shown about the particular reducibility of the solids, obtaining better performances at lower pretreatment temperatures than at high ones. Therefore, the understanding of some important parameters for M-Ce and the optimization of catalytic performance for Ni-Mg-Al-O have been studied.

The thermodynamic study allows the understanding of some crucial properties such as (i) the reason of the higher amount of H_2O at 600º than at 800ºC due to a strong competition between the main and the side reactions at the low temperature, (ii) the selective system for the periodic process thanks to the absence of reoxidation of Ni, (iii) the influence of the initial concentrations of reactants and the total pressure in the conversions, which go lower as higher are the mentioned parameters, (iv) the most feasible redox couple in ceria which is CeO_2-Ce_6O_{11} and (v) the metals which can make the function of CeO_2 or/and the one of Ni.

Periodic dry reforming of methane (P-DRM) experiments showed high performances in a wide range of conditions (different concentrations of the reactants, reaction temperature, amount and nature of the solid…). Specifically, Ni/CeO_2 formulations provide H_2/CO=2 with negligible side products, notably at 750ºC. In addition, the oxygen carrier is capable to be fully reoxidized by CO_2. Besides, two other raw materials have been tested, notably biogas and ethane, obtaining in the two cases remarkable results. A first approach on the dynamics and apparent kinetics of the periodic process is proposed showing some interesting characteristics, particularly the importance of the temperature, the crystal size and the % of Ni on oxygen diffusion. The activation energy is another parameter to take into account to know the potential selectivity on the reaction as checked on the experiments working with Ni and Co.

6.3. Outlook

One of the limiting steps is the activation energy of the “mobile” oxygen. Therefore, such parameter should be the next one to improve. A first approach has been shown working with zirconium incorporated into ceria obtaining lower performances than for Ni-Ce catalyst, but otherwise promising thermostable properties producing less sintering than working only with cerium. In addition, several pathways can be imagined for the oxygen diffusion improvement, also incorporating other additives instead of Zr, such as La. On this way, a deeper study needs to be made to better understand the reason of improving oxygen diffusion with an intermediate loading of Ni (10%), being worse at a lower (2%) or higher one (39%).

The promising carbon neutral cycle working with biogas also needs to be further investigated considering the presence of hydrogen sulfide impurity.

Another issue about DRM is the reaction pressure. Indeed methane is usually supplied under pressure and down-flow processes for syngas transformation also occur at pressures of a few tens of atm. It would thus be interesting to carry out DRM in such high pressures in order

to limit the need for decompression/compression steps. Thermodynamics of co-feed DRM considerably limit the overall conversion in this case. P-DRM will also be negatively affected by increasing reaction pressure, especially in the reductant step. Nevertheless, and in contrary to cofeed DRM, the nature of the solid has an impact on the thermodynamic equilibrium. Modification of the solid nature and composition gives an opportunity to influence the maximum conversion and therefore opens the ways for further optimization of DRM at high pressures.

In terms of process improvement, some combinations can be imagined to balance the required energy of the P-DRM, such as the one proposed by J.W. Thybaut et al [1.67]:

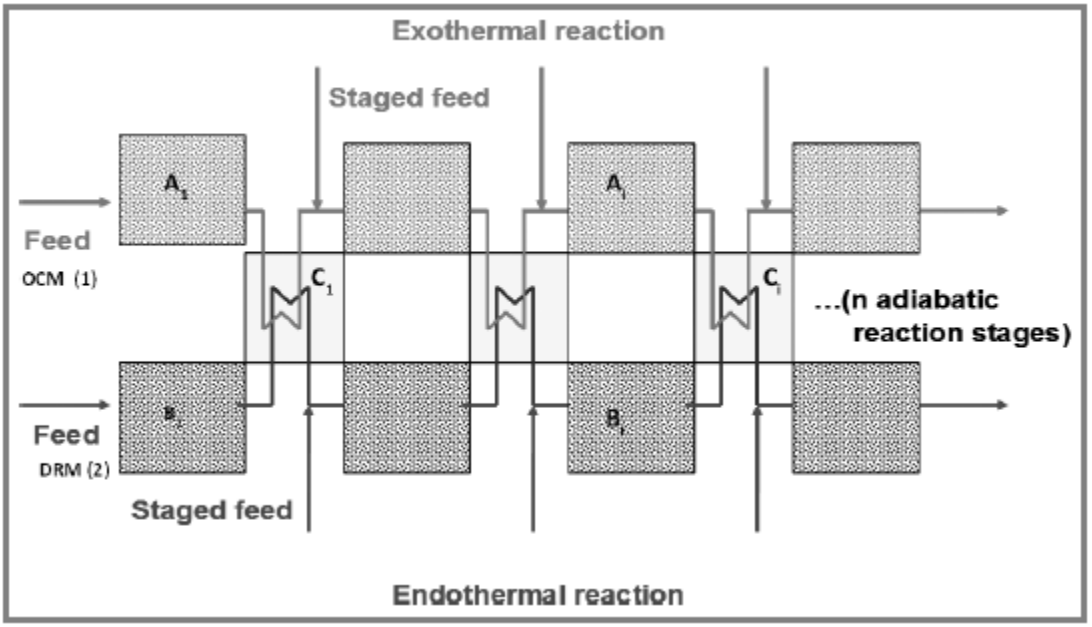

Fig 6.1 Autothermal configuration integrating ORM + DRM [1.67]

An interesting industrial process can be imagined from the combination of the autothermal configuration shown in the figure above and the advantages of working in periodic. For instance, the limited yield of 25% for the ORM can be overlapped working such process in two independent steps. Thus, this is one example of the different technology improvements which can be imagined for a large scale process by process integration.

Generally speaking, as mentioned in the first paragraph of this thesis such scientific research and development must be accompanied with the involvement of political incentives. Indeed, in the present conditions such processes are not economically viable. Such incentives should consider the real ecological cost the most pollutant technologies, and thus include expensive taxes, while providing considerable funding for the greenest ones. This could probably be one of the hot topics of the COP21 in Paris.

Annex

7. ANNEX

7.1. Set up. How it works?

In the following paragraph, the experimental work and the procedure to treat the data from the raw data obtained in the mass spectrometer to the conversions of the reactants are explained in detail. The periodic process has some particularities which need to be mentioned. Besides, some common technical details of the set up are also described in the following lines.

All the experiments were made using a quartz glass reactor. This kind of material can hold up to around 1000°C, enough for the temperature reaction required (600°C-800°C). In this context, pyrex glass can hold up to 500°C, so it is necessary to be aware about this difference in the procedure, if not the reactor would directly melt. Another aspect to underline is about the piping system (after the reactor) which is heated around 150°C in order to avoid condensation or even polymerization of some hydrocarbons.

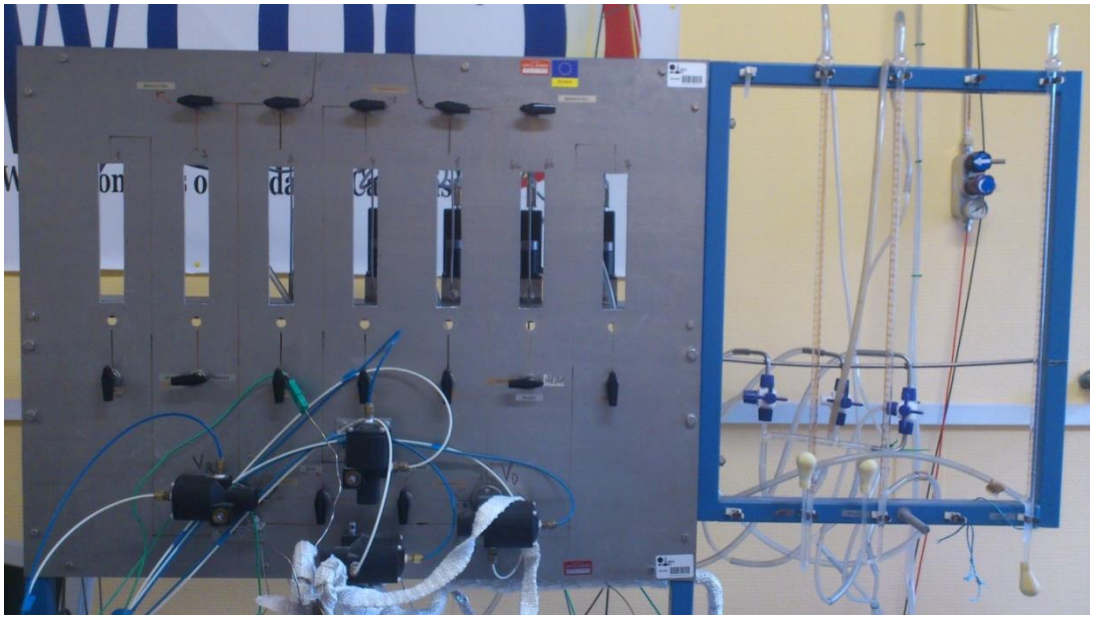

Fig 7.1 Picture of the flow's distribution (left side) and bubble flowmeters (right side)

The ***Fig 7.1*** shows a real picture of the flows distribution. Concretely, the calibration of the different flows was made once in the morning before the experiments of the day are carried. Bubble flowmeters (on the right of the picture above) were used for the precise adjustment of the flows. The importance of doing in such way is the sensitivity of the calculations using or not precisely the real flow.

Besides, the mass flowmeters (Brooks 5850S) can be partially seen behind the metallic plate. The SMARTCON software is used to connect the computer to the mass flowmeters.

There is also an important characteristic in the experimental set up concerning the valves. Automatic 4 ways valves (bottom center of the picture) equipped with air actuators are

connected to the computer through home-made software in order to automatize the system. On this way, once the experiment is launched the system is capable by itself to switch the valve eluding the annoying and waste of time procedure to switch the valves manually (a long periodic experiment is made by 60 cycles, meaning 240 movement open/close of the corresponding valves).

Fig 7.2 4-ways valve principle

The second advantage of working automatically is the quick switch of the valve, which is faster than the manually procedure, as so minimizing the perturbation in the system in order to a better reproducibility. The use of 4 way valves allows to reduce the dead volume of the piping. For instance, standard 3-ways valves would need some extra piece of pipe between them to obtain the same utility as for the 4-ways valve, so generating or increasing the dead volume which can produce memory effects in the MS). The automation is also better from the safety point of view. The software is made to close the reactants flows if they feed the system at the same time. The mixture of CH_4 with CO_2 is not concerned about this property, but it would be really useful if the set up operates with potentially flammable reactants if they were mixed (Ex. CH_4 and O_2 for the ORM in periodic).

7.1.1. Process diagram

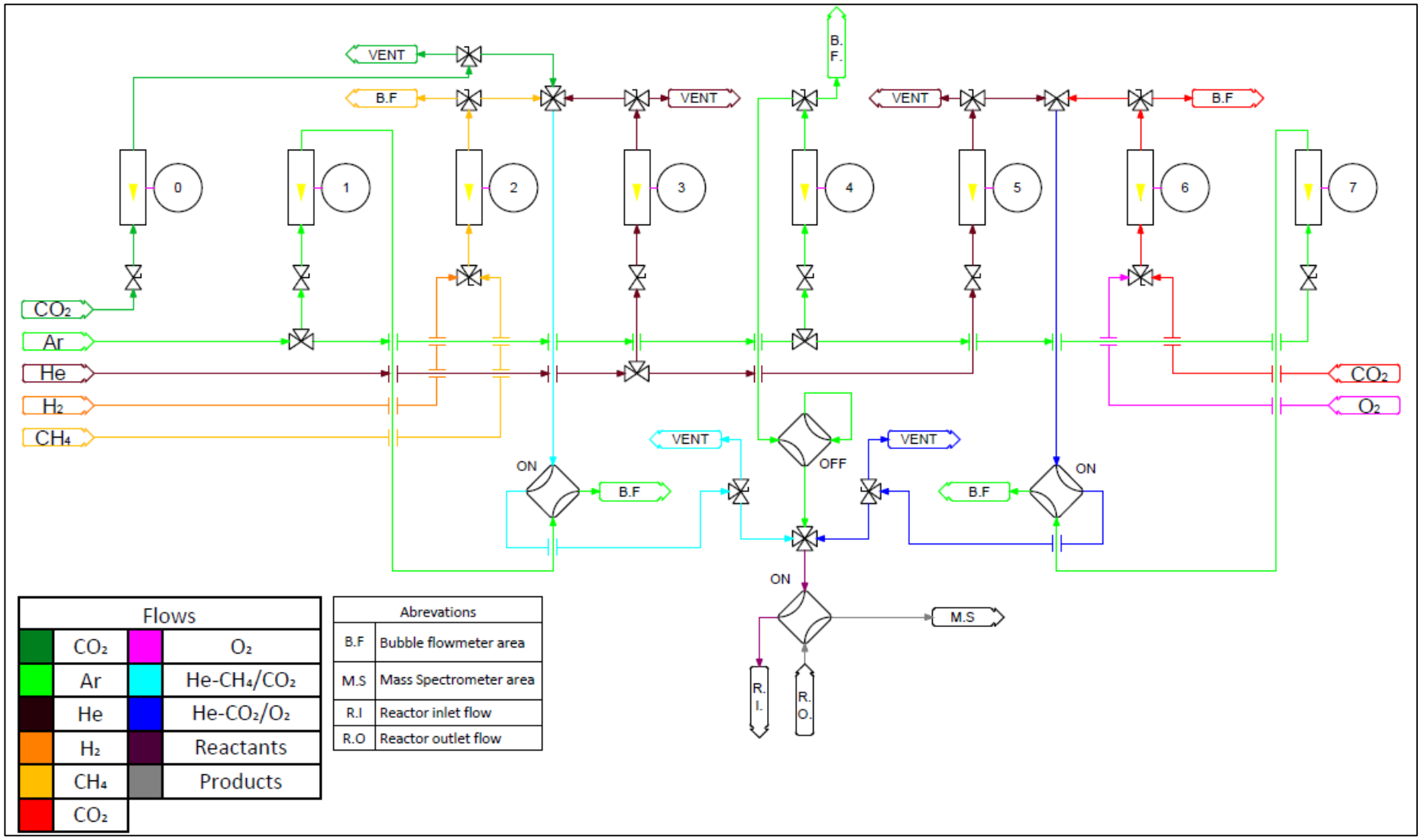

Fig 7.3 Schematic drawing of the process diagram (AutoCAD software)

The ***Fig 7.3*** shows the 8 flows present in the set-up. From left to the right: (0) CO_2 or C_2H_6 (an extension of the set up for trying biogas and shale gas compositions), (1) Ar, (2) CH_4, (3) He, (4) Ar, (5) He, (6) CO_2 and (7) Ar. Clearly, the function of methane and carbon dioxide is to use them as reactants. Otherwise, the use of helium and argon flows is described in the next paragraphs.

Argon flow

The flow of Ar is used for four main reasons. Obviously, the main one is to use it as a diluent. For instance, there is the possibility of working with different initial concentrations of the reactants without changing the total flow in the system (typically 100 mL/min). Therefore, the comparison between the different experiments would be more precise as the residence time is constant in all the cases.

In particular in the periodic mode operation each reactant gas is replaced by an equal flow of Argon, thus maintaining constant the inlet total flow rate at any time.

Example:

1. CH_4 (5%): 5 mL / min of CH_4 and 95 mL / min of Ar → F_T = 100 mL / min
2. CH_4 (25%): 25 mL / min of CH_4 and 75 mL / min of Ar → F_T = 100 mL / min

Table 7.1 Example of flows' distribution between the different steps

			Reductant	Inert	Oxidant
	Flows	F_{in} (ml/min)	ml/min	ml/min	ml/min
R 4-way valve	F_1 (Ar)	10	0	**10**	**10**
	F_2 (CH_4)	5	**5**	0	0
	F_3 (He)	5	**5**	0	0
	F_4 (Ar)	80	**80**	**80**	**80**
O 4-way valve	F_5 (He)	5	0	0	**5**
	F_6 (CO_2)	5	0	0	**5**
	F_7 (Ar)	10	**10**	**10**	0
			100	100	100

Then, another application of Ar is to use it between the two steps of the reaction in order to degas the system from the previous compound. On this way, each step of CH_4 and CO_2 are totally independent from each other, avoiding any kind of issue mixing the two flows (selectivity, flammability limits in the case of O_2…). The cycle time of the neutral step can also have an effect on the catalyst, as removing some gases adsorbed or having some time for the oxygen diffusion from the core to the surface of the solid.

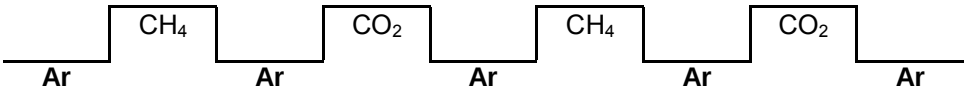

Fig 7.4 Ideal cycle steps through the experiment

Otherwise, the flow in the outlet can vary considerably as the reaction concerned has an expansion of the gases (2 to 4 moles for cofeed and 1 to 3 moles for periodic). Then, the variation on the partial pressure of argon during the reaction allows the precise calculation of the outlet flow. Concretely, an increase of the flow would be accompanied by a decrease of the Ar pressure (See ***Paragraph 7.1.3.6*** for calculation).

Finally, a flow of at least 50% of Ar is recommended when a mass spectrometer is used as analyzer. The main reason is about keeping the same viscosity of the flow at different situations (with and without reaction) because a big variation of this parameter can affect considerably the sensitivity of the MS, obtaining less precise data.

Helium flow

The flow of He is used as a marker to know the "real" inlet flow of methane and carbon dioxide at any moment taking into account the experimentally set ratios He-/-CH_4 and He-/-CO_2. This characteristic allows being more precise in the calculation of the reactant conversion instead of considering theoretical curves. Therefore the same properties for He than for CH_4 and CO_2 is assumed in the behavior towards the mass spectrometer. Thus, the instant conversion of CH_4 is calculated from the curve of He ("CH_4 inlet") and the one of CH_4 (CH_4 outlet). In addition, the integration between the two points is also made in order to take into account the variation of the outlet flow (see ***Paragraph 7.1.3.7*** for calculations).

7.1.2. Mass Spectrometer Area

A mass spectrometer is used in order to analyze the composition of the outlet flow. In the following paragraphs there is an explanation of the operating principles.

7.1.2.1. Inlet system: Capillary tube

The connection between the set up and the MS is a capillary tube. The flow though the tube is around 3-5 mL / min. Obviously, the outlet flow after the reactor must be higher than that, if not, some diffusion of air could enter back from the vent.

7.1.2.2. Vacuum system

A two stage inlet system is used. The main reason is the need to switch from viscous flow to molecular flow.

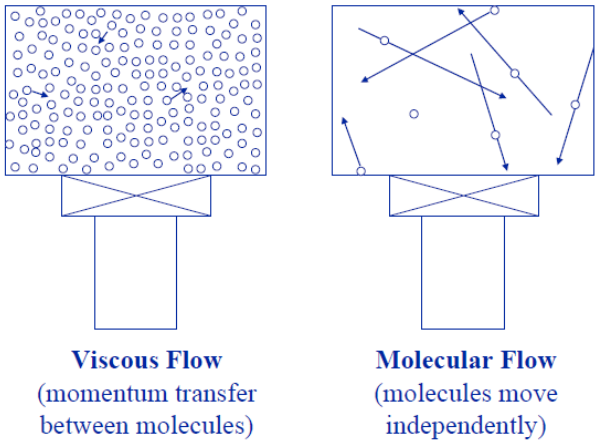

Fig 7.5 Flow regimes: viscous and molecular flow [4.1]

The viscous flow is dominated by gas-gas collisions, so the distance between molecules is small. Generally, this kind of behavior appears in pressured greater than 0.1mbar. Otherwise, pressures lower than 10^{-3} mbar are necessary to obtain a molecular flow, which is dominated by gas-wall collisions. The mean free path (the distance between molecule to molecule collisions) becomes long enough, so the molecules are more likely to impact the chamber wall than another molecule. The required high vacuum is obtained in two steps. The first one consists on a first chamber at 1 mbar (obtained through a rotary vane pump) and the second one reaches 10^{-7}-10^{-8} mbar (obtained through a combined rotary vane and turbomolecular pumping system). Therefore, gas flow properties within the first chamber are governed by viscous dynamics whereas both inlet and oulet (pumping) from the MS chamber are governed by molecular flow dynamics. This particularity allow to obtain a measurement of each gas within the analysis chamber which is directly proportional to the partial pressure of this gas in the outlet flow of the reactor at atmospheric pressure. Such linear response cannot by obtained through a single step pressure reduction system. With the inlet system open, the stationary pressure obtained is approx. 10^{-5}mbar within the MS chamber. The MS used is a Omnistar GSD200 (Pfeiffer Vacuum) quadrupole mass spectrometer equipped with a faraday collector detector and a secondary electron multiplier detector. Total pressure within the MS chamber is measured through a combined Pirani/Penning pressure Gauge (Pfeiffer Vacuum).

7.1.2.3. Cooling down: Nitrogen liquid

The most difficult molecule to take away from the system by the vacuum pump is H_2O due to the adsorption/desorption effect on the walls of the chamber. This phenomenon can modify the real instantaneous water composition of the flow. Heating or cooling the chamber is the two main solutions for such problematic. The most practical one is to cool it by liquid N_2 in order to assure that the water adsorbed on the walls keep stuck there during the experiments. As the gas inlet is placed near to the ionization source, H_2O coming from the experiment is

detected before the molecules have the possibility to encounter a cold part of the setup and thus be trapped. The cold chamber is isolated from the atmosphere with vacuum to avoid a fast evaporation of the nitrogen liquid. In addition, the tube in contact with the cooling system is made by copper as it has a high thermal conductivity. Thereby, the temperature reached is around 77°K. In such conditions, the chamber is cold enough during around 15 hours, as so being available (if necessary) to run experiments during the night. The precise quantification of the water amount is interesting to obtain accurate oxygen mass balances. For instance, the calculations about the oxygen release from the catalyst would be more precise.

7.1.2.4. Influence of the nitrogen liquid in the adsorption/desorption of CO_2:

The cold chamber allows obtaining more precise mass balance of H_2O, but on the contrary, a new issue appeared during the first experiments.

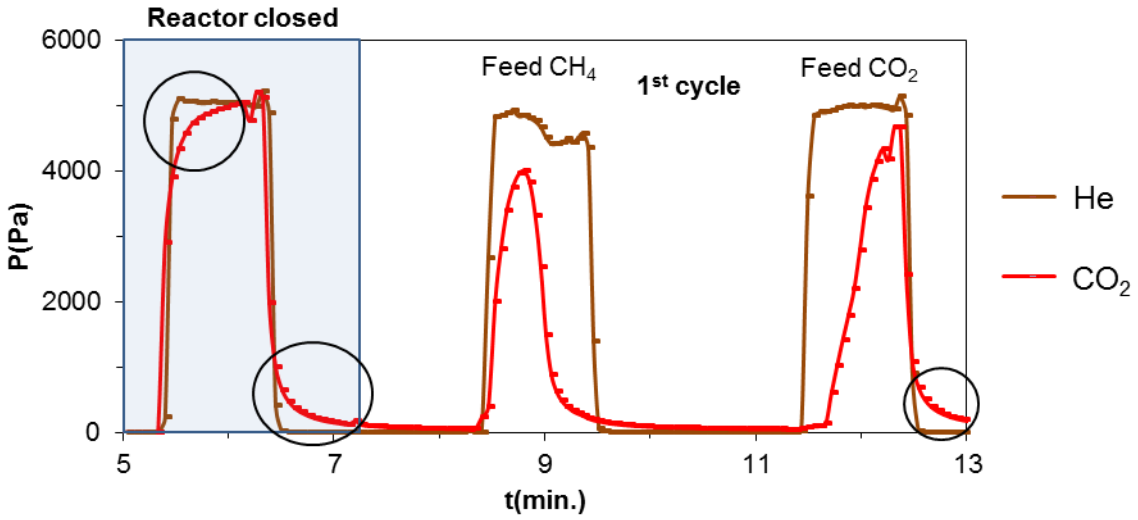

Fig 7.6 Partial pressures of He and CO_2 in the outlet flow working with 200mg of Ni(9.5)/CeO_2 at 700°C $F_{T,0}$ = 100 mL/min. Cycle: 1/2/1/2. 5% CH_4, 5 % CO_2, periodic (MS cooled down by N_2 (l))

At such low temperature (77ºK), the problematic of adsorption-desorption effect shows up for CO_2. ***Fig 7.6*** shows this type of behavior, the signal of CO_2 takes too much time to reach the nominal value (when the reactor is closed). Therefore, the calculation of the CO_2 conversion would be overestimated at that given time. Otherwise, the reverse effect is seen at the end of the step where the signal takes too much time to reach zero. In this case the data would be underestimated. In these conditions the carbon mass balance calculation would be difficult to follow. Fortunately in most of our experiments water only appear at the first cycle of the experiment. From all these facts, we decided not to use the liquid nitrogen cooling device for most of our experiments in order to give priority to precise carbon balance data.

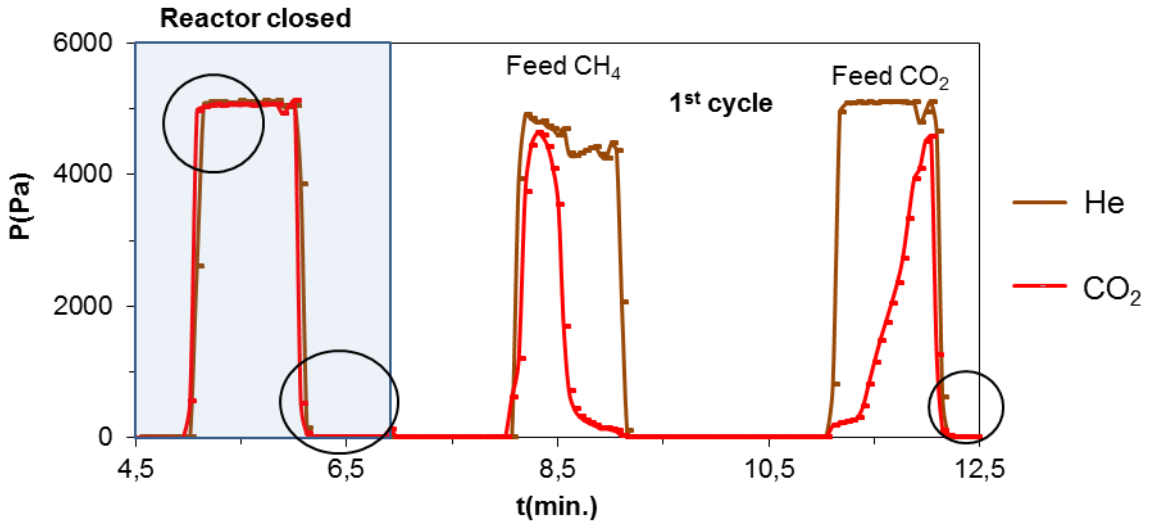

Fig 7.7 Partial pressures of He and CO_2 in the outlet flow working with 200mg of Ni(9.5)/CeO_2 at 800°C $F_{T,0}$ = 100 mL/min. Cycle: 1/2/1/2. 5% CH_4, 5 % CO_2, periodic (MS without N_2 (l))

Then, the ***Fig 7.7*** shows the improvement on the CO_2 signal. The adsorption-desorption effect disappears working without N_2 liquid, which would be more beneficial for most of the calculations.

7.1.2.5. MS elements: Ion source, mass filter, amplifier and detector

The neutral gas particles are ionized through electron bombardment. A voltage is applied between anode and cathode, which accelerates the electrons generated by the filament. The collision between the electrons and molecules produce single and multiple positive charged ions (ex. Ar → Ar^+) and fragmentation of more complex molecules (e.g. hydrocarbons). The electron energy used is 70eV.

Then, the ions are separated by the m / z ratio by a quadrupole mass filter which consists of four parallel rods arranged in the square position. Each pair of opposite rods, designated (+) or (-) is connected with the other. The ions are shot axially into the rods at approximately equal energy and velocity. The applied quadrupole field deflects the ions in the X and Y directions, causing them to undertake helical trajectories through the mass filter. The required mass range and desired resolution are governed by the dimensions of the filter and the selection of the operating frequency. Afterwards the ions go through an amplifier of the intensity (if not the intensity is too low to be detected), which in our case is a Continuous Secondary Electron Multipliers (C-SEM). Eventually, a Faraday collector detector can also be used but with much less sensitivity than the C-SEM [4.3].

7.1.3. From the raw data to the partial pressure: Methodology

The mass spectrometer provides the raw data to get the partial pressure of each gas, in the following paragraph the procedure to calculate such pressures is explained.

7.1.3.1. Baseline correction

First of all, a linear interpolation is made to adjust the baseline of each mass in the whole experiment (sometimes the loss of signal by the C-SEM can be considerable after few hours).

Eq. 7.1 $$I_{i,t} = I_{i,0} + \frac{(I_{i,f} - I_{i,0})}{(t_f - t_0)} \cdot t_t$$

$I_{i,t}$: Instantaneous intensity of the real baseline compound *i* (A) time t

$I_{i,0}$: Intensity compound *i* before the experiment (A) 0 for initial time

$I_{i,f}$: Intensity compound *i* after the experiment (A) f for final time

t_0 : Time when $I_{i,0}$ is taken (s)

t_f : Time when $I_{i,f}$ is taken (s)

t_t : Time along the experiment (s)

Eq. 7.2 $$I_{t,corr} = I_i - I_{i,t}$$

$I_{t,corr}$: Intensity at the moment *t* after baseline correction (A)

I_i : Intensity from raw data (A)

7.1.3.2. Contribution factor correction

This correction comes from the system of equations based on the fragment ion distribution of the potential compounds involved in the system. The ***Table 7.2*** helps us to know the influence of the different compounds in each mass [4.2].

Table 7.2 Main fractal ion distribution of different compounds

m/z	H_2	He	CH_4	H_2O	CO	C_2H_4	C_2H_6	O_2	Ar	CO_2	H_2S	SO_2	H_2SO_4	S_8	CH_2O	CH_3OH	CH_3CHO	CH_2O_2	C_3H_8	C_2H_5OH	$C_2H_4O_2$	m/z
1	2																					1
2	100					0,1	0,2									0,3					0,2	2
4		100																				4
14			20			2	3								1	2	11	0,4	2	1	5	14
15			89			0,3	4								2	12	36		7	7	17	15
16			100	1	2		0,1	22		10		5				0,1	6	5	0,4		2	16
17			2	21												0,3	0,3	17		1	1	17
18				100												1	1			1	3	18
20				0,3					15										1			20
26						53	23						0,2				5		9	10	1	26
27						62	33						1				4		42	22	0,1	27
28					100	100	100			10					24	5	3	17	59	3	4	28
29					1	2	22			0,1			1		100	45	100	100	100	30	8	29
30						0,1	26								58	6	1	2	2	8	0,4	30
31													0,1		1	100	0,3	1		100	2	31
32								100			44	10				74		0,2			0,1	32
34											100	0,4	0,5			0,1						34
40									100				0,1				1		3		1	40
43													0,5				48		23	11	100	43
44										100			1				83	10	27	1	3	44
45										1			1				3	48	1	52	90	45
46										0,4			0,1					61		22	1	46
48												49	51					0,3				48
60													0,1								75	60
64												100	50	100								64
80													100									80
81													72									81
96														21								96
128														55								128

From the ***Table 7.2*** a system of equations is figured out to obtain the intensity of the possible compounds in the outlet (CH_4, CO_2, H_2, CO, He, Ar and H_2O). In addition, C_2H_6 and C_2H_4 are also taken into account because the dry reforming of methane could also produce small amount of these hydrocarbons.

Eq. 7.3 $$S_{H_2} = S_2 - \frac{S_2}{S_{26}} \cdot S_{C_2H_4} - \frac{S_2}{S_{30}} \cdot S_{C_2H_6} - \frac{S_2}{S_{15}} \cdot S_{15}$$

Eq. 7.4 $$S_{He} = S_4$$

Eq. 7.5 $$S_{CH_4} = S_{15} - \frac{S_{15}}{S_{26}} \cdot S_{C_2H_4} - \frac{S_{15}}{S_{30}} \cdot S_{C_2H_6}$$

Eq. 7.6 $$S_{H_2O} = S_{18}$$

Eq. 7.7 $$S_{C_2H_4} = S_{26} - \frac{S_{26}}{S_{30}} \cdot S_{C_2H_6} - \frac{S_{26}}{S_{28}} \cdot S_{28}(28\ \text{tail})^*$$

Eq. 7.8 $$S_{CO} = S_{28} - \frac{S_{28}}{S_{26}} \cdot S_{C_2H_4} - \frac{S_{28}}{S_{30}} \cdot S_{C_2H_6} - \frac{S_{28}}{S_{44}} \cdot S_{CO_2}$$

Eq. 7.9 $$S_{C_2H_6} = S_{30} - \frac{S_{30}}{S_{28}} \cdot S_{28}(28\ \text{tail})^*$$

Eq. 7.10 $$S_{O_2} = S_{32}$$

Eq. 7.11 $$S_{Ar} = S_{40}$$

Eq. 7.12 $$S_{CO_2} = S_{44}$$

*The 28 tail means that peak at mass 28 which is usually high due to CO and CO_2 contributions has a width that may interferer on the surrounded masses, giving “false” intensities at masses 26, 27, 29 and/or 30 especially as these masses correspond to low concentrations compounds.. This effect was checked feeding CO_2 to the system with the reactor closed. Then, false production of ethane or ethylene could be taken into consideration without this correction. That is the reason of including the “28 tail” factor in the calculations.

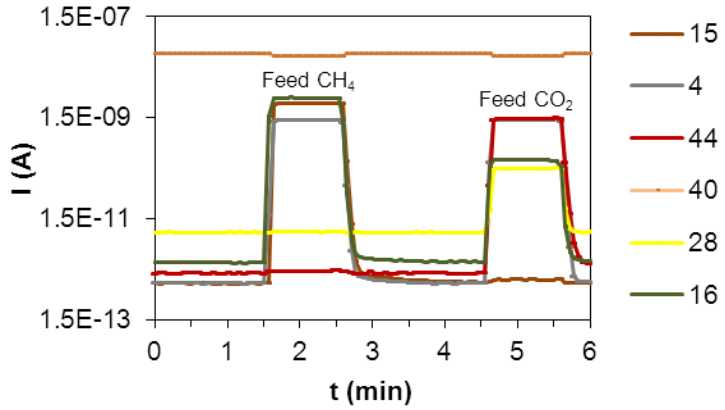

Fig 7.8 Example of signals (logarithmic scale) when the reactor is closed

In addition, a step of CH_4 and CO_2 with the reactor closed is carried before and after experiment in order to know in-situ some of the contribution factors to solve the system of equations, as shown in the ***Fig 7.8*** (the other contributions are theoretical). As an example the contribution of mass 44 in mass 28 during the step of CO_2 is around 0.10:

Eq. 7.13 $$\frac{S_{28}}{S_{44}} = \frac{1.49e{-}10}{1.44e{-}9} = 0.10$$

In this case the experimental value is the same as the theoretical one (***Table 7.2***), but as there is the easy way of checking that, the ratio is calculated at each experiment.

7.1.3.3. Importance on the order of the masses

After several experiment we realized that there was a gap between the partial pressure of He and CO_2 at the beginning and at the end of the step. One possibility about this behavior was the order of the signal capture. The measurement of each mass takes a few milliseconds, but taking into account the number of masses measured and the necessary relaxation time (electronics) between masses, this can generate some delay and have an influence on the final spectrum.

1st version: 2 / **4** /12 / 14 / **15** / 16 / 17 / 18 / 26 / 27 / 28 / 29 / 30 / 32 / 39 / 40 / 41 / **44** / T(°C)

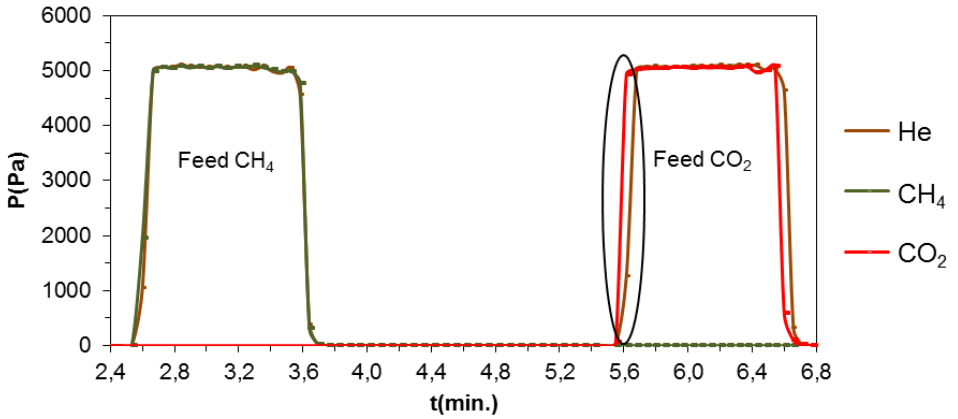

Fig 7.9 Partial pressures in the MS when the reactor is closed $F_{T,0}$ = 100 mL/min. Cycle: 1/2/1/2. 5% CH_4, 5 % CO_2, 5% He, periodic (version 1)

The ***Fig 7.9*** shows this phenomenon between the mass 4 (He) and 44 (CO_2) which are far between each other in the analysis from the MS. That would be the reason about the lower partial pressure of He in comparison with the one of CO_2 at the beginning of the oxidant step. The opposite effect appears at the end of the step. Based on this observation, the order of the signals was changed on the attempt to solve this issue. In detail, the mass 4 (for helium) was surrounded by the masses 15 (the one taken to calculate CH_4) and 44 (for CO_2). In addition, the other main masses involved in the process were also set at the beginning to get an order as follows:

2nd version: 2 / **15** / **4** / **44** / 40 / 28 / 18 / 26 / 27 / 32 / 12 / 14 / 16 / 17 / 29 / 30 / 39 / 41 / T(°C)

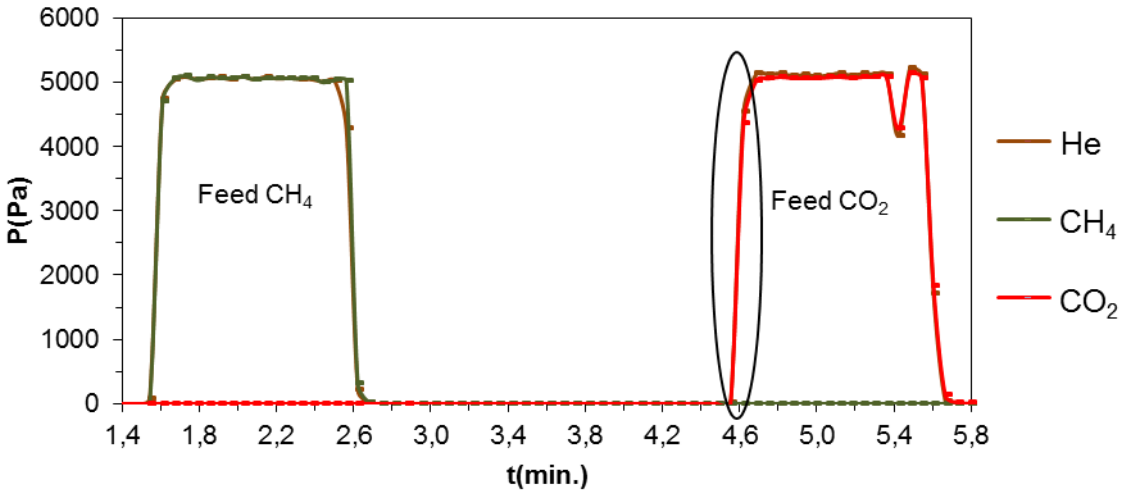

Fig 7.10 Partial pressures in the MS when the reactor is closed $F_{T,0}$ = 100 mL/min. Cycle: 1/2/1/2. 5% CH_4, 5 % CO_2, 5% He, periodic (version 2)

The difference between the two ways is clearly seen in the CO_2 step. The signal He - CO_2 in the ***Fig 7.10*** fits much better than in the ***Fig 7.9***. Thus, the calculation of CO_2 conversion

would be more precise thanks of this change. Note that the short decrease in reactants and He pressure at the end of the steps is due to the switching of the 4 way valve.

7.1.3.4. Relative sensitivity factor correction

The MS has different responses for each compound, so the last correction is based on the different sensitivities factors. The factors of the inlet flow compounds (CH_4, CO_2 and He) are calculated at the beginning and at the end of each experiment. The rest (H_2, CO, H_2O...) are calibrated time by time as it cannot be done in-situ. The argon has a factor of one (reference gas).

Table 7.3 Example of the iteration to get the relative sensitivity factor of He, CH_4, CO_2

Inlet	**He**	**CH_4**	**CO_2**
$f_{,1}$	**0,83**	**0,40**	**0,98**
$f_{,2}$	**0,82**	**0,40**	**0,99**
f_0	0,83	0,40	0,98
P_0	5066	5066	4970
P_1	5066	5066	4970
P_2	5066	5066	4970
$f_{corr,1}$	0,831	0,402	0,984
$f_{corr,2}$	0,824	0,401	0,988
$f_{corr,1} / f_1 = 1$	1,0000	1,0000	1,0000
$f_{corr,2} / f_2 = 1$	1,0000	1,0000	1,0000

An arbitrary number is assigned to f_1 and f_2 to start the iteration, which is based on the theoretical partial pressure of each reactant.

Eq. 7.14 $$f_{corr,1} = \frac{p_0}{p_1} \cdot f_1$$

$f_{corr,1}$: Correction factor before experiment

P_0 : Theoretical partial pressure of the compound (Pa)

P_1 : Partial pressure of the compound before the experiment (Pa)

Eq. 7.15 $$f_{corr,2} = \frac{p_0}{p_2} \cdot f_2$$

$f_{corr,2}$: Correction factor after the experiment

P_2 : Partial pressure of the compound after the experiment (Pa)

Eq. 7.16 $$f_0 = f_1 - \frac{(f_2 - f_1)}{(t_2 - t_1)} \cdot t_1$$

f_0 : Factor at t = 0

f_1 : Factor before experiment

f_2: Factor after experiment

t_1 : Time when P_1 is taken (s)

t_2 : Time when P_2 is taken (s)

Eq. 7.17 $$S_{corr,i} = S_{no,corr,i} \cdot \left(f_0 + \frac{(f_2 - f_1)}{(t_2 - t_1)} \cdot t_i\right)$$

$S_{corr,i}$: Intensity of the compound *i* after the sensitivity relative factor correction (A)

$S_{no,corr,i}$: Intensity of the compound *i* before the sensitivity relative factor correction (A)

7.1.3.5. From the intensity to the partial pressure

Eq. 7.18 $$S_T = \sum S_{corr,i} = S_{corr,CH_4} + S_{corr,CO_2} + \cdots$$

S_T : Total intensity in the system (sum of the intensities of all the compounds) (A)

Eq. 7.19 $$P_{i,t} = \frac{S_{corr,i}}{S_T} \cdot P_T$$

$P_{i,t}$: Partial pressure of the compound at *t* time (Pa)

P_T: Total pressure in the system (Pa)

7.1.3.6. Outlet flow (using the variation of Ar)

As explained before, the outlet flow is figured out from the variation of the Ar partial pressure with and without reaction. Example:

Eq. 7.20 $$R_{inc/dec} = \frac{P_{Ar,out}}{P_{Ar,in}}$$

$R_{inc/dec}$: variation flow factor

$P_{Ar,out}$: partial pressure of the Ar in the outlet flow (Pa)

$P_{Ar,in}$: theoretical partial pressure of the Ar in the inlet flow (Pa)

Eq. 7.21 $$F_{T,out} = \frac{F_{T,in}}{R_{inc/dec}}$$

$F_{T,out}$: total outlet flow (mL / min)

$F_{T,in}$: theoretical total inlet flow (mL / min)

7.1.3.7. Conversion with or without using the variation in the outlet flow

The conversions of the reactants are calculated by two different ways. The first one is the instantaneous conversion at a given time without taking into account the variation in the outlet flow.

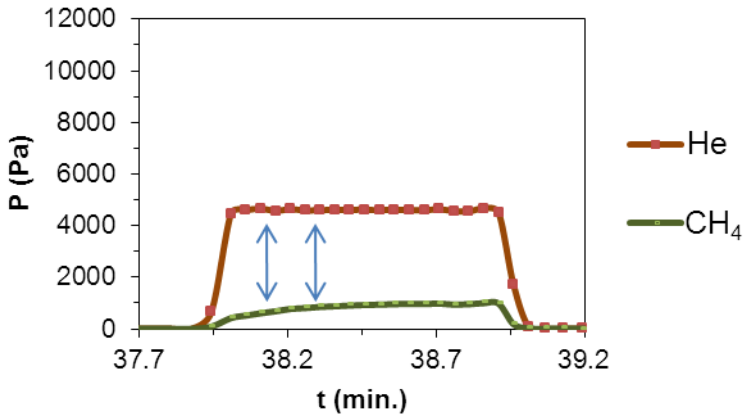

Fig 7.11 Partial pressures of CH_4 and He after the reaction

To illustrate, numerical values are taken at t = 38.3min in ***Fig 7.11***:

Eq. 7.22 $$R_{CH4/He,in} = \frac{F_{CH4,in}}{F_{He,in}} = \frac{5.0\ mL/min}{4.9\ mL/min} = 1.02$$

$R_{CH4/He,in}$: ratio between the methane and the helium flow in the inlet

$F_{CH4,in}$: inlet flow of CH_4 (mL / min)

$F_{He,in}$: inlet flow of He (mL / min)

Eq. 7.23 $$P_{CH4,in} = P_{He,out} \cdot R_{CH4/He,in} = 4590\ Pa \cdot 1.02 = 4683\ Pa$$

$P_{CH4,in}$: partial pressure of the theoretical CH_4 in the inlet (Pa)

$P_{He,out}$: partial pressure of He in the outlet (Pa)

Eq. 7.24 $$P_{CH4,con.}(Pa) = P_{CH4,in} - P_{CH4,out} = 4683\ Pa - 808\ Pa = 3875\ Pa$$

$P_{CH4,con.}$: amount of CH_4 converted (Pa)

$P_{CH4,out}$: partial pressure of CH_4 in the outlet (Pa)

Eq. 7.25 $$\%CH_{4,conversion} = \frac{P_{CH4,con.}}{P_{CH4,in}} = \frac{3875\ Pa}{4683\ Pa} \cdot 100 = 82.7\%$$

Conversion using the variation in the outlet flow (integration method)

The integration (in the inlet and in the outlet) between two points is made using the following formula in order to take into account the real outlet flow:

Eq. 7.26 $$\left[\int_{t=0}^{t}\left(P_{CH4,in,i} - P_{CH4,in,i-1}\right)(t) \cdot dt\right] \cdot F(t) = Pa \cdot s \cdot \frac{1\ min}{60\ s} \cdot \frac{mL}{min} = Pa \cdot mL$$

F (t) : outlet flow at a given time (mL / min)

To solve the integration, the trapezoidal formula is used:

Eq. 7.27 $$Int_i = \frac{(y_i + y_{i-1})}{2} \cdot (x_i - x_{i-1})$$

$$Int_{CH4,in} = \frac{\left(P_{CH4,in,i} + P_{CH4,in,i-1}\right)}{2} \cdot (t_i - t_{i-1}) = \frac{(4683\ Pa + 4732\ Pa)}{2} \cdot (2296\ s - 2293\ s)$$
$$= 14170\ Pa \cdot s \cdot \frac{1\ min}{60\ s} \cdot 107.8 \frac{mL}{min} = 25470\ Pa \cdot mL$$

Then from the ideal gas law:

Eq. 7.28 $$\mathrm{P \cdot V = n \cdot R \cdot T \rightarrow 25470\ Pa \cdot \frac{1\ atm}{101325\ Pa} \cdot mL \cdot \frac{1\ L}{1000\ mL} = n \cdot 0.082 \frac{atm \cdot L}{ºK \cdot mol} \cdot \frac{1\ mol}{1000000\ \mu mol} \cdot 298ºK \rightarrow n_{CH4,in} = 10.3\ \mu mol}$$

P : pressure (atm)

V : volume (L)

R : gas constant (atm * L / ºK * mol)

T : temperature at the mass spectrometer (ºK)

$n_{CH4,in}$: micromoles of CH_4 in the inlet at a given time (µmol)

The same procedure is considered to calculate the moles in the outlet flow:

Eq. 7.29 $$\mathrm{Int_{CH4,out} = \frac{(P_{CH4,out,i} + P_{CH4,out,i-1})}{2} \cdot (t_i - t_{i-1}) = \frac{(808\ Pa + 772\ Pa)}{2} \cdot (2296\ s - 2293\ s) = 2378\ Pa \cdot s \cdot \frac{1\ min}{60\ s} \cdot 107.8 \frac{mL}{min} = 4274\ Pa \cdot mL}$$

Eq. 7.30 $$\mathrm{P \cdot V = n \cdot R \cdot T \rightarrow 4274\ Pa \cdot \frac{1\ atm}{101325\ Pa} \cdot mL \cdot \frac{1\ L}{1000\ mL} = n \cdot 0.082 \frac{atm \cdot L}{ºK \cdot mol} \cdot \frac{1\ mol}{1000000\ \mu mol} \cdot 298ºK \rightarrow n_{CH4,out} = 1.7\ \mu mol}$$

$n_{CH4,out}$: micromoles of CH_4 in the outlet at a given time (µmol)

Eq. 7.31 $$\mathrm{\%CH_{4,conversion} = \frac{n_{CH4,in} - n_{CH4,out}}{n_{CH4,in}} = \frac{10.3\ \mu mol - 1.7\ \mu mol}{10.3\ \mu mol} \cdot 100 = 83.2\%}$$

Relative error between the two methods

Eq. 7.32 $$\mathrm{r.e\ (\%) = \frac{\Delta x}{x} = \frac{83.2 - 82.7}{83.2} \cdot 100 = 0.60\%}$$

The two methods show small differences. In this case, 0.6% seems negligible, but the variation between the outlet and the inlet flow was quiet low (108 mL/min instead of 100mL/min) thanks to the small initial concentration (5%) of the reactants. Otherwise, the difference would become more significant at high concentrations.

7.1.3.8. Conversion calculation without the helium flow

Some experiments (high initial concentrations) were carried without the helium flow, only using Ar as the inert gas. Therefore, the inlet flow is the theoretical one, without the precision of knowing the flow at each moment. The integral conversion over the full step is in this case more convenient. Then, from one side the µmols in the outlet flow is calculated as describe in the ***Eq. 7.29***. and ***Eq. 7.30***, adding the sum of it in the whole step (if the average conversion along the whole step is desired). From the other side, the theoretical µmoles of the reactants in the inlet are figured out as follows (e.g. for a 1 minute steps, 100ml/min, 25% CH_4 flow):

Eq. 7.33 $$V_i = F_i \cdot t_{step}$$

Eq. 7.34 $$n_i = \frac{V_i}{22.4 \frac{L}{mol}}$$

Eq. 7.35 $$\%CH_{4,conversion} = \frac{n_{CH4,in} - n_{CH4,out}}{n_{CH4,in}}$$

V_i : volume of the gas in the whole step (L)

F_i : flow of the gas (mL / min)

t_{step} : duration of the step (min)

n_i : µmols of the gas insert in the whole step (µmol)

22.4 L / mol : constant (one mole of an ideal gas at standard temperature and pressure occupies 22.4 liters)

Besides all the methods described above, it is necessary to keep in mind that in all the cases the main limitations are at the beginning and at the end of the step, where the partial pressures of the reactants are not constant, so obtaining instantaneous conversions which may not be reliable.

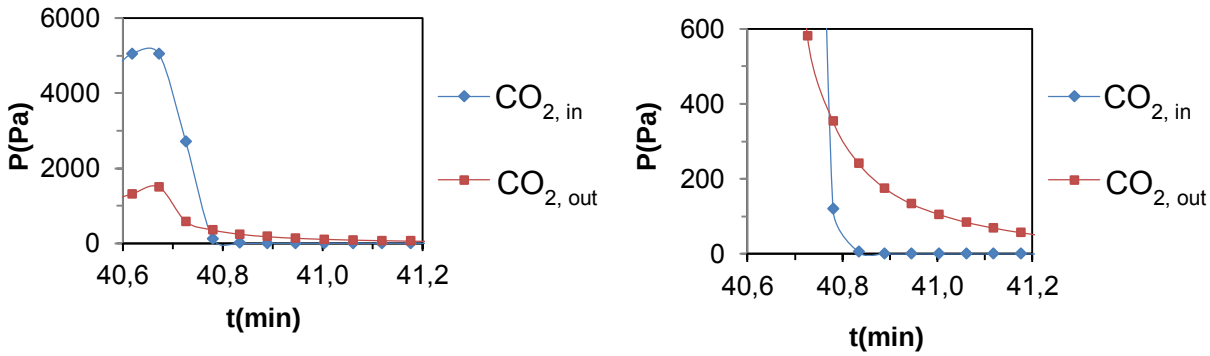

Fig 7.12 Partial pressure of CO_2 through the time

The figure above shows clearly the limitations mentioned above. For example, the instantaneous conversion at 40.83 min. would be as follows:

$$X_{CH_4} = \frac{5-240}{5} \cdot 100 = -4700\,\%$$

7.1.3.9. Selectivity reductant step: H_2 / CO and CO / (CO_2 + CO) ratios and $C_{deposited}/C_{conv.}$(%)

H_2/CO

H_2/CO ratio is calculated to have a reference about the selectivity of the reaction towards syngas. Therefore, 3 key conditions need to be considered:

- If H_2 / CO > 2, some carbon is produced because the only way to get a ratio above 2 is the decomposition of methane due to the absence of CO production.
  - $CH_4 \rightarrow C + 2\,H_2$
- If H_2 / CO = 2 and there are no other sub products (H_2O, CO_2 and C), 100% selectivity towards syngas is assumed.
  - $CH_4 + K\text{-}O \rightarrow 2\,H_2 + CO + K$
- If H_2 / CO < 2, some production of H_2O and/or CO_2 takes places at the same time as the syngas reaction
  - $CH_4 + 4\,K\text{-}O \rightarrow 2\,H_2O + CO_2 + K$

CO / (CO_2 + CO)

In addition the ratio CO/(CO_2+CO) is used to know if there is some total oxidation of CH_4, so producing CO_2.

- If CO/(CO_2+CO) = 1, there is only partial oxidation of CH_4
- If CO/(CO_2+CO) < 1, there is some total oxidation of CH_4
  - $CH_4 + 4K\text{-}O \rightarrow 2H_2O + CO_2 + K$

$C_{deposited}/C_{conv.}$(%)

Finally, $C_{deposited}/C_{conv.}$(%) is also calculated to have a reference about the % of the CH_4 converted which reacts through the cracking reaction. Specifically, the $C_{deposited}$ comes from the mass balance of carbon in the reductant step (see ***Paragraph 7.1.3.11***).

7.1.3.10. Selectivity oxidant step: $CO/CO_{2conv.}$

$CO/CO_{2conv.}$ ratio is also calculated in the oxidant step to have an idea about if the CO_2 is oxidizing the catalyst or some carbon deposited in the reductant step:

- If $CO / CO_{2,conv.}$ = 1, only reoxidation of the solid.
  - $CO_2 + K \rightarrow CO + K\text{-}O$

- If CO / $CO_{2,conv.}$ = 2, only oxidation of carbon deposit.
  - CO_2 + C → 2 CO

7.1.3.11. Mass balance of oxygen, carbon and hydrogen

The mass balance of each element involved in the reaction (O, C and H) was mainly calculated in order to get an approach of the O, C and H evolution in the solid.

Eq. 7.36 $$P_{O(catalyst)} = 2 \cdot P_{O(CO_2),in} - 2 \cdot P_{O(CO_2),out} - P_{O(CO),out} - P_{O(H_2O),out} - 2 \cdot P_{O(O_2),out}$$

Eq. 7.37 $$P_{C(catalyst)} = P_{C(CH_4),in} + P_{C(CO_2),in} - P_{C(CH_4),out} - P_{C(CO_2),out} - P_{C(CO),out} - 2 \cdot P_{C(C_2H_6),out} - 2 \cdot P_{C(C_2H_4),out}$$

Eq. 7.38 $$P_{H(catalyst)} = 4 \cdot P_{H(CH_4),in} - 4 \cdot P_{H(CH_4),out} - 2 \cdot P_{H(H_2),out} - 2 \cdot P_{H(H_2O),out} - 6 \cdot P_{H(C_2H_6),out} - 4 \cdot P_{H(C_2H_4),out}$$

Concretely, the main interest about the carbon balance is to know the eventual amount produced in the reductant step and if such quantity is reoxidized in the oxidant one:

- If $P_{C,catalyst}$ > 0 → Carbon (potentially in the reductant step)
- If $P_{C,catalyst}$ = 0 → Neither carbon deposited nor reoxidized
- If $P_{C,catalyst}$ < 0 → Oxidation of carbon (potentially in the oxidant step)

7.2. ΔG. Reduction by CH_4 and Reoxidation by CO_2

7.2.1. Complete example with Ce

Table 7.4 Reduction and oxidation reactions of the different phases of Ce

Reductant step (partial oxidation ●)	Reductant step (total oxidation ■)	Oxidant step (▲)
$(5.1) CH_4 + 2CeO_2 \rightarrow Ce_2O_3 + 2H_2 + CO$	$(5.2) CH_4 + 8CeO_2 \rightarrow 4Ce_2O_3 + 2H_2O + CO_2$	$(5.1) CO_2 + Ce_2O_3 \rightarrow 2CeO_2 + CO$
$(5.3) 2CH_4 + Ce_6O_{11} \rightarrow 3Ce_2O_3 + 4H_2 + 2CO$	$(5.4) CH_4 + 2Ce_6O_{11} \rightarrow 6Ce_2O_3 + 2H_2O + CO_2$	$(5.2) 2CO_2 + 3Ce_2O_3 \rightarrow Ce_6O_{11} + 2CO$
$(5.5) CH_4 + 6CeO_2 \rightarrow Ce_6O_{11} + 2H_2 + CO$	$(5.6) CH_4 + 24CeO_2 \rightarrow 4Ce_6O_{11} + 2H_2O + CO_2$	$(5.3) CO_2 + Ce_6O_{11} \rightarrow 6CeO_2 + CO$
$(5.7) CH_4 + Ce_2O_3 \rightarrow 2CeO + 2H_2 + CO$	$(5.8) CH_4 + 4Ce_2O_3 \rightarrow 8CeO + 2H_2O + CO_2$	$(5.4) CO_2 + 2CeO \rightarrow Ce_2O_3 + CO$
$(5.9) CH_4 + CeO \rightarrow Ce + 2H_2 + CO$	$(5.10) CH_4 + 4CeO \rightarrow 4Ce + 2H_2O + CO_2$	$(5.5) CO_2 + Ce \rightarrow CeO + CO$

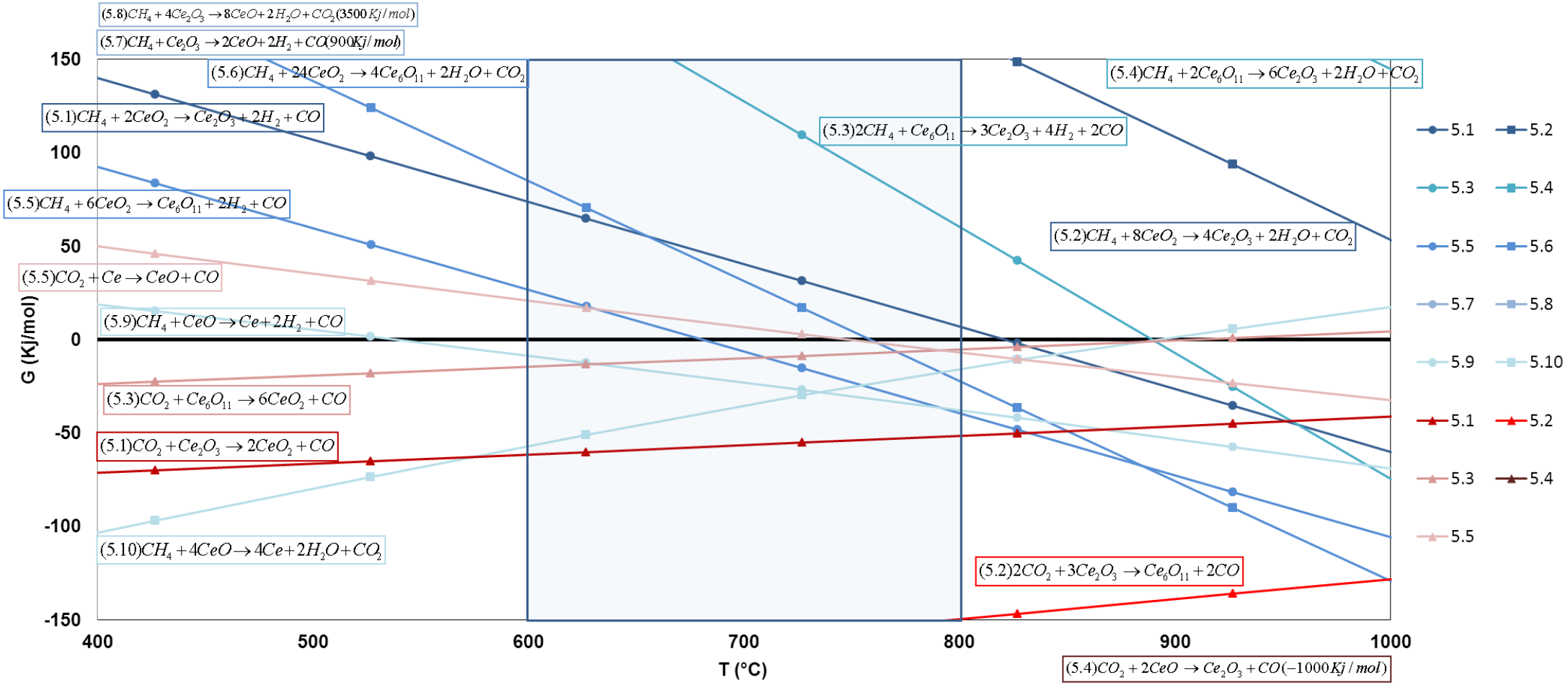

Fig 7.13 Gibbs free energy for the oxidation of CH_4 by CeO_2 and its reoxidation by CO_2

Phase diagram:

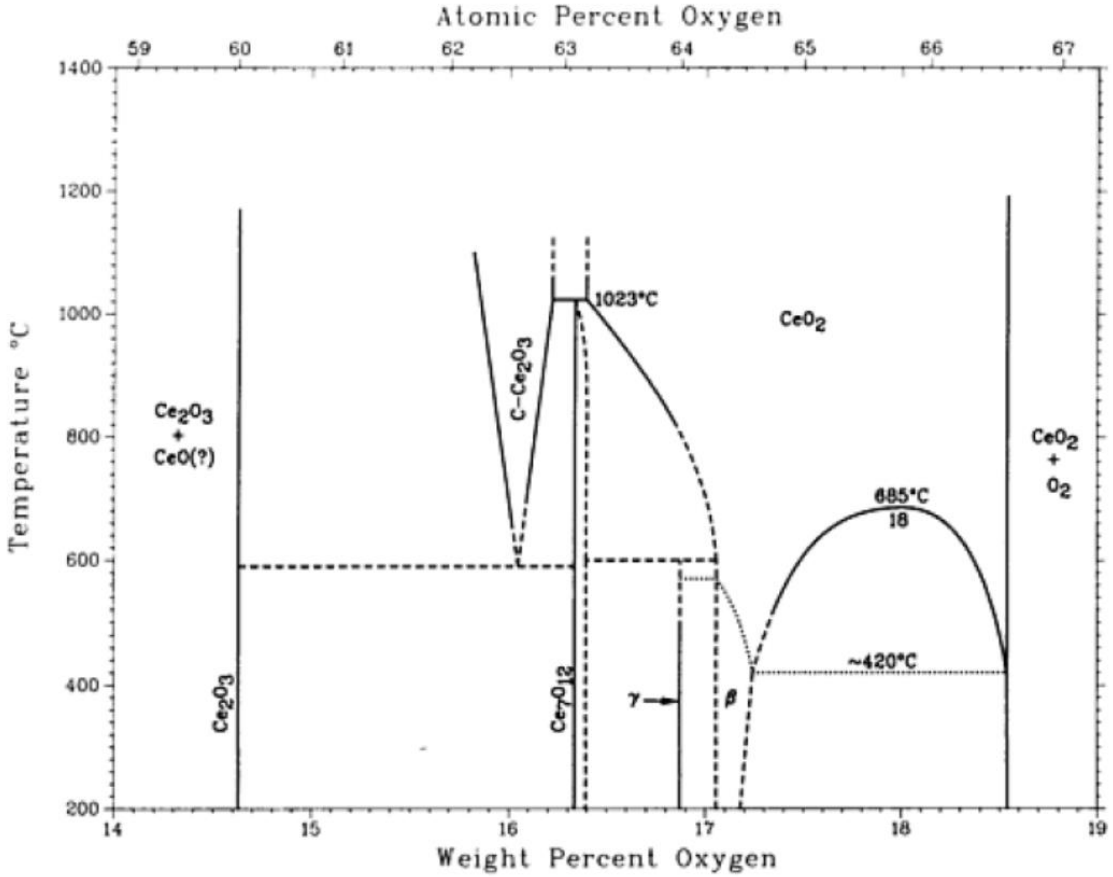

Fig 7.14 Phase diagram of Ce [3.1]

Table 7.5 Potential oxides of Ce

Ce-O crystallographic data

Phase	Composition, wt% O	Pearson symbol	Space group
$(\alpha Ce)^{(a)}$	~0	*cF*4	$Fm\overline{3}m$
$(\beta Ce)^{(b)}$	~0	*hP*4	$P6_3/mmc$
$(\gamma Ce)^{(c)}$	~0	*cF*4	$Fm\overline{3}m$
$(\delta Ce)^{(d)}$	~0	*cI*2	$Im\overline{3}m$
CeO	~10.2	*cF*8	$Fm\overline{3}m$
Ce_2O_3	~15	*hP*5	$P\overline{3}m1$
"C-Ce_2O_3" [e], [g]	15.86 to 16.16	*cI*80	$Ia\overline{3}$
Ce_7O_{12}	16.3 to 16.43	*hR*22	$R\overline{3}$
γ [f]	~16.90	*hR*?	. . .
β [g]	~17.1 to 17.2	*hR*?	. . .
Ce_6O_{11} [h]	~17.3	*mP*?	$P2_1/n$
CeO_2	~18.6	*cF*12	$Fm\overline{3}m$
CeO_2 [i]	~18.6	*hP*48	. . .
High-pressure phase			
CeO [j]	~10.2	*cF*?	. . .

Basic scheme:

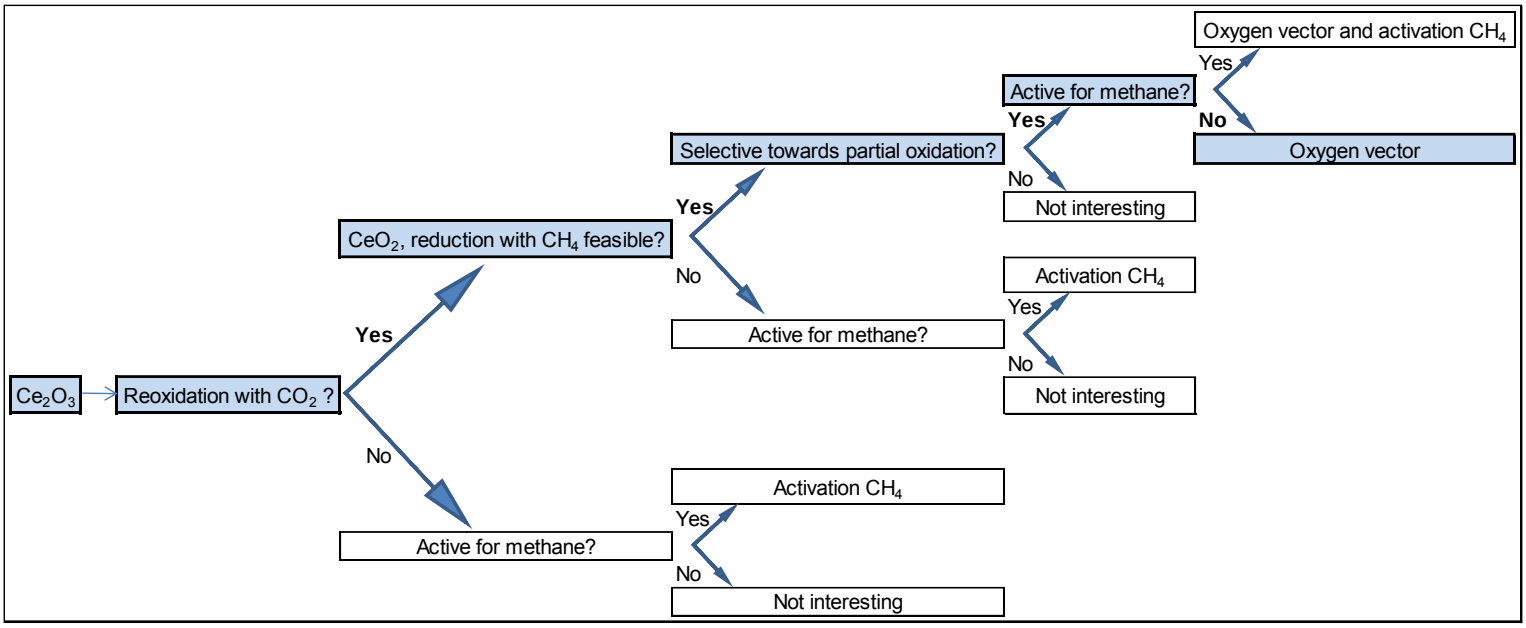

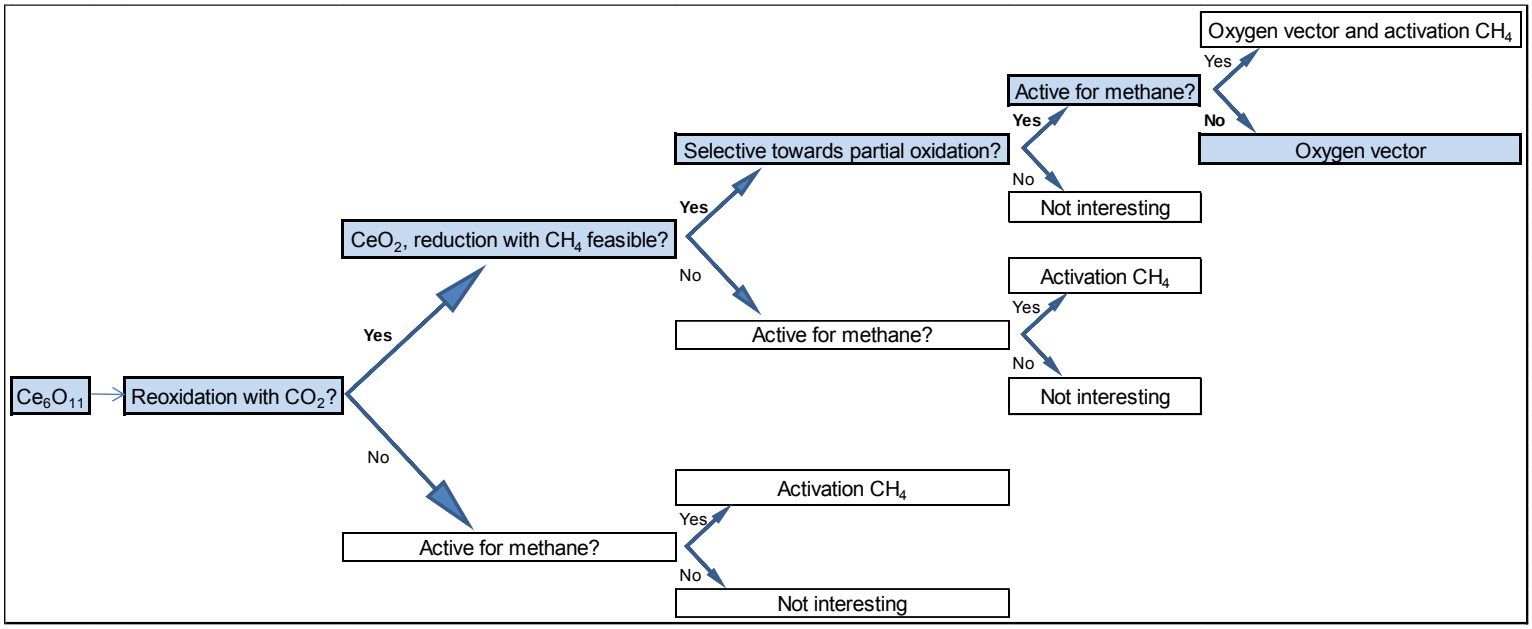

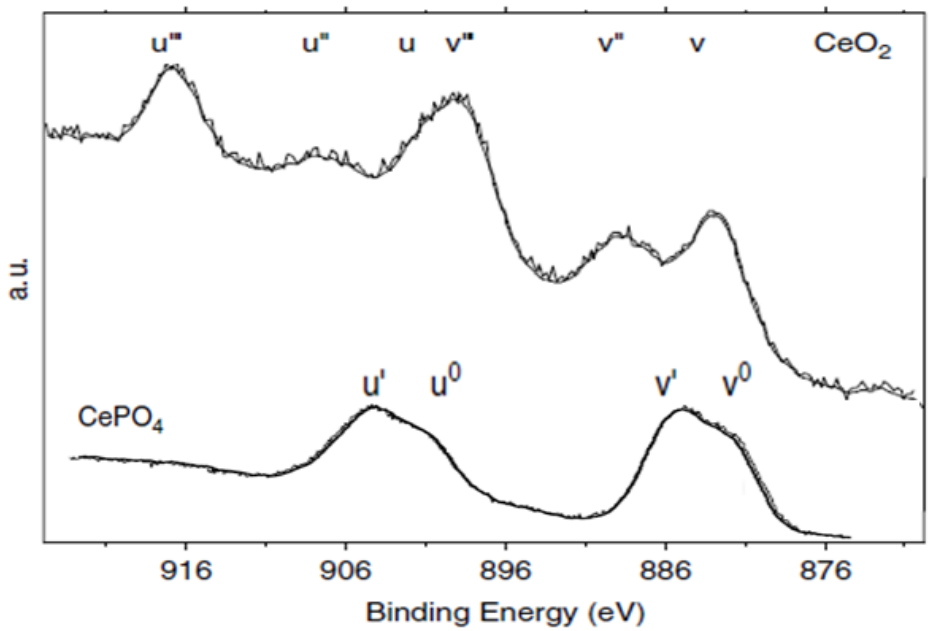

Fig 7.15 Ce 3d$_{3/2.5/2}$ XPS spectrum for Ce(IV)O$_2$ and Ce(III)PO$_4$ as references [4.21]

7.3. Example to calculate the theoretical conversion of DRM

$$CH_4 + CO_2 \rightarrow 2H_2 + 2CO$$

The equilibrium constant is found from the Gibbs free energy, according to the following equation which is the equilibrium expression in function of pressure, composition and fugacity coefficient:

$$\Pi\left(y_i \cdot \hat{\phi}_i\right)^{\nu_i} = \left(\frac{P}{P^0}\right)^{-\nu} \cdot K$$

Φ = fugacity coefficient

K = equilibrium constant

P = pressure in the system (bar)

P^0 = pressure in standard state (1 bar)

$v = \sum_i v_i$ = reactants and products coefficients

y_i = mole fraction

$$\Pi\left(y_i \cdot \hat{\phi}_i\right)^{\nu_i} = \frac{(y_{H_2} \cdot \phi_{H_2})^2 \cdot (y_{CO} \cdot \phi_{CO})^2}{(y_{CH_4} \cdot \phi_{CH_4}) \cdot (y_{CO_2} \cdot \phi_{CO_2})}$$

Mole fraction:

$$y_i = \frac{n_i}{n_T} = \frac{n_{i0} + \Delta n_i \cdot x}{n_0 + \Delta n \cdot x}$$

x = reaction coordinate

$$y_{CH_4} = \frac{1-x}{(2+2x)} \qquad y_{CO_2} = \frac{1-x}{(2+2x)} \qquad y_{H_2} = \frac{2x}{2+2x} \qquad y_{CO} = \frac{2x}{2+2x}$$

Fugacity coefficient:

$$\phi = \exp\left(\frac{P_r}{T_r} \cdot \left(B^0 + w \cdot B^1\right)\right)$$

w = acentric factor

Reduced Pressure:

$$P_r = \frac{P}{P_C}$$

Pc = critical pressure

Reduced Temperature:

$$T_r = \frac{T}{T_C}$$

Tc = critical temperature

Coefficients B_0 and B_1:

$$B^0 = 0.083 - \left(\frac{0.422}{T_r^{1.6}}\right)$$

$$B^1 = 0.139 - \left(\frac{0.172}{T_r^{4.2}}\right)$$

Equilibrium constant:

$$K = \exp\left(\frac{-\Delta G_T}{R \cdot T}\right)$$

R = 8.314 J/mol * ºK

Then, the theoretical moles in the outlet are calculated once x is obtained in function of the temperature. For instance, at 697ºC x = 0.453

$$n_{CH_4} = 1 - 0.453 = 0.547 \qquad x_{CH_4} = \frac{1-0.547}{1} \cdot 100 = 45.3\%$$